Modern Engineering Design: Analytical and Numerical Modelling of Semi-rigid Connections

A thesis submitted to The University of Manchester for the degree of Doctor of Philosophy in the Faculty of Engineering and Physical Sciences

2013

HAMEED SHAKIR TRAD AL-AASAM

SCHOOL OF MECHANICAL, AEROSPACE AND CIVIL ENGINEERING

Table of content

Abstract 16

Declaration 17

Copyright Statement 18

Acknowledgements 19

Notations 20

Publications 24

Chapter One Introduction 25

1.1. Introduction 25

1.2. Research objectives 29

1.3. Outline of the thesis 31

Chapter Two Literature review 35

2.1. Introduction 35

2.2. Semi-rigid concept 35

2.3. Main approaches to investigate the behaviour of isolated connection 36

2.3.1. Mathematical models 37

2.3.2. 2D and 3D finite element models 37

2.3.3. Component-based mechanical models 41

2.4. Main approaches to investigate the effect of a semi-rigid connection on the natural frequency of structure 43

2.4.1. Background 43

2.4.2. Beam with semi-rigid connections 44

2.4.3. Frame with semi-rigid connections 44

Chapter Three Mechanical model for predicting the rotational stiffness of a flush end-plate composite connection incorporating the effect of partial interaction 50

3.1. Introduction 50
3.2. Flush end-plate composite connection 51
3.2.1. Why flush end-plate composite connection? 51
3.2.2. Key parameters of a flush end-plate composite connection 52
3.3. Background 54
3.3.1. Requirements of an ‘‘ideal model’’ 54
3.3.2. Significant models from the literature 55
3.4. Proposed mechanical model 62
3.4.1. Basic parameters and springs in the proposed mechanical model 62
3.4.2. Derivation of the expressions for the mechanical model 64
3.5. The applicability of the proposed equation for general cases 68
3.6. Why a rotational spring? 69
3.6.1. Modelling 70
3.6.2. Results and discussion 72
3.6.3. Suggestion for modification of the conventional models 75
3.7. Main merits of the proposed model 76
3.8. Determination of the effective terms in the mathematical expression 76
3.8.1. Effect of k_c 77
3.8.2. Effect of k_b 78
3.8.3. Effect of k_r 78
3.8.4. Effect of k_s 79
3.9. Adopted procedure to calculate the key parameters 80
3.9.1. Stiffness of the top row of bolts, k_b 80
3.9.2. Stiffness of the column web in shear, k_{cws} and compression, k_{cwc} 80
3.9.3. Stiffness coefficient of the steel reinforcement, k_r 81
3.9.4. Stiffness of the shear connection, k_s 83
3.10. Validation of the proposed expression for the rotational stiffness of a composite connection 90

3.10.1. Results and conclusions 92

Chapter Four Prediction of the load-slip behaviour of a stud shear-connector 98

4.1. Background 98

4.2. Current procedures to estimate the essential properties of a stud shear-connector 98

4.2.1. Strength of the shear connector, $F_{sc,max}$ 99

4.2.2. Stiffness of a shear stud connector, k_{sc} 101

4.2.3. Empirical equations to estimate slip capacity, $S_{sc,c}$ 104

4.3. Proposed approach 104

4.3.1. Basic relations 104

4.3.2. Methodology 105

4.3.3. Strength of a stud shear-connector 110

4.3.4. Secant stiffness of a stud shear-connector 112

4.4. Validity of the proposed chart for larger diameters of shear connector 113

4.5. Multi-linear model of the load-slip curve for the shear connector 114

4.5.1. Slip at maximum strength and slip capacity of the shear connector 116

4.6. Summary and conclusion 118

Chapter Five Stiffness of a reinforced concrete slab in a composite connection 119

5.1. Introduction 119

5.2. Background 119

5.3. Brief literature review 120

5.4. Objectives 122

5.5. Proposed model for reinforced concrete composite slab, (RCCS) 123

5.5.1. Defining the behaviour of the major components 123

5.5.2. Construction of the proposed model 134

5.6. Derivation of analytical expression for the initial stiffness of composite slab with shear studs (“lump’’ component) 136

5.7. Distribution of forces in (RCC) and shear stud springs 138

5.8. Validation 139

5.8.1. Verification of the analytical expression against finite element results using ABAQUS software 139

5.8.2. Verification of the proposed model for (RCC) and shear studs against the experimental test for a composite slab 145

5.8.3. Verification of the proposed model against the experimental test for a composite connection 147

5.9. Parametric study to investigate the effect of k_{RCC}/k_{sc} on K_{lump} 154

5.9.1. Maximum and minimum ratios of k_{RCC}/k_{sc} 154

5.9.2. ABAQUS model 155

5.9.3. Results and discussion 155

5.11. Modified mechanical model of initial stiffness for a composite connection 162

5.12. Summary and conclusions 164

Chapter Six Moment resistance and Ductility of a flush end-plate composite connection 166

6.1. Introduction 166

6.2 Prediction of failure mode of a flush end-plate composite connection 167

6.3. Moment resistance of a flush end-plate composite connection 170

6.3.1. Brief literature review 170

6.3.2. Proposed procedure to calculate moment resistance of a flush end-plate composite connection 172

6.3.3. Validity of the proposed procedure to calculate the moment resistance of a flush end-plate composite connection 177

6.4. Ductility of a flush end-plate composite connection 180

6.5. Brief literature review 180
6.5.1. Rotation at yield 180
6.5.2. Rotation capacity 182
6.6. Proposed procedure to predict the rotation at yield and rotation capacity of a flush end-plate composite connection 186
6.6.1. Rotation at yield 186
6.6.2. Rotation capacity 188
6.7. Validity of the proposed procedures 191
6.7.1. Rotation at yield 191
6.7.2. Rotation capacity 192
6.8 Relation between the ductility of connection and ductility of frame 194
6.8.1. Finite element modelling 196
6.9. Summary and conclusions 203
Chapter Seven Analysis of a uniform beam with semi-rigid connections under gravity loading 204
7.1. Introduction 204
7.2. Proposed procedure 205
7.3. Eurocode 3 (2005) classification for joints 207
7.4. Comparison with (Ahmed et al., 2008)'s equations 207
7.5. Deflection of a semi-rigid beam 209
7.6. Steps for analysis of a beam with a semi-rigid connection under gravity loading 210
7.6.1 End moment and reaction V_A and V_B 210
7.6.2. Deflection at any point 210
7.7. Natural frequency of a uniform beam with semi-rigid connections using the effective length concept 213
7.8. Results and conclusion 215

Chapter Eight A simplified procedure to calculate by hand the natural periods of semi-rigid steel frames 216

8.1. Introduction 216

8.2. Brief literature review 216

8.3. Derivation of an approximate formula to calculate the natural periods of a cantilever beam 217

8.3.1. Purely flexural motion (i.e. $\lambda=\lambda_f$) 219

8.3.2. Coupled shear-flexural motion (i.e. $\lambda=\lambda_{sf}$) 220

8.3.3. Combined effect of pure flexural and shear-flexural free vibration 220

8.4. Approximate formulae for natural periods 221

8.5. Evaluation of characteristic parameters 221

8.6. Simplified procedure to calculate natural periods of a steel frame 222

8.7. Effect of connection flexibility on natural frequency of steel frames 222

8.8. Modification of the approximate formulae for semi-rigid frames 223

8.9. Parametric study on the effect of different $k\alpha H$ values 232

8.10. Summary and conclusions 234

Chapter Nine An approximate analytical method for calculating the natural periods of unbraced steel frames with semi-rigid connections 235

9.1. Introduction 235

9.2. Brief literature review 235

9.3. Muto's original method (D value method) 237

9.3.1. Equations of Muto's original method 239

9.4. Improvements of Muto's method 240

9.4.1. The position of inflection point of beams 240

9.4.2. Effect of boundary conditions of columns at the first storey on the deflection of upper storey 242

9.4.3. Storey deflection due to load applied at immediately beneath the storey in question 242
9.5. Improved equations and corresponding sub-frames 242
9.6. Proposed procedure to compute flexibility matrix for plane frame structures 246
9.7. Lumped-mass matrix for a multi-storey plane frame 247
9.8. Fundamental period of a multi-storey plane frame 248
9.9. Modified Muto's method for a semi- rigid framed structure 249
9.10. Sensitivity of the proposed procedure 252
9.11. Summary and conclusions 255
Chapter Ten Summary and Conclusions 256
10.1. Introduction 256
10.2. Mechanical model for predicting the rotational stiffness of a flush end-plate composite connection incorporating the effect of partial interaction 256
10.3. Prediction of the load-slip behaviour of a stud shear-connector 257
10.4. Stiffness of a reinforced concrete slab in a composite connection 257
10.5. Moment resistance and ductility of flush end-plate composite connections 258
10.6. Analysis of a beam with semi-rigid connections under gravity loading 259
10.7. A simplified procedure to calculate by hand the natural periods of semi-rigid steel frames 259
10.8. An approximate analytical method for calculating the natural periods of unbraced steel frames with semi-rigid connections 260
10.9. Recommendation for future work 260
References 262
Appendix-A1 269
Appendix-B 276

Word count: 60,049

Table of Figures

Figure 1.1: Types of connection and its moment- rotation curves (Chan and Chui,2000) 25
Figure 1.2: Examples of connections connected to beam UB 610x305x176 and Eurocode 3 boundaries 26
Figure 1.3: Examples of connections connected to beam UB 127x76x13 and Eurocode 3 boundaries 27
Figure 1.4: Typical moment–rotation curve of a connection .....
Figure 1.5: Logical relationship among the main chapters .....
Figure 2.1: Example of a semi-rigid composite connection 36
Figure 2.2: 2D finite element model for composite connection using DIANA software (Kattner and Crisinel, 2000) 38
Figure 2.3: General arrangement of test set-up (Fu and Lam, 2006) 39
Figure 2.4: 3D finite element model of a composite connection using ABAQUS software and only part of slab was taken and ignored the tension-stiffening effect (Fu et al., 2007) 40
Figure 2.5: The composite connection model with material model of concrete (Fu et al, 2007) 40
Figure 2.6: Example of experimental specimens (Gil and Bayo, 2008) 40
Figure 2.7: 3D Finite element model using ABAQUS software for internal and external connection incorporating the effect of tension-stiffening in concrete modelling (Gil and Bayo, 2008) 41
Figure 2.8: Example of mechanical model (Ahmed and Nethercot, 1997) 42
Figure 2.9: Test structure arrangement (Nader and Astaneh, 1991) 46
Figure 3.1: Typical flush end-plate composite connection 51
Figure 3.2: Typical model of a flush end-plate composite connection with its deformation 53
Figure 3.3: Internal forces and deformation in bare steel and composite connections ... 56
Figure 3.4: (a) Benussi and Noe's model (b) Anderson and Najafi's extended model 57
Figure 3.5: The spring model of (Ren and Crisinel 1995) 58
Figure 3.6: Ahmed and Nethercot spring's model 59
Figure 3.7: Proposed mechanical model 64
Figure 3.8: a) Proposed model b) (Ahmed and Nethercot 1997)'s model 70

Figure 3.9: Modelling of conventional mechanical model in ABAQUS 71
Figure 3.10: Modelling of the proposed mechanical model in ABAQUS 71
Figure 3.11: ABAQUS results of rotation for the S4F composite connection 72
Figure 3.12: Comparison of rotational and conventional spring's models with test results for test S4F 74
Figure 3.13: Comparison rotational and conventional spring's models with test results for test S8F 74
Figure 3.14: Comparison rotational and conventional spring's models with test results for test S12F 75
Figure 3.15: The effect of k_c on rotational stiffness 77
Figure 3.16: The effect of k_b on rotational stiffness 78
Figure 3.17: The effect of k_r on rotational stiffness 79
Figure 3.18: The effect of k_s on rotational stiffness 79
Figure 3.19: Load-slip curves for shear stud 86
Figure 3.20: Comparison of results using the proposed and Eurocode 4 procedures to calculate k_s and k_r 92
Figure 3.21: Comparison of results using the proposed and Eurocode 4 procedures to calculate k_s and k_r (after sorting the results in ascending order) 93
Figure 3.22: Comparison of the proposed procedure with other procedures to calculate the rotational stiffness of a flush end-plate composite connection 96
Figure 3.23: Comparison of the proposed procedure with other procedures to calculate the rotational stiffness of a flush end-plate composite connection (after sorting the results in ascending order) 96
Figure 4.1: Variation of α with h_{sc}/d for constant diameters of shear stud 100
Figure 4.2: Variation of α with h_{sc} or d for constant diameters or heights of the shear stud 100
Figure 4.3: Forces and deformation of shear stud 101
Figure 4.4: Values of γ for different compressive strengths of the surrounding concrete 103
Figure 4.5: Load-slip curves (experimental and numerical) of studs (22 mm diameter, 100mm high**)** for different compressive strength of concrete 106
Figure 4.6: Load-slip curves (experimental and numerical) of studs (19 mm diameter, 100mm high**)** for different compressive strength of concrete 106

Figure 4.7: Load-slip curves (experimental and numerical) of studs (16 mm diameter, 85 mm high**)** for different compressive strength of concrete 107
Figure 4.8: Load-slip curves (experimental and numerical) of studs (13 mm diameter, 65 mm high**)** for different compressive strength of concrete 107
Figure 4.9: Comparison of experimental and numerical curves for different compressive strength of concrete across four models (*d*=22mm).....108
Figure 4.10: Comparison of experimental and numerical curves for different compressive strength of concrete across four models (*d*=19mm**)**.....109
Figure 4.11: Comparison of experimental and numerical curves for different compressive strength of concrete across four models (*d*=16mm**)**.....109
Figure 4.12: Comparison of experimental and numerical curves for different compressive strength of concrete across four models (*d*=13mm**)**.....110
Figure 4.13: Secant stiffness-strength-concrete strength relationship for stud shear-connector with different d/h_{sc}.....113
Figure 4.14: Secant stiffness-strength-concrete strength relationship for large shear stud connectors 114
Figure 4.15: Multi-linear model ($F_{sc,max}$=128.7 kN) by (Queiroz et al., 2009).....115
Figure 4.16: Tri-linear model by (Titoum et al., 2008).....115
Figure 4.17: Proposed multi-linear model of load-slip curve 117
Figure 4.18: Comparison of the proposed model with experimental load-slip curves .117
Figure 5.1: Typical composite connection.....119
Figure 5.3: Idealised behaviour of a RC tension member: (a) average stress–strain relationship of a reinforcement (b) average stress–strain relationship of concrete.....124
Figure 5.2: Typical Stress-strain relationship for plain concrete .....
Figure 5.4: Tension-stiffening development (for $F_{s,T}>F_{s,cr}$) 127
Figure 5.5: Simplified load-strain relationships for bare and embedded reinforcement 127
Figure 5.6: Test arrangement (Tamai et al., 1988).....130
Figure 5.7: Comparison of the stress in a steel bar of a reinforced concrete member and in a steel bar alone using the analytical procedure (specimen No.1) 130
Figure 5.8: Comparison of analytical and experimental results for a reinforced concrete member (specimen No.1).....131
Figure 5.9: Comparison of stress of a steel bar in reinforced concrete member and a steel bar alone using an analytical procedure (specimen No. 6).....131

Figure 5.10: Comparison of analytical and experimental results for a reinforced concrete member (specimen No. 6) 131
Figure 5.11: Stress-strain relationship of the (RCC) .....
Figure 5.12: Proposed model for a composite slab 135
Figure 5.13: Simplified proposed spring model .....
Figure 5.14: Force-deformation relationship for an (RCC) spring .....
Figure 5.15: Approximate force-displacement relationship for an (RCC) spring .....
Figure 5.16: Final model for initial stiffness .....
Figure 5.17: ABAQUS model to verify the proposed analytical expressions. The part of the steel beam shaded in dark cyan (1.97 m) has been modelled by beam elements; the profile effect is due to rendering. The grey part at the right hand end (0.1 m) has been modelled by solid elements. 140
Figure 5.18: Tensile stresses in the springs from the ABAQUS deformed model 141
Figure 5.19: Moment-rotation curve 141
Figure 5.20: Distribution of forces in (RCC) springs along a composite connection ... 142
Figure 5.21: Distribution of forces acting on shear studs along a composite connection 142
Figure 5.22: Distribution of forces in (RCC) springs for increasing applied moments 143
Figure 5.23: Distribution of forces in shear studs for increasing applied moments 144
Figure 5.24: Ratio of total reinforcement force in the in every (RCC) spring from total shear force 144
Figure 5.25: Ratio from total reinforcement force in every shear stud along the composite beam 145
Figure 5.26: Sketch of the set-up used by (Rex and Easterling, 2000) 146
Figure 5.27: ABAQUS model for a composite slab with shear studs 146
Figure 5.28: ABAQUS deformed shape of a composite slab model 147
Figure 5.29: Comparison of force-deformation curves for the proposed model and experimental results 147
Figure 5.30: a) Load arrangement; b) composite beam section; c) end-plate 148
Figure 5.31: Steel end-plate connection 149
Figure 5.32: Elastic-plastic model for steel .....
Figure 5.33: Behaviour of shear studs 151
Figure 5.34: The final 3-D finite element model 152
Figure 5.35: Deformed shape of the composite connection 153

Figure 5.36: Comparison of the moment-rotation curves for experimental and numerical modelling 153
Figure 5.37: Sample of ABAQUS Model for parametric study (20 studs) (same as Figure 5.17, but with different number of studs) 155
Figure 5.38: Distribution of forces in shear studs for k_{RCC}/k_{sc} =1.0 156
Figure 5.39: Distribution of forces in shear studs for k_{RCC}/k_{sc} =10 156
Figure 5.40: Distribution of forces in shear studs for k_{RCC}/k_{sc} =50 157
Figure 5.41: Distribution of forces in shear studs for k_{RCC}/k_{sc} =100 157
Figure 5.42: Distribution of forces in shear studs for k_{sc}=150kN/mm and k_{RCC}/k_{sc} =0.01 to 100 159
Figure 5.43: First stud force ratio from reinforcement force with varying k_{RCC}/k_{sc} 160
Figure 5.44: Relationship between the maximum number of "active'' shear studs and k_{RCC}/k_{sc}. 161
Figure 5.45: The proposed mechanical model .....
Figure 5.46: Final modified mechanical model .....
Figure 6.1: Flowchart for failure mode predication .....
Figure 6.2: Proposed mechanical model with free-body diagram .....
Figure 6.3: Validity of proposed procedure to calculate the moment resistance of composite connection 177
Figure 6.4: Conventional mechanical models: a) Benussi and Noe's model; (b) Anderson and Najafi's model; c) Ahmed and Nethercot model 182
Figure 6.5: Mechanical model for calculating the rotations at yield and ultimate .....
Figure 6.6: Steel frame 194
Figure 6.7: Moment-rotation curve of isolated connections 195
Figure 6.8: Connection classification 195
Figure 6.9: Deflected shape of frame 197
Figure 6.10: load-rotation curves of connection in the frame with Conn-1 (the black dash line represents the yield limit of connection and black dots line represent the rotation capacity of connection) 198
Figure 6.11: load-rotation curves of connection in the frame with Conn-2 ((the black dash line represents the yield limit of connection and black dots line represent the rotation capacity of connection) 198
Figure 6.12: load-displacement curve of frame 200
Figure 6.13: Moment-Rotation of connection in the frame 201

Figure 6.14: Frame displacement-connection rotation curve.....201
Figure 6.15: Instant frame ductility-Instant connection ductility relationship.....202
Figure 7.1: Semi-rigid beam with a general load system.....
Figure 7.2: Example 1.....
Figure 7.3: Natural frequency for beams of uniform mass with different boundary conditions.....214
Figure 7.4: Effective length factor [ABAQUS results].....214
Figure 8.1: Plots of normalized fundamental Natural Frequency versus the joint stiffness ratio. The variable *I* in the legend indicates the second moment of area of the beam cross-section.....223
Figure 8.2: Three-bay, six-storey steel frame 225
Figure 8.3: Natural frequencies from the proposed equation and ABAQUS for the rigid connection case. 227
Figure 8.4: Natural frequencies from the proposed equation and ABAQUS for the semi-rigid connection case.....229
Figure 8.5: Joint stiffness ratio versus the fundamental natural frequency of the steel frame shown in Figure 8.2 231
Figure 8.6: Joint stiffness ration versus the second natural frequencies of the steel frame shown in Figure 8.2.....231
Figure 8.7: Joint stiffness ration versus the third natural frequencies of the steel frame shown in Figure 8.2.....232
Figure 8.8: Effect of frame parameters on shear-flexural to total periods. 233
Figure 9.1: Steel frame with multi-degree of freedom.....
Figure 9.2: Simplified sub-frame used for lateral force analysis.....
Figure 9.3: First storey-fixed base .....
Figure 9.4: First storey-pinned base.....
Figure 9.5: Middle storey model.....
Figure 9.6: Top storey model.....
Figure 9.7: Hybrid beam element with connection springs attached.....
Figure 9.8: Layout of the steel frame.....250
Figure 9.9: Relationship between relative stiffness and fundamental natural period ...253
Figure 9.10: Relationship between relative stiffness and second natural period 254
Figure 9.11: Relationship between relative stiffness and third natural period.....254

Table of Tables

Table 3.1: Main parameters for a flush end-plate composite connection 53
Table 3.2: Properties of composite connections 69
Table 3.3: Summary results of all connections (M=262 kN-m) 73
Table 3.4: Properties of Cjs-1 composite connection 77
Table 3.5: Percentage of moment for the control components in composite connection 88
Table 3.6: Results of calculations 89
Table 3.7: Adapted procedures for parameters 91
Table 3.8: Comparison of predicted and experimental results 94
Table 3.9: Comparison of predicted and other methods 97
Table 4.1: Summary of results 114
Table 5.1: Practical range of properties 154
Table 6.1: Parameters of experimental test of composite connections 168
Table 6.2:Comparison of test and predicted results of moment resistance 179
Table 6.3: Comparison between the proposed and test results for rotation at yield 192
Table 6.4: Comparison between proposed and test results for rotation capacity 193
Table 7.1: Comparison of the results of the proposed procedure with those given by ABAQUS 213
Table 7.2: Comparison with ABAQUS software for different stiffnesses and loading 215
Table 8.1: Properties of the steel frame shown in Figure 8.2 225
Table 8.2: Result of natural frequencies from the proposed equation and ABAQUS modelling for the rigid connection case 227
Table 8.3: Result of natural frequencies from the proposed equation and ABAQUS modelling for the semi-rigid connection case. 229
Table 8.4: Comparisons of fundamental time period 230
Table 9.1: Properties of the steel frame shown in Figure 9.8 251
Table 9.2: Results of natural periods 252

Abstract

The concept of semi-rigid connection and steel-concrete composite action has been extensively researched in the past. However, they are not widely used in practice due to the lack of detailed information, not only about the advantages of the semi-rigid design philosophy, but also about the potential risks if its effect is not accounted for. The above considerations were the motivations in taking up this research.

Firstly, a numerical study to investigate the effect of connection stiffness on the natural frequency of semi-rigid frame was carried out using ABAQUS software. The results of this numerical study confirmed the necessity of incorporating this effect to get safe and economical design. Consequently, an analytical procedure for a beam with semi-rigid connections under gravity load was developed which overcomes the limitations of previously published procedures. The frequency of a steel beam was also calculated using effective length concept. Furthermore, two new analytical ‘‘hand’’ calculation methods to estimate the first three frequencies of a semi-rigid frame were developed. Both methods were developed by modifying or improving for existing methods in the literature for rigid-jointed plane steel frame to incorporate the effect of connection stiffness. Fist method is suitable only for a semi-rigid plane steel frame which has uniform properties along its height so as it can be modelled as equivalent flexural-shear cantilever beam. The proposed second method is suitable for non-uniform plane steel frame. Both the above methods can be extended to composite structure using the equivalent stiffness concept of composite beam. Moreover, examples of steel frame were used to demonstrate the application of the proposed analytical methods. It was shown that the proposed methods not only can predict the difference in frequency of rigid and semi-rigid frames, but they are also simple enough to be used in day-to-day design practices.

Secondly, as the stiffness of connection is essential in the calculation of natural frequency of a semi-rigid frame, a new simple mechanical component-based model was developed to determine the initial rotational stiffness of commonly used flush end-plate steel or composite connection incorporating the partial interaction effect. The traditional axial spring of shear connectors was replaced by rotational spring to make the model suitable to extending further than the linear region. A chart was developed to estimate the appropriate values of the secant stiffness and strength of a shear stud, since the empirical equations that researchers have used in the past can lead to unrealistic results in some cases.

Thirdly, a simplified model, which combined three components of a composite connection in one ‘‘lump’’ component (RCCS), was developed. It can be used in the finite element modelling of a composite connection to overcome the convergence problems associated with cracking of concrete and also it will reduce the computational time significantly with adequate accuracy. A new procedure to determine the number of ‘‘active’’ studs was developed. The relationship between the number of ‘‘active’’ shear studs and the maximum number of shear studs required for a full shear connection was derived.

Finally, the relationship between connection ductility and frame ductility was investigated. It was found that the moment resistance and ductility of connection affect significantly the whole behaviour of a frame. Consequently, a simple flowchart to predict the failure mode of a flush end-plate composite connection was developed. A procedure to estimate the moment resistance of a flush end-plate composite connection by modifying the existing procedures in the literature to incorporate the partial shear connection effect was proposed. Also, the proposed mechanical model was further extended using the appropriate post-linear values of its components in order to calculate the rotational ductility of a connection.

All the suggested procedures have been validated with the numerical results using ABAQUS, the results from other existing models and experimental tests in the literature where available.

Declaration

No portion of the work referred to in the thesis has been submitted in support of an application for another degree or qualification of this or any other university or other institute of learning.

Copyright Statement

i. The author of this thesis (including any appendices and/or schedules to this thesis) owns certain copyright or related rights in it (the "Copyright") and s/he has given The University of Manchester certain rights to use such Copyright, including for administrative purposes.

ii. Copies of this thesis, either in full or in extracts and whether in hard or electronic copy, may be made only in accordance with the Copyright, Designs and Patents Act 1988 (as amended) and regulations issued under it or, where appropriate, in accordance with licensing agreements which the University has from time to time. This page must form part of any such copies made.

iii. The ownership of certain Copyright, patents, designs, trademarks and other intellectual property (the "Intellectual Property") and any reproductions of copyright works in the thesis, for example graphs and tables ("Reproductions"), which may be described in this thesis, may not be owned by the author and may be owned by third parties. Such Intellectual Property and Reproductions cannot and must not be made available for use without the prior written permission of the owner(s) of the relevant Intellectual Property and/or Reproductions.

iv. Further information on the conditions under which disclosure, publication and commercialisation of this thesis, the Copyright and any Intellectual Property and/or Reproductions described in it may take place is available in the University IP Policy (see http://documents.manchester.ac.uk/DocuInfo.aspx?DocID=487), in any relevant Thesis restriction declarations deposited in the University Library, The University Library's regulations (see http://www.manchester.ac.uk/library/aboutus/regulations) and in The University's policy on Presentation of Theses

Acknowledgements

I wish to express my gratitude to my supervisor, Dr. Parthasarathi Mandal, for his professionalism in providing guidance and financial support in the course of completing my work.

My deepest appreciation goes to my wife (Uhood) and my daughters (Sara and Blsm) and sons (Mohamed and Ahmed) for their unconditional, endless love and care.

Notations

Symbol	Definition	Unit
A_b	Area of beam	mm^2
A_{bf}	Area of beam flange	mm^2
A_c	Area of column	mm^2
A_{cf}	Area of column flange	mm^2
A_{cj}	Cross-sectional area of the *j*-th column	mm^2
A_r	Area of reinforcing bars	mm^2
A_{sc}	Area of a stud	mm^2
A_{vc}	Shear area of the column	mm^2
b_{bf}	Breadth of beam flange	mm
b_{cf}	Width of column flange	mm
$b_{eff,cwc}$	Effective width of column web in compression	mm
c_j	Distance of the *j*-th column from the centroid of the column assembly	mm
d	Diameter of shear connector	mm
D_b	Distance from the top row of bolts to the centre of the compression zone	mm
d_{cw}	Width of column web	mm
$D_{i,j}$	Lateral stiffness of the *i*-th storey	N/mm
D_r	Distance from the reinforcement to the centre of the compression zone	mm
d_s	Distance between the centroid of the beam section and the centroid of the reinforcement	mm
E_c	Young's modulus of concrete	N/mm^2
E_m	Mean modulus of elasticity for the embedded reinforcement	N/mm^2
E_{RCC}	Modulus of elasticity of the (RCC) component	N/mm^2
E_s	Young's modulus of steel	N/mm^2
f	Frequency	1/sec
F_b	Tensile force of the top row of bolts	N
F_{base}	Design seismic base shear force	N
F_c	Force in the centre of the compression zone	N
$F_{c,bf,Rd}$	The resistance of beam flange in compression	N
$F_{c,cw,Rd}$	The resistance of column web in compression and buckling	N
$F_{c,t}$	Force of the concrete tension member	N
f_{ck}	Characteristic cylinder compressive strength of concrete	N/mm^2
f_{cm}	Mean compression strength of concrete	N/mm^2
f_{cr}	Crack strength of concrete	N/mm^2
f_{ctm}	Mean tensile strength of concrete	N/mm^2
f_p	Tensile strength of end plate	N/mm^2
F_r	Force in reinforcement	N
$f_{r,u}$	Ultimate strength of reinforcement	N/mm^2
$f_{r,y}$	Yield strength of reinforcement	N/mm^2

F_{RCC}	Force in the (RCC) component	N
F_{s}	Force acting on the studs	N
$F_{\mathrm{s,T}}$	Tensile force of a reinforced concrete uncracked member	N
$F_{sc,k}$	Characteristic resistance of the shear stud	N
$F_{sc,max}$	Ultimate shear strength of the shear stud	N
$F_{sc,\mathrm{y}}$	Yield force of shear connector	N
f_{u}	Ultimate tensile strength of shear stud	N/mm^2
$f_{\mathrm{y,cw}}$	Yield strength of column web	N/mm^2
G	Shear modulus	N/mm^2
h	Storey height	mm
H_b	Depth of the steel beam	mm
h_{c}	Depth of column	mm
h_{d}	Bending deflection height of the shear connector	mm
h_{sc}	Height of shear connector	mm
h_{sl}	Thickness of the concrete slab	mm
I	Second moment of area of the steel beam	mm^4
$\bar{I}_b$	Modified second moment of area of a beam	mm^4
J	Lowest integer number of shear studs for full shear connection	-
k	characteristic parameter account for the effect of axial rigidity	-
k_{b}	Stiffness of bolt	N/mm
k_{bfc}	Stiffness of bottom flange of beam in compression	N/mm
k_{bt}	Stiffness of top row bolts in tension.	N/mm
k_{bwt}	Stiffness of beam web in tension	N/mm
k_{c}	Stiffness of a group of components in series at the level of the centre of the compression	N/mm
k_{cfb}	Stiffness of column flange in bending	N/mm
k_{cwc}	Stiffness of column web in compression	N/mm
k_{cws}	Stiffness of column web panel in shear	N/mm
k_{cwt}	Stiffness of column web in tension	N/mm
k_{pb}	Stiffness of end-plate in bending	N/mm
k_{r}	Stiffness of reinforcement in the concrete slab.	N/mm
k_{RCC}	Stiffness of an (RCC) spring	N/mm
k_{s}	Stiffness of shear connection; Stiffness of connection spring	N/mm
$k_{\mathrm{s,p}}$	Plastic stiffness of shear connectors	N/mm
k_{sc}	Secant stiffness of one shear connector	N/mm
K_{slab}	Stiffness of composite slab in composite connection	N/mm
L_{b}	Length of the beam under hogging bending moment adjacent to the connection	mm
l_{bi}	Span of the beam in the *i*-th bay	mm
l_{r}	Effective length of bars	mm
l_{RCC}	Length of the (RCC) component	mm
L_{t}	Transmission length of crack	mm

m	Mass per unit length of beam	kg/mm
M_{F}	Fixed end moment in beam	N-mm
$M_{j,c}$	Moment of composite connection	N-mm
$M_{j,Rd}$	Moment resistance of connection	N-mm
$M_{j,s}$	Moment of bare steel connection	N-mm
$M_{\mathrm{j,sw}}$	Moment resistance of steelwork in composite connection	N-mm
$M_{\mathrm{j,y}}$	Yield moment of connection	N-mm
N_{act}	Number of active shear studs	-
N_{full}	Maximum number of shear studs for a full shear connection	-
N_{sc}	Number of studs in the hogging moment region	-
N_{spr}	Number of (RCC) springs in series between any two consecutive shear studs	-
p	Spacing between shear studs	mm
p_0	Distance between the column face and the first shear stud	mm
q	behaviour factor	-
R_{b}	Strength force of top row of bolts	N
R_{r}	Resistance of reinforcement	N
R_{s}	Resistance of shear connectors	N
$S_{\mathrm{d}}(T_1)$	The ordinate of the design spectrum at period, T_1	m/sec^2
$S_{j,c}$	Rotational stiffness of composite connection	N-mm/rad
$S_{j,s}$	Rotational stiffness of bare steel connection	N-mm/rad
$S_{\mathrm{j,sw}}$	Stiffness of steelwork in composite connection	N-mm/rad
s_{sc}	Slip of shear connector	mm
$s_{\mathrm{sc,c}}$	Slip capacity of shear connector	mm
$s_{\mathrm{sc,u}}$	Ultimate slip of shear connector	mm
t_{bf}	Thickness of beam flange	mm
t_{bw}	Thickness of beam web	mm
t_{cf}	Thickness of column flange	mm
t_{cw}	Thickness of column web	mm
t_{p}	Thickness of end plate	mm
V_i	Shear force in the *i*-th storey	N
w_{slab}	Width of concrete slab	mm
z	Lever arm between the compressive and the tensile area	mm
H	Height of building	m
I_{bi}	Second moment of area of the beam in the *i*-th bay	mm^4
I_{cj}	Second moment of area of the *j*-th column	mm^4
T	Time period	sec
T_{sf}	Time period of coupled shear-flexural vibration	sec
κ	Effective length factor	-
μ_f	Ductility of frame. and	-
μ_j	Rotational ductility of connection	-
β	Interaction parameter	-

Δ_b	Extension of the top row of bolts	mm
Δ_c	Extension of a group of components at the level of the centre of the compression	mm
Δ_r	Extension of reinforcement	mm
δ_{red}	Reduction in deflection	mm
Δ_s	Slip of shear connection	mm
Δ_u	Top horizontal displacement at ultimate load	mm
Δ_y	Top horizontal displacement at first yield	mm
$\Delta\varepsilon_{sr}$	Increase of embedded reinforcement strain in the cracking state	-
ε_{cr}	Crack strain of concrete	-
ε_{smu}	Ultimate strain for embedded reinforcement	-
ε_{smy}	Yield strain for embedded reinforcement	-
ε_{su}	Ultimate strain of bare reinforcement	-
ε_{sy}	Yield strain of bare reinforcement	-
η	Degree of shear connection	-
κ	shape factor	-
λ	Correction factor that depends on T_1 and number of storeys; Eigenvalue of the free shear flexural vibration of a prismatic cantilever	-
ν	Poisson's ratio	-
τ_{sm}	Average bond stress along the transmission length	N/mm^2
φ_{comp}	Rotation due to the deformation of connection's components	mrad
φ_{sh}	Rotation due to shear panel of column web	mrad
ω	Angular frequency	rad/sec
α	Parameter account for the effect of flexural and shear rigidity of the assumed cantilever	$1/mm^2$
$\phi_{j,c}$	Rotation capacity of connection	mrad
$\phi_{j,ult}$	Rotation of connection at ultimate	mrad
$\phi_{j,y}$	Rotation of connection at yield	mrad
η_u	Shear connection ratio based on the ultimate strength of reinforcement	-
η_y	Shear connection ratio based on the yield strength of reinforcement	-
λ_f	Eigenvalue of purely flexural vibration	-
λ_{sf}	Eigenvalue of coupled shear-flexural vibration	-
ρ	reinforcement ratio	-
$\sigma_{c,t}$	Stress of the concrete in tension member	N/mm^2
σ_r	Stress of the reinforcement in tension member	N/mm^2

Publications

1. H. Al-Aasam and P. Mandal. A simplified procedure to calculate by hand the natural periods of semi-rigid steel frames. Journal of Structural Engineering, ASCE. 2012; DOI:10.1061/(ASCE)ST.1943-541X.0000695
2. H. Al-Aasam and P. Mandal. An approximate analytical method for calculating the natural periods of unbraced steel frames with semi-rigid connections. The first International Congress on Advances in Structural Engineering and Mechanics. *September 18-22, 2011, Sheraton Walkerhill Hotel, Seoul, Korea*
3. H. Al-Aasam and P. Mandal. Mechanical model for predicting the rotational stiffness of a flush end-plate composite connection incorporating the effect of partial interaction. To be submitted to Journal of Structural Engineering, ASCE.
4. H. Al-Aasam and P. Mandal. Stiffness of a Reinforced Concrete Slab in a Composite Connection. To be submitted to Engineering Structural Journal.
5. H. Al-Aasam and P. Mandal. Ductility of flush-end-plate composite connection. To be submitted to Engineering Structural Journal.
6. H. Al-Aasam and P. Mandal. Analysis of a beam with semi-rigid connections under gravity loading. To be submitted to Journal of Structural Engineering, ASCE.

Chapter One

Introduction

1.1. Introduction

Traditionally, the methods of analysis and design of steel and composite structures idealised the actual behaviour of beam-to-column connections into two simplified extreme cases: "perfectly rigid" or "ideally pinned". The ‘‘perfectly rigid’’ condition implies complete displacement and slope continuity between the column and the beam under all conditions of loading, whereas the "ideally pinned" condition implies that the rotation continuity is non-existent and almost free rotational movement occurs between the connected elements. Experimental investigations have clearly demonstrated that real connections have characteristics that fall between these simplified extremes. Thus, most of the practical connections of frame structures can be considered as semi-rigid connection, as shown in Figure 1.1.

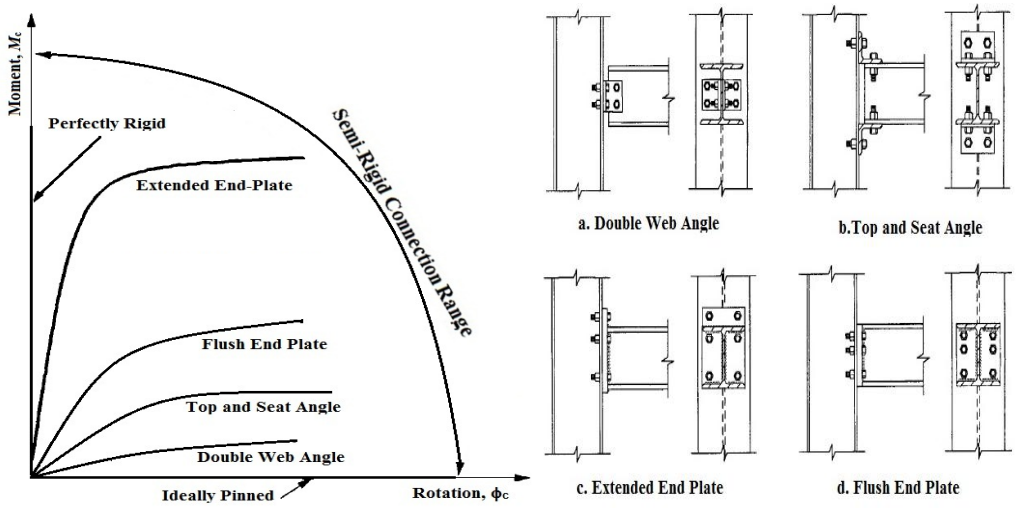

Figure 1.1: Types of connection and its moment- rotation curves (Chan and Chui,2000)

In addition, the classification of a connection as rigid, semi-rigid and nominally pinned depends essentially on the flexural stiffness of the steel beam connected to its end. This means that a certain connection may be considered rigid when connected to a steel beam with low flexural stiffness (EI_b/L_b). However, the same connection may be considered semi-rigid or even nominally pinned when connected to a steel beam with double the flexural stiffness or more. Consequently, Eurocode 3 (2005) §5.2 and

Eurocode 4 (2004) §8.2 use two procedures to classify pure steel and composite connections. Firstly, the connection may be classified as rigid, semi-rigid or nominally pinned by comparing its stiffness with the flexural stiffness of the beam (EI_b/L_b) with which it connects. Secondly, the connection may be classified as full-strength, partial strength or nominally pinned by comparing the connection design moment resistance ($M_{j,Rd}$) with the fully plastic moment (M_p) of the member adjacent to the connection. Figure 1.2 and Figure 1.3 show the classification of four types of connection when connected to two different sections of steel beam (i.e. UB 610x305x176 and UB 127x76x13). It is clear from these figures that the same connections can be considered nominally pinned when they are connected to the beam with high flexural stiffness. However, the connections are considered rigid or semi-rigid when they are connected to the beam with low flexural stiffness. These figures also show the boundaries of each category as adopted by Eurocode 3 (2005) §5.2 classification.

In summary, the category of a connection may change from rigid to semi-rigid or even to a nominally pinned connection as the flexural stiffness of the connecting steel beam increases.

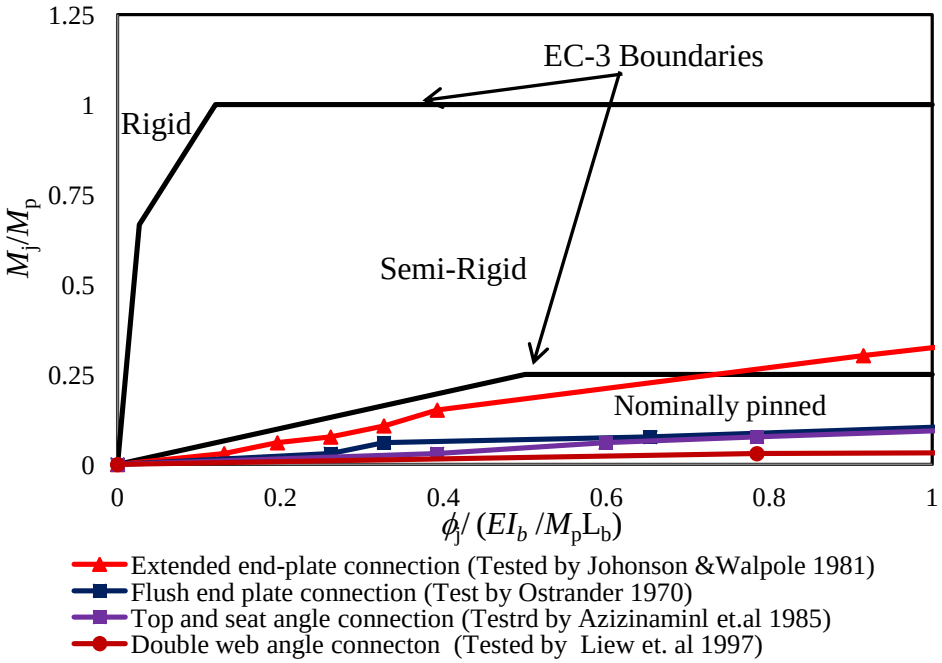

Figure 1.2: Examples of connections connected to beam UB 610x305x176 and Eurocode 3 boundaries

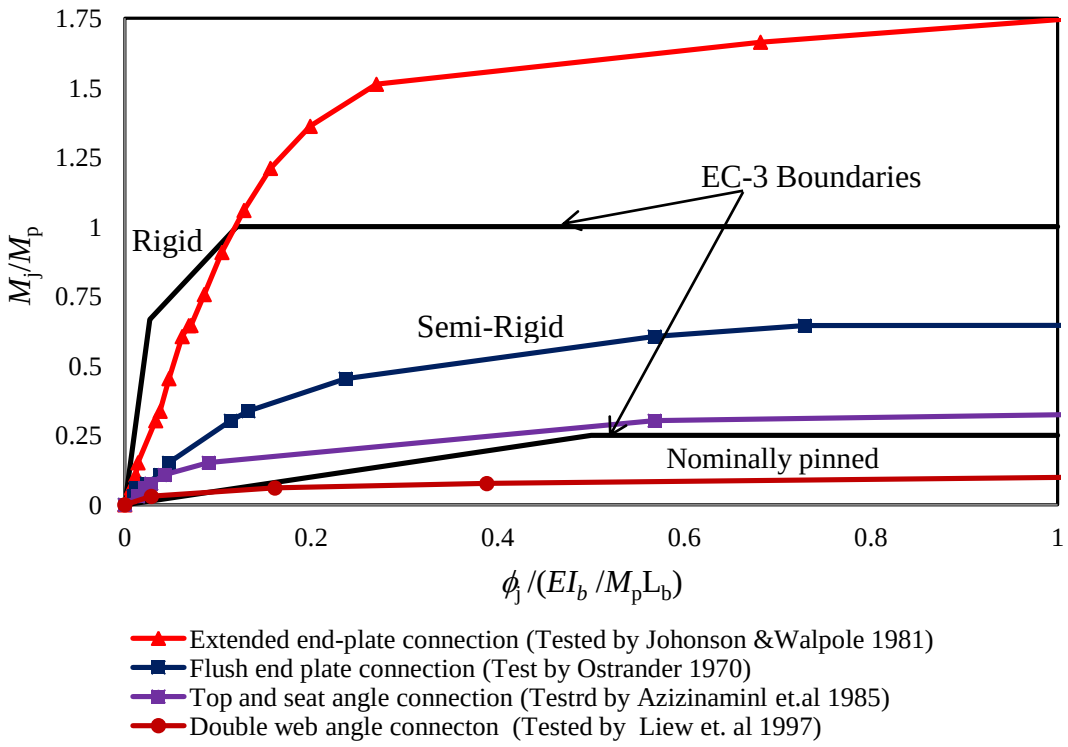

Figure 1.3: Examples of connections connected to beam UB 127x76x13 and Eurocode 3 boundaries

Modern structures use composite members for greater performance under normal service loading as well as extreme loadings such as blast, impact, fire and earthquakes. In these structures, the composite action between the steel beam and the concrete slab intensifies the importance of the semi-rigid concept, since the resultant composite beam has high stiffness compared with the bare steel beam. Consequently, high beam stiffness lead to consider the most types of connection which connect to it as semi-rigid or partial strength connection as discussed above.

Although the assumption of "perfectly rigid" or "ideally pinned" connection behaviour greatly simplifies the structural analysis and design procedures, this assumption could result in unconservative predictions of structural response. The flexibility of connections significantly affect the internal force distributions and lateral displacement magnitudes in the beams and columns of a structure. Both effects can influence structural instability and collapse modes, as they are functions of the connection flexibility.

Recently, the influence of semi-rigid connections on the realistic response of steel and composite structures has been recognized, and a provision for semi-rigid joints has been given in several national design codes. Therefore, an understanding of typical

connection behaviour under load is essential for the analysis of flexibly-connected frames.

A number of researchers have explored the performance of semi-rigid steel and composite connections under static and cyclic loadings (Azizinamini and James, 1989; Nader and Astaneh, 1991; Vellascoa et al., 2006; Cabrero and Bayo, 2007). The main conclusions from these studies are:

1. The semi-rigid approach normally results in *greater efficiency, lightness and economy* of structures;
2. The flexible and semi-rigid structures have considerable potential for resisting earthquake loading;
3. Connection flexibility and hysteresis are considered to be a significant source of damping of vibration in low-mass structures;
4. It is possible to adjust the flexibility of connections in order to control collapse mode and *the absorption capacity* of energy of frames during earthquakes; and
5. The semi-rigid frames have the advantage of a longer period and might attract lower inertial loads due to seismic ground motions.

Although the benefits of semi-rigid connections are widely documented, the semi-rigid connection design is still facing resistance from structural engineers. Reasons for this include:

1. The complexities and uncertainties in predicting connection behaviour with simple analytical models to make it suitable for practical use;
2. The lack of appropriate models, tools and design methods which incorporates the effect of semi-rigid connections in an adequate and simple way so as to bring this into everyday design-practice; and
3. The lack of detailed information, not only about the advantages of the semi-rigid design philosophy, but also about the potential risks if its effect is not accounted for.

Therefore, the first part of this research (Chapters Three, Four, Five and Six) deals with isolated connection behaviour in order to develop new simple yet accurate models and procedures to predict the main features of steel and composite connection

behaviour: (i) initial rotational stiffness; (ii) moment capacity; (iii) rotation at yield and rotation capacity to overcome the barrier described in Point 1 above.

The second part of this research (Chapter Seven, Eight and Nine) investigate the effect of semi-rigid connection on the behaviour of an isolated steel beam and a frame with semi-rigid connections. Firstly, the significant effect of a semi-rigid connection on deflection, shear forces, bending moment and frequency of an isolated beam with semi-rigid connections at its ends is presented. Secondly, the effect of a semi-rigid connection on the seismic behaviour of semi-rigid steel frame is investigated. New procedures to incorporate the effect of a semi-rigid connection in an adequate and simple way in the behaviour of a semi-rigid beam and frame are developed in order to overcome the difficulties identified in Points 2 and 3 above.

Thus, this research will cover both the behaviour of an isolated connection and the overall behaviour of semi-rigid structures.

1.2. Research objectives

The accuracy and reliability of an analysis or design depends on the degree of approximation of the model to the actual behaviour of a connection under loading. Rotational stiffness (S_j), moment capacity ($M_{j,Rd}$) and rotational ductility ($\mu=\phi_c/\phi_y$) are the key parameters for the behaviour of steel and composite connections, as shown in Figure 1.4.

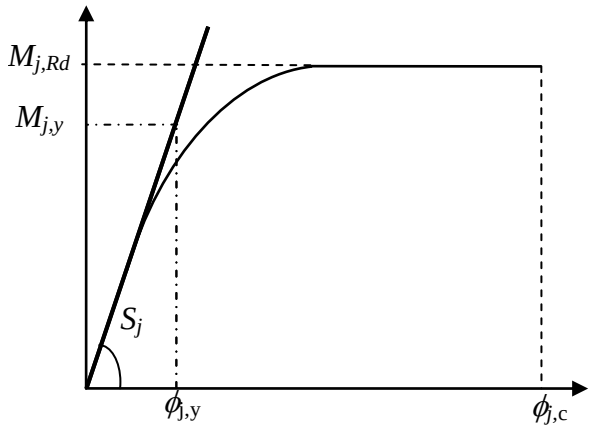

Figure 1.4: Typical moment–rotation curve of a connection

As explained above, depending on the first parameter (i.e. rotational stiffness), (Eurocode 4, 2004; Eurocode 3, 2005) classify the connections into three categories: rigid, semi-rigid and nominally pinned connections. In the same way, connections are

classified as: full strength, partial strength and nominally pinned connections in terms of the second parameter (i.e. moment capacity).

Even though the rotational ductility of a connection (μ_j) has a significant effect on the behaviour of steel and composite structures under extreme loading such as an earthquake, there is no quantification of ductility available in the literature. The design codes assume that a certain level of ductility will be achieved if the prescribed detailing rules are followed. However, this does not cover all of the connection types that are in use. Moreover, there is no direct link between the element ductility and the overall frame ductility. The lack of detail arises due to the difficulty in estimating the ductility of composite connections, which has been attempted for flush end-plate connections in the current research.

Therefore, to achieve the general aims of this research, the following specific objectives are identified:

1. Investigate, through literature, the key variables and different approaches to predict the behaviour of semi-rigid steel and composite connections. Review of the analytical and numerical models in the literature and identification of the key components of a connection;

2. Develop a simple mechanical component-based model to calculate the rotational stiffness of a flush end-plate composite connection, as this connection is a common semi-rigid connection. The model should be general for use with pure steel and composite connections, suitable for calculation by hand and with the possibility of incorporating it into any finite element software;

3. Develop a practical chart to estimate the stiffness and strength of a stud shear-connector in relation to the strength of the surrounding concrete and the diameter of the stud;

4. Develop a simple model to predict the load-slip behaviour of a stud shear-connector based on the experimental and numerical results from the literature for strength, stiffness and slip capacity;

5. Develop a new model and derive the associated expression to evaluate the behaviour of a reinforced concrete composite slab (RCCS) as one ‘‘lump’’ component;

6. Derive an expression to estimate the active number of a stud shear-connectors in the shear span of a composite connection;

7. Develop a flowchart to estimate the failure mode of a composite connection;

8. Develop a simple procedure to predict the moment capacity of a flush end-plate composite connection;

9. Develop a simple procedure to predict the rotation at yield and rotation capacity of a flush end-plate composite connection;

10. Propose a new procedure to calculate deflection, shear forces and bending moment of a steel beam with semi-rigid connections under a general loading condition. It should also possible to use the procedure to compute the deflection of a composite steel-concrete member after making some modifications for beam stiffness;

11. Modify the existing formulae in the literature for rigid plane steel frames to incorporate the effect of a semi-rigid connection in the natural periods of semi-rigid steel frames, which can be calculated by hand. In addition, conduct a parametric study to quantify the effects of semi-rigid connections on the natural periods of vibration of plane steel frames; and

12. Improve the original equations of the well-known Muto's method by introducing new factors to take into account: inflection point position, boundary conditions and deflection of an adjacent unloaded upper storey. Subsequently, construct a simple "hand'' procedure in order to determine the first three natural periods of unbraced steel frame with rigid or semi-rigid connections.

1.3. Outline of the thesis

The main contents are divided into the following ten chapters, and the logical links among them are illustrated in a flowchart shown in Figure 1.5.

Chapter One provides a brief introduction to the research background, objectives and the outline of the thesis.

Chapter Two provides a literature review on the benefit of semi-rigid concept in the design of structures. Notable experimental tests and analytical approaches in the literature are also reviewed and the key components of a connection are identified.

In **Chapter Three,** a simple mechanical component model to calculate the rotational stiffness of a composite connection is developed. The effect of each component is well studied and modelled. The traditional axial spring is replaced by a simple rotational spring to account for the actual rotation of a concrete slab under loading and to make this simple model general enough to be used for steelwork and composite connections. The validity of the model is evaluated by comparing it with the results from other existing models and experimental results.

Chapter Four presents a practical chart to evaluate the stiffness and strength of shear connectors with different diameters and for different strengths of concrete.

In **Chapter Five** a "lump'' component model of reinforced concrete composite slab (RCCS) is presented. An analytical expression for the initial stiffness of the "lump'' component is derived. The validity of the result from the proposed expression has been verified by finite element analysis using ABAQUS software.

Chapter Six presents the proposed flowchart to predict the failure mode of composite connections. In addition, the proposed procedures to estimate the moment resistance, rotation at yield and rotation capacity of composite connections are presented. The validity of these procedures is evaluated by comparing them with the results from other existing models and experimental results.

Chapter Seven presents an analytical procedure for a beam with semi-rigid connections under gravity load. The proposed procedure is based on the principle of superposition. It overcomes the limitations of previously published procedures. The accuracy of the proposed procedure has been verified by finite element analysis using ABAQUS software.

Chapter Eight presents the development of simplified formulae to calculate by hand the natural periods of semi-rigid steel frames. The proposed formulae have been developed by modifying of existing formulae in the literature for rigid-jointed plane steel frames. The accuracy of these approximate formulae has been verified by ABAQUS. Finally, a parametric study has been conducted to quantify the effects of semi-rigid connections on the natural periods of vibration of plane steel frames.

In **Chapter Nine** an approximate analytical method for calculating the natural periods of unbraced steel frames with semi-rigid connections is presented. The original equations of the well-known Muto's method are firstly improved by introducing new

factors. The improved equations are then combined with the conventional matrix method of vibration to construct a simple "hand'' procedure to determine the first three natural periods of a structure. The accuracy and sensitivity of the approximate procedure has been validated by finite element analysis of semi-rigidly jointed steel frames using ABAQUS.

Chapter Ten presents the conclusions of this study and recommendations for future work.

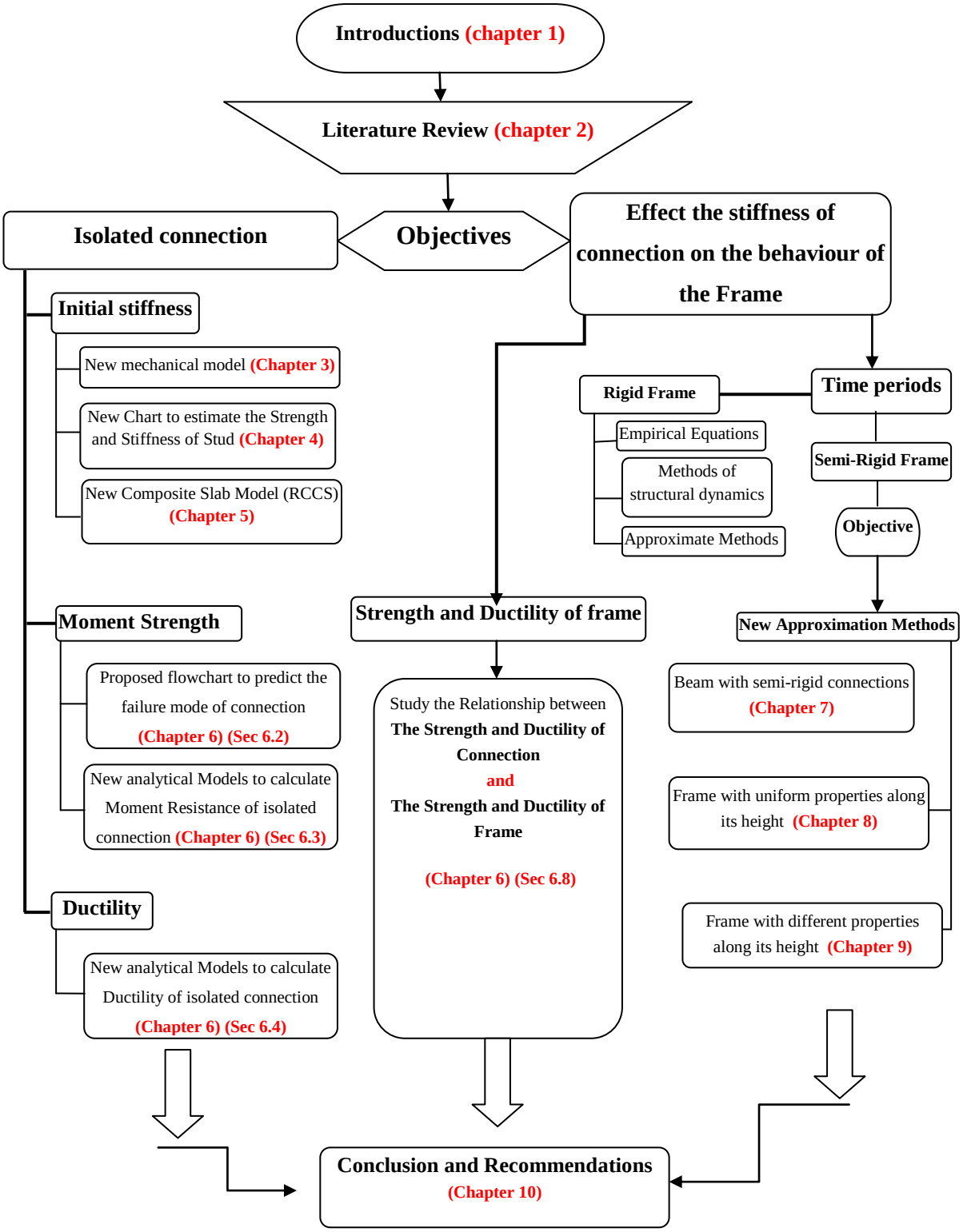

Figure 1.5: Logical relationship among the main chapters

Chapter Two

Literature review

2.1. Introduction

This chapter will give a brief overview of the experimental and numerical work recorded in the literature to investigate the behaviour of isolated semi-rigid steel and composite connections, as well as their effects on the behaviour of a structure with semi-rigid connections.

In current research, analytical models have been proposed to predict the behaviour of isolated semi-rigid connections, as well as to estimate the effect of a semi-rigid connection on the natural frequency of frames. Therefore, in this chapter, only the main features of experimental, numerical and analytical work will be briefly reviewed and discussed. A more specific literature review that clarifies the limitations of the available models and procedures will be provided in the relevant chapters.

2.2. Semi-rigid concept

In 1917, Wilson and Moore first performed experimental tests on the flexibility of riveted connections in steel structures. Since then, many experimental and numerical works have been carried out and various design methods have been proposed to incorporate the semi-rigid concept. Nevertheless, these methods did not gain much consideration because of the lengthy computational process involved when assuming semi-rigid behaviour.

In 1970, a semi-rigid composite connection was first proposed by Barnard. He continued some of the slab reinforcement across the column with enough shear studs to ensure full composite connection. Since then, extensive research has been carried out to investigate the behaviour of isolated semi-rigid composite connections and the effect of a composite connection on the behaviour of composite structures. Figure 2.1 shows an example of a semi-rigid composite connection.

The semi-rigid action in structural engineering has received much attention only during the past 20 years. The advancement of computer technology and the availability of low-cost and high-performance personal computers, together with the substantial increase in structural design knowledge, have increased awareness of the need to

include connection flexibility in the analysis and design of steel and composite structures.

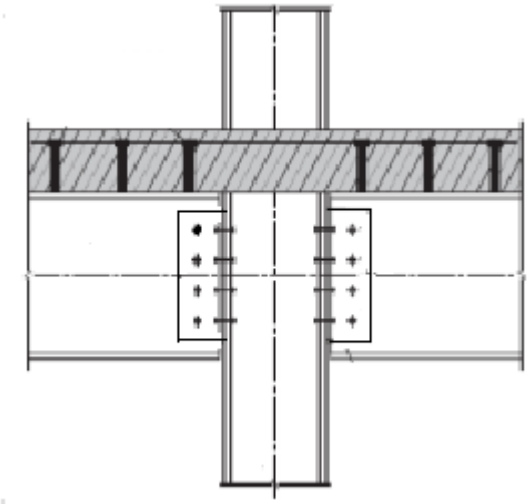

Figure 2.1: Example of a semi-rigid composite connection

2.3. Main approaches to investigate the behaviour of isolated connection

The behaviour of steel and composite structures is highly influenced by the moment-rotation characteristics of its beam-to-column connections. The moment-rotation relationship is nonlinear over the entire range of loading. The rotational stiffness (S_j), moment capacity ($M_{j,Rd}$) and rotational ductility ($\mu_j=\phi_{j,c}/\phi_{j,y}$) are the key parameters for the behaviour of composite connection, as was shown in Figure 1.4.

It is well known that the experimental test is the best way to determine the actual moment-rotation curve of any connection. However, this is very expensive and requires a great amount of time, as well as may be impractical in some cases. Nevertheless, in some cases (i.e. very important and large structures), the experimental phase is essential for the complete investigation of any structural system. Furthermore, experimental investigation plays a central role in academic studies. On the other hand, the advancement of computer technology, together with the substantial development of analytical approaches to predict the moment-rotation behaviour of a connection, makes it a potential alternative to extensive experimental tests.

Various analytical approaches exist in the literature to predict the behaviour of semi-rigid connection. These approaches can be classified into three main categories:

I. Mathematical models based on curve fitting to the available test results,

II. 2D and 3D finite element models and

III. Component-based mechanical models.

2.3.1. Mathematical models

These global models fit a skeleton curve through the experimentally obtained key parameters (i.e. initial stiffness, moment capacity, post-hardening stiffness and rotation capacity), which represent the full moment-rotation response of the connection.

Several arithmetic expressions have been proposed to fit the moment-rotation curves from the experimental data, such as linear, bilinear, tri-linear, power, the Ramberg-Osgood, the Richard-Abbott, exponential and polynomial functions. Some researchers, such as (Kishi and Chen, 1986), collected the available moment-rotation experimental data, published from 1936 up to 1986 on riveted, bolted and welded connections, and constructed steel connection data banks at the Purdue university computer centre. These models are generally not recommended for a semi-rigid composite connection, as sufficient data on this type of connection were not available. Moreover, the mode of failure of a connection may change when the connection detailing, beam and column sizes are significantly different from the available calibration experiments. Consequently, the prediction of the connection behaviour may differ substantially from its actual behaviour.

2.3.2. 2D and 3D finite element models

Another way to model the behaviour of a connection is by means of finite element idealisation. Much work had been carried out in this category. Most of them were associated with experimental test which was used to calibrate the finite element models. Only notable examples are explained here to demonstrate the main feature of this type of modelling.

Ahmed et al. (1996) used ABAQUS software to generate a numerical 3D finite element model to simulate the response of semi-rigid steel and composite connections. One bare steel and three composite flush end-plate connections, tested by (Li et al., 1996), were used to calibrate the finite element models. Due the symmetry of all of the

connections, only one side of the connection was modelled in order to reduce the size of the model. The beam, column and the end-plate were modelled using shell elements. Interaction elements were used to model the contact between the end-plate and the column flange. Bolts were modelled by joint elements. The load was applied equally on ten nodes of the beam web to overcome the local yielding problem. Since the tension-stiffening effect was not included in the concrete material model, the solution did not proceed as the concrete slab started to crack. To solve this problem, concrete was ignored in the model and multi-point constraints were used in the stud sections to transfer the tensile force to the reinforcement. Studs and the reinforcement were modelled by beam and truss elements respectively. The slip between the slab and beam and the degree of shear interaction were modelled using joint elements.

Even though this procedure of modelling provided good agreement with the specific experimental test of full interaction composite connections, completely ignoring the concrete slab in the finite element model will limit its ability to investigate the actual behaviour of composite connections with a partial shear connection. Although the tension and compression strength of concrete may have a minor effect on the behaviour of a composite connection under hogging moment, the tension-stiffening action has a significant effect on the behaviour of reinforcement in the composite connection. This effect is augmented as the shear connection decreases.

Kattner and Crisinel (2000) developed a 2D finite element model to simulate the behaviour of a semi-rigid composite connection, as shown in Figure 2.2.

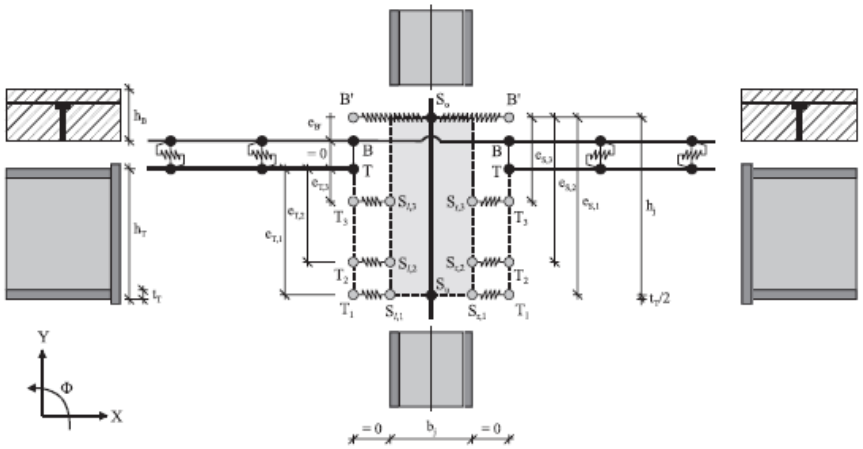

Figure 2.2: 2D finite element model for composite connection using DIANA software (Kattner and Crisinel, 2000)

The model consisted of beam elements representing the steel profile, concrete slab and steel column, and translational spring elements representing the shear connectors, steel connection and concrete slab-steel column flange interaction. The model was analysed with DIANA, a general purpose, commercial finite element system based on the displacement method. Comparisons of simulation and test results showed good agreement.

(Fu and Lam, 2006 ; Fu et al., 2007 ; Fu et al., 2008; Fu et al., 2010) examined the behaviour of eight full-scale, semi-rigid composite connections with precast hollow-core slabs (HCU), as shown in Figure 2.3. Different levels of shear connection, spacing and position of first studs from the column face were examined.

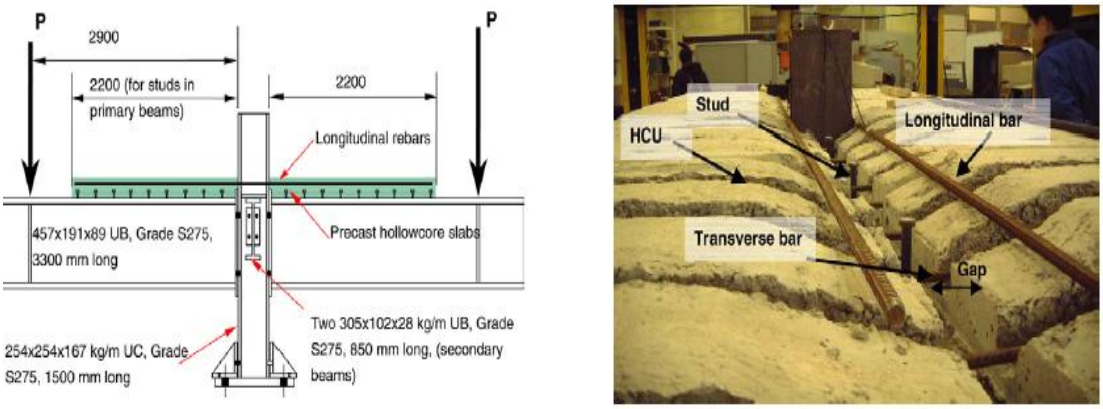

Figure 2.3: General arrangement of test set-up (Fu and Lam, 2006)

They built 3D finite element models using continuum elements with the ABAQUS package to simulate the structural behaviour of composite connections**,** as shown in Figure 2.4. The model also incorporated nonlinear material characteristics (see Figure 2.5).The same model was used to carry out parametric studies to investigate the structural behaviour with variations in size of the beam, thickness of the end-plate, thickness of the column web and the depth of precast hollow-core slab. The model could predict the mode of failure of all the tests and the moment–rotation response of the composite connections with minimal discrepancy.

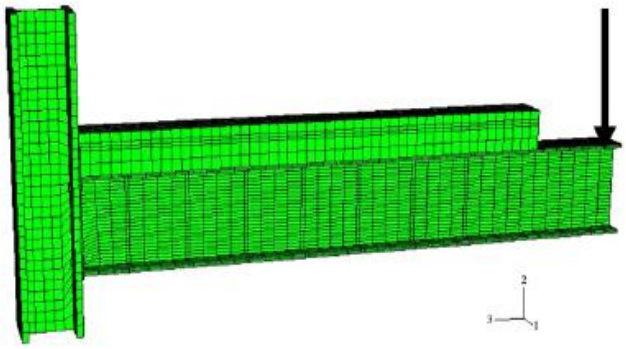

Figure 2.4: 3D finite element model of a composite connection using ABAQUS software and only part of slab was taken and ignored the tension-stiffening effect (Fu et al., 2007)

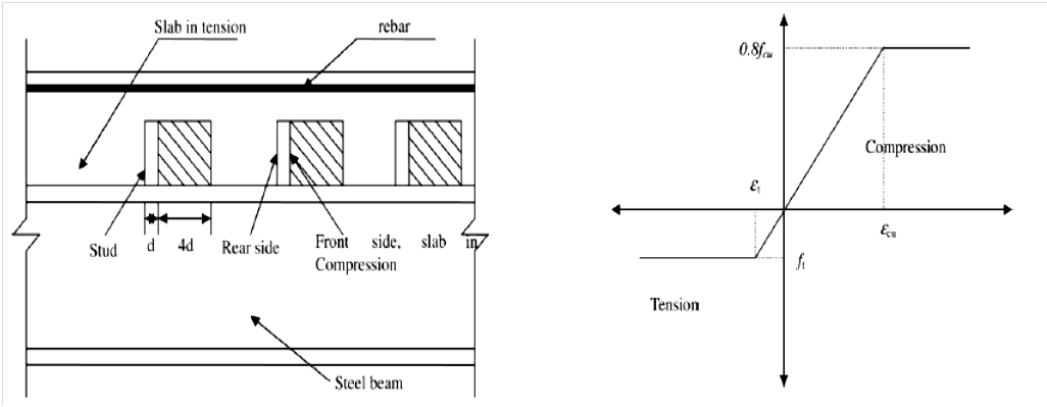

Figure 2.5: The composite connection model with material model of concrete (Fu et al, 2007)

Gil and Bayo (2008) carried out an experimental program to test internal and external semi-rigid composite connections, as shown in Figure 2.6. Three tests were performed on semi-rigid composite joints with flush end-plates. One of the tests dealt with an internal joint with asymmetrical loads, while the other two focused on external connections.

Figure 2.6: Example of experimental specimens (Gil and Bayo, 2008)

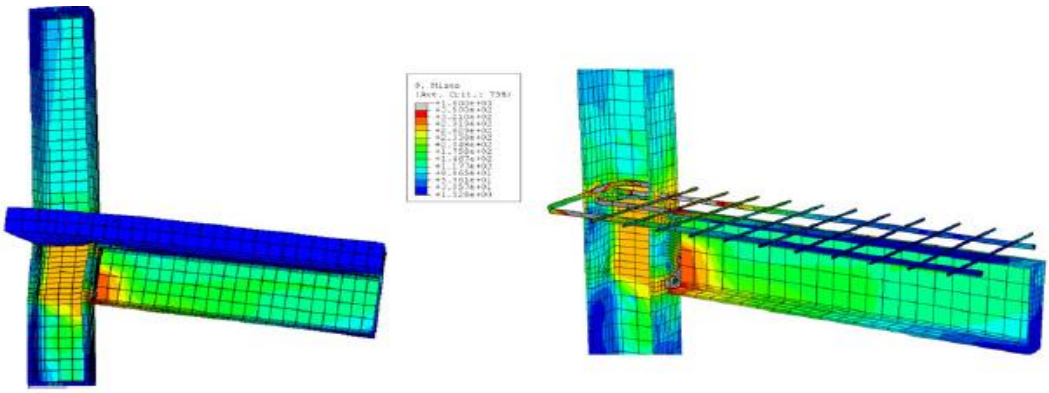

Figure 2.7: 3D Finite element model using ABAQUS software for internal and external connection incorporating the effect of tension-stiffening in concrete modelling (Gil and Bayo, 2008)

The experimental results were used to calibrate the finite element models. The ABAQUS finite element models show limitations in modelling the interactions between different types of elements and surfaces. Moreover, it was found that solution-processing of a finite element model is very sensitive to the chosen values of tension-stiffening in the concrete characteristics model. Improper values can cause conflict in the convergence.

Many other researchers have used 2D and 3D finite element modelling to investigate the behaviour of steel and composite connections, such as (Kattner and Crisinel, 1997; Queiroza et al., 2007; Titoum et al., 2008; Dabaon et al., 2009; Queiroz et al., 2009; Gizejowski et al., 2010).

In fact, some of the finite element models were able to predict the behaviour of semi-rigid composite connections accurately, i.e. the results were close to the experimental observations. A well-calibrated finite element model can reduce the number of experiments that needs to be carried out in order to understand certain behaviour in a parametric sense. However, the FE models incorporating semi-rigid connections require intensive computational effort and time which may be impractical for the analysis of large structures.

2.3.3. Component-based mechanical models

The mechanical models lie between the mathematical models and finite element models. The main feature of mechanical models is that they simplify the process of dealing with the complex behaviour of a connection. In addition, the degree of accuracy and applicability of this model without intensive computations compared with the detailed

finite element models make it the best practical tool to analyse a semi-rigid composite connection. Furthermore, it is the more realistic option from a perspective design.

The component-based method combines the analytical model of the individual connection's components to model the complex behaviour of connections using only the material and geometrical properties of these components. Equilibrium and compatibility requirements are used in its formulation without the very high computational effort required by the finite element method. The connection is modelled through a series of mechanical springs (components), as shown in Figure 2.8.

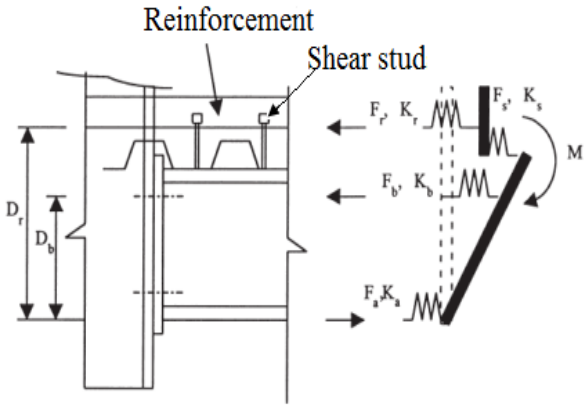

Figure 2.8: Example of mechanical model (Ahmed and Nethercot, 1997)

Every spring is modelled using the stiffness and strength of the associated component by a process of simple bilinear modelling with the aid of experimental evidence. Silva et al. (2002) also incorporated the ductility of each component in one such model.

The main outputs of a mechanical model are stiffness, moment capacity and rotational capacity of steel or composite connections.

A number of mechanical models exist in the literature. Most of them are adequate to simulate semi-rigid steel connections. Very few of the models are suitable for the simulation of semi-rigid composite connections. Furthermore, these models ignored or played down the effect of some of the important characteristics of semi-rigid composite connections, such as the slip between a concrete slab and steel beam in the case of partial shear interaction, the effect of the bond forces between concrete and the reinforcement between adjacent cracks and the effect of compression forces between the steel column and the concrete aligned to it.

The accuracy of any spring model not only depends on the number of component springs or procedures to find the equivalent spring for the whole composite connection,

but the results are also very sensitive to the stiffness of each individual spring. Therefore, an accurate model must be capable of representing not only the true relation between its components but also the stiffness of each effective parameter in the connection.

In Chapter Three, a literature review of notable mechanical models will be presented, as the main objective of that chapter is to develop a new mechanical model with a rotational spring to represent the shear connection effect. The proposed model may be used to calculate the rotational stiffness of bare steel and a composite flush end-plate connection. In Chapter Six, the same model will be used, with necessary modifications to calculate the moment resistance, rotation at yield and rotational capacity of a connection.

2.4. Main approaches to investigate the effect of a semi-rigid connection on the natural frequency of structure

As the second part of this research focuses on the effect of a semi-rigid connection on the whole behaviour of a steel beam (Chapter Seven) and on the natural frequency of a steel frame (Chapters Eight and Nine), this part of the literature briefly review the notable works in the literature in this field which confirm the necessity of considering the effect semi-rigid connection in the analysis or design of any structural system. A more specific literature review which critically analyses the available procedures will be provided in the relevant chapters.

2.4.1. Background

Recently, the influence of semi-rigid connections on the realistic response of steel and composite structures has been documented, and specification for semi-rigid connections has been given in several national design codes. Connection flexibility is the crucial source of non-linearity in the behaviour of structures under static and dynamic loading, and it plays an essential role in structure behaviour which is dominated by a deflection limit state, instability or vibration. Flexible connections affect significantly the deformations, stress distributions and dynamic responses of a structure. Moreover, connection flexibility and hysteresis are considered to be a significant source of damping for vibration in low-mass structures.

2.4.2. Beam with semi-rigid connections

Jones et al. (1983) demonstrated that the semi-rigid approach leads to smaller beam sizes and their rotational stiffness can be adjusted for an optimal distribution of the bending moments in the beams.

Nethercot et al. (1988) reviewed the effect of three cases of connection: fixed, semi-rigid and nominally pinned on the behaviour of a steel beam. The end moments are critical for the design of an isolated beam with fixed connections, whereas the span moment is critical for the design of a simply supported beam. However, the end and span moments may be nearly balanced for a beam with semi-rigid connections. Also, the elastic deflection is reduced by end fixity compared to the simply-supported condition. Columns are another source of economy, where the consideration of actual restraint conditions may lead to more reliable methods of design.

McGuire (1995) performed a NASTRAN normal modes analysis to the finite element model of steel beam with semi-rigid connections in order to calculate the minimum natural frequency of beam for various values of connection stiffness. It was found that the beam behaves as pinned-pinned beam when the connection stiffness ratio (i.e. $k_s/ (EI/L)_b$) is less than 1.0 and as fixed-fixed beam when the connection stiffness ratio is more than 100. Consequently, the beam behaves as semi-rigid beam for the connection stiffness ratio between 1.0 and 100.

Chan and Chui (2000) investigated the effect of changing the stiffness of end connections on the natural frequency of beams. It was found analytically that the change of the stiffness of connection has the significant effect on the natural frequency of beams and ignoring this effect may lead to significant error in vibration analysis of semi-rigid beams.

The above discussion clearly demonstrates the necessity of considering the semi-rigid concept in the design of a beam in order to develop a safe and economical design.

2.4.3. Frame with semi-rigid connections

In earthquake engineering, the estimation of the level of design seismic base shear force (F_{base}) of a structure requires the fundamental period to be determined in advance. Eurocode 8 (2004) §4.3.3.2.2.(1) presents the following expression to compute the seismic base shear force for multi-storey buildings which can be transformed into an

equivalent Single Degree of Freedom (SDOF) system using the procedure of (Eurocode 8, 2004)-Annex B:

$$F_{base} = S_d\left(T_1\right) m.\lambda \tag{2.1}$$

where S_d (T_1) is the ordinate of the design spectrum at period, T_1,

T_1 is the fundamental period of vibration,

m is the total mass of the building,

λ is a correction factor that depends on T_1 and number of storeys.

In addition, Eurocode 8 (2004) §3.2.2.5 states that the design spectrum ($S_d(T_1)$), which is the reduced spectrum to avoid inelastic structural analysis explicitly in design, accounts for the capacity of the structure to dissipate energy through its ductile behaviour. Three different expressions have been given in (Eurocode 8, 2004) §3.2.2.5.(4) to calculate the design spectrum for different ranges of fundamental period. These expressions relate the design spectrum to fundamental period and the behaviour factor (q). The behaviour factor is given for various materials and structural systems according to the relevant ductility classes of the structure.

It is clear from the above discussion that the natural period (or frequency) and ductility are the most important properties of a structure for seismic design.

2.4.3.1. Experimental works

Many tests are reported in the literature which has focused on the behaviour of semi-rigid frames. Since the behaviour of any structure under seismic loading is related to the combined effects of its ductility and natural period, the determination of these properties is one of the objectives of this research.

Gerstle (1988) carried out a numerical study to investigate the effects of the rotational stiffness of connections on the overall behaviour of unbraced frames. These effects were found to be in the following two categories: (i) the reduction in connection stiffness for a nominally rigid frame will increase the frame sway deformation under lateral loads, and will increase the natural period of vibration of the frame; (ii) the connection rotation will influence the distribution of the internal forces and moments in beams and columns. Therefore, ignoring the connection flexibility in analysis may lead to unrealistic predictions of stresses and deflections. Gerstle (1988) also investigated the effect of connection flexibility on the top storey sways of many frames with heights

ranging from 5 to 25 stories (3.6 m per storey) with (height/width) ratio ranging between 0.5 and 3. The results of the investigation indicated that the sway of a semi-rigid frame is about 40% over that predicted by assuming rigid-frame, and the sway for a nominally pinned-frame may exceed 100 to 200% of that of a rigid frame. Therefore, it was concluded that the share of connection rotation ranges from 1/3 to 2/3 of total sway. The result of the above study supports the previous conclusion for the necessity of considering the semi-rigid concept in design of frame structures under static or dynamic loading in order to get safe and economical design.

Nader and Astaneh (1991) investigated experimentally the effects of connection flexibility on the dynamic response of a single storey steel structure, as shown in Figure 2.9.

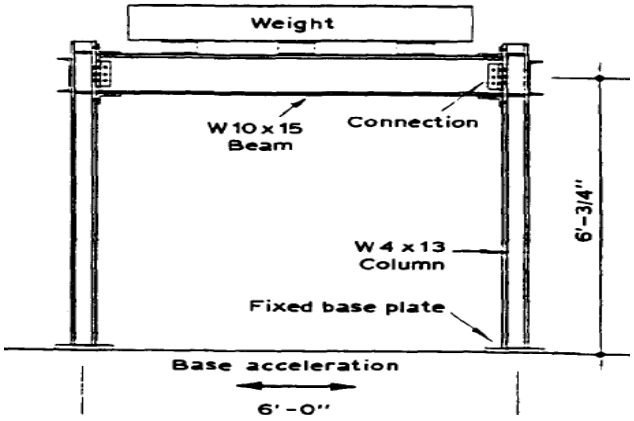

Figure 2.9: Test structure arrangement (Nader and Astaneh, 1991)

Three types of connection had been used: nominally pinned, semi-rigid and rigid connections. Each of these structures was subjected to three types of earthquake with maximum peak acceleration ranges between 0.05 g and 0.5 g. These types of earthquake were the 1940 El Centro S00E, the 1985 Mexico S60E and the 1952 Taft N21E.

From these tests, it was found that:

1. The response of the nominally pinned structure was considerably nonlinear. The rigid structure was almost elastic and the semi-rigid structure showed more inelastic hysteresis response, but with almost no degeneration in stiffness;

2. The maximum base shear in the rigid structure was about 2.5 times of the maximum base shear for the nominally pinned structure;

3. The maximum lateral drift in the nominally pinned structure was only 30% more than the maximum lateral drift in the rigid structure. The base shear and lateral drift

in the semi-rigid structure was in between the ranges for rigid and nominally pinned structures; and

4. The semi-rigid connection had 20% more rotation than the rigid connection, while its maximum moment was only 15% less than the maximum moment for the rigid case.

In summary, an increase in connection stiffness results in an increase in the base shear forces for the same ground motion, while the associated lateral drift did not decrease in the same proportion. This conclusion reveals that the rigid connection is not the optimal solution for dynamic loading, since the optimal design of a structure should ensure the lowest possible base shear forces associated with an acceptable amount of lateral deformations. The test structures with semi-rigid connections behaved well and had moderate base shear forces and yet they did not develop large lateral deformations.

Moreover, Nader and Astaneh (1991) found that the semi-rigid connections can dissipate the energy in hysteresis behaviour better than the other type of connections. This virtue may improve the dynamic performance of semi-rigid frames in low-rise buildings. Furthermore, the moment capacity of the semi-rigid connections was higher than expected. Based on these results, it was concluded that the semi-rigid structures have considerable potential for resisting earthquake loading. Further experimental and numerical work on the effect of semi-rigid connections on the seismic behaviour of structure was recommended; the aforementioned is one of the objectives of the current research.

Ohi and Hyoukchoi (2006) investigated the effect of semi-rigid connections on the dynamic behaviour of structures under earthquake. It was shown that it is possible to adjust the flexibility of connections in order to control the collapse mode and the energy absorption capacity of frames during earthquakes.

Several authors, such as (Azizinamini and James, 1989; Dhillon and Malley, 1999; da S. Vellasco et al., 2006; Ihaddoudène et al., 2009), studied the performance of semi-rigid steel beam-to-column connections under static and cyclic loadings. It was found that the use of semi-rigid connections for building frames will lead to potential economies by adjusting connection stiffness to achieve optimal distribution of the bending moments of the connected members.

All of the above numerical and experimental works confirm the potential effect of semi-rigid connection on the behaviour of structures under static and dynamic loading.

2.4.3.2. Approximate procedures

Since one of the objectives of this research is to develop new hand calculation procedures to estimate the natural frequency of structures with semi-rigid connections, only a brief review of some of these procedures documented in the literature is presented here. A more specific literature review which identifies the shortcomings of the available procedures will be provided in the relevant chapters.

Current seismic design codes provide empirical equations which relate the fundamental period to the height of the frame, and the code implicitly assumes that the contribution from higher modes of vibration is insignificant. These formulae are usually dependent on the building material, building type (frame, shear wall, etc.) and overall dimensions. These formulas take the form:

$$T = \alpha H^{\beta} \tag{2.2}$$

in which α and β are constants which depend on the building behaviour. In addition, there are many other empirical formulae in the literature which have the same general form as Eq. (2.2) but with different constants. None of these empirical formulae take into account the effect of connection behaviour on the behaviour of a frame.

Also, the design codes allow estimation of the fundamental natural period using more complex procedures, such as Rayleigh's method and computer-based eigenvalue analysis, which makes them impractical for many situations. Consequently, many researchers have investigated the applicability of using approximate hand calculation methods which have the merits of simplicity while maintaining the required degree of accuracy.

Goel and Chopra (1998) developed a formula to calculate the fundamental natural frequency of concrete shear wall building as equivalent cantilever beam using Dunkerley's method by calibrating a theoretical formula with the measured period data. This formula takes this form:

$$T = \frac{4\sqrt{\frac{m}{\kappa G}}}{\sqrt{\frac{A}{1+\frac{1}{1+\nu}\left(\frac{H}{D}\right)^2}}} H \tag{2.3}$$

in which m is the mass per unit height; G is the shear modulus; A is the cross-sectional area of the equivalent beam; ν is Poisson's ratio and κ is the shape factor (=0.8333 for rectangular sections) and D is the plan dimension of the cantilever in the direction in question.

Assuming the frame as equivalent shear-flexure cantilever beam, Chrysanthakopoulos et al. (2006) proposed a procedure to estimate the first three vibration periods. A plane frame which has uniform properties along its height was modelled as equivalent flexural-shear cantilever beam for which the analytical expression of its natural period has the form (Smith and Crowe, 1986; Chrysanthakopoulos et al., 2006):

$$T = \frac{2\pi}{\lambda^2}\sqrt{\frac{m}{EI}} \tag{2.4}$$

Where $$\lambda^4 = \frac{\omega^2 m}{EI}$$

in which m and EI are the approximate mass per meter and flexural rigidity of an equivalent uniform cantilever beam respectively. The ω is the circular natural frequency. Similar to the empirical equations, all of the approximate methods above assumed the beam-column connections as rigid, even though the period of a semi-rigid frame can be twice that of a rigid frame (Smith and Crowe, 1986).

In this research, two new approximate procedures have been developed, taking into account the effects of semi-rigid connections by modifying some of the previous methods in the literature.

Chapter Three

Mechanical model for predicting the rotational stiffness of a flush end-plate composite connection incorporating the effect of partial interaction

3.1. Introduction

The behaviour of a composite structure is highly influenced by the moment-rotation characteristics of beam-to-column connections. The rotational stiffness, ultimate moment and rotational capacity are key parameters in defining the aforementioned characteristics. Experiments, simplified analytical models, finite element models, and empirical equations based on existing experimental data are the main approaches to derive these parameters for a particular type of connection. Simplified models are the most realistic option from a design perspective.

A number of researchers in the past developed various simplified models to predict each of these parameters as closely to the experimental results as possible. These models may differ in form, but all of them are based on: spring models to estimate the equivalent rotational stiffness for the whole connection, a block model to estimate the ultimate moment, and the compatibility requirement in plastic range to predict the rotational capacity of the connection.

The rotational stiffness is more important than the other parameters, due to its use in classification of structures as rigid or semi-rigid. Rotational stiffness also plays a key role in the vibration design of composite structures. All simplified spring models have similar forms, but the springs vary in number; the number of springs represents the number of effective parameters in the composite connection. The accuracy of any spring model depends not only on the number of component springs or procedures to find the equivalent spring for the whole composite connection, but the results are also very sensitive to the stiffness of each individual spring. Therefore, an accurate model must be capable of representing not only the true relationship between its components but also the stiffness of each effective parameter in the connection.

In this work, a simple mechanical component model is developed. The effect of each component is well studied and modelled. The traditional axial spring which is used to model the effect of shear connectors is replaced by a simple rotational spring to account for the actual rotation of a concrete slab under loading and to make this simple model suitable for using with steelwork and composite connections, appropriate for modelling with any finite element software and able to extend further than the linear region with valid values for the stiffness of components, since it is based on the equilibrium and compatibility requirements. The theoretical basis of this model is also derived. Furthermore, a simple and effective procedure to evaluate the equivalent stiffness of the shear connection is developed. The validity of the model is evaluated by comparing the results with those recorded from other existing models and experimental tests.

3.2. Flush end-plate composite connection

Some of the common bolted composite connections that can be classified as semi-rigid or partial strength are double web cleat, flush end-plate, and top and seat angle. Figure 3.1 shows a typical flush end-plate composite connection.

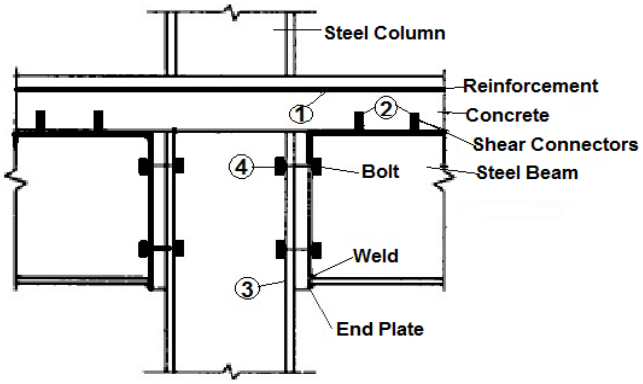

Figure 3.1: Typical flush end-plate composite connection

3.2.1. Why flush end-plate composite connection?

A Flush end-plate composite connection (Figure 3.1) was selected in this study for a number of reasons:

1. Due to economic factors and ease of construction, it is the most common choice in design (Loh et al., 2006);

2. Experimental tests carried out by (Nethercot, 1995) showed that flush end-plate connections generally provide the appropriate rotational stiffness and considerably greater levels of moment capacities than the other types of connections; and

3. The majority of the experimental work on composite connections published from 1989 to 2006 involves composite flush end-plate connections to I-beam sections connected with H-section columns, as presented in the literature survey carried out by (Loh et al., 2006). As the current research does not have an experimental component, data from the literature are vital to validate the analytical and numerical models.

3.2.2. Key parameters of a flush end-plate composite connection

The most effective parameters for the behaviour of a composite connection under symmetrical loading are the following (see Figure 3.1):

1. The stiffness and ductility of the reinforcement in the concrete slab.

2. The stiffness and ductility of the shear connectors.

3. The stiffness and ductility of the components in the level of the bottom flange of the beam (i.e. the column web in compression, bottom flange of the beam in compression, buckling strength of the column web and beam bottom flange if no stiffener of the column web is present in this level).

4. The stiffness and ductility of the components at the level of the top row of bolts. These components consist of the column web in tension, the column flange in bending, the beam web in tension, the end-plate in bending and the top row of bolts in tension.

If there is asymmetrical loading, the effect of shear deformation of the column panel zone should be taken into account. Table 3.1 lists the effective components and their symbols which are used in the calculation of the rotational stiffness of a flush end-plate composite connection. A typical model of a flush end-plate composite connection with its force distribution and deformation is shown in Figure 3.2.

Table 3.1: Main parameters for a flush end-plate composite connection

Component Stiffness	symbol
Reinforcement in the concrete slab.	k_r
single shear connecter	k_{sc}
shear connection	k_s
column web in compression	k_{cwc}
column web in tension	k_{cwt}
column flange in bending	k_{cfb}
bottom flange of beam in compression	k_{bfc}
beam web in tension	k_{bwt}
end-plate in bending	k_{pb}
top row bolts in tension.	k_{bt}

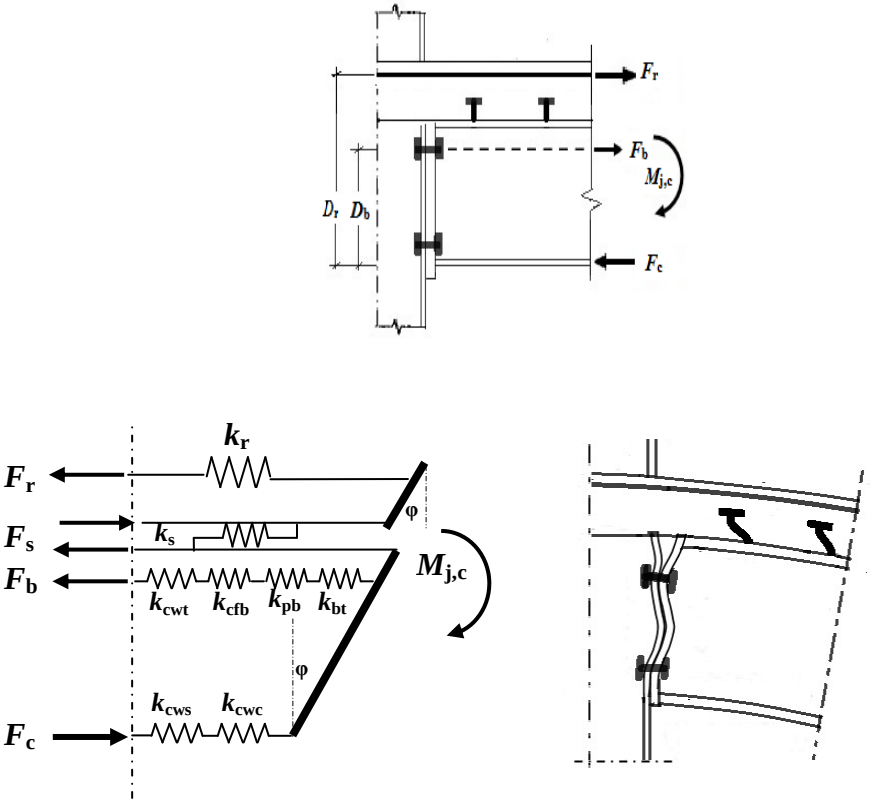

Figure 3.2: Typical model of a flush end-plate composite connection with its deformation

In reference to Figure 3.2 , the following points should be noted:

1. All forces and deformations shown in the figure are within the range of serviceability limit states.

2. F_r and F_s are the forces acting on the reinforcement and studs respectively.

3. F_b is the force acting on the top row of bolts, but k_b is the stiffness of a group of components in series at the level of top row of bolts.

4. F_c is the force in the centre of the compression and k_c is the stiffness of a group of components in series at the level of the centre of the compression (Eurocode 3, 2005) which are the column web in compression, k_{cwc}, and column web panel in shear, k_{cws} for the asymmetrical loading case.

3.3. Background

To date, various finite element and mechanical models have been developed and introduced to predict the rotational stiffness of beam-to-column connections. Most of them are applicable for pure steelwork connections and few of the models are applicable to predict the rotational stiffness of a composite connection. The mechanical models simplify the behaviour of the connection and approximate the response of the key elements. Furthermore, most of these models assume full interaction between the concrete slab and the steel beam, excluding the possibility of slip at the interface. Aribert (1996) carried out experimental tests and finite element numerical simulations on flush end-plate composite connections with different degrees of shear connection. Significant effect of interface slip was observed on the overall behaviour, even in the case of a full shear connection. Only a few models in the literature considered the slip when calculating the rotational stiffness.

3.3.1. Requirements of an "ideal model''

In order to investigate the advantages and limitations of the previous simplified mechanical models, the basic requirements of an "ideal model'' are described first. These are as follows:

1. It should be simple;

2. The model should be applicable to both composite and bare steel flush end-plate connections;

3. The actual behaviour of the composite connection should be considered;
4. The actual configuration of the composite connection after deformation should be reflected;
5. The derivation of mathematical expressions to calculate rotational stiffness should use all existing forces and moments in the configured model;
6. It should be possible to model it easily in any finite element software;
7. The results of the analytical expressions and finite element modelling of the mechanical model should be identical;
8. It should be able to extend further than the linear region, with valid values for the stiffness of the components, since it is based on the equilibrium and compatibility requirements; and
9. It should use appropriate procedure to estimate the stiffness of each component.

3.3.2. Significant models from the literature

Aribert and Lachal (1992) carried out eight tests on a flush end-plate composite connection in order to evaluate the effective components of a composite connection and to investigate the whole behaviour of a composite connection. Based on these tests, they derived expressions to calculate the rotational stiffness of the composite connection $S_{j,c}$ using a simple summation of the moment resistance of the steel connection $M_{j,s}$ and the moment resistance of concrete slab M_{slab} for the same rotation θ, as follows:

$$M_{j,c} = M_{j,s} + M_{slab} \rightarrow S_{j,c}\theta = S_{j,s}\theta + S_{slab}\theta \tag{3.1}$$

$$S_{j,c} = S_{j,s} + S_{slab} \rightarrow S_{j,c} = S_{j,s} + K_{slab}D_r^2 \tag{3.2}$$

The term K_{slab} accounts for the contribution of the reinforcement and shear studs to the rotational stiffness of the connection:

$$S_{j,c} = S_{j,s} + \frac{D_r^2}{\frac{1}{k_r} + \frac{\alpha}{N_{sc}k_{sc}}\left(\frac{D_r}{H_b}\right)} \tag{3.3}$$

where D_r is the distance from the reinforcement to the centre of the compression in the lower flange of the steel beam; H_b is the depth of the steel beam; N_{sc} and k_{sc} are the number and secant stiffness of the shear connector; α is the increase factor, taken as ≈2. This simple approach did not consider the additional increase in compressive force, F_c

(see Figure 3.2), which leads to an increase in tensile force of the top row of bolts, F_b The difference between the moment resistance of the bare steel connection, $M_{j,s}$, and the moment resistance of the steelwork in the composite connection, $M^*_{j,s}$, for the same rotation can be calculated as follows (see Figure 3.3):

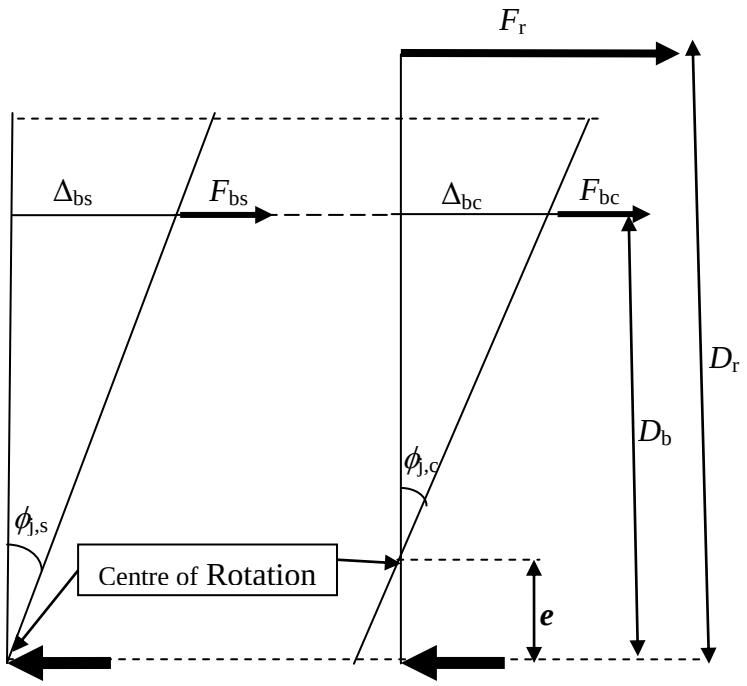

a) Bare steel connection b) Composite connection

Figure 3.3: Internal forces and deformation in bare steel and composite connections

$$\text{For} \quad \phi_s = \phi_{co} = \phi \rightarrow \frac{\Delta_{bs}}{D_b} = \frac{\Delta_{bc}}{D_b - e} \tag{3.4}$$

$$\frac{\Delta_{bs}}{\Delta_{bc}} = \frac{D_b}{D_b - e} \rightarrow \Delta_{bc} = \Delta_{bs} \frac{D_b - e}{D_b} \tag{3.5}$$

$$F_{bs} = k_b \Delta_{bs} \quad \& \quad F_{bc} = k_b \Delta_{bc} \rightarrow \Delta_{bs} = \frac{F_{bs}}{k_b} \quad \& \quad \Delta_{bc} = \frac{F_{bc}}{k_b} \tag{3.6}$$

where

Δ_{bs} is the deformation of a bolt in a bare steel connection
Δ_{bc} is the deformation of a bolt in a composite connection
F_{bs} is the force of a bolt in a bare steel connection
F_{bc} is the force of a bolt in a composite connection

Substituting Eq. (3.6) in Eq. (3.5):

$$\frac{F_{bc}}{k_b} = \frac{F_{bs}}{k_b}\frac{D_b - e}{D_b} \tag{3.7}$$

$$\therefore F_{bc} = F_{bs}\frac{D_b - e}{D_b} \tag{3.8}$$

$$\because M_{j,s}(\phi) = F_{bs}D_b \qquad \text{and} \qquad M_{j,c}(\phi) = F_{bc}D_b + F_rD_r \tag{3.9}$$

$$\therefore M_{j,c}(\phi) = F_{bs}\frac{D_b - e}{D_b}D_b + F_rD_r = F_{bs}D_b - F_{bs}e + F_rD_r \tag{3.10}$$

$$M_{j,c}(\phi) = \left[M_{j,s}(\phi) - F_{bs}e\right] + F_rD_r = M^*_{j,s}(\phi) + F_rD_r \tag{3.11}$$

$$\therefore M^*_{j,s}(\phi) = M_{j,s}(\phi) - F_{bs}e \tag{3.12}$$

The moment resistance of the bare steel connection ($M_{j,s}$) can only be equal to the moment resistance of the steelwork in a composite connection ($M^*_{j,s}$) if there is a very low reinforcement ratio or at a lower applied moment, i.e. $e \approx 0$.

Benussi and Noe (1994) proposed a simple spring model to predict the rotational stiffness of a partial-depth end-plate composite connection without taking into account the slip of the shear connectors.

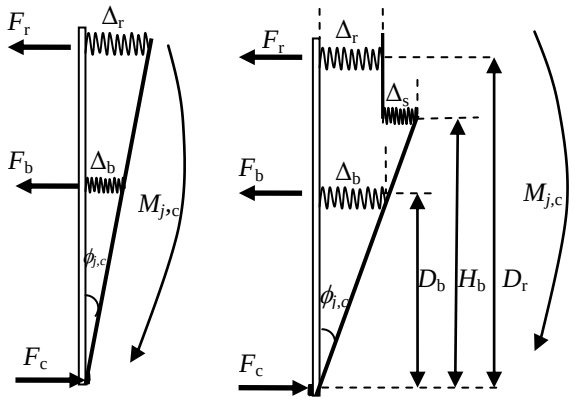

Figure 3.4: (a) Benussi and Noe's model (b) Anderson and Najafi's extended model

This model was extended to an end-plate composite connection incorporating the effect of the slip of the shear connectors by (Anderson and Najafi, 1994), as shown in Figure 3.4. They also performed four experimental tests on a flush end-plate composite connection in order to assess their model. In this model, the effect of the shear connectors was modelled as an axial spring at the level of the slab-beam interface, which has a stiffness of k_s. The components of the steelwork connection were modelled

as one spring at the top row of bolts level, D_b, with a stiffness of k_b, and assumed that the rotation of the connection is around the centre of the bottom beam flange. The concrete was assumed to be cracked. From the equilibrium and compatibility the following equation was derived to evaluate the rotational stiffness of the whole flush end-plate composite connection:

$$S_{j,c} = k_b D_b^2 + \frac{D_r H_b}{\frac{1}{k_r} + \frac{1}{k_s}} \tag{3.13}$$

The model did not consider the actual deformations of the compression components, as it was limited to a special case of stiffened column web, as in the experimental tests. Therefore, the stiffness of the column web, k_c, was assumed to be equal to infinity, which may have a finite value in many situations, even if the column web is stiffened. Also, the stiffness of the shear connectors, k_s, was calculated based on the assumption that the slip at the connection depends only on the nearest stud to the column; the stiffness of the shear connectors was therefore taken to be a constant value (200kN/mm) for all cases of the composite connection. In fact, a number of theoretical and experimental studies have shown that all shear connectors shared the longitudinal shear resistance in the interface between the concrete slab and the steel beam (Ahmed and Nethercot, 1996; Aribert and Dinga, 2000). In addition, the model did not reflect the actual configuration of the composite connection after deformation, as it used a vertical rigid bar to connect the axial studs' spring with the reinforcement's spring.

Ren and Crisinel (1996) proposed a simple mechanical model which reflected the actual configuration of the composite connection after deformation, as shown in Figure 3.5.

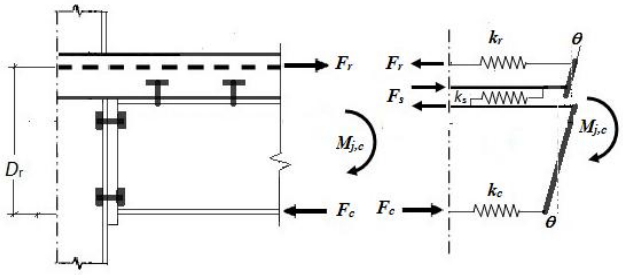

Figure 3.5: The spring model of (Ren and Crisinel 1995)

They incorporated the column web deformation at the level of the beam's bottom flange in the derivation of a formula to relate the moment applied to the composite connection

with its rotation. This formula can be used to calculate the rotational stiffness of the flush end-plate composite connection:

$$S_{j,c} = \frac{D_r^2}{\frac{1}{k_r} + \frac{1}{k_s} + \frac{1}{k_c}} \tag{3.14}$$

where D_r, k_r, k_s and k_c have the same definition as before. This derivation is based on the simple summation of the reinforcement and bare steel connection capacities to calculate the moment capacity of the composite connection. This simple approach did not consider the actual behaviour of the steelwork component in composite connection, as explained before in (Aribert and Lachal, 1992)'s model.

Ahmed and Nethercot (1997) developed a simple mechanical model which is the most common current model to predict the rotational stiffness of a flush end-plate composite connection, as shown in Figure 3.6. It also considered the increase in F_c and the effect of deformation of the compression zone. Based on this mechanical model, they derived mathematical expressions to calculate the rotational stiffness of a flush end-plate composite connection as follows:

$$S_{j,c} = \frac{H_b D_r \left(\frac{1}{k_b} + \frac{1}{k_c}\right) + D_b^2 \left(\frac{1}{k_r} + \frac{1}{k_s} + \frac{1}{k_c}\right) - D_b \left(H_b + D_r\right) \frac{1}{k_c}}{\left(\frac{1}{k_r} + \frac{1}{k_s} + \frac{1}{k_c}\right)\left(\frac{1}{k_b} + \frac{1}{k_c}\right) - \frac{1}{k_c^2}} \tag{3.15}$$

The definition of all symbols is the same as before.

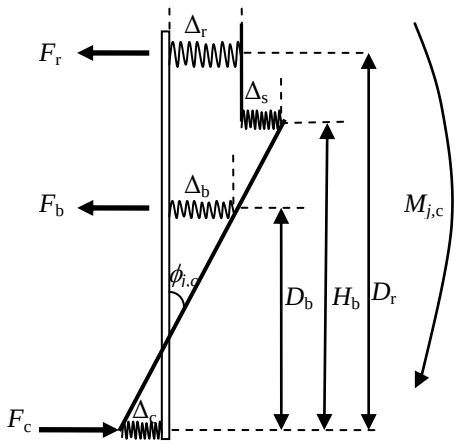

Figure 3.6: Ahmed and Nethercot spring's model

In fact, they simply modified the mechanical model of (Anderson and Najafi, 1994) (see Figure 3.4) to incorporate the effect of the stiffness of the compression zone in their model. Therefore, the centre of rotation of the composite connection will not be in the centre of the beam's bottom flange, as assumed in (Anderson and Najafi, 1994)‘s model. (Ahmed and Nethercot, 1997)'s model did not consider the effect of shear in the column web panel, which is a very important factor in the overall behaviour of asymmetrical composite connections and its effect should be considered, as stated by (Eurocode 3, 2005). Furthermore, the procedure employed to calculate the stiffness of all of the key parameters in this model was based on a statistical study of all previous available procedures and then the value which gave the best agreement for this specific model with the experimental results was chosen. These values may not represent the actual stiffness of these parameters and may not be valid for other cases. Furthermore, the model did not reflect the actual configuration of the composite connection after deformation, as the concrete slab rotates with the steel beam and this affects the deformation of the reinforcement. In addition, the derivation of the mathematical expression to calculate the rotational stiffness of the composite connection did not take into account the fixed moment required to keep the rigid bar, which connects the studs' spring with the reinforcement's spring, in a vertical orientation. Therefore, the mathematical expression did not represent the associated mechanical model. This inconsistency in reaction's forces leads to inconsistency in the gained results from the mathematical expression and the finite element modelling of the mechanical model. The expression always gives larger values of rotational stiffness and consequently less rotation for the same applied moment, as will be explained in detail in the following section. It may have little effect on the rotational stiffness of the composite connection in the linear region of the moment-rotation curve for some cases, but it will limit the ability of this model to extend further than the linear region, with valid values for the stiffness of the components.

Liew et al. (2000) used a procedure similar to (Aribert and Lachal, 1992)‘s model that was calculated the rotational stiffness of composite connection, $S_{j,c}$, by adding the stiffness of the steelwork, $S_{j,s}$, to the stiffness of the reinforced slab, which was considered to be made up of the combination of the reinforcement stiffness, k_r, and the summation of the stiffness of shear connectors, $N_{sc}\, k_{sc.}$

$$S_{j,c} = S_{j,s} + \frac{\left(\frac{k_r h_{rs}^2 + N_{sc} k_{sc} h_{ss}^2}{k_r h_{rs} + N_{sc} k_{sc} h_{ss}}\right)^2}{\frac{1}{N_{sc} k_{sc}} + \frac{1}{k_r}} \tag{3.16}$$

where h_{rs}, h_{ss} are the equivalent lever arm of the reinforcement and shear connectors in the slab and N_{sc} is the number of shear connectors. This approach did not consider the difference in behaviour of the steelwork component in the composite connection and the bare steel connection, as explained before with (Aribert and Lachal, 1992)'s model.

Eurocode 4 (2004) used another approach to calculate the initial rotational stiffness of the composite connection. The effect of shear connectors was taken into account by modifying the stiffness of the reinforcement spring, k_r, multiplied by a reduction factor, K_{slip}:

$$K_{slip} = \frac{1}{1 + \frac{E k_r}{k_s}} \tag{3.17}$$

The stiffness of all of the studs in the slab-beam interface, k_s, was calculated by an equation developed by (Aribert, 1996). This equation was derived assuming cracked composite cross-sections and using the elastic interaction theory of a composite beam, as will be explained in Section 3.9.4. In fact, this approach was an extension of the component model for the steelwork connection to be used with a composite connection by considering the reinforcement component as an additional row of bolts located at the level of reinforcement. This type of modelling did not consider the difference in behaviour of the concrete slab with shear connectors and the behaviour of an additional row of bolts, from the perspective of the distribution of forces and deformations. Also, this procedure combined the reinforcement steel and shear connectors in the same spring, despite the fact that they are on different levels. These considerations may have little effect on the rotational stiffness of high to full shear connection ratios of a composite connection, but this effect may be unacceptable in the case of partial shear connections. In addition, this will limit the ability of the model to extend further than the linear region of the moment-rotation curve using valid stiffness of the components.

It should be noted that even though the symbols of the key parameters for all of the previous models have the same meaning, different procedures were used by different researchers to calculate them; this will be discussed in the following sections.

3.4. Proposed mechanical model

3.4.1. Basic parameters and springs in the proposed mechanical model

In general, the rotation of a composite connection, which is defined as the change in angle between the steel beam axes and the column axis, consists of two parts:

(i) The rotation due to the deformation of the connection's components, $\varphi_{comp.}$

(ii) The rotation due to the shear panel of the column web, $\varphi_{sh.}$ (for asymmetrical loading).

The total rotation of the connection is:

$$\varphi_{total} = \varphi_{comp} + \varphi_{sh} \tag{3.18}$$

In order to construct the proposed mechanical model, the following considerations were taken into account in order to make the model compatible with (Eurocode 4, 2004) requirements:

1. The tensile strength of the concrete was ignored.

2. Typical components of a flush end-plate composite connection are (see Figure 3.1): (i) longitudinal steel reinforcement in tension, k_r, which has a vital effect on the overall behaviour of a composite connection; (ii) shear connectors located in the concrete slab–steel beam interface, k_s, since the degree of interaction between them greatly affects the behaviour of composite connection; (iii) the column web panel in shear, k_{cws}; (iv) end-plate in bending, k_{pb}; (v) column flange in bending, k_{cfb}; (vi) column web in compression, k_{cwc}; (vii) column web in tension, k_{cwc}; (viii) bolts in tension, k_{bt}.

3. Eurocode 3 (2005) §6.3.2 states that the stiffness coefficients of the following components need not be taken into account in calculation of the rotational stiffness of connections (i.e. stiffness coefficients equal to infinity): (i) beam's web in tension, (ii) beam's flange and web in compression and (iii) end-plate in tension or compression. Its deformations were assumed to include in the deformation of the beam in bending and does not contribute to the flexibility of the connection (Weynand et al., 1996).

4. Eurocode 3 (2005) §6.3.1(3) states that "for a bolted end-plate joint with more than one row of bolts in tension, the stiffness coefficients for the related basic components should be combined''. Therefore, for simplicity, the flush end-plate with only one row of bolts will be considered.

5. According to (Eurocode 3, 2005), the stiffness coefficient of the combined components at the level of the top row of bolts, k_b, which are: column web in tension, k_{cwt}; column flange in bending, k_{cfb}; end-plate in bending, k_{pb}; and bolts in tension, k_{bt} is given by:

$$k_b = \frac{1}{\left[\frac{1}{k_{cwt}} + \frac{1}{k_{cfb}} + \frac{1}{k_{pb}} + \frac{1}{k_{bt}}\right]} \tag{3.19}$$

6. Following the procedure of (Eurocode 3, 2005), the column web panel in shear and the column web in compression were combined to yield an equivalent component with a stiffness coefficient, k_c, which is given by:

$$k_{\mathrm{c}} = \frac{1}{\frac{1}{k_{cws}} + \frac{1}{k_{cwc}}} \tag{3.20}$$

Therefore, only four springs should be modelled in the mechanical model, as shown in Figure 3.7, in order to simulate:

(i) Longitudinal steel reinforcement in tension, k_r.

(ii) Shear connectors located in the concrete slab–steel beam interface, k_s.

(iii) Combined components at the level of the top row of bolts, k_b, from Eq. (3.19).

(iv) Combined column web in shear and compression, k_c, from Eq. (3.20).

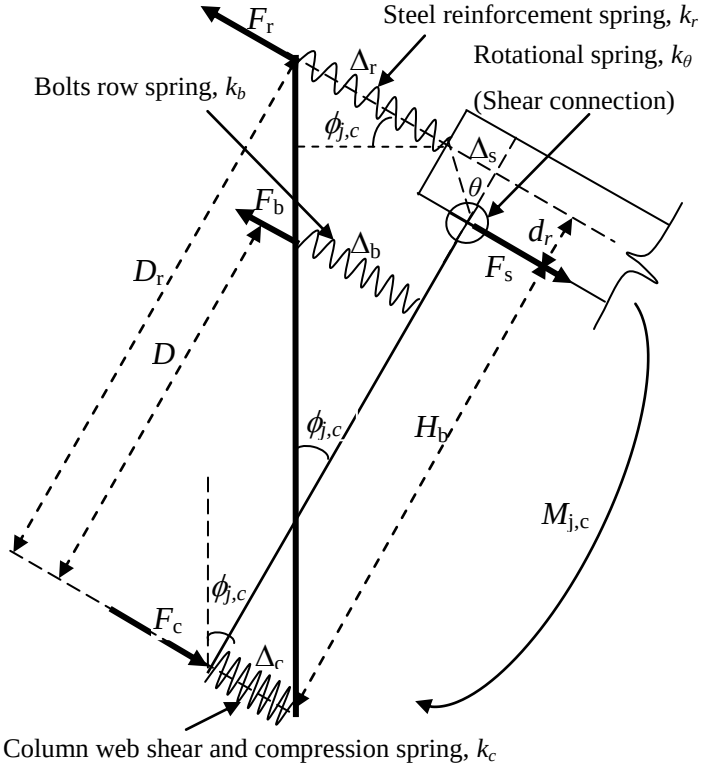

Figure 3.7: Proposed mechanical model

3.4.2. Derivation of the expressions for the mechanical model

To define the rotational stiffness of the shear connection spring, k_θ, in terms of linear spring stiffness, the moment in this spring, M_θ, can be written using the following equation:

$$M_\theta = k_\theta \theta = k_\theta \frac{\Delta_s}{d_r} \tag{3.21}$$

From the equilibrium of the upper part of the composite connection, the following relationship can be written:

$$M_\theta = F_r d_r = F_s d_r = k_s \Delta_s d_r \tag{3.22}$$

From Eq. (3.21) and Eq. (3.22) we get: $$k_\theta \frac{\Delta_s}{d_r} = k_s \Delta_s d_r \tag{3.23}$$

$$\therefore k_\theta = k_s d_r^2 \tag{3.24}$$

The stiffness deformation relations are:

$$F_b = k_b \Delta_b, \qquad F_r = k_r \Delta_r, \qquad F_c = k_c \Delta_c \tag{3.25}$$

The compatibility condition gives:

$$\Delta_s = \theta d_r \tag{3.26}$$

$$\Delta_r + \Delta_s + \Delta_c = D_r \tan\phi \tag{3.27}$$

$$\Delta_b + \Delta_c = D_b \tan\phi \quad \Rightarrow \Delta_c = D_b \tan\phi - \Delta_b \tag{3.28}$$

For the small angle ($\tan\phi = \phi$) where ϕ is the total rotation of the composite connection, as mentioned in Eq. (3.18). Subtracting Eq. (3.28) from Eq. (3.27) results, in the following:

$$\Delta_r + \Delta_s - \Delta_b = \left(D_r - D_b\right)\phi \tag{3.29}$$

The equilibrium condition gives:

$$F_c = F_r + F_b \Rightarrow \Delta_c = \frac{k_r\Delta_r + k_b\Delta_b}{k_c} \tag{3.30}$$

$$F_s = F_r \quad \Rightarrow \quad \Delta_s = \frac{k_r\Delta_r}{k_s} \tag{3.31}$$

Substituting Eq. (3.30) in Eq. (3.28) results in:

$$D_b\phi - \Delta_b = \frac{k_r\Delta_r + k_b\Delta_b}{k_c} \rightarrow \Delta_b = \frac{D_b k_c\phi - k_r\Delta_r}{\left(k_c + k_b\right)} \tag{3.32}$$

Substituting Eq. (3.31) and Eq. (3.32) in Eq. (3.29) results in:

$$\Delta_r + \frac{k_r\Delta_r}{k_s} - \frac{D_b k_c\phi - k_r\Delta_r}{\left(k_c + k_b\right)} = \left(D_r - D_b\right)\phi \tag{3.33}$$

$$\Delta_r + \frac{k_r\Delta_r}{k_s} + \frac{k_r\Delta_r}{\left(k_c + k_b\right)} = \left(D_r - D_b\right)\phi + \frac{D_b k_c\phi}{\left(k_c + k_b\right)} \tag{3.34}$$

$$\Delta_r k_r\left[\frac{1}{k_r} + \frac{1}{k_s} + \frac{1}{\left(k_c + k_b\right)}\right] = \left[D_r - D_b\left(1 - \frac{k_c}{\left(k_c + k_b\right)}\right)\right]\phi \tag{3.35}$$

$$\Delta_r = \frac{\left(D_r - D_b\left(\frac{k_b}{k_c + k_b}\right)\right)}{k_r\left(\frac{1}{k_r} + \frac{1}{k_s} + \frac{1}{\left(k_c + k_b\right)}\right)}\phi \tag{3.36}$$

$$\therefore F_r = \frac{\left(D_r - D_b\left(\frac{k_b}{k_c + k_b}\right)\right)}{\left(\frac{1}{k_r} + \frac{1}{k_s} + \frac{1}{\left(k_c + k_b\right)}\right)}\phi \tag{3.37}$$

Substituting Eq. (3.36) in Eq. (3.32) results in:

$$\Delta_b = \frac{\dfrac{1}{(k_c+k_b)}\left[D_b k_c\left(\dfrac{1}{k_r}+\dfrac{1}{k_s}+\dfrac{1}{(k_c+k_b)}\right) - \left(D_r - D_b\left(\dfrac{k_b}{k_c+k_b}\right)\right)\right]}{\left(\dfrac{1}{k_r}+\dfrac{1}{k_s}+\dfrac{1}{(k_c+k_b)}\right)}\phi \tag{3.38}$$

$$\therefore F_b = \frac{\dfrac{k_b}{(k_c+k_b)}\left[D_b k_c\left(\dfrac{1}{k_r}+\dfrac{1}{k_s}+\dfrac{1}{(k_c+k_b)}\right) - \left(D_r - D_b\left(\dfrac{k_b}{k_c+k_b}\right)\right)\right]}{\left(\dfrac{1}{k_r}+\dfrac{1}{k_s}+\dfrac{1}{(k_c+k_b)}\right)}\phi \tag{3.39}$$

By taking the moment about the centre of compression and assuming that there is no compression force in the beam web, provided that the internal forces for the calculation of rotational stiffness are low, then:

$$M_{j,c} = F_r D_r + F_b D_b \tag{3.40}$$

Substituting Eq. (3.37) and Eq. (3.39) in Eq. (3.40) results in:

$$M_{j,c} = \left[\frac{D_r\left(D_r - D_b\left(\dfrac{k_b}{k_c+k_b}\right)\right) + \dfrac{D_b k_b}{(k_c+k_b)}\left[D_b k_c\left(\dfrac{1}{k_r}+\dfrac{1}{k_s}+\dfrac{1}{(k_c+k_b)}\right) - \left(D_r - D_b\left(\dfrac{k_b}{k_c+k_b}\right)\right)\right]}{\left(\dfrac{1}{k_r}+\dfrac{1}{k_s}+\dfrac{1}{(k_c+k_b)}\right)}\right]\phi \tag{3.41}$$

$$\because \quad M_{j,c} = S_{j,c}\phi, \tag{3.42}$$

and rearranging Eq. (3.41) gives:

$$\therefore \quad \mathrm{S}_{j,c} = \frac{D_b^2 k_b k_c}{(k_c+k_b)} + \frac{\left(D_r - D_b\left(\dfrac{k_b}{k_c+k_b}\right)\right)^2}{\left(\dfrac{1}{k_r}+\dfrac{1}{k_s}+\dfrac{1}{(k_c+k_b)}\right)} \tag{3.43}$$

Many researchers attempted to provide methods to estimate the rotational stiffness which will be applicable for both composite and bare steel connections. This required that the rotational stiffness of bare steel connection, $S_{j,s}$, could be obtained when no reinforced concrete slab was present in the composite arrangement. To achieve this consistency, they derived their mathematical expressions by separating the moment resistance of the bare steel connection and the slab independently in advance (such as Eq. (3.1)). However, the moment resistance of the steelwork component and the reinforced slab are inter-related. As explained in Section 3.3, there is an additional increase in compressive force, F_c, which leads to increase in the tension force in the top

row of bolts, F_b. Hence, the moment resistance of the steelwork component in a composite connection is less than the moment resistance of the bare steel connection for the same amount of rotation (see Eq. (3.12)).

The required consistency can be achieved in the proposed model, as it dealt with the whole composite connection. The components of the bare steel connection were separated to obtain two terms in Eq. (3.43). The first term represents the effect of the steelwork components only and the other term is the effect of the correlation between the bare steel connection and the reinforced slab. The following procedure was used:

1. **Steelwork stiffness, $S_{j,sw}$ (i.e. no reinforcement and F_r=0)**

From Eq. (3.30)

$$F_c = F_b \Rightarrow k_c\Delta_c = k_b\Delta_b \Rightarrow \Delta_c = \frac{k_b\Delta_b}{k_c} \tag{3.44}$$

Substituting Eq. (3.44) in Eq. (3.28) gives:

$$\Delta_b = \phi D_b - \frac{k_b\Delta_b}{k_c} \Rightarrow \Delta_b = \frac{D_b}{\left(1+\frac{k_b}{k_c}\right)}\phi \tag{3.45}$$

$$M_{j,sw} = F_b D_b \Rightarrow M_{j,sw} = k_b\Delta_b D_b \Rightarrow M_{j,sw} = \frac{k_b D_b^2}{\left(1+\frac{k_b}{k_c}\right)}\phi \tag{3.46}$$

$$S_{j,sw} = \frac{M_{j,sw}}{\phi} = \frac{k_b D_b^2}{\left(1+\frac{k_b}{k_c}\right)} \tag{3.47}$$

Anderson and Najafi (1994) derived an equation to calculate the rotational stiffness of bare steel connection as follows:

$$S_{j,s} = k_b D_b^2 \tag{3.48}$$

It is clear that Eq. (3.48) is a special form of Eq. (3.47) corresponding to the assumption of an infinite stiffness for the column web (i.e. k_c=∞), as the connections that were tested by (Anderson and Najafi, 1994) had a stiffened column.

Eq. (3.47) can be rewritten in this form: $S_{j,sw} = \frac{k_b k_c D_b^2}{k_c + k_b}$ (3.49)

2. Concrete slab stiffness, K_{slab}

$$K_{slab} = \frac{k_r k_s}{k_r + k_s} \tag{3.50}$$

Substituting Eq. (3.49) and Eq. (3.50) in Eq. (3.43) gives:

$$\therefore \quad \mathrm{S}_{j,c} = \mathrm{S}_{j,sw} + \frac{\left(D_r - \frac{\mathrm{S}_{j,sw}}{D_b k_c} \right)^2}{\left(\frac{1}{K_{slab}} + \frac{\mathrm{S}_{j,sw}}{D_b^2 k_c k_b} \right)} = \mathrm{S}_{j,sw} + \mathrm{S}_{j,sws} \tag{3.51}$$

Eq. (3.51) is a general equation to calculate the rotational stiffness for flush end-plate steelwork or composite connections and for stiffened or unstiffened column cases.

3.5. The applicability of the proposed equation for general cases

The applicability of Eq. (3.51) to calculate the rotational stiffness for all cases of flush end-plate connection can be checked as follows:

1. Steelwork connection case (K_{slab}=0)

i. Unstiffened connection ($k_c \neq \infty$)

$$\therefore \quad \mathrm{S}_{j,c} = \mathrm{S}_{j,sw} + K_{slab} \frac{D_b^2 k_c k_b \left(D_r - \frac{\mathrm{S}_{j,sw}}{D_b k_c} \right)^2}{\left(D_b^2 k_c k_b + K_{slab} \mathrm{S}_{j,sw} \right)} = \frac{k_b D_b^2}{\left(1 + \frac{k_b}{k_c} \right)} \tag{3.52}$$

ii. Stiffened connection ($k_c = \infty$)

$$\therefore \quad \mathrm{S}_{j,c} = \mathrm{S}_{j,sw} = k_b D_b^2 \tag{3.53}$$

Eq. (3.53) is the same as (Anderson and Najafi, 1994)'s equation (i.e. Eq. (3.48)) for calculating the rotational stiffness of a stiffened bare steel connection.

2. Composite connection cases

i. Unstiffened connection ($k_c \neq \infty$)

Same as Eq. (3.51)

ii. Stiffened composite connection ($k_c = \infty$)

$$S_{j,c} = S_{j,sw} + K_{slab} D_r^2 = k_b D_b^2 + \frac{k_r k_s}{k_r + k_s} D_r^2 \qquad (3.54)$$

In summary, Eq. (3.51) gives the same result as (Ahmed and Nethercot, 1997)'s equation (i.e. Eq. (3.15)) for calculating the rotational stiffness of an unstiffened composite connection, but after replacing (H_b) with (D_r) to take into account the actual position of the concrete slab after deformation. The effect of the column web panel in shear should be considered in k_c. Also, Eq. (3.54) is similar for (Anderson and Najafi, 1994) and (Ahmed and Nethercot, 1997)'s equations (i.e. Eqs. (3.13) & (3.15)) for calculating the rotational stiffness of a stiffened composite connection, but after carrying out the same adjustment above for D_r and k_c. This means that Eq. (3.51) is an improved form of (Ahmed and Nethercot, 1997)'s equation for unstiffened case of composite connection as well as Eq. (3.54) is an improved form of (Anderson and Najafi, 1994; Ahmed and Nethercot, 1997)'s equations for a stiffened composite connection.

3.6. Why a rotational spring?

In order to show the considerable advantage of using the proposed rotational spring over the conventional axial spring in the modelling of shear connectors, three composite connections that had been tested by (Anderson and Najafi, 1994) were used to carry out this comparison. The details of these tests are listed in Table 3.2.

Table 3.2: Properties of composite connections

TEST	k_r kN/mm	k_s kN/mm	$k_\theta = k_s d_r^2$ kN.mm/rad	k_c kN/mm	k_b kN/mm	D_r mm	D_b mm	H_b mm	d_r mm
S4F	220	602	5548032	68861	155	400	254	304	96
S8F	435	509	4690944	68861	155	400	254	304	96
S12F	654	433	3990528	68861	155	400	254	304	96

(Ahmed and Nethercot, 1997)'s model was selected for the comparison, as shown in Figure 3.8.

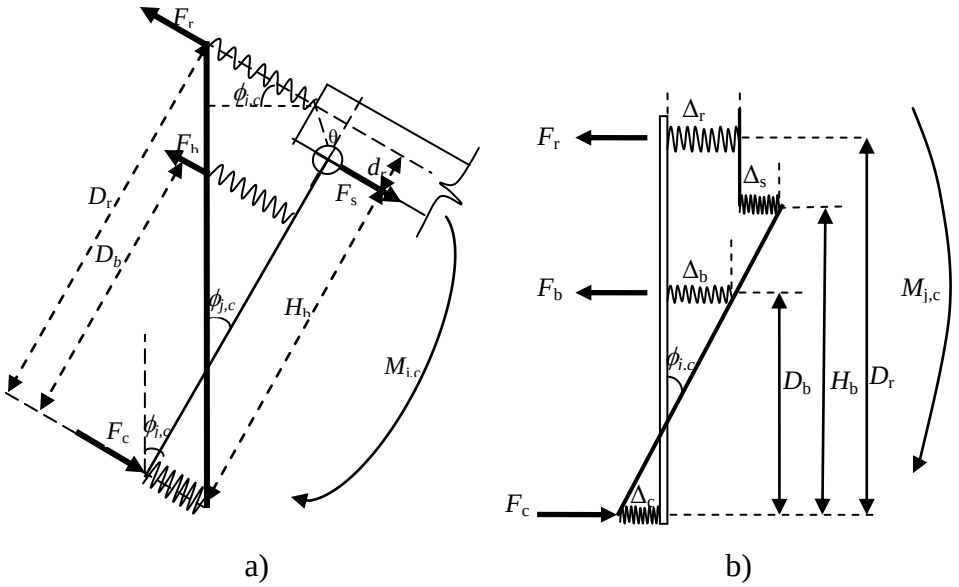

Figure 3.8: a) Proposed model b) (Ahmed and Nethercot 1997)'s model

3.6.1. Modelling

ABAQUS software was used to evaluate the advantage of using the rotational spring over the conventional linear spring. Linear springs were used in the conventional models to represent: (i) the column compression zone, (ii) the top row of bolts, (iii) the reinforcement, and (iv) shear connectors. Linear spring of shear connectors was replaced by rotational spring in the proposed model. The column and lines of rotation of the steel beam and slab were modelled by rigid bars. In the conventional model, the connection between the shear connectors' spring and slab was modelled using a fixed joint on roller support. However, they were directly joined using a rotational spring in the proposed model. Sketches of the conventional model and the proposed model are illustrated in Figure 3.9 and Figure 3.10 respectively.

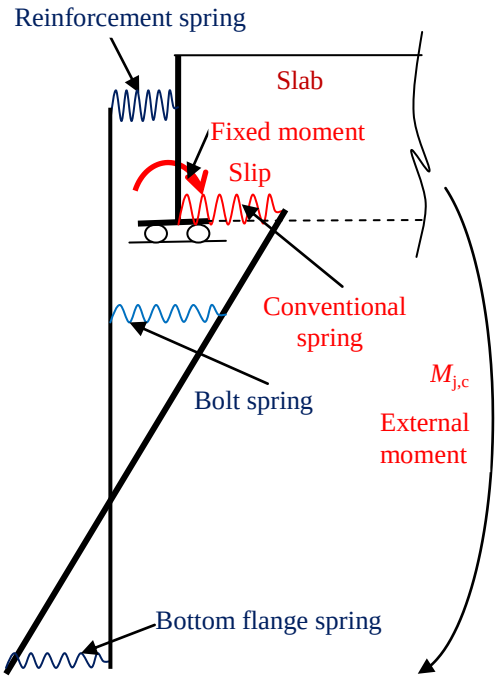

Figure 3.9: Modelling of conventional mechanical model in ABAQUS

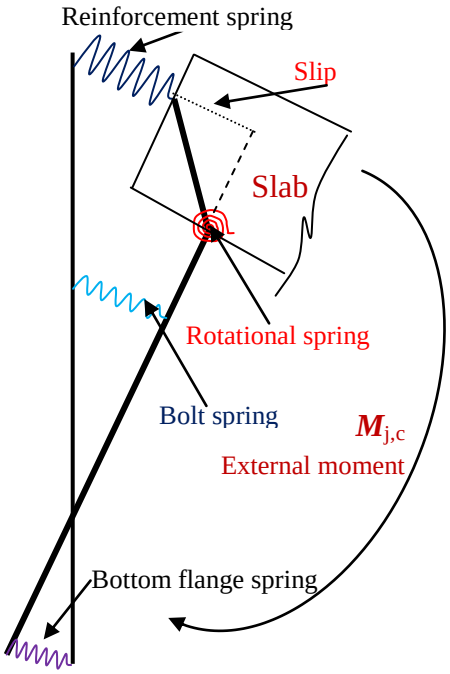

Figure 3.10: Modelling of the proposed mechanical model in ABAQUS

All models of the composite connection were subjected to the same external moment, $M_{j,c}$. The magnitude of the external moment was 262 kN-m. This value of moment was higher than the elastic range of the experimental moment-rotation curve for all connections, in order to show the whole available range where the stiffness of components are valid or the region where the post-linear stiffness of components should be used.

This comparison using ABAQUS aims to verify the results from the conventional [Eq. (3.15)] and the proposed [Eq. (3.51)] analytical expressions in terms of satisfying the equilibrium and compatibility requirements.

3.6.2. Results and discussion

Figure 3.11 shows the result of rotations of the conventional and the proposed models due to the applied moment for the S4F composite connection.

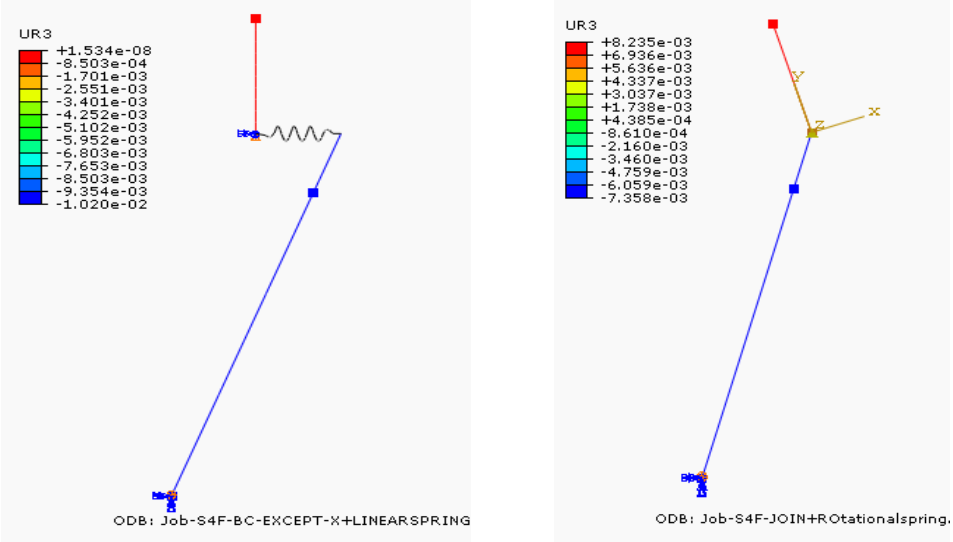

Figure 3.11: ABAQUS results of rotation for the S4F composite connection

Table 3.3 summarizes the results from ABAQUS modelling for both the conventional and the proposed models in column 2 and 4 respectively. Also, the results from the conventional mathematical expression (i.e. Eq. (3.15)) and the proposed mathematical expression (i.e. Eq. (3.51)) are listed in column 1 and 3.

In the conventional model the rigid bar connecting the horizontal springs for the reinforcement and shear studs had been assumed to remain vertical. However, in order to maintain the assumed configuration, a restraining bending moment would have been necessary, which was not considered in the analytical expression. The corresponding ABAQUS model using appropriate constraints ensured both equilibrium and compatibility. Hence the results were different for the conventional model using ABAQUS and the analytical expressions (columns 3 and 4).

For the proposed model, the ABAQUS and the analytical expression produces similar results (columns 1 and 2) ensuring the compatibility and equilibrium requirements being satisfied in the analytical expression.

The restraining bending moment in the conventional model will increase the total applied moment or decrease the resistance moment of connection. As a result, it leads to an increase in rotation and a decrease in the stiffness of the composite connection shown in the ABAQUS model. In (Ahmed and Nethercot, 1997)'s model, this internal fixed moment was not included in the derivation of the mathematical expression, even though its effect (i.e. vertical orientation) was included in the configuration of the model. Therefore, the mathematical expression underestimates the rotation (i.e. overestimates stiffness) by about 20% for these cases of composite connections. This difference will increase significantly as the rotation increases beyond the elastic range. This inaccuracy may be acceptable in the elastic range for some cases of connections, especially when the thickness of the slab is very small compared to the depth of the steel beam, as the internal moment at the base of the vertical rigid bar will be minimal. Nevertheless, this makes the conventional mechanical model unsuitable for extending further then the elastic range to estimate the moment-rotation curve of composite connections using the elasto-plastic behaviour of its components, and limits it from being used with any other modelling software like ABAQUS. Since the proposed model connects the steel beam directly to the slab by a rotational spring to model the effect of the shear connectors, this overcomes all of these shortcomings of the conventional model.

Table 3.3: Summary results of all connections (M=262 kN-m)

Connection	Parameter	Expression (Proposed) 1	ABAQUS Modelling (Proposed) 2	Expression (Conventional) 3	ABAQUS Modelling (Conventional) 4	1/2	3/4
S4F	Stiffness (kN/mm)	35.63	35.65	29.46	25.69	0.99	1.15
	Rotation (mrad)	7.35	7.35	8.89	10.2	1.00	0.87
S8F	Stiffness kN/mm	47.27	46.80	38.31	31.50	1.01	1.22
	Rotation (mrad)	5.54	5.60	6.84	8.32	0.99	0.82
S12F	Stiffness (kN/mm)	51.39	50.87	41.43	33.87	1.01	1.22
	Rotation (mrad)	5.10	5.15	6.32	7.73	0.99	0.82

Furthermore, Figure 3.12 to Figure 3.14 show the applicability of the proposed model to predict the actual behaviour of composite connections in the whole linear range of the moment-rotation curve.

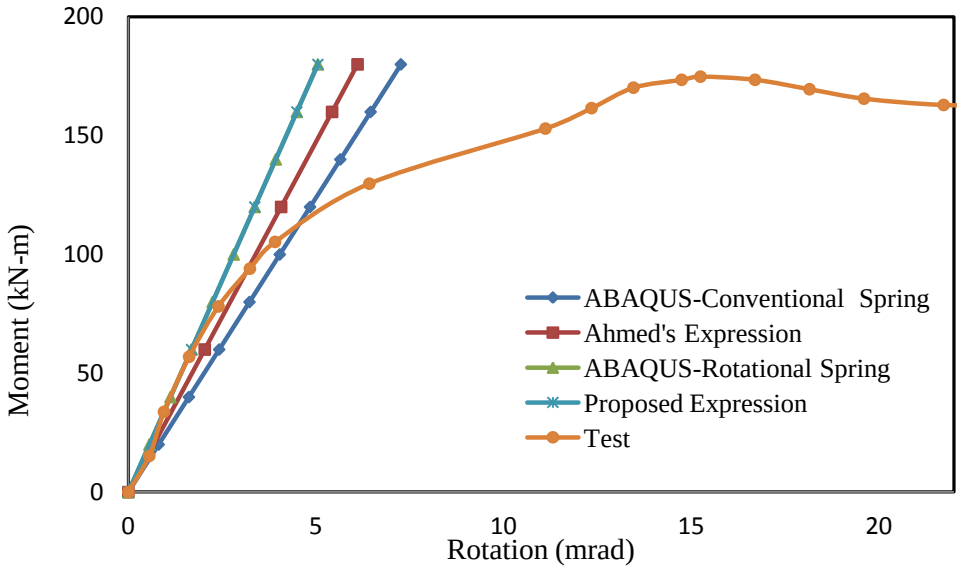

Figure 3.12: Comparison of rotational and conventional spring's models with test results for test S4F

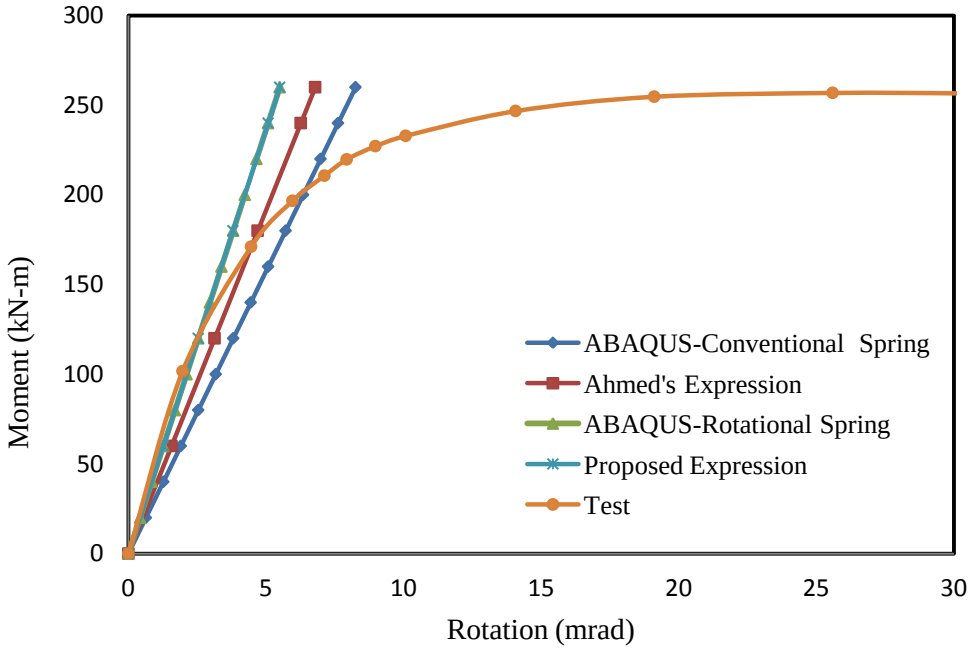

Figure 3.13: Comparison rotational and conventional spring's models with test results for test S8F

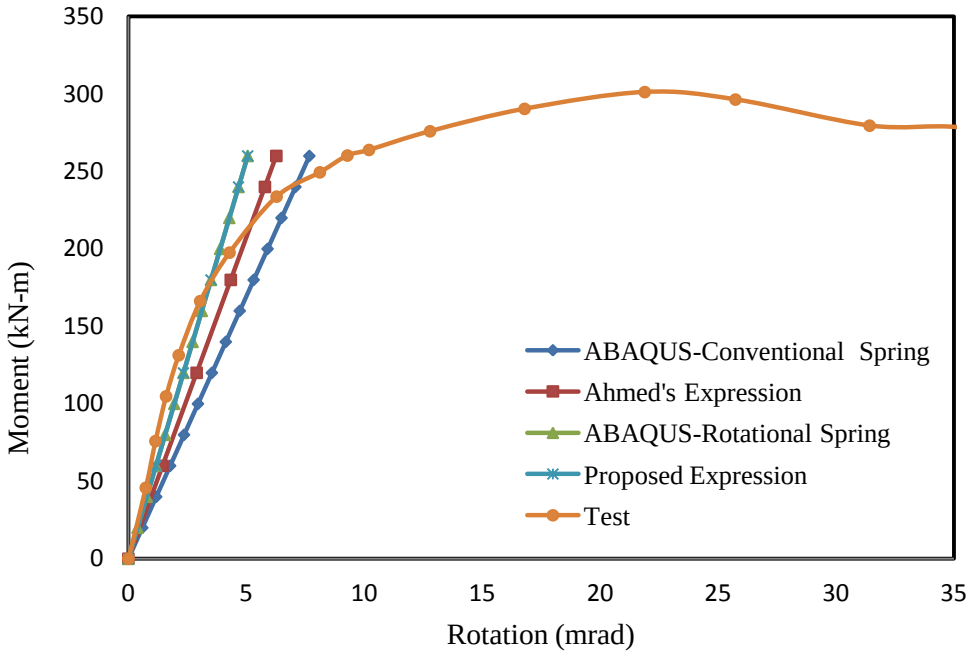

Figure 3.14: Comparison rotational and conventional spring's models with test results for test S12F

In summary, using the rotational spring to simulate the shear connection can capture the actual behaviour of the composite connection in a linear range. In addition, it makes the proposed model better suited for estimating the rotation of the composite connection in the post-linear range using appropriate elasto-plastic behaviour for every component.

3.6.3. Suggestion for modification of the conventional models

In order to modify the conventional mathematical expression to match the mechanical model, the implicit internal moment should be deducted from the moment resistance of the connection, as follows:

$$M_{j,c} = F_r D_r + F_b d_b - F_r d_r \Rightarrow M_{j,c} = F_r \left(D_r - d_r\right) + F_b d_b \tag{3.55}$$

Therefore, the modified stiffness expression for the conventional model (Eq. (3.15)) will be:

$$S_{j,c} = \frac{H_b \left(D_r - d_r\right)\left(\frac{1}{k_b}+\frac{1}{k_c}\right) + D_b^2\left(\frac{1}{k_r}+\frac{1}{k_s}+\frac{1}{k_c}\right) - D_b\left(H_b + \left(D_r - d_r\right)\right)\frac{1}{k_c}}{\left(\frac{1}{k_r}+\frac{1}{k_s}+\frac{1}{k_c}\right)\left(\frac{1}{k_b}+\frac{1}{k_c}\right) - \frac{1}{k_c^2}} \tag{3.56}$$

$$S_{j,c} = \frac{H_b^2\left(\frac{1}{k_b}+\frac{1}{k_c}\right)+D_b^2\left(\frac{1}{k_r}+\frac{1}{k_s}+\frac{1}{k_c}\right)-\frac{2H_bD_b}{k_c}}{\left(\frac{1}{k_r}+\frac{1}{k_s}+\frac{1}{k_c}\right)\left(\frac{1}{k_b}+\frac{1}{k_c}\right)-\frac{1}{k_c^2}}$$

This modified expression ensures *only* the matching in results with the ABAQUS modelling for the associated mechanical model. However, it increases the underestimation of the rotational stiffness (or overestimation of rotation) due to the implicit fixed moment. The exclusion of the implicit fixed moment from the derivation of the conventional expression reduced the underestimation of stiffness due to the use of a linear spring in the conventional model. However, this omission does not have a reasonable structural basis.

3.7. Main merits of the proposed model

In summary, the main merits of the proposed model are

1. Its simplicity.
2. It can be applied both to bare steel connections as well as composite connections.
3. It includes all the important aspects of behaviour of steelwork in a composite connection, as explained in Section 3.3.2 and Figure 3.3.
4. It incorporates the rotation of the slab.
5. The derivation of a mathematical expression to calculate the rotational stiffness includes all of the relevant forces.
6. It can be modelled easily in any finite element software such as ABAQUS.
7. It can be extended in the post-elastic non-linear region, with valid values for the stiffness of components, since it satisfies the equilibrium and compatibility conditions at large displacements.

3.8. Determination of the effective terms in the mathematical expression

The degree of accuracy of any mathematical expression for the rotational stiffness of a composite connection depends to a large extent on the accuracy of its effective parameters. Therefore, a parametric study was carried out to evaluate the effect of every

key parameter in the mathematical expression, k_c, k_b, k_r, k_s, on the rotational stiffness. The composite connection, CJS-1, which was tested by (Li et al., 1996), was selected in this parametric study. The properties of this composite connection and the basic stiffness coefficient of its components are shown in Table 3.4.

Table 3.4: Properties of Cjs-1 composite connection

Beam	Column	H_b (mm)	D_r (mm)	D_b (mm)	k_r kN/mm	k_s kN/mm	k_c kN/mm	k_b kN/mm
254x102UB25	203x203UC46	257.2	338	203	350	2800	6500	155

The results of the parametric study are shown in Figure 3.15 to Figure 3.18.

3.8.1. Effect of k_c

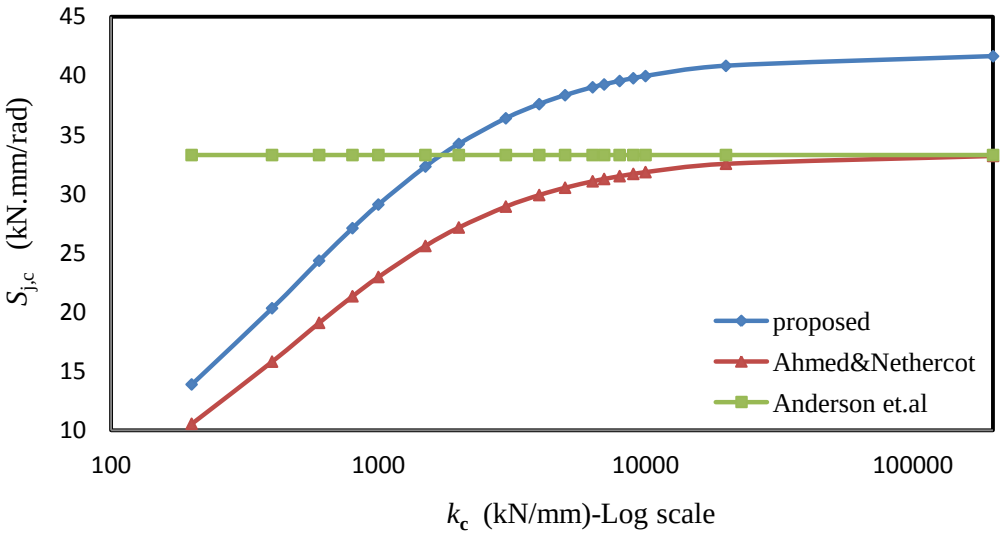

Figure 3.15: The effect of k_c on rotational stiffness

Figure 3.15 shows that the rotational stiffness of the connection is affected by the combined stiffness coefficients of the column web in shear and compression, k_c, if all other coefficients are constant. This effect is minimal for high values of k_c (i.e. a stiffened composite connection with a symmetrical loading system). However, it has a significant effect in the lower range of k_c, (100 to 1000 kN/mm). This highlights the importance of using a stiffener at the column web to increase the rotational stiffness of the composite connection. On the other hand, it indicates the necessity of including the stiffness of the column web in shear into the proposed model. The model used by (Anderson and Najafi, 1994) is not affected by this factor since it was based on the

assumption of infinite stiffness of the compression zone (i.e. the fully stiffened case). Also, (Ahmed and Nethercot, 1997)'s model matches with (Anderson and Najafi, 1994)'s model for higher values of stiffness, since the latter model was modified from the former model by including the stiffness of the column web in compression effect only. However, the effects of the column web in shear were not included. The additional difference between the proposed model and (Ahmed and Nethercot, 1997)'s model for higher values of k_c, is due to the reasons which have been explained in the previous section.

3.8.2. Effect of k_b

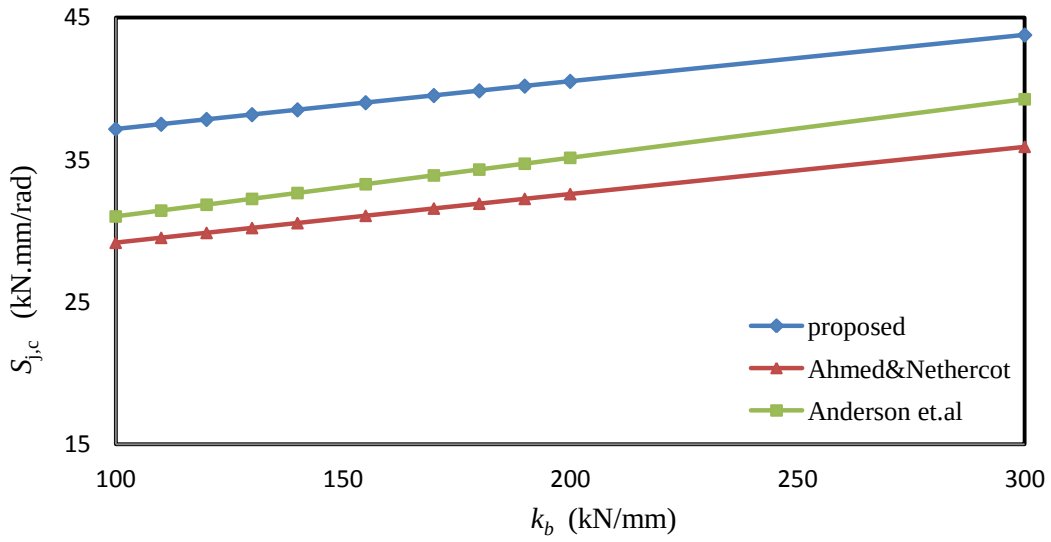

Figure 3.16: The effect of k_b on rotational stiffness

Figure 3.16 shows the effect of changing the stiffness coefficient of the row of bolts, k_b, on the rotational stiffness of the composite connection. It is clearly seen that k_b has little effect on the rotational stiffness. Also, the acceptable value for this parameter was taken as 155 kN/mm for all composite connections by a number of researches such as (Anderson and Najafi, 1994; Ahmed and Nethercot, 1997; Loh et al., 2006).

3.8.3. Effect of k_r

Figure 3.17 shows the significant effect of the stiffness coefficient of steel reinforcement, k_r, on the rotational stiffness of the composite connection, which increases steeply from about 15 to 80 kN-mm/mrad for changes in k_r, from 100 to 1000 kN/mm. This result is expected, since all of the previous numerical and

experimental studies confirmed considerable effect of steel reinforcement ratio on overall behaviour of the composite connection especially for small reinforcement ratios.

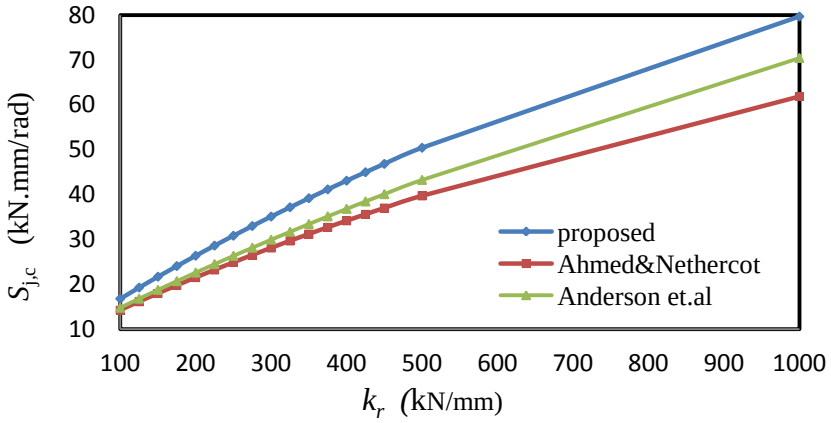

Figure 3.17: The effect of k_r on rotational stiffness

3.8.4. Effect of k_s

The effect of shear connection on the rotational stiffness of the connection can be seen in Figure 3.18. (Anderson and Najafi, 1994)'s model has a constant value of stiffness, since it was based on a constant value of shear connection, k_s, and equal to 200 kN/mm for all cases. Figure 3.18 also shows that the rotational stiffness of the composite connection is very sensitive to the changes in stiffness coefficient of the shear connection, k_s, especially for a partial shear connection. This effect is reduced when the connection is close to full interaction. Since the partial interaction is commonly used in practice, the simple and reliable procedure to evaluate this factor is highly necessary.

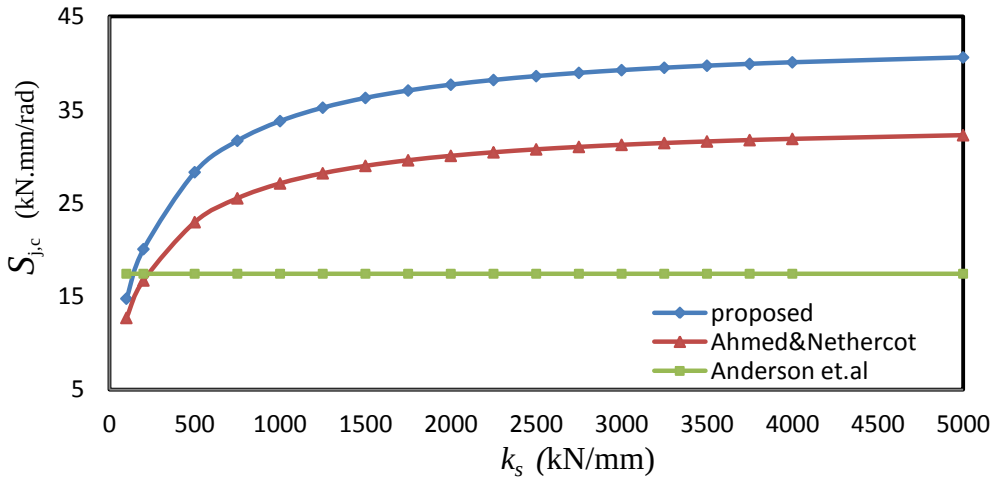

Figure 3.18: The effect of k_s on rotational stiffness

3.9. Adopted procedure to calculate the key parameters

As mentioned above, the accuracy of the results depends to a large extent on the successful selection of key parameters. In order to make the proposed model compatible with (Eurocode 3, 2005) and (Eurocode 4, 2004), the stiffness parameters k_b and k_c were calculated using the procedures in (Eurocode 3, 2005) §6.3.2 (1),Table 6.11 and (Eurocode 4, 2004) §A.2.1.1,Table (A.1). The procedures of calculation are demonstrated in Sections 3.9.1 and 3.9.2. Meanwhile the procedure to estimate the stiffness of reinforcement, k_r, is explained in Section 3.9.3. A new procedure to estimate the stiffness of the shear connection, $k_{s,}$ is proposed in Section 3.9.4.

3.9.1. Stiffness of the top row of bolts, k_b

This parameter can be calculated according to (Eurocode 3, 2005) using Eq. (3.19) as the stiffness coefficient of the combined components at the level of the top row of bolts. This was taken to be 155 kN/mm by (Anderson and Najafi, 1994) corresponding to the approximate linear stiffness of the steelwork connection. Ahmed and Nethercot (1997) adopted the same value, based on a statistical study of its variation with the results of their model. The same value was taken by (Loh et al., 2006). To simplify the comparison with other models, the same value was used in the current research if there was no sufficient data to calculate it using Eq. (3.19), since variation of this value has little effect on the rotational stiffness of the composite connection, as explained and shown in Figure 3.16 in the previous section.

3.9.2. Stiffness of the column web in shear, k_{cws} and compression, k_{cwc}

The column web panel in shear is a very important component in the overall behaviour of the connection, but it has little effect on the rotational stiffness for a stiffened composite connection or for symmetrical loading, as explained in the previous section. According to (Eurocode 3, 2005), the stiffness coefficient, k_{cws}, for an unstiffened web is calculated using the following equation:

$$k_{cws} = \frac{GA_{vc}}{\beta z} = \frac{0.38E_s A_{vc}}{\beta\left(H_b - t_{bf}\right)} \tag{3.57}$$

where A_{vc} is the shear area of the column and z denotes the lever arm between the compressive and the tensile area. E_s is the Young's modulus of steel. β is the interaction

parameter to account for asymmetrical loading and it is defined in (Eurocode 3, 2005) §5.3. (8). Its value varies in the range of $0 \leq \beta \leq 2$.

The stiffness coefficient of the column web in compression, k_{cwc}, is defined in (Eurocode 3, 2005) for an unstiffened web case as follows:

$$k_{cwc} = EA_c \frac{1}{h_c} = E \frac{0.7 b_{eff,cwc} t_{cw}}{h_c} \tag{3.58}$$

where, A_c and h_c are the area and depth of column respectively. $b_{eff,cwc}$, is the effective width of the column web in compression and it is computed as follows:

$$b_{eff,cwc} = t_{bf} + 2\left(\sqrt{2}a_b + t_p\right) + 5\left(t_{cf} + r_c\right) \tag{3.59}$$

where all of the above terms are defined in (Eurocode 3, 2005) §6.2.6.2. For the stiffened web case, k_{cwc}, is taken as equal to infinity.

3.9.3. Stiffness coefficient of the steel reinforcement, k_r

This coefficient is based on the assumption that the reinforcement obeys Hooke's law:

$$F_r = k_r \Delta_r = \left(\frac{E_s A_r}{l_r}\right) \Delta_r \tag{3.60}$$

where, A_r, is the area of reinforcing bars. The main difficulty in calculating the stiffness of reinforcing bars is the assumed effective length, l_r, of bars, having extension Δ_r. This length is measured from the centreline of the column and is extended along the reinforcement up to the point where considerable stress is attained. Nevertheless, this length is not the same along all parallel reinforcing bars, but it is commonly greater as the reinforcing bar is positioned further away from the column (Gil and Bayo, 2008).

Anderson and Najafi (1994) assumed this length to be equal to half the depth of the column, h_c. However, they stated that if the flexibility of the shear connectors is taken into consideration, this length needs to increase up to the first row of shear connectors in order to overcome the overestimation of the stiffness of the reinforcing bars:

$$l_r = \frac{h_c}{2} + p_0 \tag{3.61}$$

where p_0 is the distance between the column flange and the first shear stud. The same expression was used by (Liew et al., 2000; Brown and Anderson, 2001; Queiroz et al., 2005; Titoum et al., 2009).

Ren and Crisinel (1996) proposed the following empirical equation to calculate the effective length, l_r, in (mm) as:

$$l_r = 0.7\left(60 + 1.3ks\right) \tag{3.62}$$

where k =0.5 for simple bending and k=1 for pure tension, and s is the spacing of the reinforcing bars in (mm).

Ahmed and Nethercot (1997) reviewed the effective length expressions adopted by various authors and concluded that if the first stud is very near the column's flange, the distance to the next stud should be used. They used the following expression to calculate l_r:

$$l_r = \frac{h_c}{2} + p_0 + p \tag{3.63}$$

where p_0 is as above and p is the spacing between shear studs.

Rassati et al. (2004) developed the following equation to calculate the effective length:

$$l_r = h_c\left(1 + 2.8 - 0.5K_{trans}\right) \quad \text{where} \quad K_{trans} = A_r \,/\left(A_{s,rb} + 0.64t_{bf}\, b_b\right) \tag{3.64}$$

where $A_{s,rb}$ is the area of longitudinal reinforcement in the composite beam's section adjacent to the connection, and A_r is the area of longitudinal reinforcement in the effective width of the slab. t_{bf} and b_b, are the thickness and the breadth of the steel beam flange respectively.

Eurocode 4 (2004) used several expressions which depend on the interaction parameter, β. The estimation of this parameter was explained in Section 3.9.2.

Gil and Bayo (2008) used the finite element method to carry out a parametric study for composite connections with different load conditions, varying the profiles, bolts and reinforcement ratio. Based on the reasoning and observation of the simulation results, an effective length was chosen for each case. They then established an expression to determine the effective length of the reinforcement, as follows:

$$l_r = \frac{h_c}{2} + 0.8D_r \tag{3.65}$$

It is clear from the above brief discussion that there is no guideline to favour any approach over the others, as some of them were empirical equations from limited tests and others were outcomes of statistical analysis for available data or simulation results.

In Chapter Five, we will propose another procedure to combine the effect of reinforcement effect with the effect of the shear connector in one component, thus eliminating the need to estimate the effective length. In current chapter, Eq. (3.61) was adopted to simplify the comparison with other models.

3.9.4. Stiffness of the shear connection, k_s

It has been demonstrated by many experimental and numerical studies that the slip in the interface between the concrete slab and the steel beam has a significant effect on the rotational stiffness and overall behaviour of a composite connection, even in full shear connection conditions (Aribert, 1996; Loh et al., 2006). This effect is more significant for partial shear connections as explained and shown in Figure 3.18. The elastic stiffness of a stud shear is:

$$k_{sc} = \frac{F_{sc,k}}{s_{sc}} \tag{3.66}$$

where $F_{sc,k}$ is the characteristic resistance of the stud and s_{sc} is the corresponding slip. Anderson and Najafi (1994) reviewed and assessed the available push-out tests data of the load-slip behaviour of welded studs. The assessment led to assume the stiffness of stud, k_{sc} to be 200 kN/mm. Furthermore, they interpreted the result of the assessment by assuming that the first stud provides resistance to slip under increasing load until it reaches its maximum resistance and becomes plastic. Its force then remains constant and any additional load is resisted by the next stud until it also reaches its maximum resistance, and so forth. Based on this behaviour, they concluded that the slip at the connection depends initially on the nearest stud to the column and the stiffness of the shear connection, k_s, was taken as the stiffness of one stud (i.e. 200 kN/mm). The numerical study that was carried out by (Ahmed and Nethercot, 1996) showed that all studs shared the longitudinal shear force in the interface between the concrete slab and the steel beam even for the studs located at the end of the shear span, but with different loading ratio.

Ren and Crisinel (1996) suggested the following equation:

$$k_s = \text{smaller}\begin{cases} \dfrac{0.6R_r}{\Delta_s} \\ \dfrac{0.6R_s}{\Delta_s} \end{cases} \tag{3.67}$$

where R_r and R_s are the resistances of the reinforced concrete slab and the shear connectors in the hogging moment region, respectively. Δ_s is the interface slip, taken as 0.5mm for 19x100mm welded shear connectors. The assumption of a constant slip value of 0.5mm for complete, full and all partial shear connection conditions is not compatible with the experimental and numerical results. Lawson (1989) found that this slip may have negligible value for full shear interaction, and lower values for some partial shear interaction cases at average working load. Therefore, the estimated stiffness of the shear connection may be unsafe.

Ahmed and Nethercot (1997) reviewed and assessed the available push-out test data of the load-slip behaviour of welded studs. They stated that the elastic tangential stiffness of a shear stud vary between 110 and 350 kN/mm at 45% of its load- carrying capacity. They suggested the following expression to calculate the stiffness of the shear connection:

$$k_s = 200 N_{sc} \tag{3.68}$$

where N_{sc} is the smaller number of studs in the hogging moment region or studs required for full interaction. The same expression was taken by (Gil and Bayo, 2008; Queiroz et al., 2009; Titoum et al., 2009) but with different values, ranging between 100 and 350 kN/mm for the stiffness of a stud. The assumption of a constant stiffness of the shear connector for all cases is not reasonable, since the stiffness of the shear connector is related to the diameter and length of shear connector as well as to the compressive strength of the surrounding concrete. Therefore, the adoption of constant value of 100kN/mm or 200kN/mm for all cases may overestimate or underestimate the actual stiffness. A practical chart to estimate the secant stiffness of a stud depending on the above considerations has been proposed and is described in Chapter Four.

Eurocode 4 (2004), Annex A.3, adopts the following expressions to calculate the stiffness of the shear connection, k_s.

$$k_s = \frac{N_{sc} k_{sc}}{v - \left(\frac{v-1}{1+\xi}\right)\frac{D_r}{d_s}} \text{ where } \quad v = \sqrt{\frac{(1+\xi) N_{sc} k_{sc} l d_s^2}{E_a I_a}} \ \& \ \xi = \frac{E_a I_a}{d_s^2 E_s A_s} \tag{3.69}$$

where E_r, A_r are the modulus of elasticity and area of reinforcement respectively. E_a, I_a are the modulus of elasticity and second moment of area of the steel beam respectively. l is the length of the beam adjacent to the connection in hogging bending.

d_s is the distance between the centroid of the beam's steel section and the centroid of the reinforcement. All other symbols are as defined previously.

These expressions are based on the procedure which had been developed by (Anderson et al., 2000). It was derived assuming cracked composite cross-sections and using the elastic interaction theory of a composite beam, making it unsuitable to extend into the post-linear range.

3.9.4.1. Proposed procedure to calculate the stiffness of the shear connection, k_s

The behaviour of a shear stud is generally defined by a non-linear load-slip curve which is obtained from a push-out test. Ollgaard et al. (1971) proposed one of the most cited analytical functions for a shear stud which can be used to model the behaviour of a shear stud in a composite connection. This exponential function takes the following general form:

$$\frac{F_{sc}}{F_{sc,max}} = \left(1 - e^{-\lambda s_{sc}}\right)^{\alpha} \tag{3.70}$$

where F_{sc} is the shear force acting on the stud connector; s_{sc} is the corresponding slip; α is a non-dimensional parameter (its value being 0.5-1.5). The value of the parameter λ is 0.5-2 mm^{-1}. $F_{sc,max}$ is the ultimate shear strength of a stud connector, which can be determined by the following equation, given by Eurocode 4 (2004) for a stud connector in a solid slab:

$$F_{sc,\max} = \min \begin{cases} 0.8 A_{sc} f_u \\ 0.37 A_{sc} \sqrt{f_{ck} E_c} \end{cases} \tag{3.71}$$

where, f_u, is the ultimate tensile strength of the shear stud; f_{ck} and E_c are the compressive strength and modulus of elasticity of concrete, respectively. A_{sc} is the cross-sectional area of the stud. Eq. (3.71) is multiplied by a factor, k_t, which ranges between 0.6 and 1.0 for a stud used with profiled steel sheeting. The details of calculating this factor are presented in (Eurocode 4, 2004) §6.6.4 The same forms of Eq. (3.70) were used by many researchers such as (Aribert and Labib, 1982; Aribert and Al Bitar, 1989; Razaqpur and Nofal, 1989; Johnson and Molenstra, 1991; Loh et al., 2004; Nie et al., 2004; Titoum et al., 2009; Vasdravellis et al., 2009) with different combinations of α and λ to model shear stud behaviour. Figure 3.19 shows some examples of these load–slip curves.

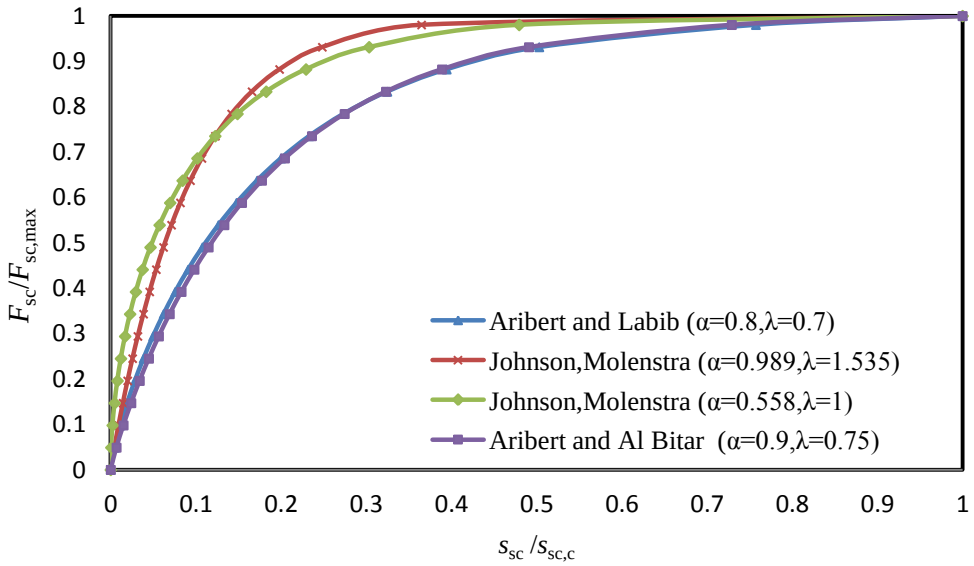

Figure 3.19: Load-slip curves for shear stud

The numerical study by (Ahmed and Nethercot, 1996) demonstrated that all studs in the shear span share the developed force, F_{shear}, in the interface between the concrete slab and the steel beam. Therefore, based on this study:

$$F_{shear} = \sum_{i=1}^{N_{sc}} F_{sc,i} \tag{3.72}$$

where N_{sc} is the number of studs in the shear span. All shear studs in the shear span are replaced by one equivalent shear stud which has the equivalent force, $F_{eq} = F_{shear}$ and equivalent slip, Δ_{eq}, then:

$$F_{eq} = k_s \Delta_{eq} \tag{3.73}$$

$$F_{eq} = F_{shear} = \sum_{i=1}^{N_{sc}} F_{sc,i} \tag{3.74}$$

$$F_{eq,max} = N_{sc} F_{sc,max} \tag{3.75}$$

Even though Eq. (3.70) was developed from push-out tests of a single or two shear connectors, it is still valid to simulate the group of shear connectors as the equivalent shear stud, since it has the same overall behaviour. Then:

$$\frac{F_{eq}}{N_{sc} F_{sc,max}} = \left(1 - e^{-\lambda \Delta_{eq}}\right)^{\alpha} \quad \text{and} \quad F_{eq} < N_{sc} F_{sc,max} \tag{3.76}$$

$$\left(\frac{F_{eq}}{N_{sc} F_{sc,max}}\right)^{\frac{1}{\alpha}} = 1 - e^{-\lambda \Delta_{eq}} \tag{3.77}$$

$$\Delta_{eq} = \frac{\ln\left[1-\left(\frac{F_{eq}}{N_{sc}F_{sc,max}}\right)^{\frac{1}{\alpha}}\right]}{-\lambda} \tag{3.78}$$

$$k_s = \frac{F_{eq}}{\Delta_{eq}} = -\frac{\lambda F_{eq}}{\ln\left[1-\left(\frac{F_{eq}}{N_{sc}F_{sc,max}}\right)^{\frac{1}{\alpha}}\right]} \tag{3.79}$$

In the current research the combination of α=0.8 and λ=0.7 mm^{-1} was used in all calculations when there was no information about the behaviour of studs, since this curve is close to the real behaviour of a 19mm diameter headed stud, as this stud was used in most experimental tests of composite connections. The ultimate shear strength of connector $F_{sc,max}$ was taken to be 120 kN if there was not enough data to calculate it from Eq. (3.71).

3.9.4.2. Estimation of F_{eq}

The rotational stiffness of a connection is always calculated for the average working load or where the moment–rotation curve of the connection can safely be assumed to be linear. This range is between 40% to 60% of the ultimate moment capacity of the connection. It was taken to be 50% of the maximum experimental moment of the composite connection by (Anderson and Najafi, 1994), while Ahmed and Nethercot (1997) assumed it to be 45% of the ultimate moment capacity. Based on this explanation, there are three requirements that must be satisfied in selecting the value of equivalent shear force, F_{eq}:

1. It should be in the level of moment where the moment–rotation curve of connection can be assumed to be linear up to this limit. In most cases, this limit is after the cracking of concrete and prior to the yield moment of the connection. Also, (Johnson and May, 1975; Lawson, 1989) found that the average working load of a shear connector is about 0.5 $F_{sc,max}$.

2. It should be ensured that this limit of moment is in the linear range of the moment–rotation curve. It was taken as 40-60% of the ultimate moment capacity of connection even when the linear range may be further then 60%.

3. It should be based on the force in the component which controls the behaviour of the connection in this range (i.e. the yield force in the reinforcing bar, $A_r f_{r,y}$, or the strength of the shear studs, $\sum F_{sc,max}$).

By studying the experimental results from (Li et al., 1996; Fu and Lam, 2006) for different reinforcement and partial shear connection ratios as shown in Table 3.5, it is clear that the yielding of reinforcement or the fracture of shear studs takes place after 50% of the maximum moment for all complete, full and partial shear connection ratios. Hence, it was decided to calculate the equivalent shear force, F_{eq}, as follows:

$$F_{eq} = \begin{cases} 0.5 N_{sc} F_{sc,max} & \text{for} \quad \eta < 1 \\ \dfrac{0.5}{\eta} N_{sc} F_{sc,max} & \text{for } \eta \geq 1 \end{cases} \qquad \text{where} \quad \eta = \frac{N_{sc} F_{sc,max}}{A_r f_{y,r}} \tag{3.80}$$

where η is the degree of the shear connection.

Table 3.5: Percentage of moment for the control components in composite connection

Test	Shear Connection Ratio η	Ultimate Moment (kN-m)	% of ultimate moment for the control components		Mode of failure
			Yield of Reinforcement	Fracture of Shear Studs	
CJS-1	≥300%	181.5	77%	>100%	Excessive deformation
CJS-2	≥300%	176	77%	>100%	Excessive deformation
CJS-3	≥300%	148.5	86%	>100%	Excessive deformation
CJS-4	≥300%	177.5	66%	>100%	Excessive deformation
CJS-5	≥300%	197.2	68%	>100%	Excessive deformation
CJS-6	≥300%	174	84%	>100%	Excessive deformation
CJ-1	271%	370	67%	>100%	Reinforcement fracture
CJ-2	155%	363	65%	>100%	Reinforcement fracture
CJ-3	78%	250	>100%	≤100%	Connector fracture
CJ-4	116%	368	73%	≤100%	Connector fracture
CJ-5	116%	363	92%	≤100%	Connector fracture
CJ-6	120%	425	67%	>100%	Reinforcement fracture
CJ-7	120%	274	71%	>100%	Reinforcement fracture

This value of the equivalent shear force will ensure that the above three requirements of the equivalent shear force are satisfied. The resulting equations for shear stiffness are:

$$k_s = \begin{cases} -\dfrac{0.5\lambda N_{sc} F_{sc,max}}{\ln\left[1-(0.5)^{\frac{1}{\alpha}}\right]} & \text{for} \quad \eta \le 1 \\ -\dfrac{\dfrac{0.5\lambda}{\eta} N_{sc} F_{sc,max}}{\ln\left[1-\left(\dfrac{0.5}{\eta}\right)^{\frac{1}{\alpha}}\right]} & \text{for} \quad \eta > 1 \end{cases} \tag{3.81}$$

Eq. (3.81) overcomes the shortcomings of Eq. (3.67) and Eq. (3.68) by considering the shear connection ratio in the calculation of shear stiffness.

3.9.4.3. Validity of the proposed procedure for, k_s

Five experimental composite connections (CJ1, CJ2, CJ3, CJ4 and CJ6) were selected from the experimental study on semi-rigid flush end-plate composite connections with steel beams and precast hollowcore slabs which were performed by (Fu and Lam, 2006). These samples represent the cases of complete interaction, full and partial shear connection respectively. The results of the shear stiffness calculations are listed in Table 3.6.

Table 3.6: Results of calculations

Test	Degree of shear connection %	Area of reinforc-ement (mm^2)	No. of studs	Final end slip (Test) (mm)	Mode of failure (Test)	k_s (kN/mm)				
						Proposed	Anderson & Najafi	Ahmed & Nethercot	Ren & Crisinel	EC 4
CJ1	271%	628	7	0.34	RF*	912	200	1400	402	237
CJ2	155%	628	4	0.8	RF	421	200	800	402	174
CJ3	78%	628	2	5.8	CF&SF	166	200	400	312	118
CJ4	116%	828	3	3.5	CF	274	200	600	402	148
CJ6	121%	800	4	0.84	RF	374	200	800	514	201

*RF-Reinforcement Fracture; CF-Connector Fracture; SF-Slab shear failure

Based on the degree of connection and mode of failure in the test, these results show clearly that (Anderson and Najafi, 1994)'s procedure underestimated the shear stiffness for most connections, as it did not take into account the effect of the shear connection ratio and used the same value for complete, full and partial shear connections, since the procedure depended on just the first shear connector for all cases. Ahmed and Nethercot

(1997)'s procedure overestimated the shear stiffness of all connections and estimate the same value for shear stiffness for CJ2 and CJ6, even though they have different shear connection ratios. This is because this procedure depended only on the number of studs, N_{sc}, and its stiffness, k_{sc}, and did not take into account the effect of the partial shear connection ratio. The assumption of constant slip (0.5mm) by (Ren and Crisinel, 1996)'s procedure leads to the estimation of a higher stiffness of the full shear connection (i.e. CJ6) than for a complete interaction (i.e. CJ1). The experimental results indicated that this estimation was not valid, since the end slip in CJ6 was more than twice the end slip in CJ1. Also, the results give the same stiffness for CJ4 and CJ1, even though the experimental failure mode showed that the failure of the CJ4 connection occurred due to the shear failure of the connection, while the failure of CJ1 connection took place because of the fracture of reinforcement. The Eurocode 4 (2004) procedure underestimated the shear connection stiffness for all connections. Furthermore, the stiffness of CJ2 is lower than the stiffness of CJ6, which is not consistent with the experimental results for the final slip of these connections. The proposed procedure can predict the actual differences in the shear stiffness of the connection due to the variation of the shear connection ratios.

3.10. Validation of the proposed expression for the rotational stiffness of a composite connection

The proposed expression for calculating the rotational stiffness of a composite connection was validated using the test results from many published papers. These tests can be divided into three groups of flush end-plate composite connections. These groups include:

1. a conventional flush end-plate connected to an H-section steel column with metal deck flooring and solid concrete slabs as in (Anderson and Najafi, 1994; Xiao et al., 1994; Li et al., 1996; Liew et al., 2000)'s tests;

2. a flush end-plate connected to a square hollow steel column filled concrete with metal deck flooring and solid concrete slabs as in (Loh et al., 2006)'s tests; and

3. a flush end-plate connected to H-section steel column with precast hollowcore slab as in (Fu and Lam, 2006) tests.

Two comparisons were carried out as follows:

1. the test results were compared with the results from the proposed expression (i.e. Eq. (3.51)) of rotational stiffness of a composite connection using the calculated values of k_r and k_s, by:

   i. the Eurocode 4 procedure;

   ii. the procedure in Section 3.9.3 to calculate k_r and the proposed procedure in Section 3.9.4 to calculate k_s.

   The results of comparison are shown in Figure 3.20 and Figure 3.21.

2. the same test results were compared with the calculated values of rotational stiffness using:

   i. the results from the proposed expressions in (1(ii)) above;

   ii. (Anderson and Najafi, 1994) expressions;

   iii. (Ren and Crisinel, 1996) expressions; and

   iv. (Ahmed and Nethercot, 1997) expressions.

The results of comparison are shown in Figure 3.22 and Figure 3.23. Table 3.7 lists the final procedures which were adopted in the proposed expression to calculate the rotational stiffness of flush end-plate composite connections.

Table 3.7: Adapted procedures for parameters

k_b	k_c		$k_r = \frac{E_r A_r}{l_r}$ / l_r		k_s	
	k_{cws}	k_{cwc}	Eurocode 4	Proposed	Eurocode 4	Proposed
Eq. (3.19) or 155 kN/mm	Eq. (3.57)	Eq. (3.58)	Annex A, §A.2.1.1, Table (A.1)	Eq. (3.61)	Eq. (3.69)	Eq. (3.81)

3.10.1. Results and conclusions

It can be seen from Figure 3.20 and Figure 3.21 that the proposed expressions to calculate the stiffness of the steel reinforcement, k_r, and the stiffness of the shear connection, k_s, can give better results than the results using the calculated values of k_s and k_r from the Eurocode 4 procedure. However, the difference is minimal but the proposed procedure is simpler. Moreover, the procedure proposed to calculate the stiffness of the shear connection, k_s, in elastic range can be extended easily to calculate the stiffness of the shear connection at any stage of loading where the Eurocode 4 procedure is applicable only to the elastic range, since it is based on the elastic interaction theory of composite beams.

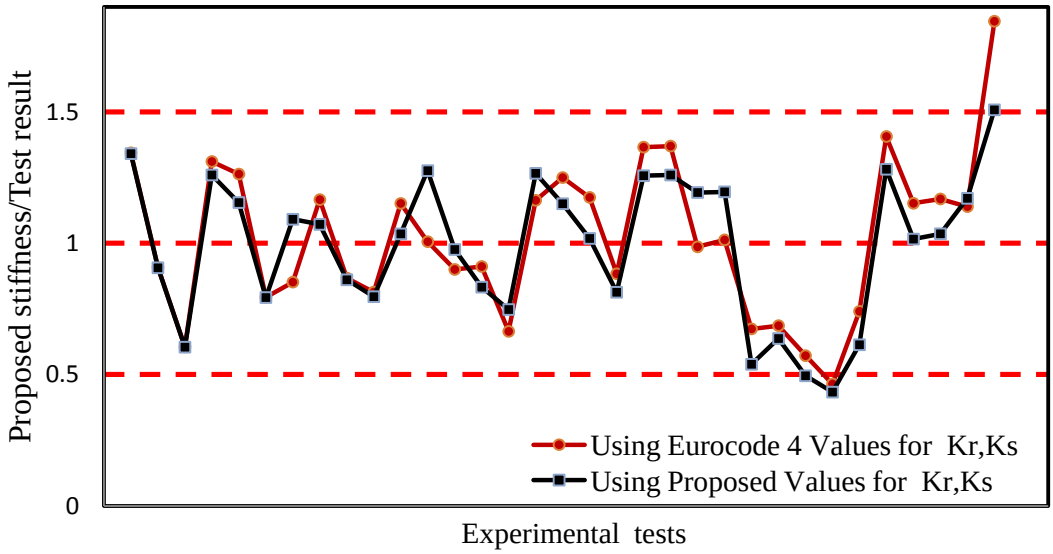

Figure 3.20: Comparison of results using the proposed and Eurocode 4 procedures to calculate k_s and k_r

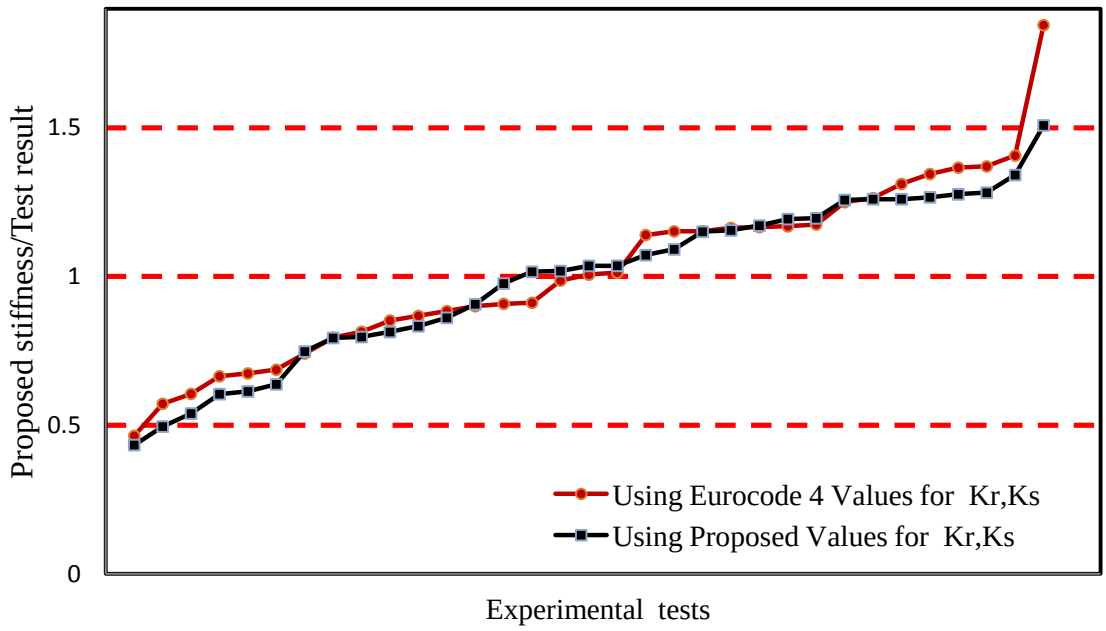

Figure 3.21: Comparison of results using the proposed and Eurocode 4 procedures to calculate k_s and k_r (after sorting the results in ascending order)

Table 3.8: Comparison of predicted and experimental results

Reference	Test	K_b kN/mm	K_c kN/mm	$S_{j,c}$ kN/mm (Test)	Eurocode 4 Procedure (1)		Proposed Procedure (2)		$S_{j,c}$ (kN/mm) Proposed Using		$S_{j,c}$/Test	
					K_r kN/mm	K_s kN/mm	K_r kN/mm	K_s kN/mm	Eurocode 4 Values (1)	Proposed Values (2)	(1)/T	(2)/T
Li et al. (1996)	CJS-1	155	1008	31	1509	866	760	1961	41.7	41.57	1.34	1.34
	CJS-2	155	373	28	1509	866	760	1961	25.4	25.38	0.91	0.91
	CJS-3	155	373	42	1509	866	760	1961	25.4	25.38	0.61	0.6
	CJS-4	155	1008	33	1509	960	760	1961	43.3	41.57	1.31	1.26
	CJS-5	155	1008	36	1509	1112	760	1961	45.5	41.57	1.26	1.15
	CJS-6	155	373	32	1509	866	760	1961	25.4	25.38	0.79	0.79
Xiao et al. (1994)	SCJ-3	155	1140	29	446	183	238	1045	24.7	31.64	0.85	1.09
	SCJ-4	155	1140	49	2250	624	1201	662	57.1	52.51	1.17	1.07
	SCJ-5	155	1140	61	2250	535	1201	662	52.9	52.51	0.87	0.86
	SCJ-6	155	1140	65	2250	535	1201	639	52.9	51.77	0.81	0.8
	SCJ-7	155	1140	50	2696	606	1439	588	57.6	51.78	1.15	1.04
Anderson and Najafi (1994)	S4F	155	1301	35	884	291	472	936	35.2	44.67	1.01	1.28
	S8F	155	1301	55	1769	463	944	740	49.5	53.69	0.9	0.98
	S12F	155	1301	66	2653	608	1416	617	60.2	54.96	0.91	0.83
	S8FD	155	1305	141	1769	425	944	740	93.7	105.4	0.66	0.75
Liew et al. (2000)	SCCB1	155	1094	36	1781	369	944	555	41.9	45.58	1.16	1.27
	SCCB2	155	1094	60.1	3958	1023	2099	1047	75.1	69.14	1.25	1.15
	SCCB3	155	1094	84	5541	1930	2938	1627	98.7	85.53	1.17	1.02
	SCCB4	155	1094	85	3958	1023	2099	1047	75.1	69.14	0.88	0.81
	SCCB5	155	1094	55	3958	1023	2099	1047	75.1	69.14	1.37	1.26
	SCCB6	155	1124	55.5	3958	1023	2099	1047	76	69.92	1.37	1.26
Fu and Lam (2006)	CJ1	155	3125	90	868	237	330	912	88.8	107.4	0.99	1.19
	CJ2	155	3125	74	868	175	330	421	74.9	88.48	1.01	1.2
	CJ3	155	3125	90	868	118	120	166	60.7	48.52	0.67	0.54
	CJ4	155	3125	100	868	149	191	274	68.6	63.72	0.69	0.64
	CJ5	155	3125	120	868	149	159	274	68.6	59.45	0.57	0.5
	CJ6	155	3125	180	1106	202	262	374	83.6	77.98	0.46	0.43
	CJ7	155	3125	70	553	92	76	187	51.9	42.94	0.74	0.61
Loh et al. (2006)	CJ1	155	2683	37	1600	405	842	391	52	47.42	1.41	1.28
	CJ2	155	2683	38.3	1600	266	842	211	44.1	38.9	1.15	1.02
	CJ3	155	2683	33.3	1600	189	842	141	38.9	34.5	1.17	1.04
	CJ4	155	2683	32.5	800	182	421	257	37	38.06	1.14	1.17
	CJ5	155	2683	40	2400	828	1263	647	73.8	60.31	1.85	1.51
										Average	1.02	0.99
										Stdev.	0.30	0.28

Table 3.8 and Table 3.9, Figure 3.22 and Figure 3.23 indicate that (Anderson and Najafi, 1994)'s procedure underestimated the rotational stiffness of the composite connection for most cases, while Ren and Crisinel (1996)'s procedure overestimated the rotational stiffness for many cases. This means that these methods represent the lower and upper bound of rotational stiffness. Ahmed and Nethercot (1997)'s procedure gave a better agreement with the test results than the other procedures for many cases, but it overestimated the rotational stiffness for some cases. However, the expression proposed to calculate the rotational stiffness of a composite connection associated with the proposed procedure to calculate the stiffness of shear connection can predict well the rotational stiffness of a composite connection for most cases. In addition, comparison with the other procedures shows that the proposed procedure has the best average ratio, standard division and absolute error ratio (0.99, 0.28 and 0.23 respectively). The differences for some cases can be related to the assumptions made in calculating the effective length of reinforcement, since all other procedures show the same trend for these cases. Also, all of the procedures underestimated the rotational stiffness of the group of tests carried out by (Fu and Lam, 2006), since these tests incorporated recent precast concrete hollowcore slabs which may require modified procedures to calculate the stiffness of its components.

In summary, besides the generality of the proposed model for bare steel and composite connections, the other merit of the proposed procedure is its ability to be extended further than the linear range of the moment-rotation curve of connection using the proper component stiffness values for the non-linear range.

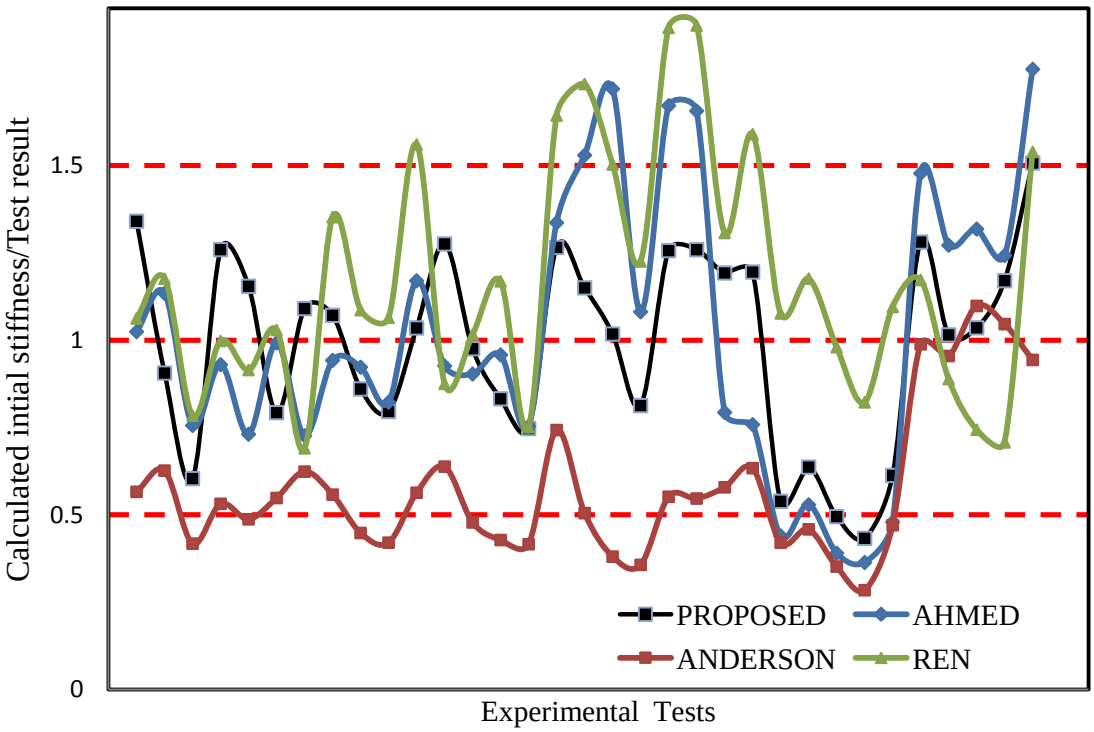

Figure 3.22: Comparison of the proposed procedure with other procedures to calculate the rotational stiffness of a flush end-plate composite connection

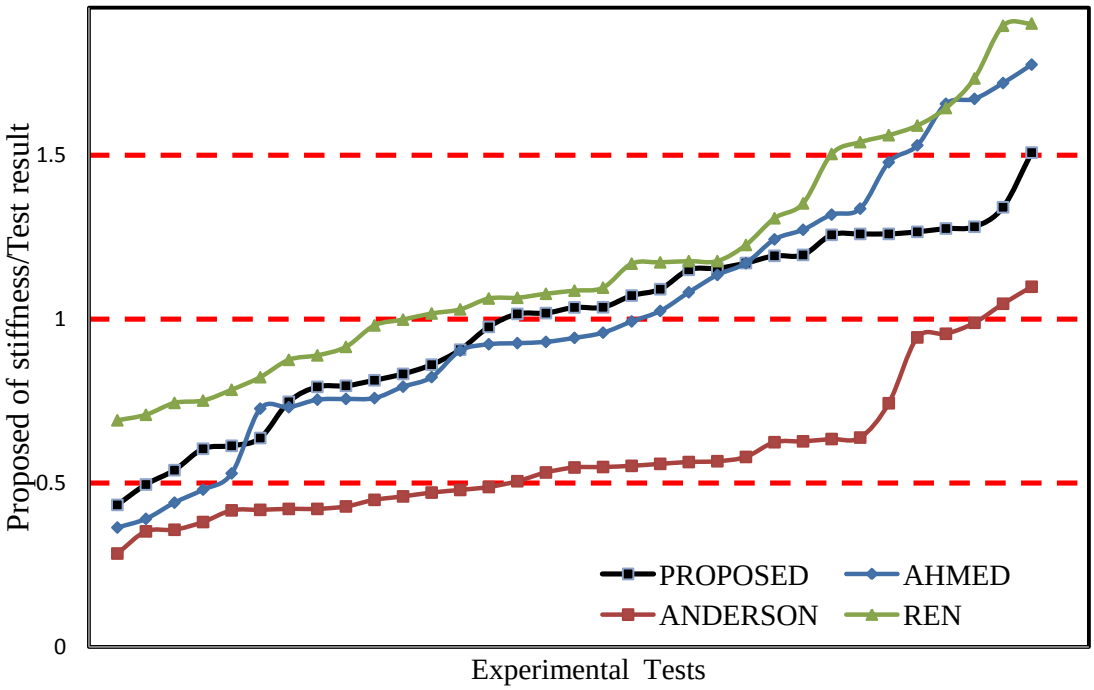

Figure 3.23: Comparison of the proposed procedure with other procedures to calculate the rotational stiffness of a flush end-plate composite connection (after sorting the results in ascending order)

Table 3.9: Comparison of predicted and other methods

Reference	Test	$S_{j,c}$ kN/mm	$S_{j,c}$ kN/mm				Ratio				Abs(Error)/T			
			Proposed (P)	Ahmed and Nethercot (1997)	Anderson and Najafi (1994)	Ren and Crisinel (1996)	(P)/T	(1)/T	(2)/T	(3)/T	P/T	(1)/T	(2)/T	(3)/T
Li et al. (1996)	CJS-1	31	41.57	31.77	17.56	32.95	1.04	1.02	0.57	1.06	0.34	0.02	0.43	0.06
	CJS-2	28	25.38	31.77	17.56	32.95	1.17	1.13	0.63	1.18	0.09	0.13	0.37	0.18
	CJS-3	42	25.38	31.77	17.56	32.95	1.51	0.76	0.42	0.78	0.4	0.24	0.58	0.22
	CJS-4	33	41.57	30.71	17.56	32.95	1.26	0.93	0.53	1	0.26	0.07	0.47	0
	CJS-5	36	41.57	26.32	17.56	32.95	1.15	0.73	0.49	0.92	0.15	0.27	0.51	0.08
	CJS-6	32	25.38	31.77	17.56	32.95	0.79	0.99	0.55	1.03	0.21	0.01	0.45	0.03
Xiao et al. (1994)	SCJ-3	29	31.64	21.08	18.11	20.04	1.09	0.73	0.62	0.69	0.09	0.27	0.38	0.31
	SCJ-4	49	52.51	46.19	27.36	66.29	1.07	0.94	0.56	1.35	0.07	0.06	0.44	0.35
	SCJ-5	61	52.51	56.32	27.36	66.29	0.86	0.92	0.45	1.09	0.14	0.08	0.55	0.09
	SCJ-6	65	51.77	53.49	27.36	69.23	0.8	0.82	0.42	1.07	0.2	0.18	0.58	0.07
	SCJ-7	50	51.78	58.54	28.19	78.05	1.04	1.17	0.56	1.56	0.04	0.17	0.44	0.56
Anderson and Najafi (1994)	S4F	35	44.67	32.43	22.35	30.65	1.28	0.93	0.64	0.88	0.28	0.07	0.36	0.12
	S8F	55	53.69	49.71	26.33	55.94	0.98	0.9	0.48	1.02	0.02	0.1	0.52	0.02
	S12F	66	54.96	63.26	28.28	77.16	0.83	0.96	0.43	1.17	0.17	0.04	0.57	0.17
	S8FD	141	105.42	106.34	58.73	105.96	0.75	0.75	0.42	0.75	0.25	0.25	0.58	0.25
Liew et al. (2000)	SCCB1	36	45.58	48.13	26.76	59.18	1.27	1.34	0.74	1.64	0.27	0.34	0.26	0.64
	SCCB2	60.1	69.14	91.95	30.37	104.22	1.15	1.53	0.51	1.73	0.15	0.53	0.49	0.73
	SCCB3	84	85.53	144.48	32	126.3	1.02	1.72	0.38	1.5	0.02	0.72	0.62	0.5
	SCCB4	85	69.14	91.95	30.37	104.22	0.81	1.08	0.36	1.23	0.19	0.08	0.64	0.23
	SCCB5	55	69.14	91.95	30.37	104.22	1.26	1.67	0.55	1.89	0.26	0.67	0.45	0.89
	SCCB6	55.5	69.92	91.95	30.37	105.54	1.26	1.66	0.55	1.9	0.26	0.66	0.45	0.9
Fu and Lam (2006)	CJ1	90	107.37	71.44	52.15	117.68	1.19	0.79	0.58	1.31	0.19	0.21	0.42	0.31
	CJ2	74	88.48	56.16	46.92	117.68	1.2	0.76	0.63	1.59	0.2	0.24	0.37	0.59
	CJ3	90	48.52	39.61	37.89	96.95	0.54	0.44	0.42	1.08	0.46	0.56	0.58	0.08
	CJ4	100	63.72	52.93	45.91	117.68	0.64	0.53	0.46	1.18	0.36	0.47	0.54	0.18
	CJ5	120	59.45	46.89	42.29	117.68	0.5	0.39	0.35	0.98	0.5	0.61	0.65	0.02
	CJ6	180	77.98	65.54	51.27	148.08	0.43	0.36	0.28	0.82	0.57	0.64	0.72	0.18
	CJ7	70	42.94	33.59	32.95	76.71	0.61	0.48	0.47	1.1	0.39	0.52	0.53	0.1
Loh et al. (2006)	CJ1	37	47.42	54.7	36.58	43.4	1.28	1.48	0.99	1.17	0.28	0.48	0.01	0.17
	CJ2	38.3	38.9	48.74	36.58	34.06	1.02	1.27	0.96	0.89	0.02	0.27	0.04	0.11
	CJ3	33.3	34.5	43.91	36.58	24.79	1.04	1.32	1.1	0.74	0.04	0.32	0.1	0.26
	CJ4	32.5	38.06	40.4	34.02	23.01	1.17	1.24	1.05	0.71	0.17	0.24	0.05	0.29
	CJ5	40	60.31	71.05	37.76	61.59	1.51	1.78	0.94	1.54	0.51	0.78	0.06	0.54
						AVER.	0.99	1.02	0.58	1.17	0.23	0.31	0.43	0.28
						Std.Dev	0.28	0.39	0.21	0.34	0.15	0.23	0.19	0.25
						Max	1.51	1.78	1.10	1.9	0.57	0.78	0.72	0.90
						Min	0.43	0.36	0.28	0.69				

Chapter Four

Prediction of the load-slip behaviour of a stud shear-connector

4.1. Background

The stiffness, strength and ultimate slip capacity of a stud shear-connector are essential properties in the analysis and design of composite beams and connections with full or partial shear interaction. These parameters can be estimated from push-out tests. These test data are not always available in practice, and a set of empirical equations are used which may give unsafe or overly conservative values of stiffness. All of the available experimental and numerical studies clearly indicated that the strength and stiffness of a stud shear-connector are related. In addition, all of these properties are related to the diameter of the stud and the compressive strength of the concrete (Oehlers and Coughlan, 1986). Therefore, a simple and practical method for predicting the load-slip behaviour of stud shear-connectors incorporating these factors is highly desirable. One such model has been developed in this study which is based on the experimental and numerical results of the initial stiffness available in the literature. The complete load-slip model was also compared with other test data that are available in the literature for different diameters of shear studs and concrete compressive strength.

4.2. Current procedures to estimate the essential properties of a stud shear-connector

In most composite construction calculations, the strength, stiffness and slip capacity of a stud shear-connector are necessary. Both strength and stiffness are fundamental in calculating the initial stiffness of composite beam or connection. Only the strength of a stud shear-connector is required to find the moment capacity. Slip capacity is essential to estimate the rotation capacity or ductility. However, all of the above are necessary to investigate the whole behaviour of a composite beam or connection from the start of applying load until the point of failure. The current procedures to calculate each of the above properties are as follows:

4.2.1. Strength of the shear connector, $F_{sc,max}$

Eurocode 4 (2004) §6.6.3.1 presents two formulae for determining the maximum strength of the shear connector, $F_{sc,max}$.

$$F_{sc,max}/\gamma_v = \text{smaller of} \begin{cases} 0.8 f_u \left(\frac{\pi d^2}{4}\right) \\ 0.37\alpha\sqrt{f_{ck}E_{cm}}\left(\frac{\pi d^2}{4}\right) \end{cases} \quad \text{where} \quad \alpha = \begin{cases} 0.2\left(h_{sc}/d + 1\right) & \text{for } 3 \le h_{sc}/d \le 4 \\ 1 & \text{for } h_{sc}/d > 4 \end{cases} \tag{4.1}$$

It is clear that the first equation is dominated when the ultimate tensile strength of the material of a stud shear-connector, f_u, controls the behaviour of a shear connector (i.e. shear failure), but this value should not be greater than 500 N/mm^2 for a solid slab and 450 N/mm^2 for a slab with profiled steel sheeting, as stated by (Eurocode 4, 2004) §6.6.3.1 and §6.6.4.2. Conversely, the second equation is dominated when the characteristic cylindrical compressive strength of the concrete, f_{ck}, and its corresponding modules of elasticity, E_{cm}, are determining factors for failure, typically the failure of the concrete around the connector (i.e. bearing failure). The reduction factor (α) is taken to account for the ratio of the height (h_{sc}) to diameter (d) of a shear connector and its value ranges (0.8-1). Most shear studs were used in composite building have, $h_{sc}/d>4$. Therefore, the reduction factor (α) is equal to unity.

Rocha et al. (2012) studied the influence of concrete strength and stud diameter variation on the reduction factor. The results from this study are summarized in Figure 4.1. It can be seen that (Eurocode 4, 2004)'s equation underestimates the reduction factor for high strength concrete. In addition, Figure 4.2 shows the variation of α with h_{sc} for constant (d=19 mm) and the variation of α with d for constant (h_{sc}=45 mm). It is clear that the reduction factor (α) is more influenced by height than by diameter. This behaviour can be interpreted as follows (see Figure 4.3): as the shear stud is subjected to the force transferred from the beam, the concrete around the shear stud is in bearing stress and the maximum stress is at the base of shear stud. As the load increases, the slip occurs between the steel beam and the slab. Also, the concrete at the base of the shear stud will become plastic, causing the shear stud to rotate. The resistance to this rotation comes from the bending moment, M_B (see Figure 4.3), which correlates directly with the height of the shear stud, h_{sc}. This moment plays a role of transferring some of the stress from the plastic zone at the base of the shear stud to the adjacent nonplastic zone.

This behaviour will increase the ability of the shear stud to resist greater loads before the concrete fails.

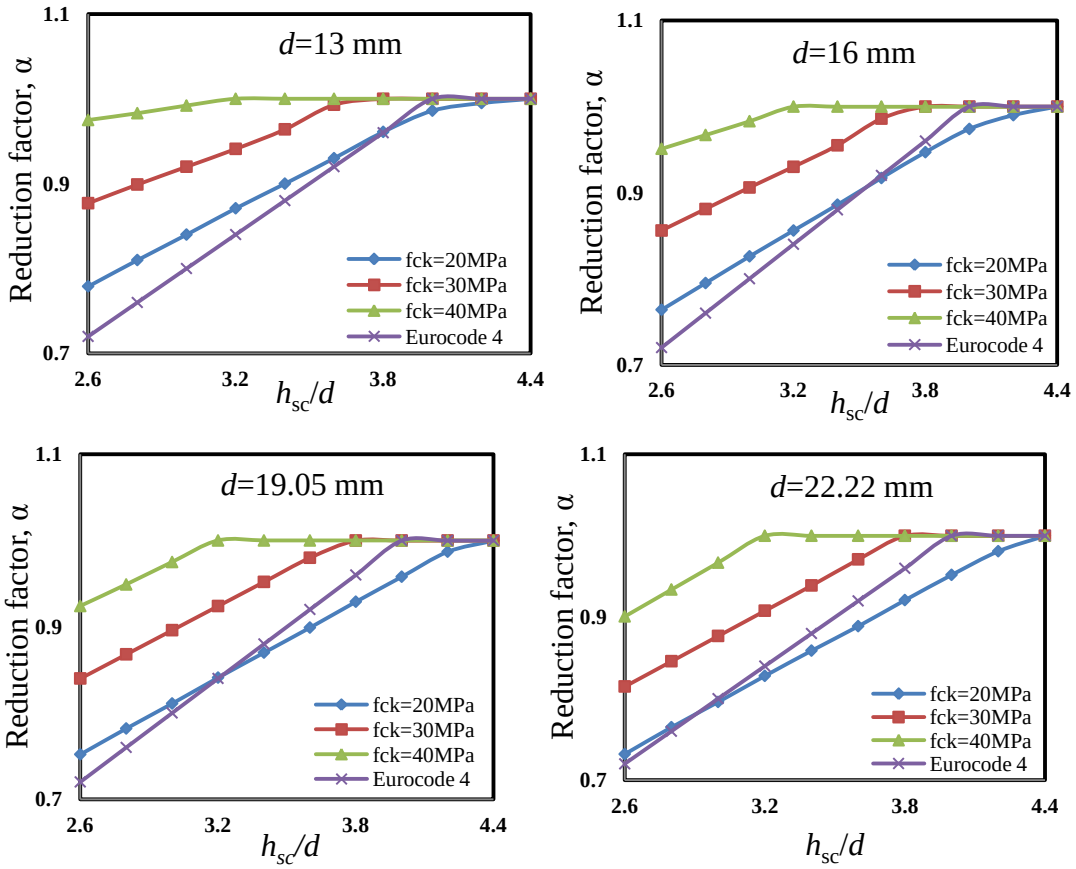

Figure 4.1: Variation of α with h_{sc}/d for constant diameters of shear stud

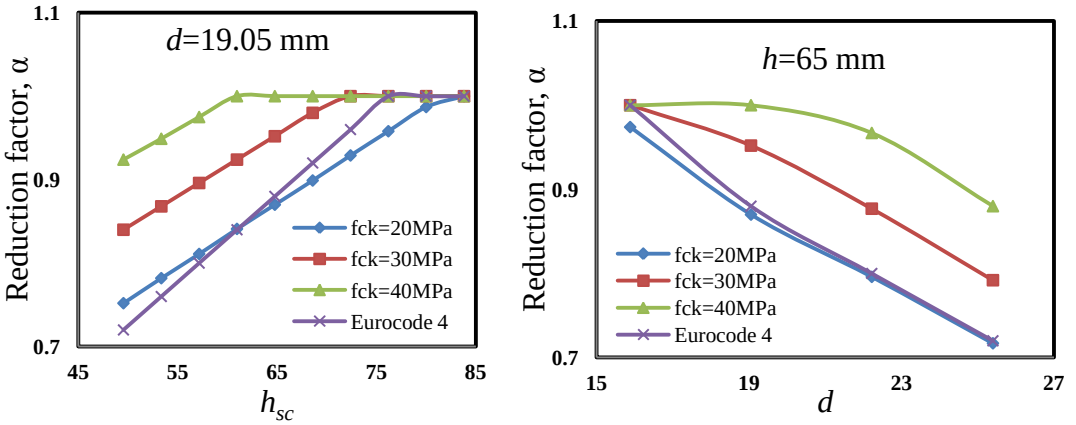

Figure 4.2: Variation of α with h_{sc} or d for constant diameters or heights of the shear stud

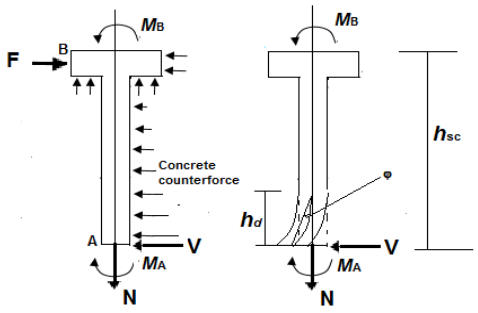

Figure 4.3: Forces and deformation of shear stud

In addition, Eq. (4.1) is multiplied by a factor k_t, which ranges between 0.6 and 1.0 for a stud used in a slab with profiled steel sheeting. The details of calculating this factor are presented in (Eurocode 4, 2004) §6.6.4. The partial safety factor for shear connection, γ_v, is taken as 1.25.

4.2.2. Stiffness of a shear stud connector, k_{sc}

4.2.2.1. Assumed constant value of k_{sc}

All of the previous experimental and numerical work by many researchers indicated clearly that the stiffness of a shear stud is related to the compressive strength of the concrete and the diameter of the shear stud, as in the works of (Ollgaard et al., 1971; Oehlers and Coughlan, 1986; Mottram and Johnson, 1990; Lam and El-Lobody, 2005; Xue et al., 2009; Wang et al., 2011; Xue et al., 2012). However, in many other works the stiffness of a shear stud was calculated or assumed unrelated to the compressive strength of the concrete.

A value of 200 kN/mm was assumed by (Anderson and Najafi, 1994) to compute the initial rotational stiffness of a flush end-plate composite connection for four experimental cases with different compressive strengths of concrete. The same value was also taken by (Gil and Bayo, 2008). Also, Al-Jabri (2004) used the same value in his component-based model to estimate the initial rotational stiffness of flexible end-plate connection at elevated temperatures.

Based on the assessment of many experimental and numerical works by several researchers, Ahmed and Nethercot (1997) stated that the shear stiffness of the shear connector can range between 110 kN/mm and 350 kN/mm; however, no guidance was given for adopting a specific value from the above range. They adopted a value of 200 kN/mm to calculate the initial rotational stiffness for the 32 cases of flush end-plate composite connections with different shear connectors that they investigated and

compressive strengths of concrete. Based on the previous range, Queiroz et al. (2009) assumed a value of 350 kN/mm in their two-dimensional FE model for the evaluation of composite beams. Eurocode 4 (2004) (Annex A) allows the assumption of an approximate value of (100 kN/mm) for headed studs with 19mm diameter when no push-out test data is available.

The above discussion indicates clearly the necessity for guidelines to choose certain values of shear stiffness or strength for the shear stud from the above range or a procedure to calculate it depending on its properties or the properties of the surrounding concrete.

4.2.2.2. Equations to calculate the value of k_{sc}

Based on the analysis of 116 push-out tests, Oehlers and Coughlan (1986) suggested the following empirical equation to calculate the stiffness of a stud shear-connector, assuming that the load-slip behaviour is nearly linear up to 0.5 $F_{sc,max}$.

$$k_{sc} = \frac{F_{sc,max}}{(0.16 - 0.0017 f_{cm})d} \tag{4.2}$$

where $F_{sc,max}$ is the maximum strength of the stud shear-connector in N/mm^2, d is the diameter of the shear connector in mm and the (f_{cm}) is the mean compressive strength of the surrounding concrete which ranged from 20 to 70 N/mm^2. Shim et al. (2004) stated that the value of 0.16 in Eq. (4.2) should be replaced by 0.08 and 0.24 to obtain the lower and upper limits of the characteristic stiffness, respectively. Eq. (4.2) can be rewritten in the form:

$$k_{sc} = \gamma F_{sc,max} \tag{4.3}$$

It is clear from Figure 4.4 that factor γ ranges from 0.4 to 12 (1/mm) for the compressive strength of concrete with ($20 < f_{cm} < 90$) in N/mm^2. The empirical equation may overestimate or underestimate the actual value of stiffness of the shear connector, especially for low or high strength concrete.

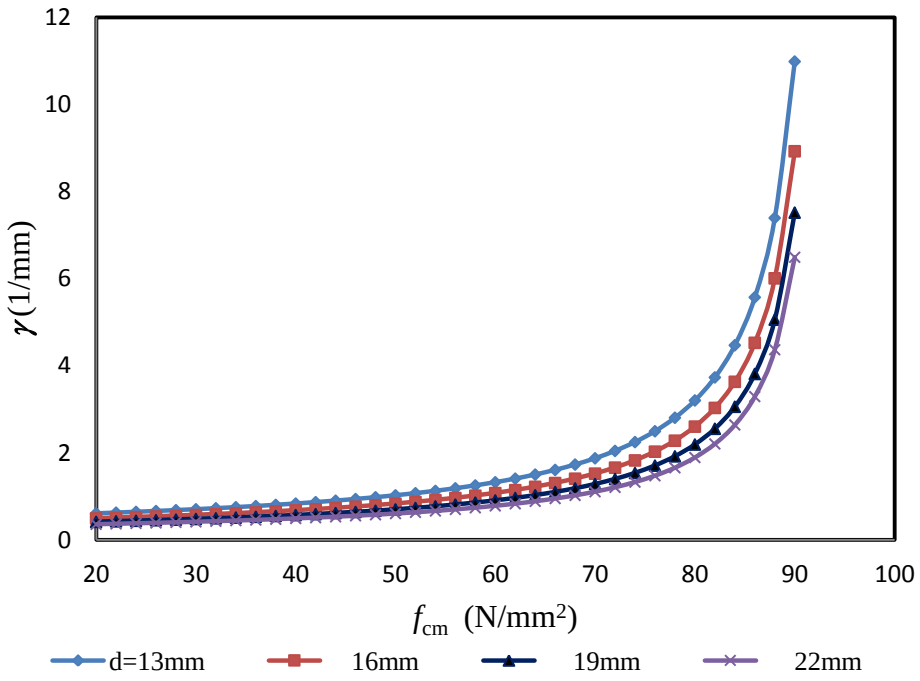

Figure 4.4: Values of γ for different compressive strengths of the surrounding concrete

Wang (1998) presented a practical procedure to estimate the stiffness of a stud shear-connector as the secant stiffness at the shear connector design strength ($0.8F_{sc,max}$) with an equivalent slip of 0.8 mm. Liew et al. (2000) presented a similar procedure but with ($0.6F_{sc,max}$) and limited the slip to 0.5 mm to calculate the stiffness of the stud shear-connector:

$$k_{sc} = 1.2F_{max,sc} \tag{4.4}$$

Nie et al. (2004) proposed a similar equation to estimate the shear connector stiffness as:

$$k_{sc} = 0.66F_{max,sc} \tag{4.5}$$

The assumption of a constant slip for all conditions is not compatible with the experimental and numerical studies, since the slip of a shear connector in the elastic range may vary from negligible to more than 0.8 mm. Therefore, this assumption may unsafely underestimate or overestimate the stiffness of stud shear-connectors in some cases.

4.2.3. Empirical equations to estimate slip capacity, $S_{sc,c}$

Oehlers and Coughlan (1986) defined the slip capacity of a stud shear-connector as the slip at failure when the peak load has reduced by 5%. Based on an analysis of 53 push-out tests with different stud diameters and compressive strengths of concrete, they established the following empirical equation to estimate the slip capacity (in mm) of a shear stud:

$$S_{sc,c} = (0.453 - 0.0018 f_c)d \tag{4.6}$$

They also stated that the mean of the experimental slip capacity was 0.34*d*. Furthermore, they proposed the following empirical equation to estimate the slip at ultimate load capacity as:

$$S_{sc,u} = (0.389 - 0.0023 f_c)d \tag{4.7}$$

A number of researchers adopted the above empirical equations to estimate the ultimate slip and slip capacity of a stud shear in their studies such as (Johnson and Molenstra, 1991; Shim et al., 2004; Titoum et al., 2009).

Xue et al. (2008) conducted thirty push-out tests on stud shear-connectors to investigate the effects of stud diameter and height and concrete strength on the stud failure mode. They proposed the following empirical equation to estimate the slip capacity:

$$S_{sc,c} = h_d \tan\varphi \tag{4.8}$$

where h_d is the bending deflection height of the shear stud, which is about 0.18–0.33 times of the height of the shear stud (h_{sc}) and φ ranges between 27-35° for the stud shank failure and 55-65° for the concrete failure. The selection of φ depends on the expected mode of failure (Eq. (4.1)). If the concrete controls the behaviour of the shear stud, the average value of φ (i.e. 60^0) will be selected. The average adopted value of φ for stud shank failure is 31^0.

4.3. Proposed approach

4.3.1. Basic relations

The load-slip curve of shear connectors is generally nonlinear. Johnson and May (1975) found that it was too difficult to find a reliable formula for the shear connector stiffness due to the scattering of test results and there are too many parameters which affect its

magnitude. The proposed approach is based on the definition of the shear stud stiffness given by Johnson and May (1975) - as the secant stiffness at half the ultimate load of the shear connector. Empirical equations developed by (Ollgaard et al., 1971; Gattesco and Giuriani, 1996; Gattesco et al., 1997) were used to model the typical load-slip curves of a stud shear-connector in the present work. It is also based on the experimental and numerical results on the shear capacity of headed shear studs carried out by (Ollgaard et al., 1971; An and Cederwall, 1996; Gattesco and Giuriani, 1996; Kim et al., 2001; Shim et al., 2004; Dai and Liao, 2005; Lam and El-Lobody, 2005; Ellobody and Young, 2006; Lam, 2007; Xue et al., 2008) in order to select an appropriate model to calculate the stiffness of shear connector. The four most practical dimensions of shear connectors (i.e.13mmx65mm, 16mmx85mm, 19mmx100mm and 22mmx100mm) have been used in this study to construct a set of design charts. The collection of the experimental data is comprised of tests conducted by different researchers with different set-ups. As a result, the slip capacity shows high degree of scatter depending on when the tests were stopped in a particular situation. In the absence of detailed information of the test procedure, a maximum slip value of 0.34*d* was adopted in the current study for all of the experimental data which was the mean slip value suggested by (Oehlers and Coughlan, 1986). Moreover, the emphasis of the present study is on the initial stiffness and the maximum load capacity of the shear studs, for which a slip capacity of 0.34 *d* will be sufficient.

4.3.2. Methodology

The following steps were used to construct a design chart for the strength and secant stiffness for different values of shear stud diameter.

Step 1: Draw all available load-slip curves for each diameter with different compressive strength of concrete, as shown in Figure 4.5 to Figure 4.8.

Step 2: The most cited analytical model of stud shear-connector behaviour which was proposed by (Ollgaard et al., 1971) was used to construct the typical load-slip curves. The model is as follows:

$$\frac{F_{sc}}{F_{sc,max}} = \left(1 - e^{-\beta S_{sc}}\right)^{\alpha} \tag{4.9}$$

As explained in Chapter Three (Section 3.9.4.1), Aribert and Labib (1982) presented a combination of α=0.8, β=0.7 mm^{-1}. Johnson and Molenstra (1991) provided another two combinations of α=0.558, β=1.0 mm^{-1} and α=0.989, β=1.535 mm^{-1}.

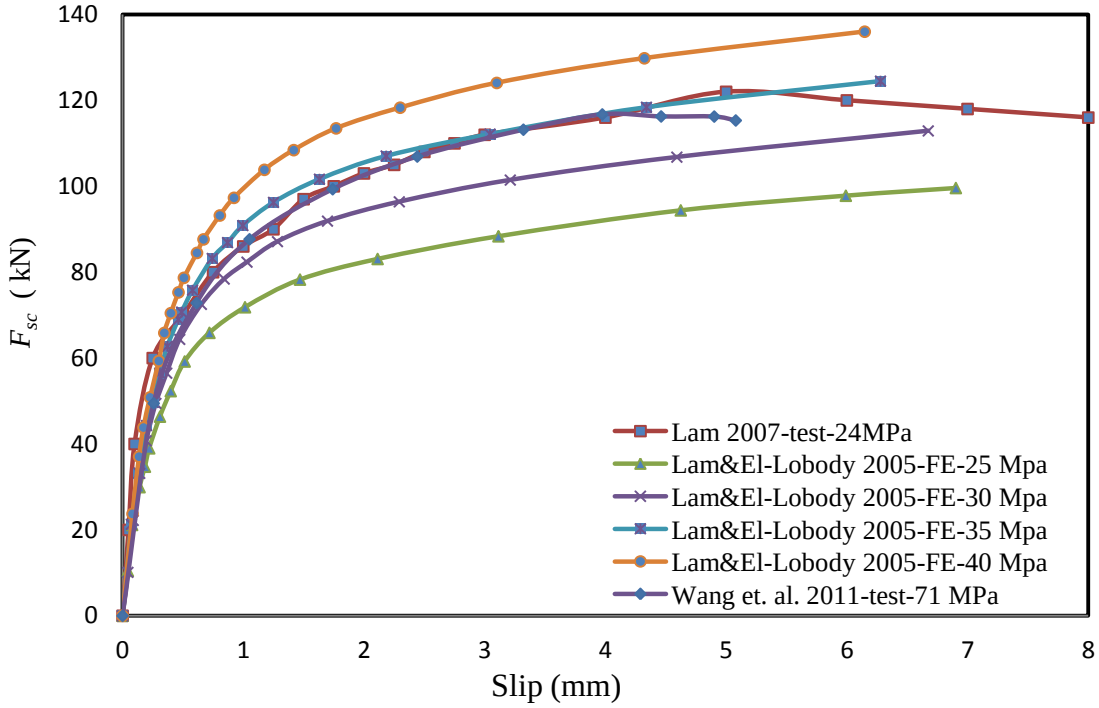

Figure 4.5: Load-slip curves (experimental and numerical) of studs

(22 mm diameter, 100mm high**)** for different compressive strength of concrete

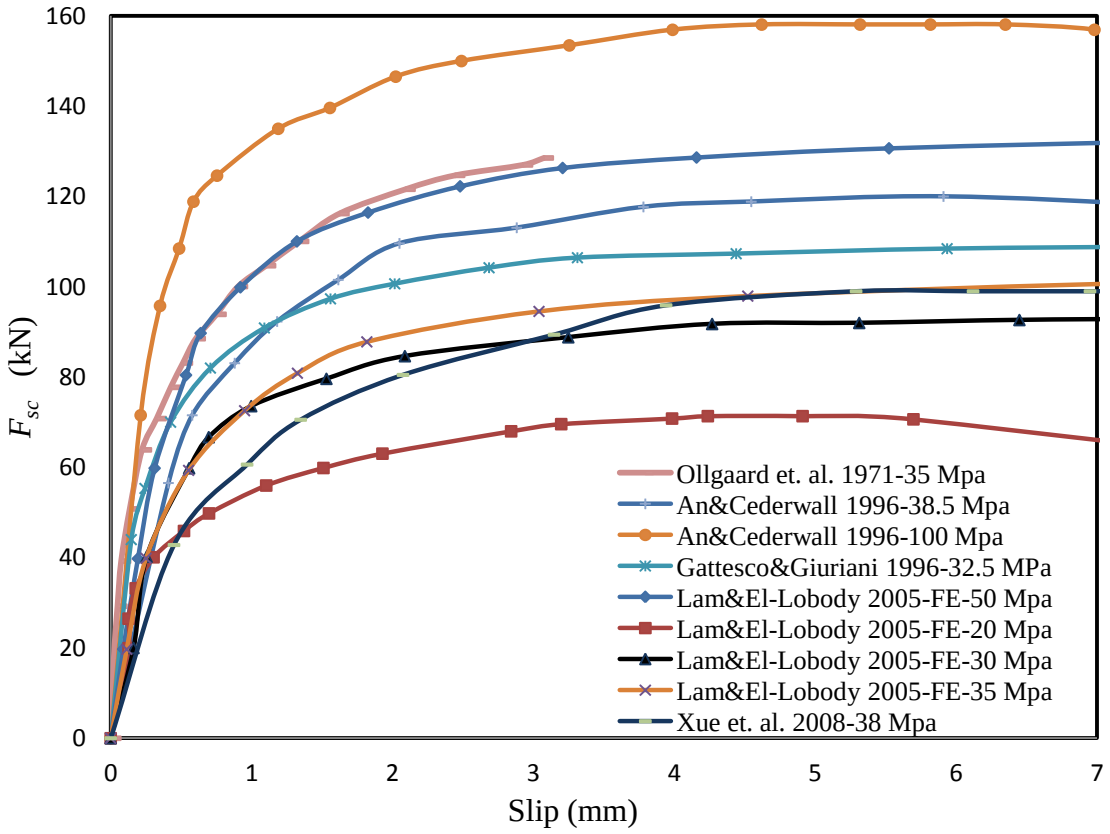

Figure 4.6: Load-slip curves (experimental and numerical) of studs

(19 mm diameter, 100mm high**)** for different compressive strength of concrete

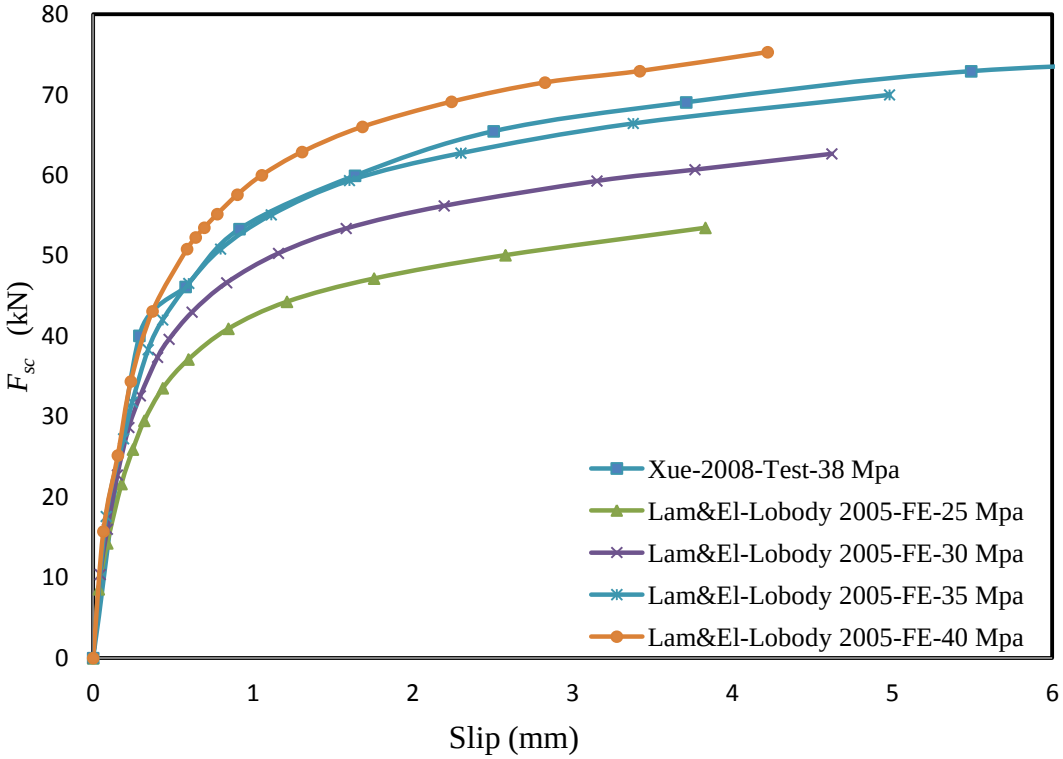

Figure 4.7: Load-slip curves (experimental and numerical) of studs (16 mm diameter, 85 mm high**)** for different compressive strength of concrete

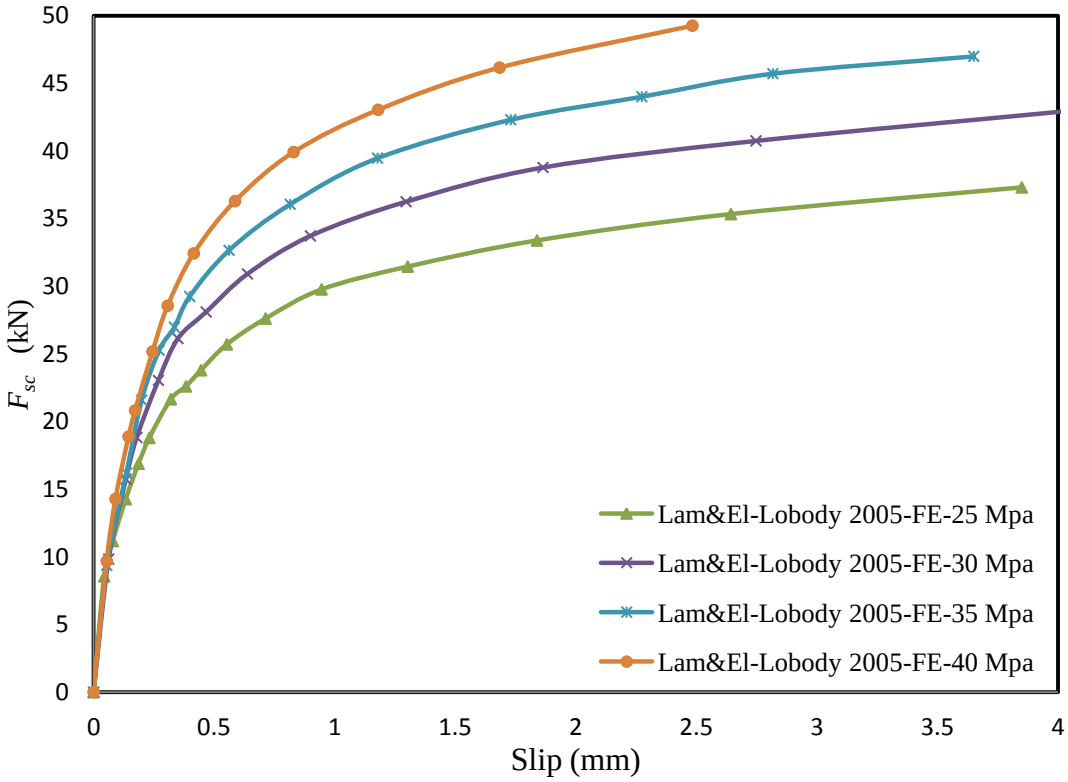

Figure 4.8: Load-slip curves (experimental and numerical) of studs (13 mm diameter, 65 mm high**)** for different compressive strength of concrete

Based on an experimental study on shear connectors subjected to cyclic loading, Gattesco and Giuriani (1996) proposed the following equation to simulate the behaviour of the shear connector with α=0.97, β=1.3 mm^{-1} and γ=0.0045 mm^{-1}:

$$\frac{F_{sc}}{F_{sc,max}} = \alpha\sqrt{\left(1-e^{-\beta S_{sc}/\alpha}\right)} + \gamma s_{sc} \qquad (4.10)$$

In this study, four combinations of (α, β) were used to determine an optimum model for capturing the actual behaviour of a shear connector, particularly in the elastic range. These models are:

Model 1: Eq. (4.10) with α=0.97, β=1.3 mm^{-1} and γ=0.0045 mm^{-1}

Model 2: Eq. (4.9) with α=0.558, β=1.0 mm^{-1}

Model 3: Eq. (4.9) with α=0.989, β=1.535 mm^{-1}

Model 4: Eq. (4.9) with α=0.8, β=0.7 mm^{-1}

It should be noted that there are many other empirical relationships (An and Cederwall, 1996; Xue et al., 2008) which are in between the curves for Model-1 and Model-4. The normalised experimental and numerical load-slip curves with the selected models are shown in Figure 4.9 to Figure 4.12.

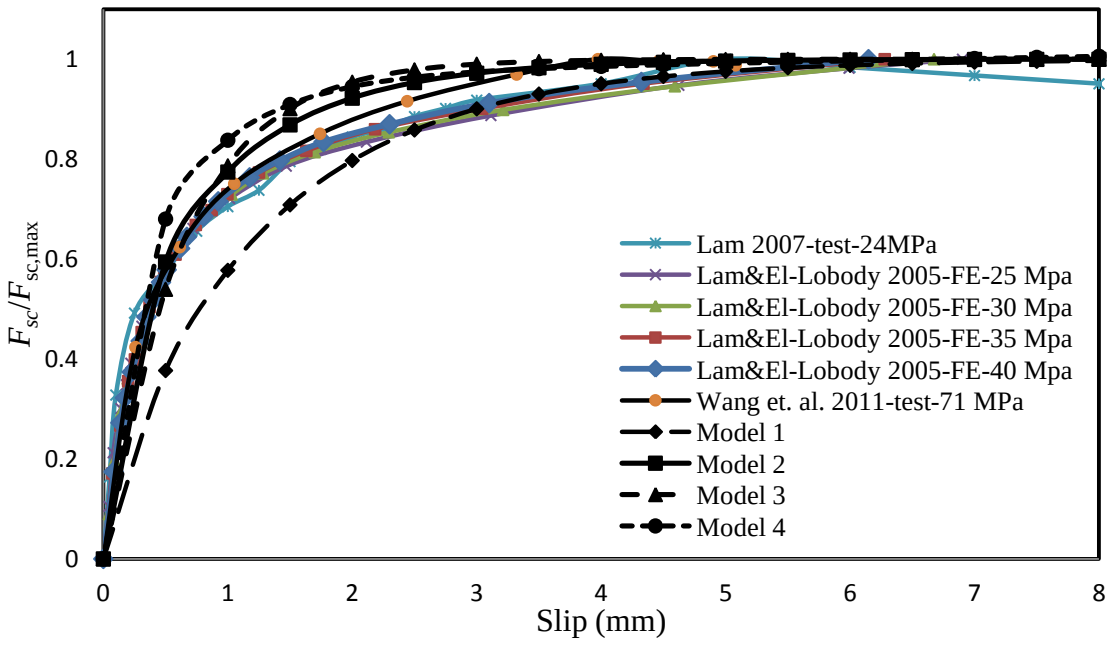

Figure 4.9: Comparison of experimental and numerical curves for different compressive strength of concrete across four models (d=22mm)

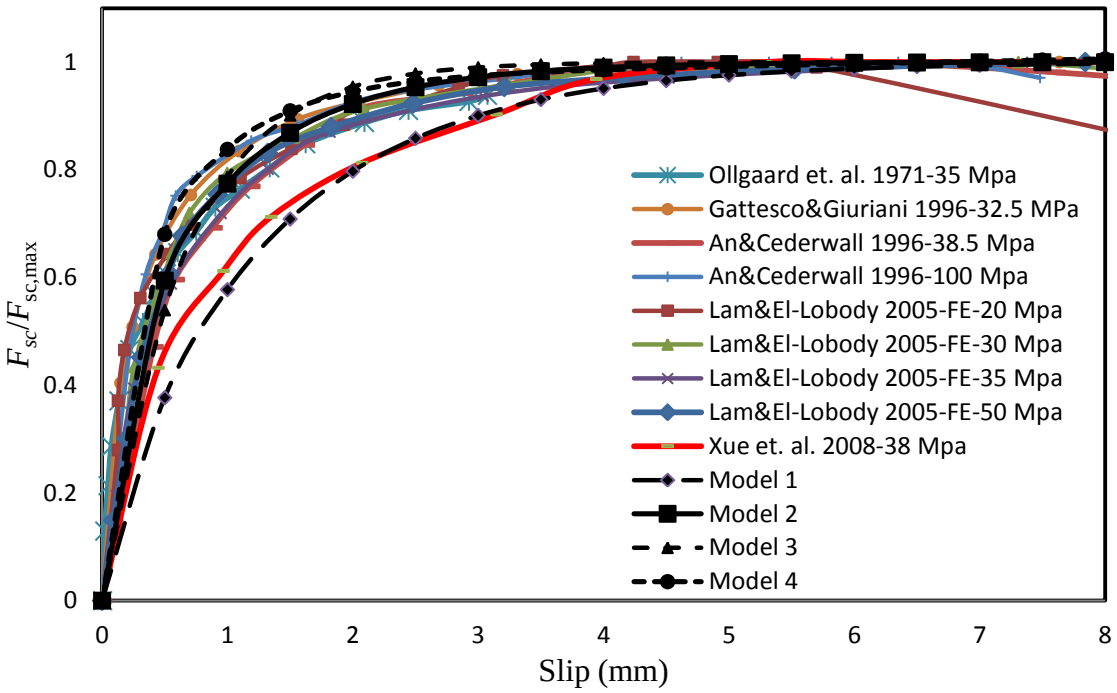

Figure 4.10: Comparison of experimental and numerical curves for different compressive strength of concrete across four models (*d*=19mm**)**

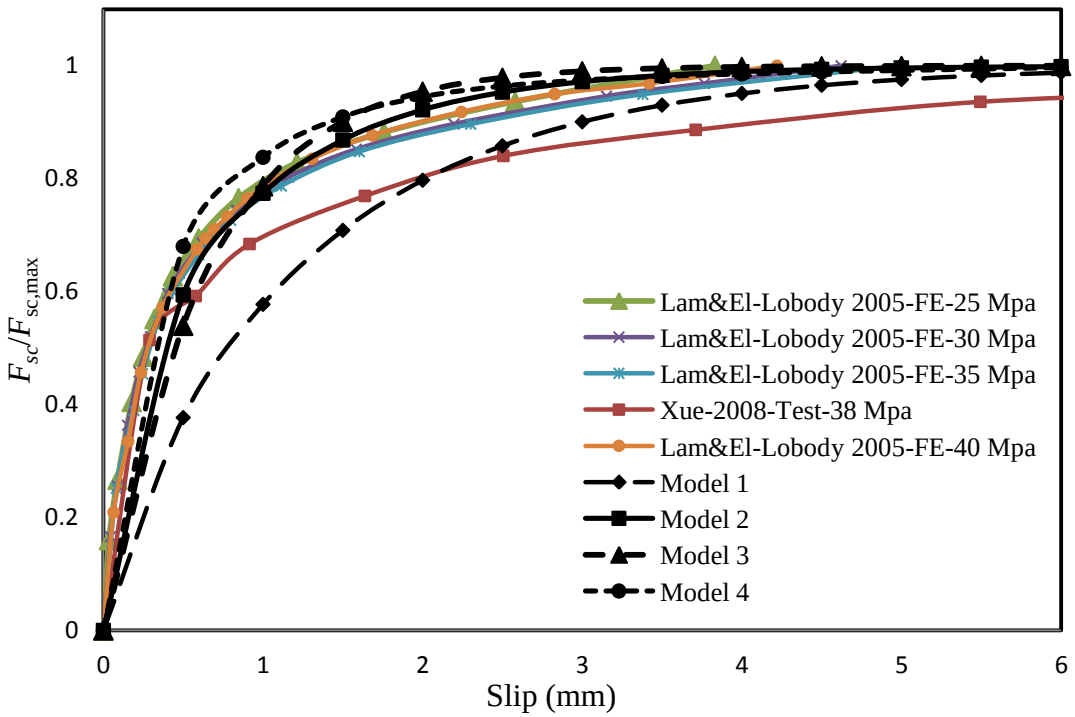

Figure 4.11: Comparison of experimental and numerical curves for different compressive strength of concrete across four models (*d*=16mm**)**

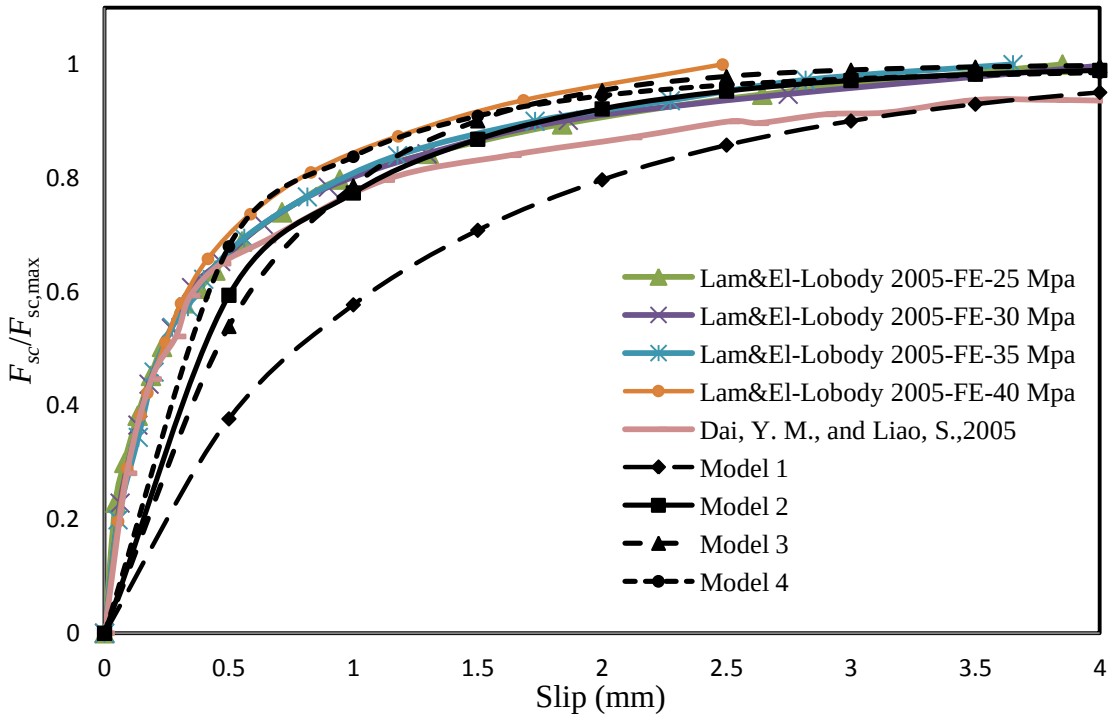

Figure 4.12: Comparison of experimental and numerical curves for different compressive strength of concrete across four models (*d*=13mm**)**

It can be seen clearly from the above figures that Model-1 and Model-4 represent the lower and upper bound respectively and Model-2 is the best model for all the cases which have been investigated, particularly in the elastic range.

Step 3: The best model (Model-2) and Eq. (4.1) were used to construct the proposed practical chart to estimate the strength and stiffness of shear connectors.

4.3.3. Strength of a stud shear-connector

The boundary between the stud shank mode failure and concrete mode failure can be determined as follows:

(i) BSI (2005) §6.1.7(b) states that "the minimum ultimate tensile strength of the material of a headed stud is usually specified in the UK as 495 N/mm^2''.

(ii) Eurocode 4 (2004) §6.6.3. 1(1) states that "the specified ultimate tensile strength of the material of the stud '' should not be greater than 500 N/mm^2.

Therefore, the limiting value of the cylindrical compressive strength of concrete can be calculated as follows:

$$0.8 f_u A_{sc} = 0.37 \alpha A_{sc} \sqrt{(f_{ck})_{control} E_{cm}} \rightarrow \sqrt{(f_{ck})_{control} E_{cm}} = \frac{2.16 f_u}{\alpha} \qquad (4.11)$$

There are many procedures to calculate the modulus of elasticity of concrete based on its compressive strength, such as the formulas given in ACI code, BS 8110 (BSI 1997) and Eurocode 2 (2004). The Eurocode 2 (BS EN 1992-1-1:2004) relationship is as follows:

$$\because E_{cm}\ (\text{MPa}) = 22000\left[f_{cm}/10 \right]^{0.33} = 22000\left[(f_{ck}+8)/10 \right]^{0.33} \qquad (4.12)$$

$$\sqrt{(f_{ck})_{control} \times 22000 \times \left[\left((f_{ck})_{control} + 8 \right)/10 \right]^{0.33}} = \frac{2.16 f_u}{\alpha} \qquad (4.13)$$

Also, the curve fitting of the left side of Eq. (4.13) for the whole range of compressive strength of concrete results:

$$(f_{ck})_{control} \approx \left(\frac{f_u}{56\alpha} \right)^{1.6} \qquad (4.14)$$

$$\text{If} \quad (f_{ck})_{actual} \begin{cases} \leq (f_{ck})_{control} \Rightarrow \text{Concrete failure mode} \Rightarrow F_{sc,\max} = 0.37 \alpha \sqrt{f_{ck} E_{cm}} \left(\frac{\pi d^2}{4} \right) \\ > (f_{ck})_{control} \Rightarrow \text{Stud shank failure mode} \quad F_{sc,\max} = 0.8 f_u \left(\frac{\pi d^2}{4} \right) \end{cases}$$

It is clear from Eq. (4.14) that the mode of stud failure (i.e. the shear connector shearing off or failure of the concrete) depends on the tensile strength of the shear connector. Ollgaard et al. (1971) analysed statistically the test data of his push-out tests in addition to a number of other investigations. It was found that an upper bound to the shear connector strength is approached when $\sqrt{f_{ck} E_c} \approx 897 \text{MPa}$ and E_c was calculated using the ACI formula. This experimental relation gives the estimation of $f_{ck} \approx 28$ MPa, which corresponds to $f_u \approx 450$ MPa. This experimental result is compatible with Eq. (4.14).

From Eq. (4.14):

$$\text{If} \quad f_u \leq 500\text{MPa} \quad \Rightarrow \quad (f_{ck})_{control} \simeq 34\text{MPa} \quad \Rightarrow \quad (f_{cu})_{control} \simeq 43.4\text{MPa}$$

4.3.4. Secant stiffness of a stud shear-connector

The shear stiffness of a stud shear-connector is calculated as follows:

$$\frac{F_{sc}}{F_{sc,max}} = \left(1 - e^{-\beta S_{sc}}\right)^{\alpha} \qquad \Rightarrow \qquad s_{sc} = \frac{\ln\left(1 - \left(\frac{F_{sc}}{F_{sc,max}}\right)^{\frac{1}{\alpha}}\right)}{-\beta} \tag{4.15}$$

As noted in Section 4.3.1, the present work is based on Johnson and May (1975)'s definition of the stud shear-connector stiffness as the secant stiffness at half the ultimate load of the shear connector:

$$k_{sc} = \frac{0.5F_{sc,\max}}{s_{sc}} = \frac{-0.5\beta F_{sc,\max}}{\ln\left(1-(0.5)^{\frac{1}{\alpha}}\right)} \tag{4.16}$$

$$k_{sc} = \begin{cases} 1.47F_{sc,\max} & \text{using} \quad \text{Model}-2 \quad \text{for} \quad \alpha = 0.558,\ \beta = 1.0\ \text{mm}^{-1} \\ 1.12F_{sc,\max} & \text{using} \quad \text{Model}-3 \quad \text{close to Eq.(4.4)} \\ 0.64F_{sc,\max} & \text{using} \quad \text{Model}-4 \quad \text{close to Eq.(4.5)} \end{cases} \tag{4.17}$$

The results from Eq. (4.17) using the combinations of (α, β) for model-2, were used to construct a practical chart to the estimate strength and stiffness of stud shear-connectors, as shown in Figure 4.13. For a lower concrete strength (f_{cu}-control zone at the left) the stiffness and strength both are governed by concrete failure. Whereas for higher concrete strength ($f_{u,sc}$-control zone at the right), the stiffness is governed by the properties of stud material (shown by dashed horizontal lines).

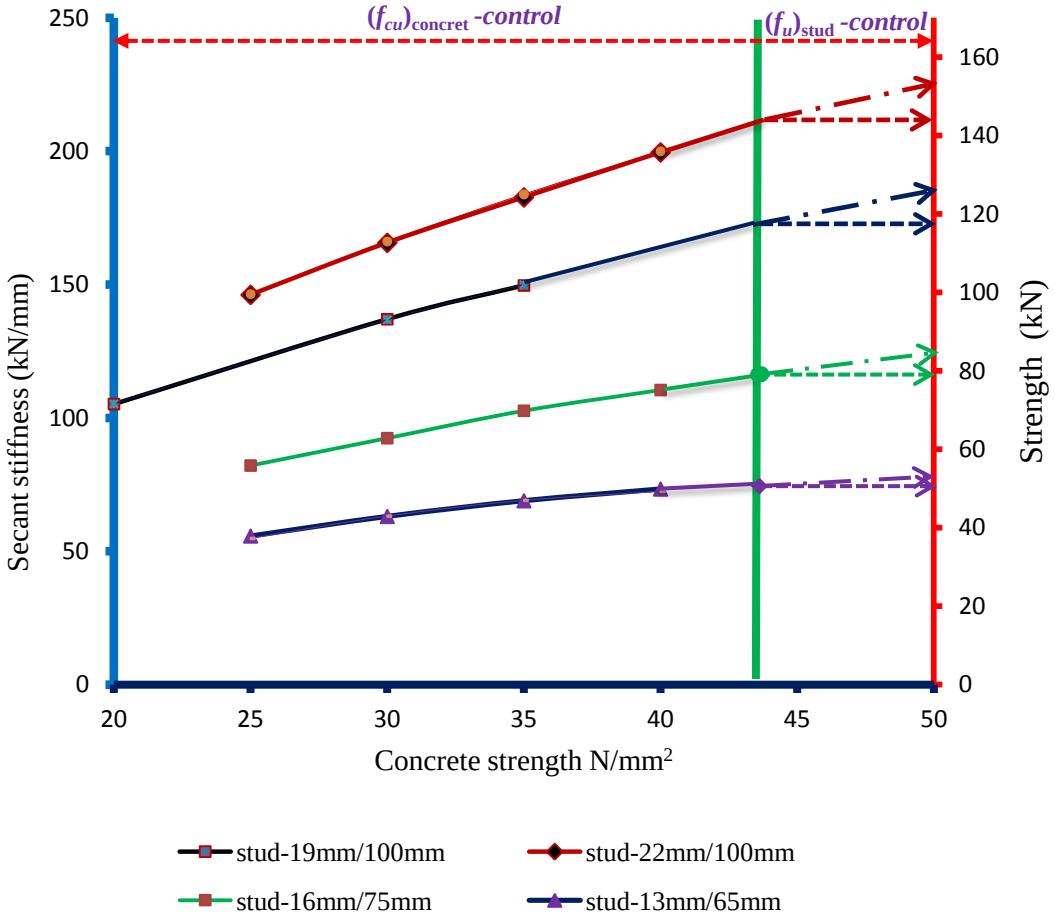

Figure 4.13: Secant stiffness-strength-concrete strength relationship for stud shear-connector with different d/h_{sc}

4.4. Validity of the proposed chart for larger diameters of shear connector

Shim et al. (2004) conducted push-out tests on studs with 25, 27, and 30 mm of diameter to investigate the static behaviour of large studs which are beyond the scope of current design codes. The shear stiffness of the stud shear-connector, which was calculated using the empirical equation (i.e. Eq. (4.2)), was in the range of 25-50% of the test results. The proposed chart in Figure 4.13 was used to find the stiffness and strength of the stud shear-connector for the above diameters by constructing parallel lines at an appropriate level in the chart, as shown in Figure 4.14. The values from the proposed chart were compared with the average of the push-out test results; and a good agreement was found which is summarised in Table 4.1. It is clear from the results in the table that the proposed chart can predict the strength and stiffness of the shear connector, even for large diameters.

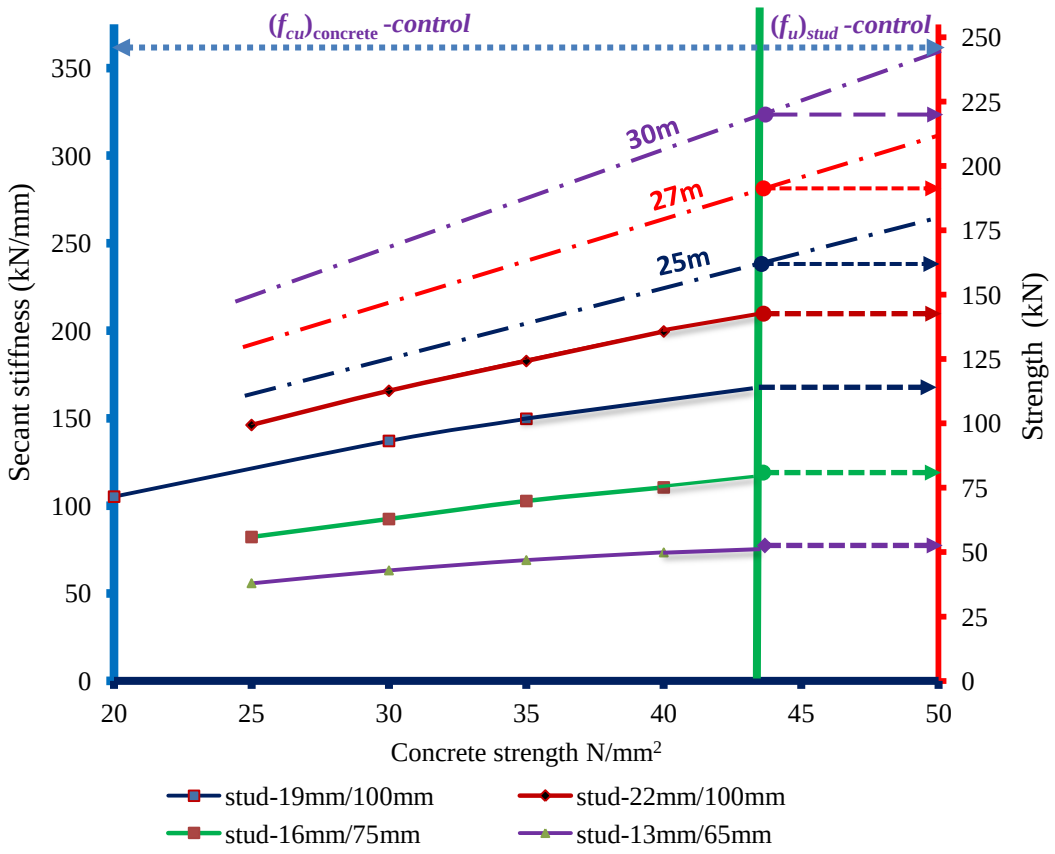

Figure 4.14: Secant stiffness-strength-concrete strength relationship for large shear stud connectors

Table 4.1: Summary of results

Stud diameter (mm)	Concrete strength (MPa)	Average stud strength (kN)			Average stud stiffness (kN/mm)				
		Test	Proposed chart	EC-4	Test	Proposed chart	Eq. (4.2)	Eq. (4.4)	Eq. (4.5)
25	35.4	156	160	167	275	245	78	200	110
25	49.3	180.1	181	167	366.3	290	96	200	110
27	35.4	186.3	190	195	341.7	290	75	234	129
27	64.5	211.2	215	195	304	330	155	234	129
30	35.4	191.9	215	240	292.5	300	70	288	159
30	64.5	232.3	240	240	290	325	154	288	159

4.5. Multi-linear model of the load-slip curve for the shear connector

For numerical analysis of composite beams and connections, a simple and accurate load-slip curve for the shear connector must be assumed in advance. The accuracy of the numerical analysis depends to a large extent on this assumed load-slip curve, especially for the partially interaction cases in which the shear connector behaviour

plays the main role in the whole behaviour of composite beams and connections. Queiroz et al. (2009) assumed a multi-linear model for stud shear-connectors with ($F_{sc,max}$=128.7 kN) in their finite element parametric study for the evaluation of composite beams. This model is shown in Figure **4.15**.

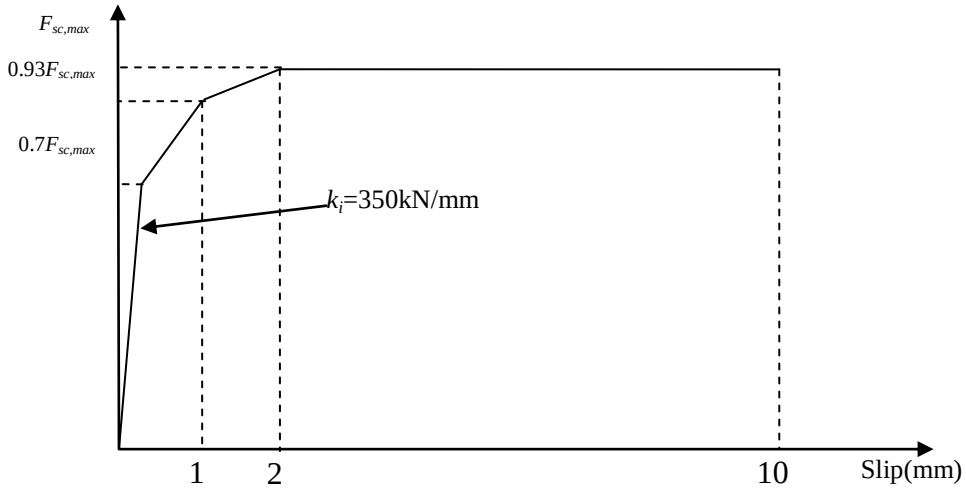

Figure 4.15: Multi-linear model ($F_{sc,max}$=128.7 kN) by (Queiroz et al., 2009)

The assumed high initial stiffness (350 kN/mm) and constant values of slip at different levels of load in this model were due to the difference in the behaviour of the studs in a composite beam from those in a push-out test. They also found from a 2D FE model that the difference in various load-slip curves has insignificant effect on the behaviour of beams in the hogging moment region.

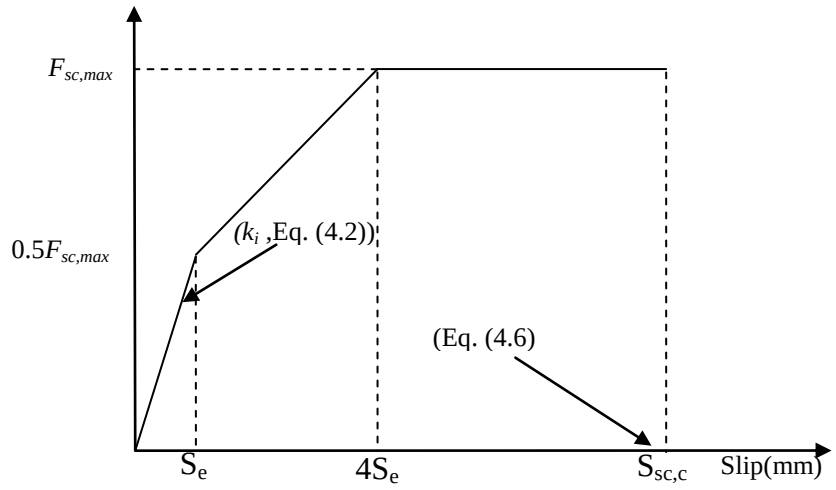

Figure 4.16: Tri-linear model by (Titoum et al., 2008)

Titoum et al. (2008) proposed a tri-linear model for a stud shear-connector, to be used in their 2-D finite element approach to analyse semi-continuous composite beams with partial shear connection, as shown in Figure 4.16. The model was based on Eq. (4.2) to calculate the initial stiffness of a stud shear-connector and the slip at ultimate load. However, this equation may overestimate or underestimate the stiffness for many cases, as explained in Section 4.2.2.2.

In the present work, a multi-linear model of the load-slip curve of a shear connector was constructed using the proposed chart in Figure 4.13 to find the initial stiffness ($k_{sc,i}$), and strength ($F_{sc,max}$) of the shear connector. Then, using Model-2 (Eq. (4.9)), the post-yield stiffness ($k_{sc,p-1}$) of the shear connector was calculated. In addition, based on the study of Wang (1998), it was assumed that the maximum load for the second part of the multi-linear curve was the design strength of the shear connector ($0.8F_{sc,max}$). The post-limit stiffness for the second part of the multi-linear curve, $k_{sc,p-1}$, can be calculated as follows:

$$F_{sc} / F_{sc,\max} = (1 - e^{-s_{sc}})^{0.558} \Rightarrow s_{sc} = -\ln\left(1 - \sqrt[0.558]{F_{sc} / F_{sc,\max}}\right) \tag{4.18}$$

$$k_{sc,p-1} = \frac{0.3}{\frac{1.11}{F_{sc,\max}} - \frac{1}{2k_{sc,i}}} \tag{4.19}$$

4.5.1. Slip at maximum strength and slip capacity of the shear connector

Eq. (4.6) and Eq. (4.7) were used to find the slip at maximum strength ($s_{sc,u}$) and slip capacity ($s_{sc,c}$) of shear connector. The ratio ($s_{sc,u}$ /$s_{sc,c}$) for different compressive strength of concrete is:

$$R = s_{sc,c} / s_{sc,u} = 0.783 + 0.148 / (0.389 - 0.0023 f_c) \tag{4.20}$$

Therefore, the post-limit stiffness for the third part of multi-linear curve ($k_{sc,p-2}$) can be calculated as follows:

$$k_{sc,p-2} = \frac{0.2F_{sc,\max}}{s_{sc,u} - 1.11} \tag{4.21}$$

The final multi-linear curve is shown in Figure **4.17**.

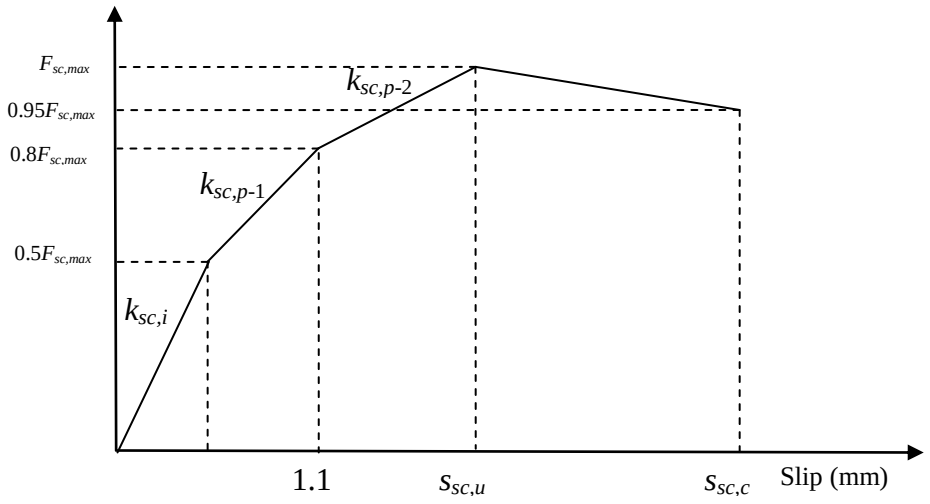

Figure 4.17: Proposed multi-linear model of load-slip curve

The validity of the proposed multi-linear load-slip curve is verified against some of experimental load-slip curves, as shown in Figure 4.18. It can be seen clearly from the figure that the proposed multi-linear model agrees well with the experimental results.

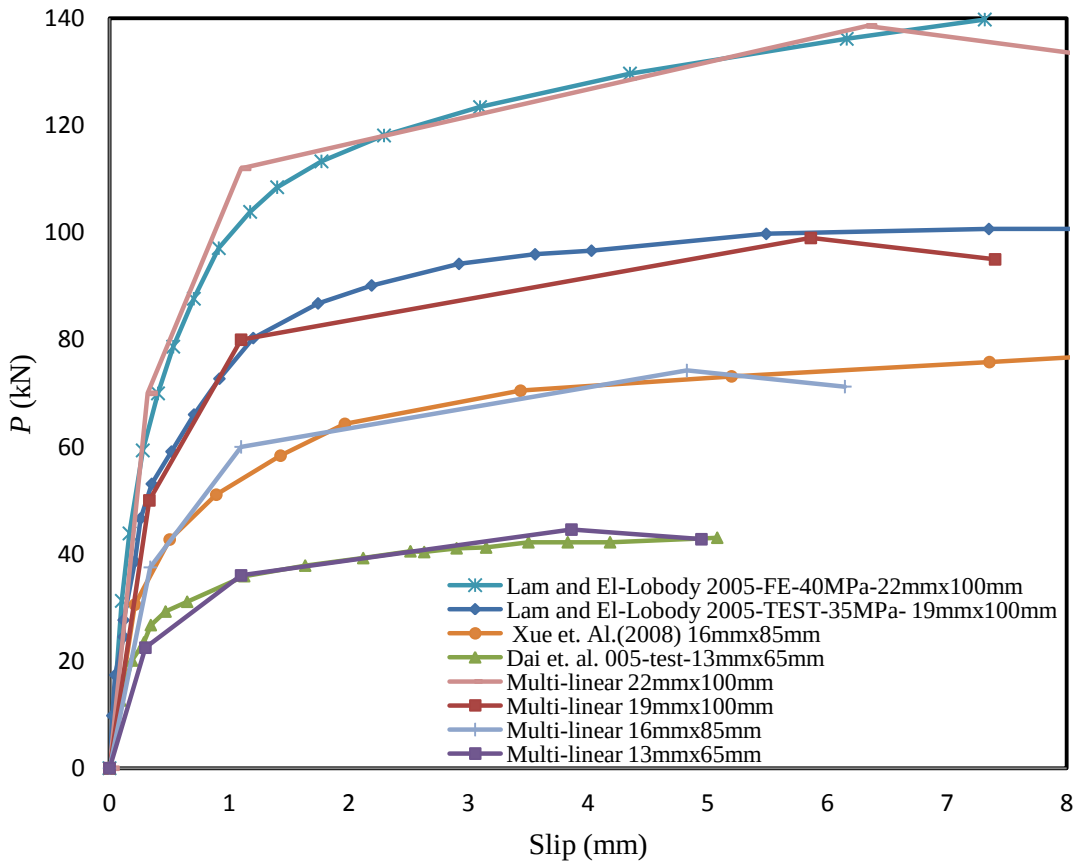

Figure 4.18: Comparison of the proposed model with experimental load-slip curves

4.6. Summary and conclusion

The chart in Figure 4.13 demonstrates a simple approach to estimate the appropriate values of the secant stiffness and strength of a shear connector for different compressive strength of concrete. It can be used when no push-out test curve is available. The empirical equations that researchers have used in the past can lead to unrealistic shear stiffness of the shear connector in some cases. In addition, Figure 4.13 shows clearly that the secant stiffness and strength of the shear connector are highly related. Furthermore, the proposed chart can be used to estimate the secant stiffness and strength for other diameters of shear connectors by drawing parallel lines at the required levels. A simplified multi-linear load-slip curve was also derived based on the proposed chart for initial stiffness, as well as the derivation of post-yield stiffness from empirical equations in the literature. The proposed model is in agreement with the test results, as shown in Figure 4.18.

Chapter Five

Stiffness of a reinforced concrete slab in a composite connection

5.1. Introduction

The fundamental assumption of the present research task is that a beam-column composite connection can be modelled as a combination of components. These components can be divided into two main groups: a reinforced concrete slab and a steelwork connection. Shear studs connect these two groups compositely. Furthermore, the term ‘‘reinforced concrete composite slab’’ (RCCS) represents three components: the reinforcement, the concrete slab and the shear studs (S). In addition, each group can be subdivided into many components as explained in Chapter Three, where the components of the (RCCS) were modelled separately. However, the behaviour of the (RCCS) can be modelled as one ‘‘lump’’ component. Consequently, a model of the behaviour of this ‘‘lump’’ component is required; this is therefore the main objective of this chapter.

5.2. Background

In a composite beam-column connection, the reinforced concrete composite slab is mainly under the tension force of the reinforcement F_r (see Figure 5.1) which develops due to transfer of longitudinal shear force from the beam to the concrete through the shear studs. A model combining the three main components - the concrete, the reinforcement and the shear studs - is essential for understanding the behaviour of composite slabs under tensile load.

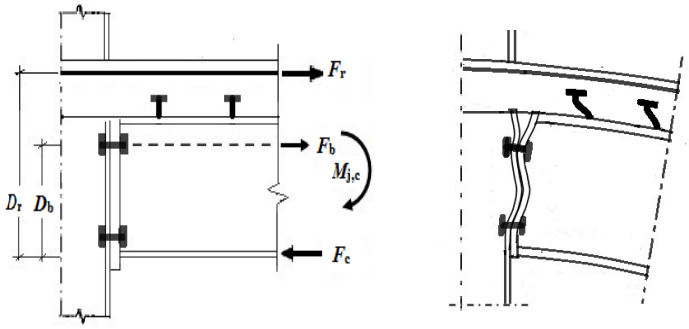

Figure 5.1: Typical composite connection

5.3. Brief literature review

In the literature, three basic procedures are used to model the beam-column composite connection. These are simplified mechanical models, finite element models and empirical models based on the available experimental data.

In most of the simplified mechanical models, the components of (RCCS) are modelled separately, as in the works of (Anderson and Najafi, 1994; Ren and Crisinel, 1996; Ahmed and Nethercot, 1997; Liew et al., 2000). In Chapter Three, the simplified mechanical models were explained in detail eliminating the need to repeat them here.

Eurocode 4 (2004) uses different procedure which combines the stiffness of the reinforcement (k_r) and stiffness of the shear studs (k_s) into one component which represents the stiffness of the composite slab (k_{slab}).

$$k_{slab} = \frac{k_r k_s}{k_s + k_r} \tag{5.1}$$

In this procedure, all shear studs are modelled as one component (k_s) which can be calculated by (Anderson et al., 2000)'s formulae assuming cracked composite cross-sections and using the elastic interaction theory of a composite beam, as explained in Chapter Three (Section 3.9.4). Only a fraction of the reinforcement (l_r) along the composite beam of the connection was assumed to influence the stiffness of the reinforcement (k_r). It is also suggested that the effective length (l_r) for reinforcement is to be measured from the centreline of the column up to the point where an assumed considerable stress is attained.

For the stiffness of the shear studs (k_s), a numerical study was performed by (Ahmed and Nethercot, 1996) which showed clearly that the effect of each shear stud along the composite beam of the connection depends on its distance from the centreline of the column and on the degree of shear connection.

In addition, an experimental and numerical studies carried out by (Gil and Bayo, 2008) found that the effective length (l_r) is not the same along all parallel reinforcing bars, therefore an average length was suggested.

In Chapter Three (Sections 3.6.3 and 3.6.4), various other procedures to estimate the effective length and stiffness of shear studs had been described. These procedures were shown to give considerably different results. Therefore, potentially inaccurate estimation of the effective length and equivalent stiffness for all shear studs along the

composite beam of the connection is the main shortcoming which limits the accuracy of all the current mechanical models in the literature. Furthermore, all of the simplified mechanical models dealt with a cracked composite section; the tensile strength of the concrete and the effect of the concrete between cracks on the behaviour of the reinforcement (i.e. tension-stiffening effect) were thereby ignored.

A number of researchers used the finite element approach to simulate the beam-column composite connection. In comparison with the simplified mechanical models, this approach is more realistic but it is computationally more expensive. The composite concrete slab (RCCS) components (concrete, reinforcement and shear connectors) are modelled in different ways, as follows.

As the main role of the concrete in the reinforced slab is to transfer the longitudinal shear force from the shear studs to the reinforcement, the concrete was ignored in the modelling of the composite connection using ABAQUS software by (Ahmed et al., 1996) and replaced by multi-point constraints to join the shear stud (modelled as a beam element) to the reinforcement (modelled as a truss element). This procedure may reduce the computational time, but it also reduces the accuracy of the model, since the concrete plays another important role in increasing the stiffness of the reinforcement in tension. Therefore, if this effect is not taken into account, the stiffness of the reinforced bars will be underestimated.

Other researchers (Salvatore et al., 2005; Queiroza et al., 2007; Queiroz et al., 2009; Vasdravellis et al., 2009) modelled the concrete explicitly using finite element software such as ABAQUS, ANSYS and ADINA to model the beam-column composite connection. The behaviour of the plain concrete was considered independently of the behaviour of the reinforcement. The reinforcing bars were modelled as one-dimensional rods that can be defined either singly (as beam or truss elements) or embedded in oriented surfaces using elasto-plastic with strain hardening behaviour of the bare steel bars both in compression and tension. The bond interaction effects, such as bond slip and dowel action, were considered approximately by using the ‘‘tension-stiffening’’ concept in the concrete modelling to simulate load transfer across the cracks through the reinforcing bar. The shear studs were modelled as non-linear springs using different load-slip curves. Gil and Bayo (2008) used the same approach but with linear springs for modelling the shear studs and assuming a stiffness of 200 kN/mm. Solid elements with elasto-plastic material behaviour was used to model the shear connectors by (Fu et al., 2007 ; Fu et al., 2008).

In summary, to date, two procedures have been used to model the reinforced concrete component (RCC). The first ignored the concrete completely and replaced it with multi-point constraints to join the shear studs to the reinforcement. The second modelled the concrete explicitly and the behaviour of the plain concrete was considered independently of the behaviour of the reinforcement. The tension-stiffening effect was considered in terms of the behaviour of the concrete. However, the reinforcement was modelled as bare steel bars. The second approach required extensive computational effort and often experienced convergence problem. A parametric study covering all possible parametric combinations will be difficult to achieve using this method.

In the present work, a new procedure, serving as a compromise between the two methods described above, has been developed to model the (RCC).

5.4. Objectives

The main objectives of this chapter are:

1. To propose a mechanical component model for an (RCCS) which can be used as a simplified model in the finite element modelling of a composite connection to overcome the convergence problems in explicit modelling of concrete when the concrete slab begins to crack. This will also reduce the computational time significantly with adequate accuracy.

2. To verify the proposed model against experimental tests.

3. To derive analytical expression for the initial stiffness of (RCCS) to be used in the manual calculation of the initial stiffness of an overall composite connection. The target expression should combine the effect of the reinforcement, concrete and shear studs components in one "lump'' component, avoiding the assumption of the effective length of reinforcement (l_r) in calculating the stiffness of the reinforcement component (k_r) and should not ignore the effect of the concrete (i.e. tension-stiffening), as in the procedures detailed in Chapter Three (Section 3.6.3).

4. To verify the analytical expression against finite element results using ABAQUS software.

5. To carry out parametric study using ABAQUS software to investigate the effect of the relative stiffness of the reinforced concrete component and the shear stud

component - k_{RCC}/k_{sc} - on the initial stiffness of the composite slab (RCCS) as a "lump'' component.

6. To modify the proposed mechanical model of initial stiffness for a composite connection developed in Chapter Three in order to combine the effects of the reinforcement, the concrete, and the shear studs into one "lump'' component.

5.5. Proposed model for reinforced concrete composite slab, (RCCS)

The hypothesis of the proposed model is that the force-deformation behaviour of the (RCCS) under tension can be modelled as a combination of the fundamental components: reinforcement, concrete and shear studs. In addition, the reinforcement and the concrete may be combined as one component which should be referred to as the reinforcement- concrete component (RCC). Therefore, only two major components are used to construct the proposed model of (RCCS): the (RCC) and the shear studs (S).

The proposed model can be achieved by following two steps:

1. Define the behaviour of each major component (i.e. the (RCC) and the shear studs (S)) ;

2. Develop an approach to combine the major component behaviours in order to produce the approximate force-deformation behaviour of the (RCCS).

5.5.1. Defining the behaviour of the major components

5.5.1.1. Reinforcement- concrete component, (RCC)

5.5.1.1.1. Plain concrete

Plain concrete is a brittle material which has high compressive strength, f_c'. However, it has a low tensile strength, f_{cr}, with very limited crack strain, ε_{cr}, as shown in Figure 5.2.

As most concrete in a composite connection is under tension, the cracking and postcracking of the concrete are the most important aspects of its behaviour, and dominate its modelling. Therefore, only the behaviour of concrete under tension associated with the embedded reinforcement behaviour is discussed in this chapter.

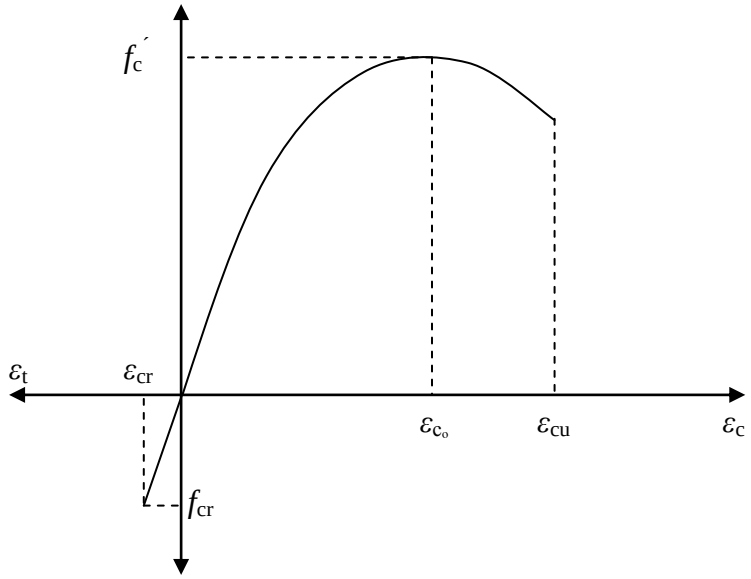

Figure 5.2: Typical Stress-strain relationship for plain concrete

5.5.1.1.2. Tension-stiffening effect

The proposed model for the (RCC) takes into account the tension-stiffening effect. explanations of this effect are given in (CEB-FIP model code 1990, 1993; Kwak and Kim, 2006) along with Figure 5.3 below.

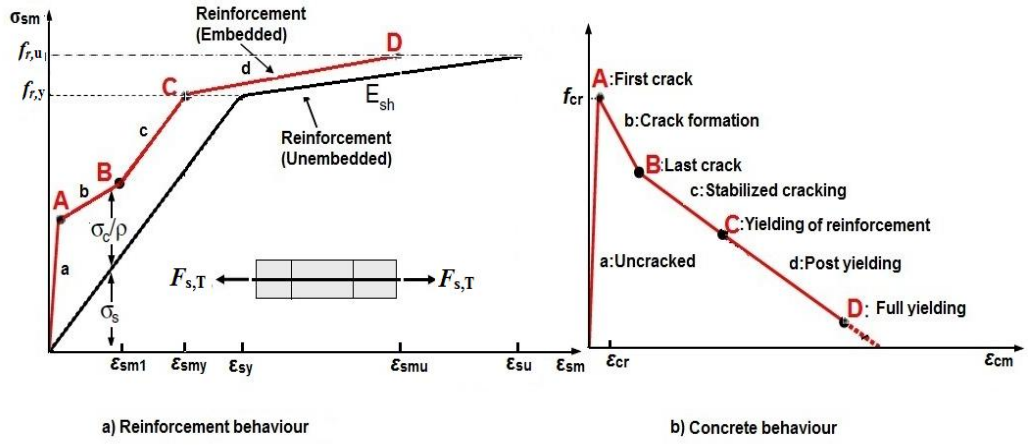

Figure 5.3: Idealised behaviour of a RC tension member: (a) average stress–strain relationship of a reinforcement (b) average stress–strain relationship of concrete

When a reinforced concrete uncracked member is loaded in tension, the tensile force, $F_{s,T}$, is distributed between the reinforcement and the concrete in proportion to their relevant stiffness. The first crack in the concrete occurs when the mean strain, ε_{sm}, reaches the crack strain of the concrete, ε_{cr}, (point A). The crack formation phase continues or the concrete contribution decreases significantly until the last crack form

(point B). A stabilized cracking phase then begins. In this phase, all tensile forces are balanced by the reinforcement alone in a cracked cross-section. However, tensile forces are transmitted from the embedded reinforcement to the surrounding concrete by bond forces in sections between any two successive cracks. As loading increases, the cracks gradually widens without the appearance of any additional crack, until the reinforcement at the cracked-sections yields (point C). Any additional increases in load after the reinforcement yields (i.e. in the post yielding phase) lead to an increase in the strain until the point of fracture of the reinforcement at the cracked section with a maximum strain that is less than the maximum strain of the bare steel bar. In this phase, the contribution of the concrete to the strength of a tension member comes through the remaining bond resistance.

5.5.1.1.3. Combined reinforcement-concrete behaviour

To date, the behaviour of the plain concrete has been considered independently of the behaviour of the reinforcement in finite element modelling of composite connections. In this type of modelling, the stress-strain relationship of the embedded reinforcement is the stress-strain relationship of the bare steel bar (see Figure 5.3-a) and the tension-stiffening effect is taken into account by modifying the stress-strain relationship of the plain concrete, as in Figure 5.3-b.

In the proposed model, the contribution of the reinforcement and the concrete to the behaviour of the composite connection will be considered using a different approach. The proposed approach is based on the following considerations:

1. The main roles of concrete in the composite connection are:
    i. To transfer the tensile force to the reinforcement from the shear studs and
    ii. To increase the stiffness of the reinforcement in tension by way of the tension-stiffening effect.
2. The embedded reinforcement has greater stiffness and lower ductility than the bare reinforcement, due to the tension-stiffening effect.
3. The tension-stiffening effect should be taken into account in force-deformation relationship of the (RCC) as stated in Eurocode 4 (Annex L).

Based on the above considerations, the roles of concrete were taken into account in the proposed model as follows:

1. The reinforcement is connected directly to the shear studs by multi point constraints to simulate the first role of concrete (1(i)) as described above.

2. The second role of concrete (1(ii)) can be interpreted as increasing the stiffness of the reinforcement in tension by modifying the stress-strain relationship of the embedded reinforcement, as shown in Figure 5.3-a. This means that the significant effect of concrete on the reinforcement stiffness is taken implicitly into account in the stress-strain relationship of the embedded reinforcement.

3. The insignificant tensile strength of concrete is ignored. As mentioned in Section 5.3, Ahmed et al. (1996) ignored the concrete and all its contributions in their finite element modelling of composite connections. Nevertheless, they achieved adequate agreement with some experimental results.

The simplified proposed approach will reduce the computational time significantly and overcome the convergence problems in explicit modelling of concrete that occurred when the concrete slab begins to crack. Nevertheless, the most important role of concrete (i.e. transfer the tensile force to the reinforcement and tension-stiffening effect) are reflected implicitly by modifying the behaviour of the reinforcement.

In order to determine the stress-strain relationship for the (RCC) components, the basic properties of bare reinforcement should be used, which are the yield strain, ε_{sy}, and ultimate strain, ε_{su}. The corresponding mean yield strain, ε_{smy}, and ultimate mean strain, ε_{smu}, for modifying the behaviour of the embedded reinforcement can be calculated from the relationships shown in the next section.

5.5.1.1.3.1. Pure tension member

The behaviour of a reinforced concrete member under tension as shown in Figure 5.4 can be described using the simplified stress-strain relationship for an embedded reinforcement, as shown in Figure **5.5**. The total tensile force, $F_{s,T}$, can be calculated as follows:

$$F_{s,T} = F_{c,t} + F_r = A_c\sigma_{c,t} + A_r\sigma_r \qquad (5.2)$$

where $F_{c,t}$, $\sigma_{c,t}$ and A_c are the force, stress and area of the concrete respectively. F_r, σ_r and A_r are the force, stress and area of the reinforcement respectively.

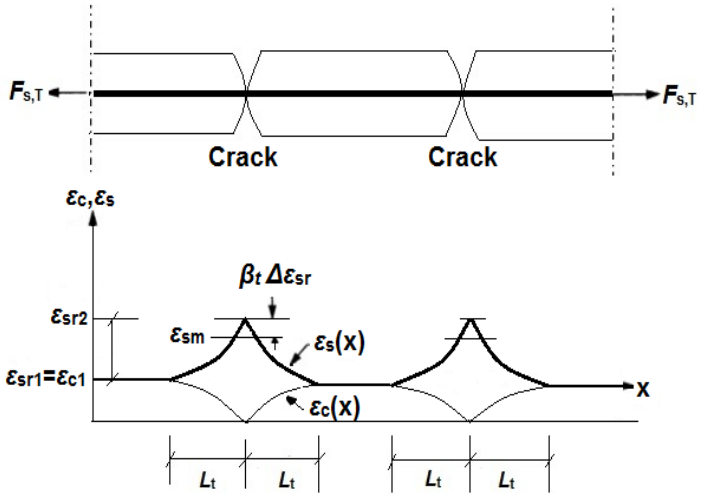

Figure 5.4: Tension-stiffening development (for $F_{s,T}>F_{s,cr}$)

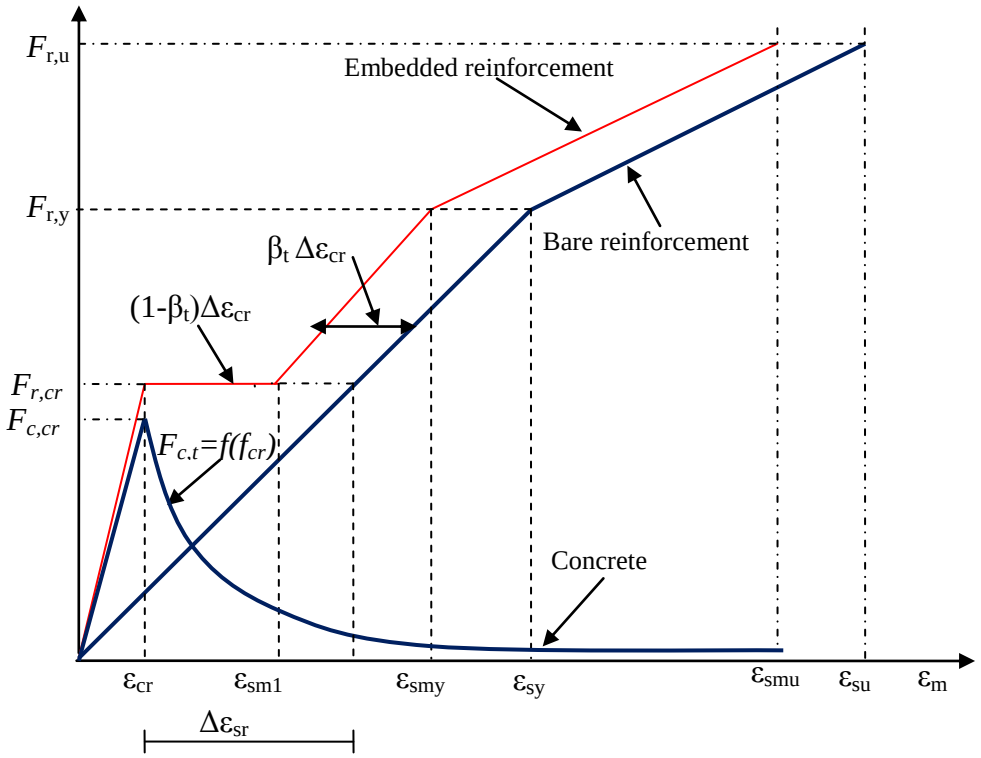

Figure 5.5: Simplified load-strain relationships for bare and embedded reinforcement

Before first crack $\Rightarrow$ $F_{s,T} \le F_{s,cr} \Rightarrow F_{s,T} = A_c E_c \varepsilon_{c,t} + A_r E_r \varepsilon_r$ (5.3)

where $\varepsilon_{c,t}$ and ε_r are the strain in the concrete and the reinforcement respectively.

$\because \varepsilon_{c,t} = \varepsilon_r = \varepsilon_m \Rightarrow F_{s,T} = A_c E_c \varepsilon_m (1+\rho n)$ where $\rho = \dfrac{A_r}{A_c}$ and $n = \dfrac{E_r}{E_c}$ (5.4)

where ε_m is the mean strain in the (RCC).

At first crack $\Rightarrow$ $\varepsilon_m = \varepsilon_{cr}$ and $F_{s,T} = F_{s,cr}$ (5.5)

$$F_{s,cr} = A_c E_c \varepsilon_{cr} (1+\rho n) = A_c f_{cr} (1+\rho n) \quad (5.6)$$

where ε_{cr}, f_{cr} are the cracking strain and stress in concrete respectively.

In the stabilized cracking phase $\Rightarrow$ $F_{s,cr} < F_{s,T} \le F_{s,y}$ (5.7)

$$\therefore F_{s,T} = A_c f_{c,t} + A_r \sigma_r \quad (5.8)$$

In the literature, there are many relationships between the tensile strength of concrete after cracking, $f_{c,t}$, and the crack strength, f_{cr}. Hwang and Rizkalla (1983) performed 34 experimental tests on rectangular reinforced concrete panels under uniaxial load. Based on the experimental results, they proposed the following relationship for the behaviour of concrete after cracking:

$$f_{c,t} = f_{cr} e^{-1000(\varepsilon - \varepsilon_{cr})} \quad (5.9)$$

Gupta and Maestrini (1990) proposed the same form of relationship as

$$f_{c,t} = f_{cr} e^{-550(\varepsilon - \varepsilon_{cr})} \quad (5.10)$$

Tamai et al. (1988.) proposed a power relationship for the tensile strength of concrete after cracking. It takes the form:

$$f_{c,t} = f_{cr} \left(\frac{\varepsilon_{cr}}{\varepsilon} \right)^c \quad (5.11)$$

where the cracking strain, ε_{cr} is taken as 0.0002 and c is a constant depending on the bond characteristic, taken as 0.4 for a deformed bar. Jaeyeol et al. (2003) proposed the same form of Eq. (5.11) but after replacing 0.0002 with 0.000113 for the cracking strain. In the present work, the behaviour of the concrete after cracking was taken as exponential form (Eq. (5.9)), since this form represent the true trend for most cases. Therefore, Eq. (5.8) will be rewritten as:

$$F_{s,T} = A_c \left(f_{cr} e^{-1000(\varepsilon_m - \varepsilon_{cr})} + \rho \sigma_r \right) = A_c \left(f_{cr} e^{-1000(\varepsilon_m - \varepsilon_{cr})} + \rho E_r \varepsilon_m \right) \quad (5.12)$$

At yield $\Rightarrow$ $\varepsilon_m = \varepsilon_{cmy}$ and $f_{c,t} \approx 0 \Rightarrow F_{s,y} = A_r f_{r,y}$ (5.13)

At ultimate $\Rightarrow$ $\varepsilon_m = \varepsilon_{cmu}$ and $f_{c,t} \approx 0 \Rightarrow F_{s,y} = A_r f_{r,u}$ (5.14)

In order to find the relevant strain at every load value, $F_{s,T}$, the increase in strain on the embedded reinforcement in the cracking state, $\Delta\varepsilon_{sr}$, should first be calculated as follow:

$$\Delta\varepsilon_{sr} = \frac{F_{s,cr}}{A_r E_r} - \varepsilon_{cr} = \frac{A_c f_{cr}(1+\rho n)}{A_r E_r} - \frac{f_{cr}}{E_c} = \frac{f_{cr}}{\rho E_r} \tag{5.15}$$

$$\therefore \varepsilon_{sm1} = \varepsilon_{cr} + (1-\beta_t)\Delta\varepsilon_{sr} \tag{5.16}$$

$$\varepsilon_{cmy} = \varepsilon_{sy} - \beta_t \Delta\varepsilon_{sr} \tag{5.17}$$

In the (CEB-FIP model code 1990, 1993), β_t was defined as the integration factor for the steel strain along the transmission length, L_t. β_t was taken to be 0.4 for instantaneous loading. The ultimate strain in post-yielding state was also calculated, using the following relation (Anderson et al., 2000):

$$\varepsilon_{smu} = \varepsilon_{sy} - \beta_t \Delta\varepsilon_{sr} + \delta\left(1 - \frac{\sigma_{sr1}}{f_{sy}}\right)\left(\varepsilon_{su} - \varepsilon_{sy}\right) \tag{5.18}$$

$$\sigma_{sr1} = \frac{F_{s,cr}}{A_{s,r}} = \frac{A_c f_{cr}(1+\rho n)}{A_{s,r}} = \frac{f_{cr}}{\rho}\left[1+\rho n\right] \tag{5.19}$$

where σ_{sr1} is the stress in the reinforcement when the first crack has initiated. δ is the coefficient that accounts for the ratio of ultimate strain to the yield strength of the reinforcement. It was taken as 0.8 for ductile steel with yield strength of 500 MPa.

5.5.1.1.3.2. Verification of the procedure for pure tension against test results

Tamai et al. (1988) conducted six uniaxial tests on prismatic reinforced concrete specimens. Steel stress distribution and elongations of each specimen were measured in order to evaluate the tension-stiffening effect on the average stress-strain relationship of a steel bar in the post-yield range. The main parameters of these tests are the concrete strength, reinforcement ratio, yield strength of steel and curing conditions. A deformed steel bar with a diameter of 19 mm was arranged in the centre of rectangular concrete cross-sections of 150 mm x 200 mm and 200 mm x 250 mm, reinforcement ratios of 0.6% and 1% respectively. The length of all specimens was 2700 mm. The testing apparatus was set up horizontally, as shown in Figure 5.6.

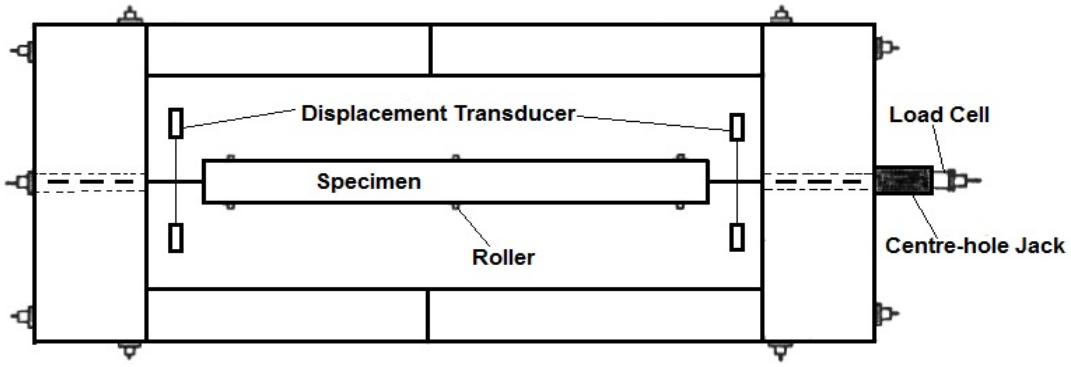

Figure 5.6: Test arrangement (Tamai et al., 1988)

Two specimens (No.1 and No.6) were selected from the experimental tests to verify the applicability of the analytical procedure to estimate the load-deformation curve of a reinforced concrete member under pure tension. The results of the analytical procedure and experimental tests are compared in Figure 5.7 to Figure 5.10. It is clear from these figures that the analytical procedure can predict the behaviour of a reinforced concrete member under pure tension sufficiently accurately.

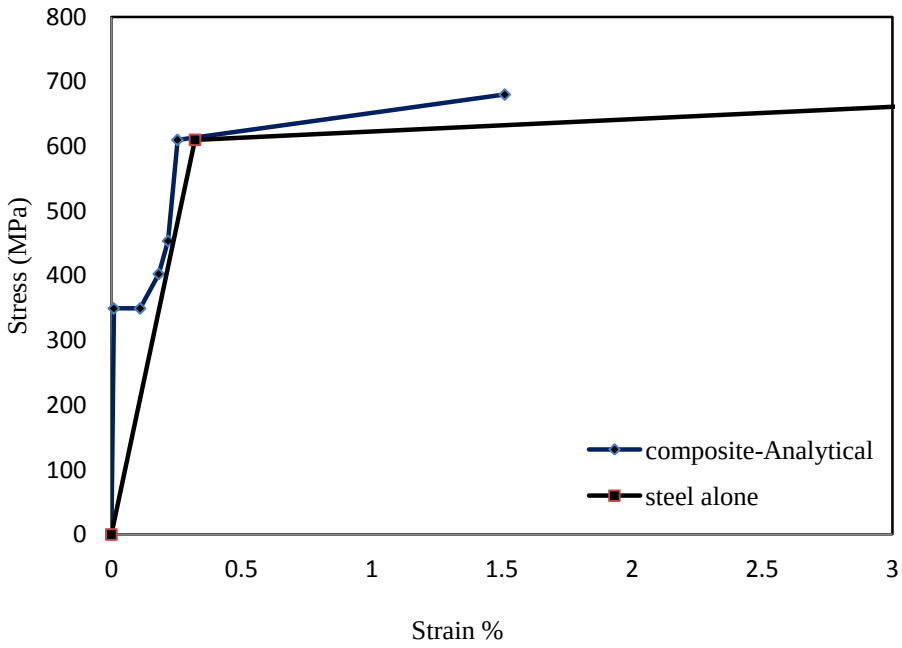

Figure 5.7: Comparison of the stress in a steel bar of a reinforced concrete member and in a steel bar alone using the analytical procedure (specimen No.1)

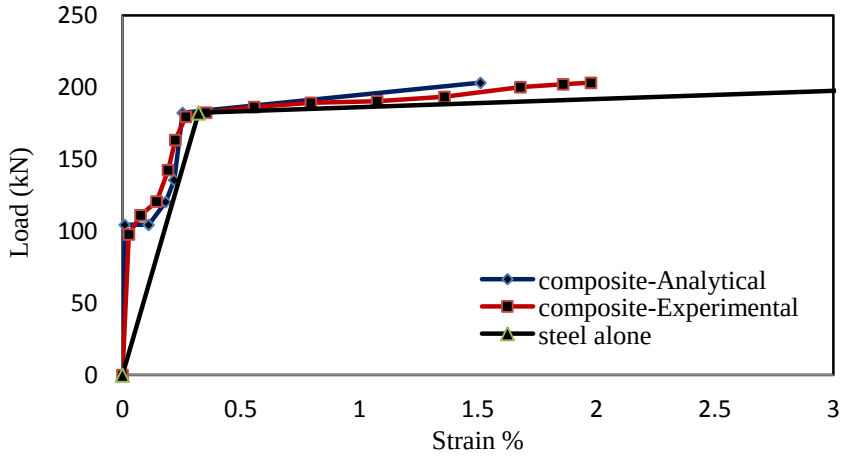

Figure 5.8: Comparison of analytical and experimental results for a reinforced concrete member (specimen No.1)

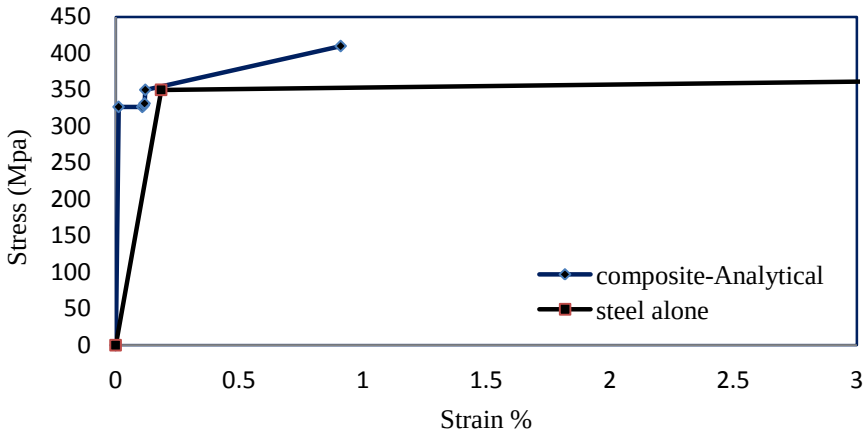

Figure 5.9: Comparison of stress of a steel bar in reinforced concrete member and a steel bar alone using an analytical procedure (specimen No. 6)

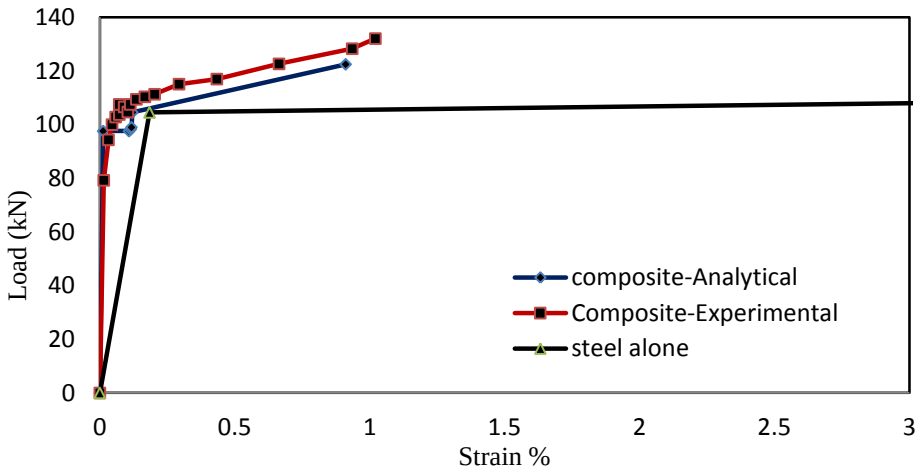

Figure 5.10: Comparison of analytical and experimental results for a reinforced concrete member (specimen No. 6)

5.5.1.1.3.3. Modification for the combined actions of tension and bending

Anderson et al. (2000) modified the relevant relationships for pure tension state in order to account for the combined action of tension and bending in the reinforced concrete slab. They defined the cracking moment of a composite connection as the moment that causes the mean tensile strength of concrete (f_{ctm}) to be reached at the upper fibre of the uncracked slab. Eurocode 4 (2004) gives the following expressions to calculate the mean tensile strength of concrete, f_{ctm}:

$$f_{ctm} = \begin{cases} 0.3\left(f_{ck}\right)^{2/3} & \leq \text{C50/60} \\ 2.12\ln(1+(f_{ck}+8)/10) & >\text{C50/60} \end{cases} \tag{5.20}$$

The cracking strength, f_{cr}, was replaced by the mean tensile strength (f_{ctm}) multiplied by the factor (k_{cm}) in all relevant relations for pure tension. k_{cm} is a coefficient to account for the self-equilibrating stresses in the slab prior to cracking:

$$k_{cm} = \frac{1}{1+\frac{h_{sl}}{2Z_0}} \tag{5.21}$$

where h_{sl} is the thickness of the concrete slab and Z_0 is the vertical distance between the centroid of the uncracked, unreinforced concrete slab and the neutral axis of the uncracked, unreinforced transformed composite section.

The resultant stress-strain relationship for the modified behaviour of the embedded reinforcement is shown in Figure 5.11. In addition, the mean modulus of elasticity (E_m) for the embedded reinforcement in the elastic range is shown in the same figure.

This stress-strain curve is required when undertaken finite element modelling of the (RCC). It should be noted that the length of the (RCC) element should be short enough to capture the cracking effect of the concrete adequately. The length of the (RCC) element (s_e) should be in the range:

$$L_t \leq s_e \leq 2L_t \Rightarrow \left(s_e\right)_{av} = 1.5L_t \quad \text{and} \quad L_t \leq p \tag{5.22}$$

where p is the spacing between the shear studs. L_t is the transmission length, as shown in Figure 5.4. It can be calculated as follows (Anderson et al., 2000):

$$L_t = \frac{k_{cm} f_{ctm} \phi}{4\rho\tau_{sm}} \tag{5.23}$$

where ϕ is the diameter of the reinforcement and τ_{sm} is the average bond stress along the transmission length, taken as 1.8 f_{ctm}.

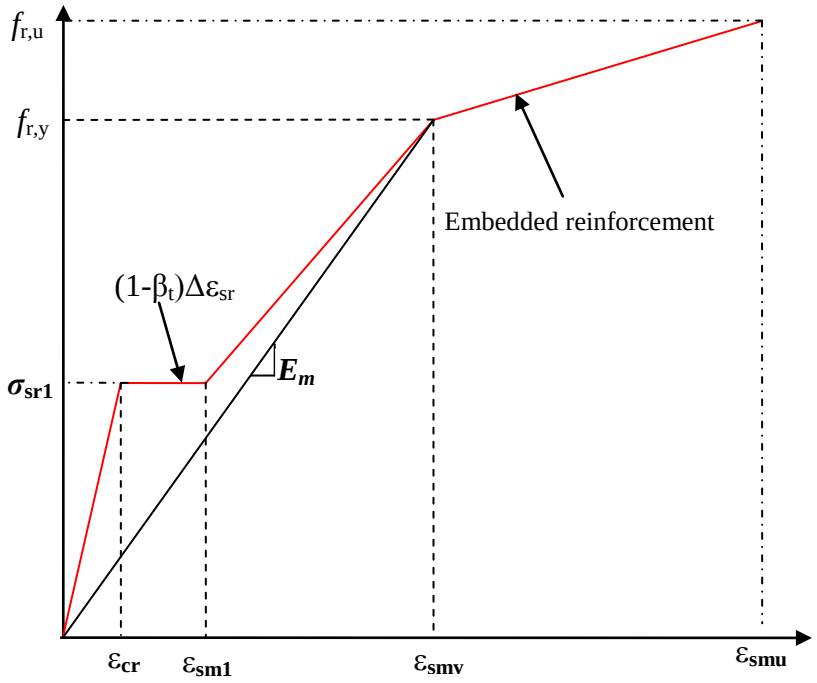

Figure 5.11: Stress-strain relationship of the (RCC)

In addition, the width of the (RCC) element (w_e) should be equivalent to the width of the transformed concrete slab:

$$w_e \approx \frac{w_{slab}}{n} \qquad \text{where} \quad n = \frac{I_c}{I_r} \tag{5.24}$$

5.5.1.2. Shear stud component

The load-slip curve for a shear stud is required in the proposed model for nonlinear analysis of the composite connection up to failure. However, only the linear stiffness of a shear stud may be required in the proposed model for (RCCS), depending on the following considerations:

1. Eurocode 4 (2004) (Annex A.3) assume that the linear stiffness of an individual shear connector may be taken as up to 70% of its strength. The same percentage

was taken by (Queiroz et al., 2009). Johnson and May (1975) assumed this linear range to be up to 50% of the strength. Ren and Crisinel (1996) assumed the whole stiffness of the shear connection may be taken as linear up to a value of 60%. The chart proposed in Chapter Four for estimating the initial stiffness of a shear connector was constructed based on the percentage of (Johnson and May, 1975).

2. The linear stiffness of a shear connector, k_{sc}, can be used in the analysis when it is expected that the maximum load on a shear connector is equal to or less than half its strength, $F_{sc,max}$, depending on the shear connection ratio.

3. Since the maximum expected load on all shear connectors along the length of beam of a composite connection is equal to the maximum expected load in the reinforcement up to failure, $F_{r,u}$, then the use of the linear stiffness of the shear connector, k_{sc}, may be required if the number of shear connectors satisfies the following condition:

$$N_{sc,\min} \geq \frac{2A_r f_{r,u}}{F_{sc,\max}} \tag{5.25}$$

where A_r and $f_{r,u}$ are the area and ultimate strength of the reinforcement respectively. $F_{sc,max}$ is the strength of the shear connector, which can be determined easily from the proposed chart in Chapter Four.

4. If the number of shear connectors did not satisfy the condition in Eq. (5.25), then the load-slip curve of the shear connector will be required for analysis of the composite connection. The proposed multi-linear load-slip curve in Chapter Four may be used for this purpose.

5.5.2. Construction of the proposed model

Only two major components are used to construct the proposed model of a composite slab. These are the (RCC) and the shear studs (S), as shown in Figure 5.12. Moreover, every region of the (RCC) between the shear studs is modelled individually, as the strain along the (RCC) is not uniform and depends on the distance from the centreline of the column. Furthermore, in order to make the proposed model appropriate for both finite element modelling and manual calculations in the linear-elastic range, the conventional (RCC) are replaced by (RCC) springs, as shown in Figure 5.13.

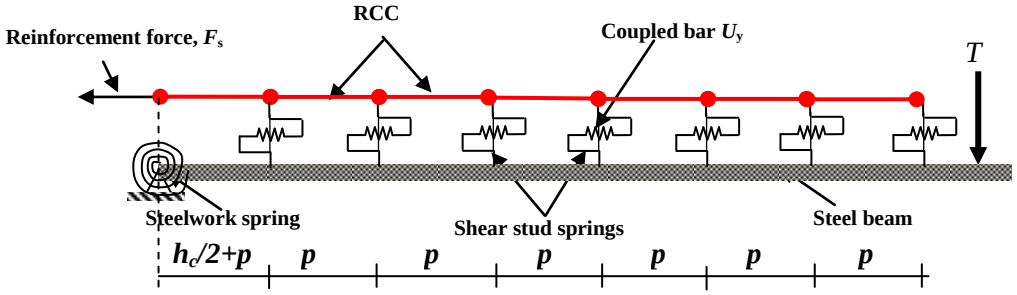

Figure 5.12: Proposed model for a composite slab

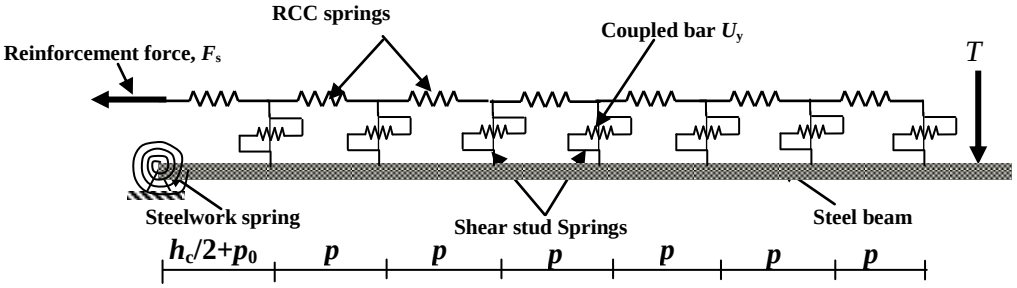

Figure 5.13: Simplified proposed spring model

In addition, the number of (RCC) springs in series between any two consecutive shear studs, N_{spr}, depends on p and s_e. This number is equal to the integer number of:

$$N_{spr} \geq \frac{p}{s_e} \tag{5.26}$$

Hence, the force-displacement relationship of the (RCC) springs is required in the simplified spring model. The stress-strain relationship of the (RCC) in Figure 5.11 is converted to a force-displacement relationship for the (RCC) springs, as shown in Figure 5.14. This relationship is defined by multiplying all stresses by the area of reinforcement and all strain by the length of reinforcement over which this strain can be assumed to act.

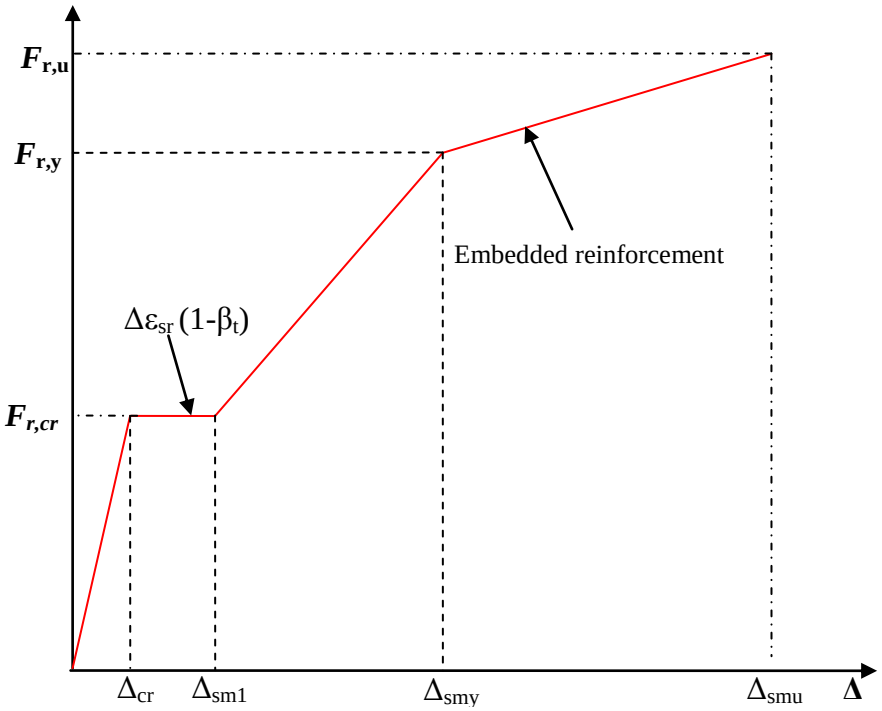

Figure 5.14: Force-deformation relationship for an (RCC) spring

5.6. Derivation of analytical expression for the initial stiffness of composite slab with shear studs (“lump’’ component)

The analytical expression for the “lump’’ component is required to be used in the manual calculation of the initial stiffness of the overall composite connection. This expression combines the effects of the concrete, the reinforcement and the shear studs components in one “lump’’ component. Derivation of this expression is based on the principle of finding the equivalent stiffness of a group of springs in parallel and in series. Therefore, the stiffness of every spring should first be calculated; in this instance, the stiffnesses of the (RCC) springs and the shear stud springs must be derived.

The stiffness of an (RCC) spring, k_{RCC}, can be determined using the axial stiffness of the (RCC) component as follows:

$$k_{RCC} = \frac{E_{RCC} A_r}{l_{RCC}} \tag{5.27}$$

where A_r is the area of reinforcement. l_{RCC} and E_{RCC} are the length and the modulus of elasticity of the (RCC) component respectively.

As the initial stiffness of the composite connection is assumed to be calculated at 50% of the ultimate moment capacity of the connection, all (RCC) components can be

assumed to be in the elastic range, but they may be at any one of the three zones in the elastic range shown in Figure 5.15, depending on their distance from the centreline of the column. As an approximation, the stiffness of (RCC) spring, k_{RCC}, can be taken as $k_{RCC,m}$, for all (RCC) springs, as shown in Figure 5.15.

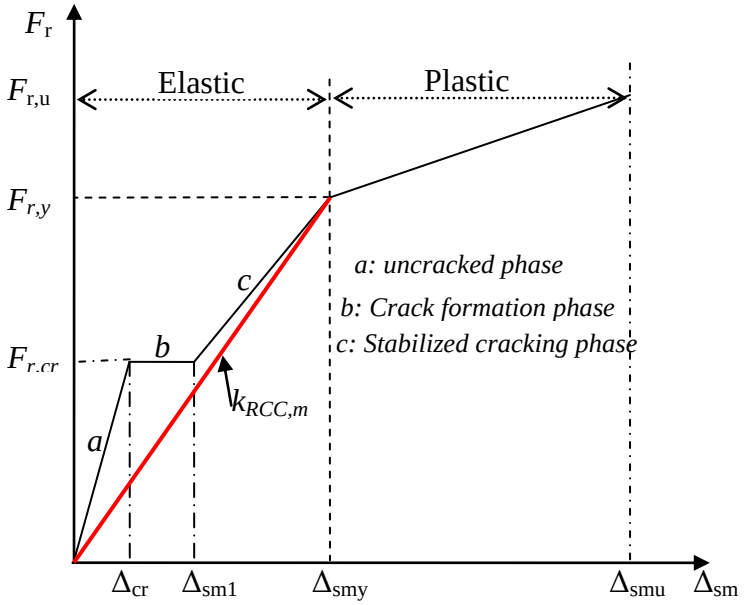

Figure 5.15: Approximate force-displacement relationship for an (RCC) spring

In addition, the initial stiffness of a shear stud, k_{sc}, can be easily determined from the proposed chart in Chapter Four. This stiffness is representative of all parallel shear studs in the same row if there is more than one stud in every row. The final model for the initial stiffness is shown in Figure 5.16.

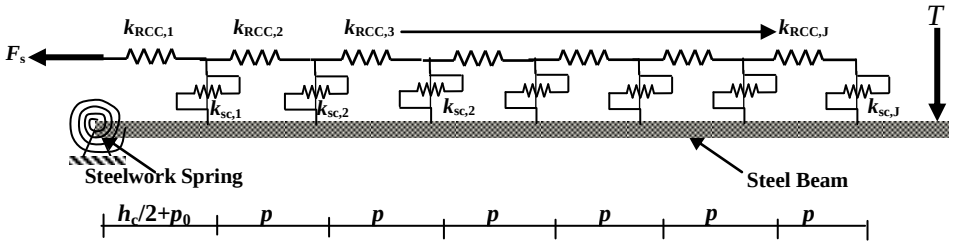

Figure 5.16: Final model for initial stiffness

The equivalent stiffness of all (RCC) and shear stud springs (S), K_{lump}, can be calculated as follows:

1. The equivalent stiffness of the $k_{RCC,J}$ and $k_{sc,J}$ (the set of springs at the extreme right as shown in Figure 5.16) is

$$K_{eq,J} = \frac{k_{sc,J} k_{RCC,J}}{k_{sc,J} + k_{RCC,J}} \tag{5.28}$$

2. This equivalent spring, $K_{eq,J}$, is in parallel with the previous shear stud spring, $k_{sc,J-1}$, and is in series with the previous (RCC) spring, $k_{RCC,J-1}$. Therefore:

$$K_{eq,J-1} = \frac{\left(K_{eq,J} + k_{sc,J-1}\right) k_{RCC,J-1}}{\left(K_{eq,J} + k_{sc,J-1}\right) + k_{RCC,J-1}} \tag{5.29}$$

and so on.

3. The equivalent stiffness of all (RCC) and shear stud springs, K_{lump} is

$$K_{eq,J+1} = 0 \tag{5.30}$$

$$K_{eq,J} = \frac{\left(K_{eq,J+1} + k_{sc,J}\right) k_{RCC,J}}{\left(K_{eq,J+1} + k_{sc,J}\right) + k_{RCC,J}}$$

$$K_{eq,J-1} = \frac{\left(K_{eq,J} + k_{sc,J-1}\right) k_{RCC,J-1}}{\left(K_{eq,J} + k_{sc,J-1}\right) + k_{RCC,J-1}}$$

$$K_{eq,2} = \frac{\left(K_{eq,3} + k_{sc,2}\right) k_{RCC,2}}{\left(K_{eq,3} + k_{sc,2}\right) + k_{RCC,2}}$$

$$K_{eq,1} = \frac{\left(K_{eq,2} + k_{sc,1}\right) k_{RCC,1}}{\left(K_{eq,2} + k_{sc,1}\right) + k_{RCC,1}} \tag{5.31}$$

$$K_{lump} = K_{eq,1} \tag{5.32}$$

where J is the lowest integer number of shear studs for full shear connection but not greater than the total number of shear studs:

$$J \le \frac{A_s f_{sy}}{F_{sc,\max}} \quad \text{and} \quad J \le N_{sc,all} \tag{5.33}$$

5.7. Distribution of forces in (RCC) and shear stud springs

The proposed procedure can be used to calculate the distribution of forces in the elastic range for all (RCC) and shear stud springs as follow:

1. Forces in (RCC) springs

$$F_{RCC,1} = F_s \tag{5.34}$$

$$F_{RCC,2} = \frac{k_{eq,2}}{k_{eq,2} + k_{sc,1}} F_{RCC,1}$$

$$F_{RCC,3} = \frac{k_{eq,3}}{k_{eq,3} + k_{sc,2}} F_{RCC,2}$$

$$F_{RCC,i} = \frac{k_{eq,i}}{k_{eq,i} + k_{sc,i-1}} F_{RCC,i-1} \tag{5.35}$$

2. Forces in shear stud springs

$$F_{sc,1} = \frac{k_{sc,1}}{k_{eq,2} + k_{sc,1}} F_{RCC,1}$$

$$F_{sc,2} = \frac{k_{sc,2}}{k_{eq,3} + k_{sc,2}} F_{s,2}$$

$$F_{sc,i} = \frac{k_{sc,i}}{k_{eq,i+1} + k_{sc,i}} F_{s,i} \tag{5.36}$$

5.8. Validation

5.8.1. Verification of the analytical expression against finite element results using ABAQUS software

5.8.1.1. ABAQUS model

The analytical expressions used to calculate the equivalent stiffness of all (RCC) and shear stud springs, K_{lump}, were verified against finite element modelling using ABAQUS software. In this modelling, the rotational stiffness of a steelwork connection was modelled as a pinned boundary condition in order to evaluate the rotational stiffness of the (RCC) and shear studs alone. The steel beam is 203x102UB23 and is 2.07m long. It was divided into two parts: one part was modelled with a beam element with a length of 1.97m and the other part was modelled as a solid element with a length of 0.1m in order to calculate the rotation of the beam as the difference between the displacement at the top and bottom of the beam. These parts were connected using a coupling constraint. Both parts were assigned a high modulus of elasticity, $10E_s$, in order to account for the rotational stiffness of the composite connection due to the effect of composite slab with shear studs only. Nine shear studs were used which were distributed at 230mm c/c. The shear studs were modelled as rigid bars with rotational springs at the base, with stiffness

equal to 6600 kN-m/rad. This rotational stiffness is equivalent to 150 kN/mm of linear stiffness, which is the initial stiffness of a 19mm x100mm shear stud in concrete with a compressive strength of 30 MPa, as determined from the proposed chart in the previous chapter. The (RCC) springs were assigned 560 kN/mm of axial stiffness, equivalent to an axial stiffness of 4-ϕ12mm of reinforcement. The modulus of elasticity was set at 285 GPa, which is the modified modulus to account for the tension-stiffening effect, as explained in Section 5.5 and Figure 5.15. A concentrated load was applied at the left-hand end of the steel beam. The final model in ABAQUS is shown in Figure 5.17.

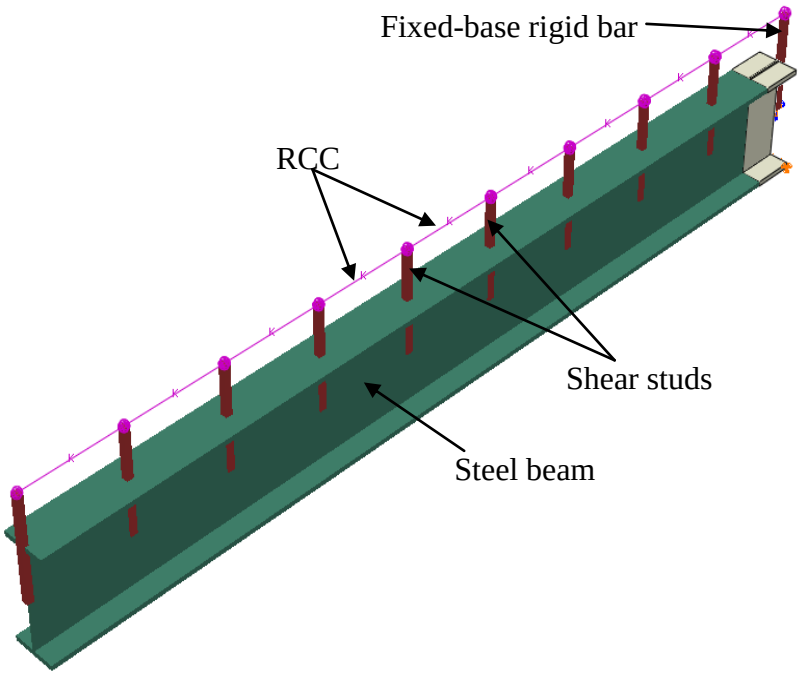

Figure 5.17: ABAQUS model to verify the proposed analytical expressions. The part of the steel beam shaded in dark cyan (1.97 m) has been modelled by beam elements; the profile effect is due to rendering. The grey part at the right hand end (0.1 m) has been modelled by solid elements.

5.8.1.2. Results and discussion

The results of tensile stresses in the springs from the ABAQUS deformed model are shown in Figure 5.18.

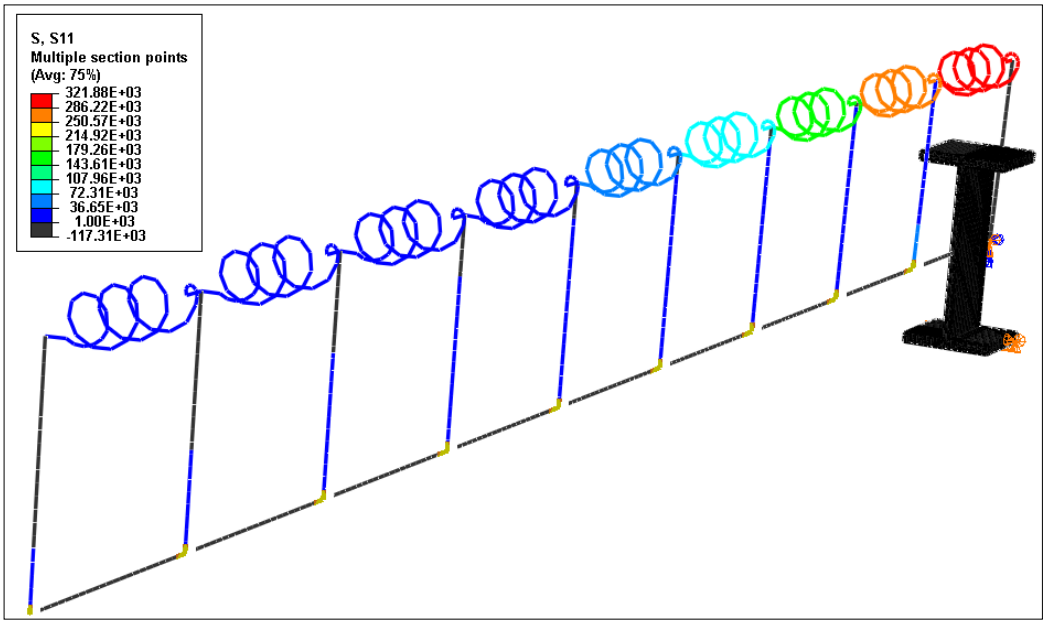

Figure 5.18: Tensile stresses in the springs from the ABAQUS deformed model

The moment-rotation curve is shown in Figure 5.19. The load was applied such that the moment was in the linear range in order to calculate initial stiffness of the composite connection.

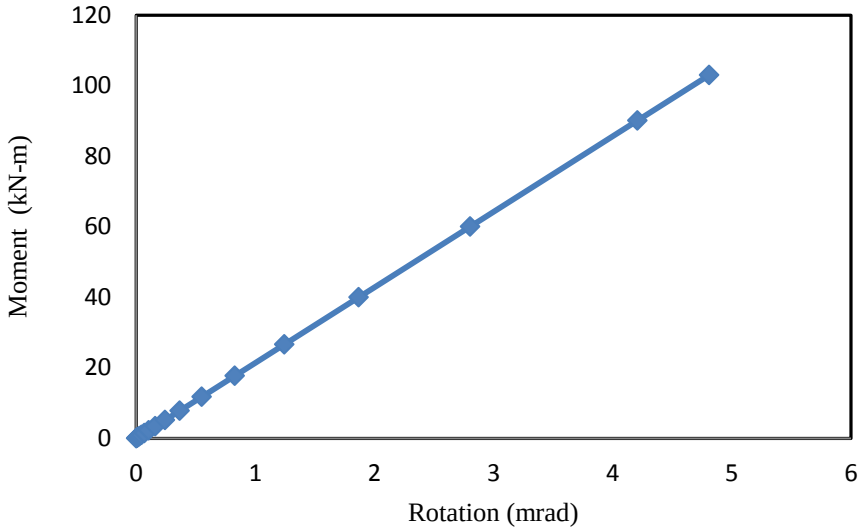

Figure 5.19: Moment-rotation curve

In addition, Figure 5.20 and Figure 5.21 show a comparison between the analytical and numerical results using ABAQUS software for the distribution of forces acting on the (RCC) springs and shear studs along the composite connection. Both results are

identical. These show the validity of the proposed expressions to calculate stiffness and forces in (RCC) springs and shear studs along a composite connection.

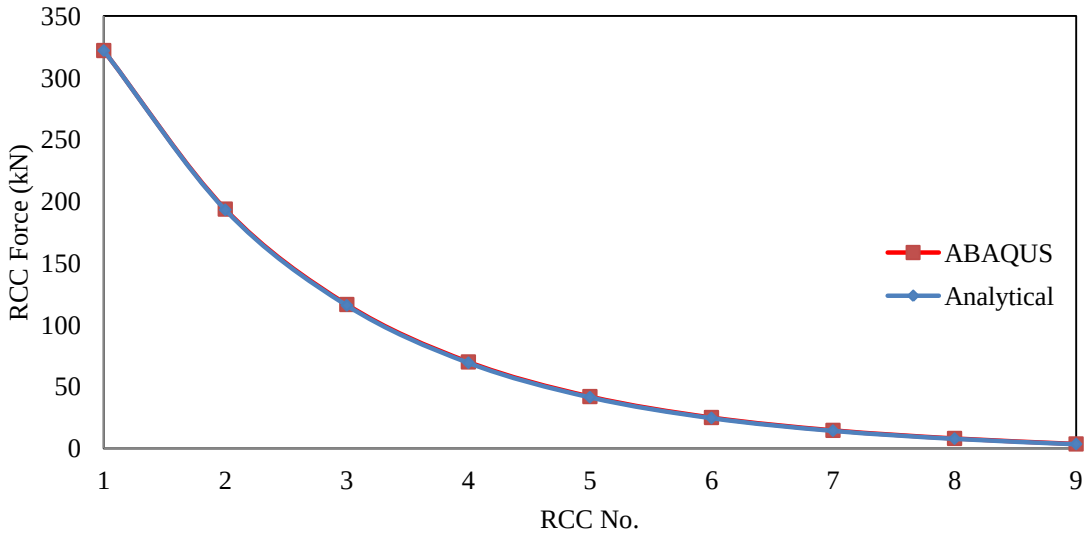

Figure 5.20: Distribution of forces in (RCC) springs along a composite connection

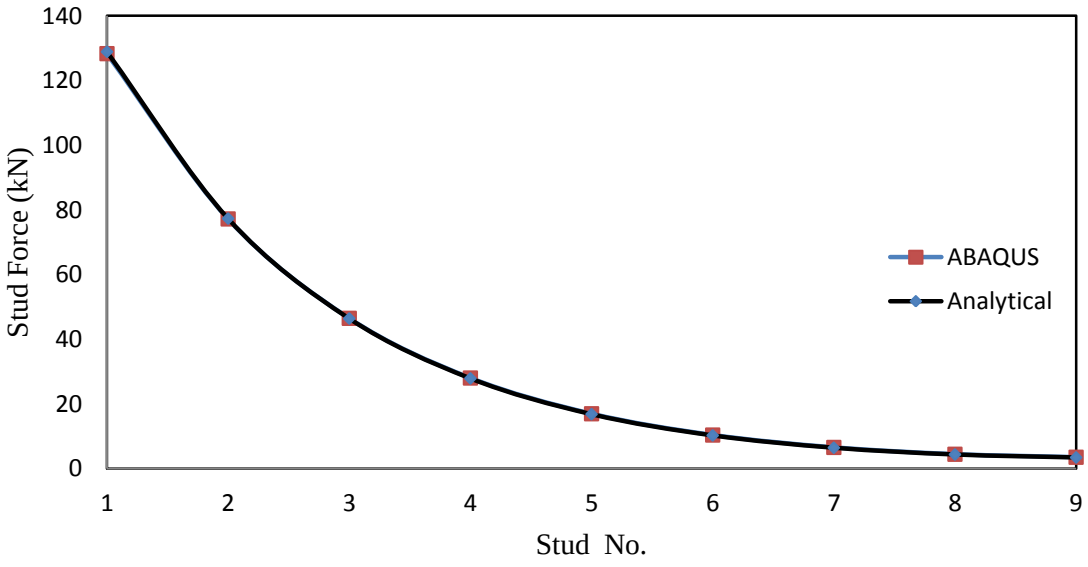

Figure 5.21: Distribution of forces acting on shear studs along a composite connection

Furthermore, Figure 5.22 and Figure 5.23 show the distribution of forces in the (RCC) springs and shear studs as applied moments increase. These figures, along with Figure 5.24 and Figure 5.25 show the ratio of (RCC) springs and the shear studs forces respectively from total reinforcement force. The results clearly show that the first and

second shear studs and first and second reinforcement zones (i.e. between the centreline of the column and the second stud) provide the most resistance to the longitudinal shear force in the composite connection. In addition, the first three studs provide 80% of the total shear resistance and the following six studs provide just 20%. This result is in good agreement with the experimental test results by many researchers such as (Loh et al., 2006; Fu and Lam, 2006). What is more, Anderson and Najafi (1994) assessed their four experimental tests of composite connections for different reinforcement ratios and concluded that the majority of resistance to longitudinal shear force in the steel-concrete interface depends on the first shear stud. Therefore, they considered only this shear stud in their procedure to calculate the initial stiffness of a composite connection. Furthermore, Ahmed and Nethercot (1996) performed numerical studies on a number of cases of composite connections with different shear connection ratios. From the results of the study, they concluded that all shear studs along the composite connection take a share of the longitudinal shear force but in different ratios, depending on their distance from the centreline of the column and the nearest shear stud providing the most resistance to slip. Their modelling was validated against the experimental results of (Li et al., 1996). In principle, their conclusions are compatible with the results from the present work, as shown in Figure 5.24 and Figure 5.25.

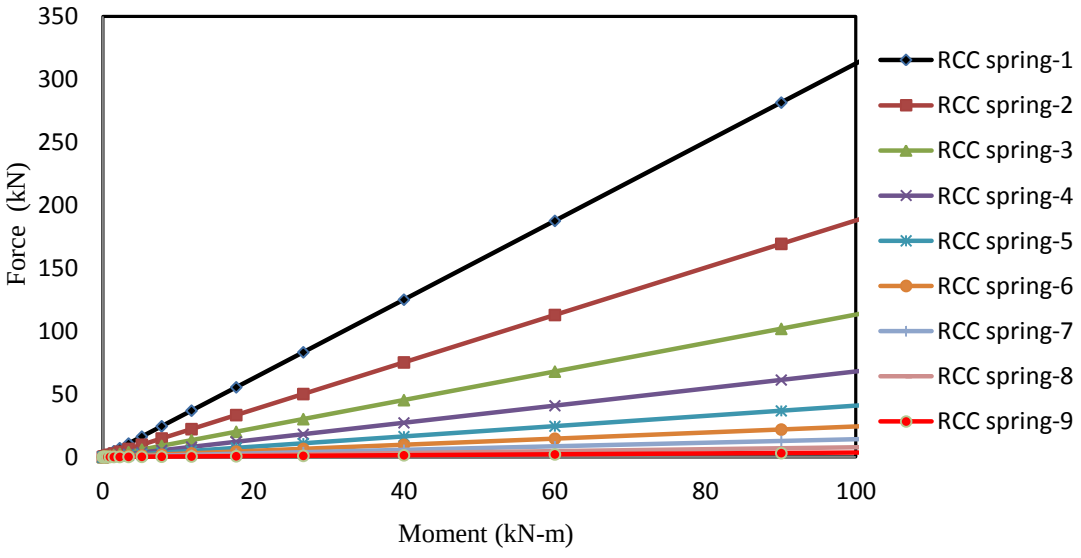

Figure 5.22: Distribution of forces in (RCC) springs for increasing applied moments

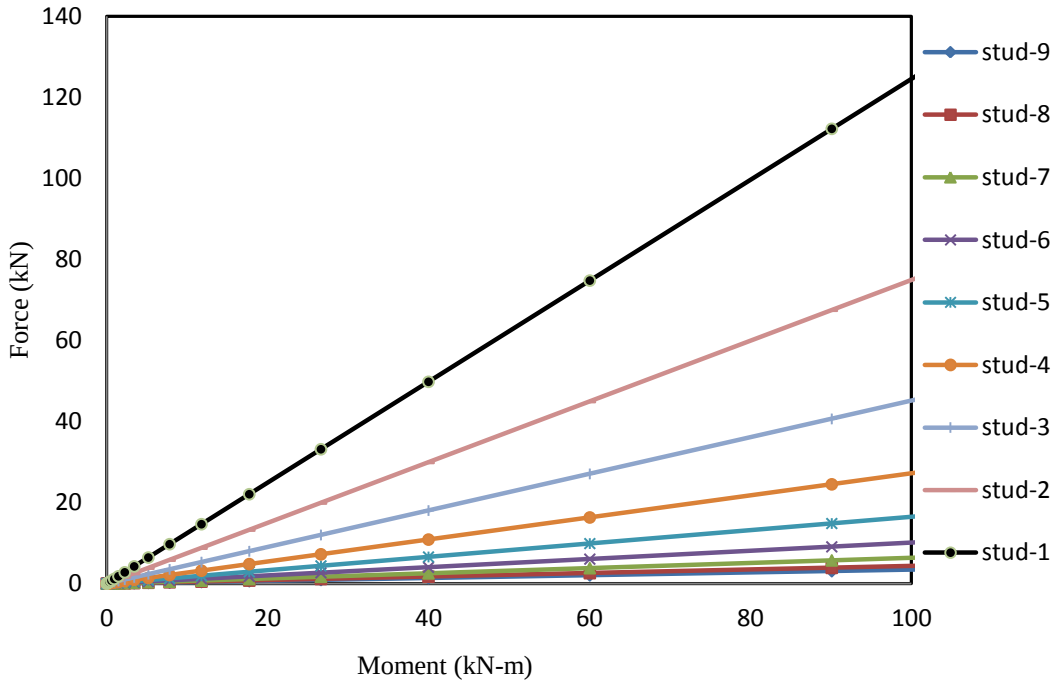

Figure 5.23: Distribution of forces in shear studs for increasing applied moments

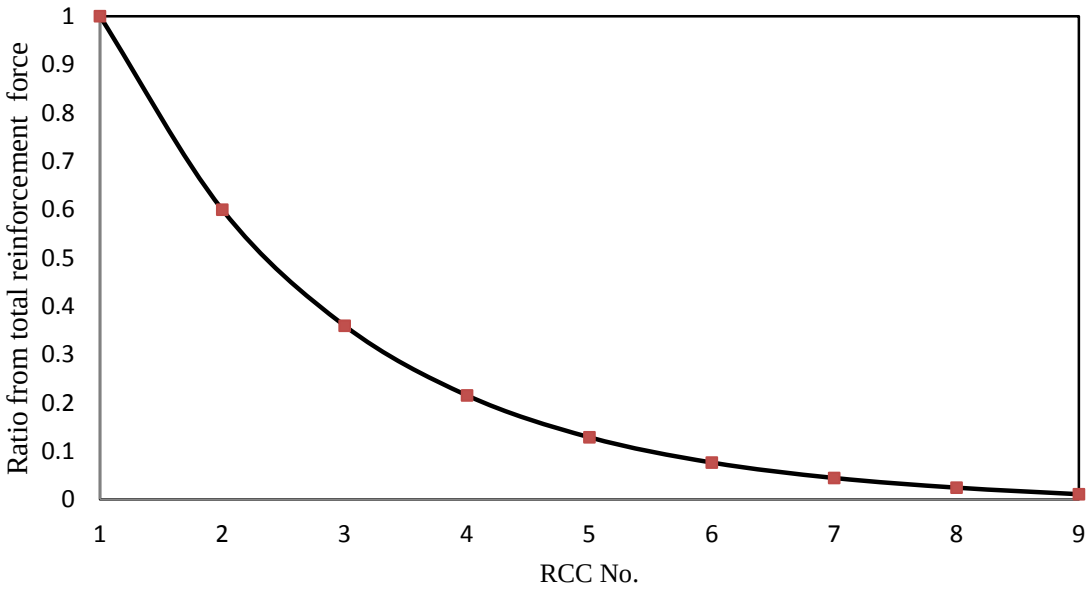

Figure 5.24: Ratio of total reinforcement force in the in every (RCC) spring from total shear force

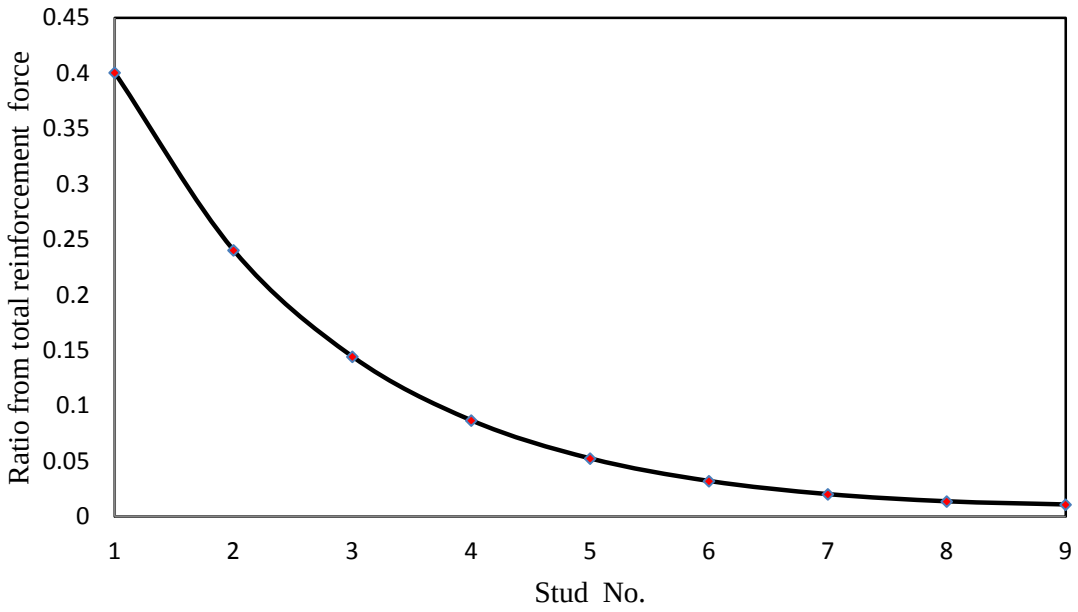

Figure 5.25: Ratio from total reinforcement force in every shear stud along the composite beam

On the other hand, the proposed procedure can be used to overcome the shortcoming in the estimation of the effective length of reinforcement, l_r, as this length is measured from the centreline of the column up to the point where the assumed considerable stress is attained, as explained in Section 5.3.

5.8.2. Verification of the proposed model for (RCC) and shear studs against the experimental test for a composite slab

In literature, limited experimental tests have been conducted on an isolated composite slab. Rex and Easterling (2000) performed experimental tests on four full-scale composite slabs with different numbers and positions of shear studs. The load-deformation behaviour of an isolated composite slab under tension and bending was the main objective of these tests. In addition, a component model was developed to predict the load-deformation behaviour of an isolated composite slab and was compared with the experimental results. This model took into account the effect of concrete on reinforcement (i.e. tension-stiffening) by modelling the concrete as an axially loaded fictitious member with a special stress-strain behaviour acting in parallel with the reinforcing steel. The strain in the concrete was assumed to be the same as the strain in the reinforcing steel (i.e. a perfect bond). This type of modelling did not represent the actual behaviour in reinforcement due to the tension-stiffening effect, as explained in the previous section. A sketch of the test set-up is shown in Figure 5.26.

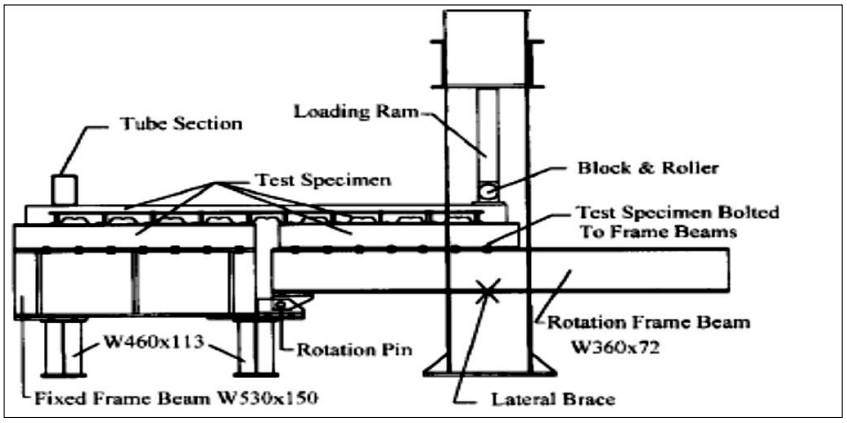

Figure 5.26: Sketch of the set-up used by (Rex and Easterling, 2000)

One of the four slab tests (slab #1) was selected to verify the applicability of the proposed model for (RCC) and shear studs, in order to predict the force-deformation behaviour of the composite slab. The same modelling procedure used in the previous section was used to model the steel beam and the shear studs using ABAQUS software. The embedded reinforcement was modelled as a beam element with modified stress-strain behaviour, as shown in Figure 5.11, in order to account for the tension-stiffening effect. The guideline for modelling in Eq. (5.22) and Eq. (5.24) was used to assign the profile of reinforcement. The final ABAQUS model is shown in Figure 5.27.

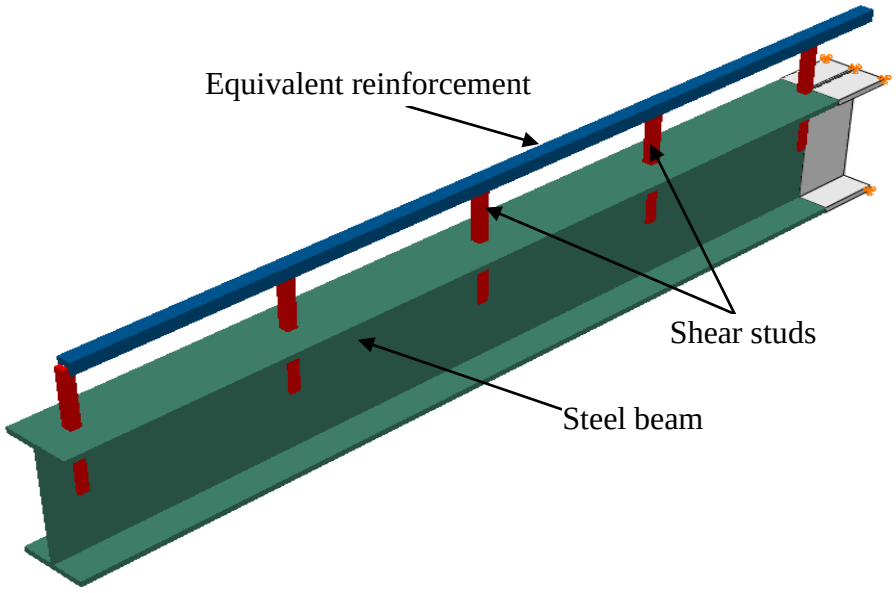

Figure 5.27: ABAQUS model for a composite slab with shear studs

The result of the deformed shape of the model is shown in Figure 5.28. A comparison of the experimental and numerical force-deformations is shown in Figure 5.29, which

clearly shows that the proposed model can reliably predict the force-deformation behaviour of a composite slab with shear studs up to the maximum load.

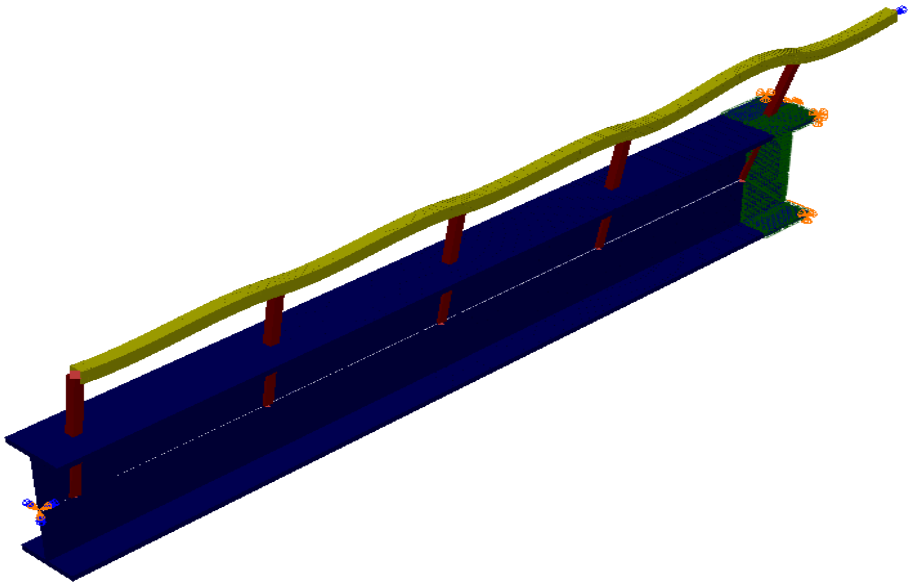

Figure 5.28: ABAQUS deformed shape of a composite slab model

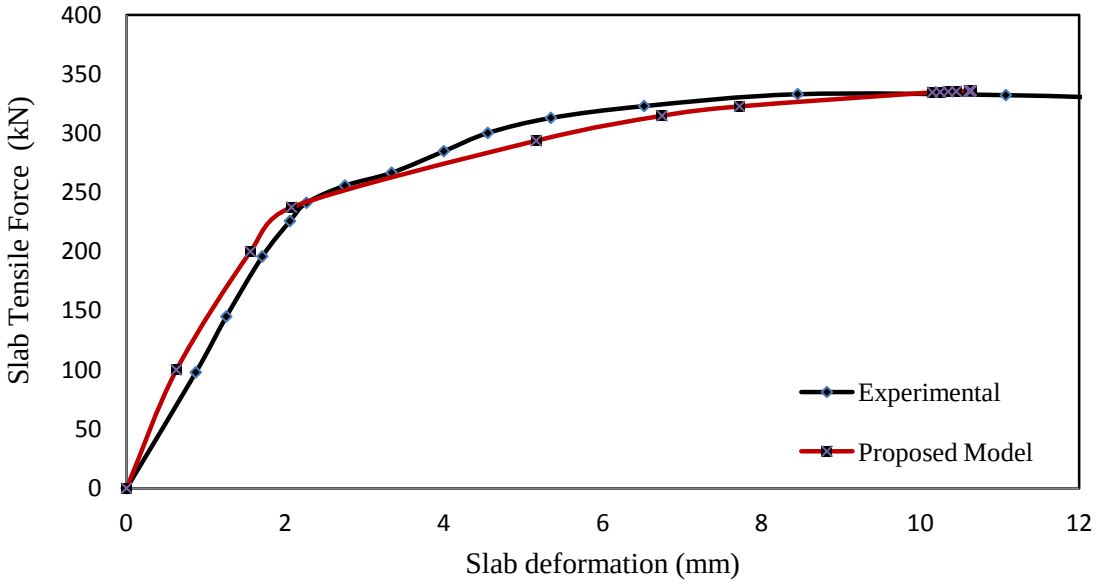

Figure 5.29: Comparison of force-deformation curves for the proposed model and experimental results

5.8.3. Verification of the proposed model against the experimental test for a composite connection

In this section, a 3-D finite element model is constructed using ABAQUS software to verify the proposed model against the experimental test for a composite connection.

The model is based on the experimental tests of (Li et al., 1996). They performed a series of six end-plate beam-to-column composite connection tests. All composite connections were the same with variable shear/moment ratios. A seventh test was carried out on a pure steel connection for the sake of comparison. The specimens were assembled from 254x102UB25 beams and 203x203UC46 columns. Details of the composite connection and load arrangement are shown in Figure 5.30.

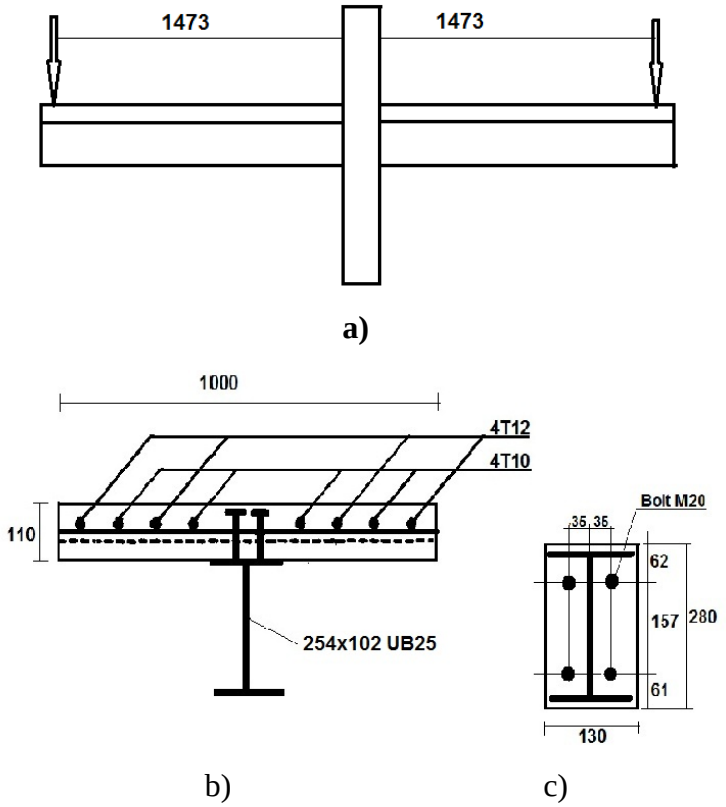

Figure 5.30: a) Load arrangement; b) composite beam section; c) end-plate

5.8.3.1. Modelling of composite connection

5.8.3.1.1. Modelling of steel connection

A 3-D finite element model was constructed to simulate the rotational behaviour of end-plate connections. (Bursi and Jaspart, 1997; Bursi and Jaspart, 1998) suggested one of the three solid elements (C3D8, C3D3I and C3D8R) to be used to model the end-plate connection. A set of simulations were carried out to select the best element out of those three. It was found that the C3D8R element with the reduced integration is the best one considering accuracy, computational time and convergence problems.

All components of the end-plate steel connection were modelled using C3D8R solid elements, as shown in Figure 5.31. Surface-to-surface contact interaction elements were used to simulate the function between:

1. End-plate,
2. column flange,
3. Shank, front and back nuts of bolts.

The pre-tension in the shank of the bolt was modelled by applying contact pressure between the front nut and the end-plate and back nut of the bolts and flange of column. The normal and tangential contact properties were defined using the interaction type option in ABAQUS with a friction coefficient of 0.25.

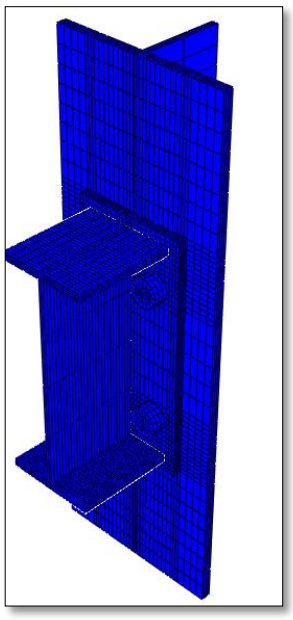

Figure 5.31: Steel end-plate connection

A sensitivity study was conducted to determine an optimum mesh size. Furthermore, interaction elements were used to simulate all of the constrained surfaces. As the composite connection is symmetrical, only one side of the connection was modelled in order to reduce computing time.

5.8.3.1.2. Modelling the steel beam and column

C3D8R solid elements were used to simulate the neighbouring zones of the end-plate connection in order to avoid any conflicts between different types of contact elements.

As the steel beam and upper and lower parts of the column have relatively small strain for all stages of loading, beam element with a coarse mesh was used to model the remaining parts of the steel beam and column to reduce computation time. The surface-to-surface constrain *Tie* option in ABAQUS was used to connect the steel beam and the end-plate; however, coupling constrains were used to connect both parts of the steel beam and column.

5.8.3.1.3. Material modelling

In order to reduce numerical problems, a simplified elastic-plastic model with symmetrical behaviour in both tension and compression was used to simulate all the structural steel components such as the beam, column, shank and nuts of bolts and the end-plate. The linear elastic part was defined by the ELASTIC option in ABAQUS using an elastic modulus of elasticity value of E_s=200 GPa. This behaviour continues up to the experimental yield stress. Based on a study by (Amadio and Fragiacomo, 2003), the assumed linear post-limit part was modelled using the PLASTIC option using an assumed hardening modulus of E_h=0.015E_s. This behaviour continues up to the ultimate stress, as shown in Figure 5.32. In ABAQUS material model, there are two automatic options to compute the stress for any strain greater than ε_{su} by extending the last part of the stress-strain curve indefinitely along a direction of (i) constant slope, (ii) zero slope.

The first option was taken in order to overcome the problem of convergence.

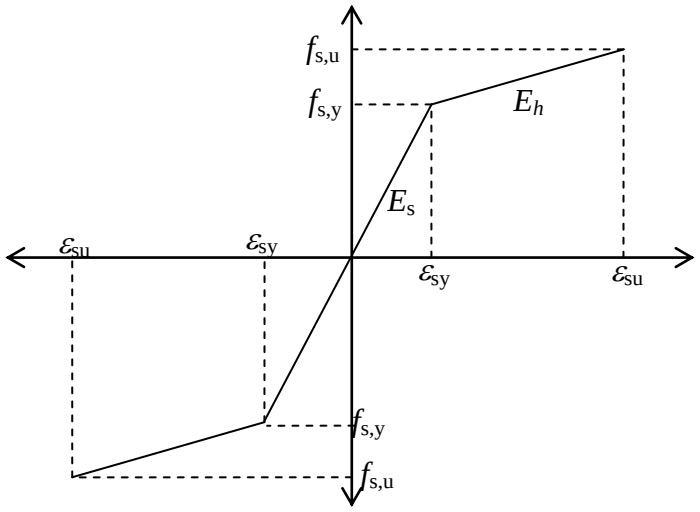

Figure 5.32: Elastic-plastic model for steel

5.8.3.2. Modelling of a reinforced concrete slab

The proposed model in Section 5.5 was used to simulate the embedded reinforcement incorporating the effects of concrete, which were taken implicitly. Eq. (5.22) and Eq. (5.24) were used to select appropriate dimensions for the element in order to capture the actual behaviour of a reinforced concrete slab. The embedded reinforcement and shear studs were connected by multi-point constraints.

5.8.3.3. Modelling of shear studs

As there were two shear studs in every row along the composite connection, their effects were combined into one equivalent shear stud using the principle of equivalent springs in parallel. The resultant shear studs were modelled as rotational springs at the base of a rigid bar which was connected to the centreline of the beam with a modified embedded reinforcement. The non-linear moment-rotation behaviour of the rotational spring is shown in Figure 5.33.

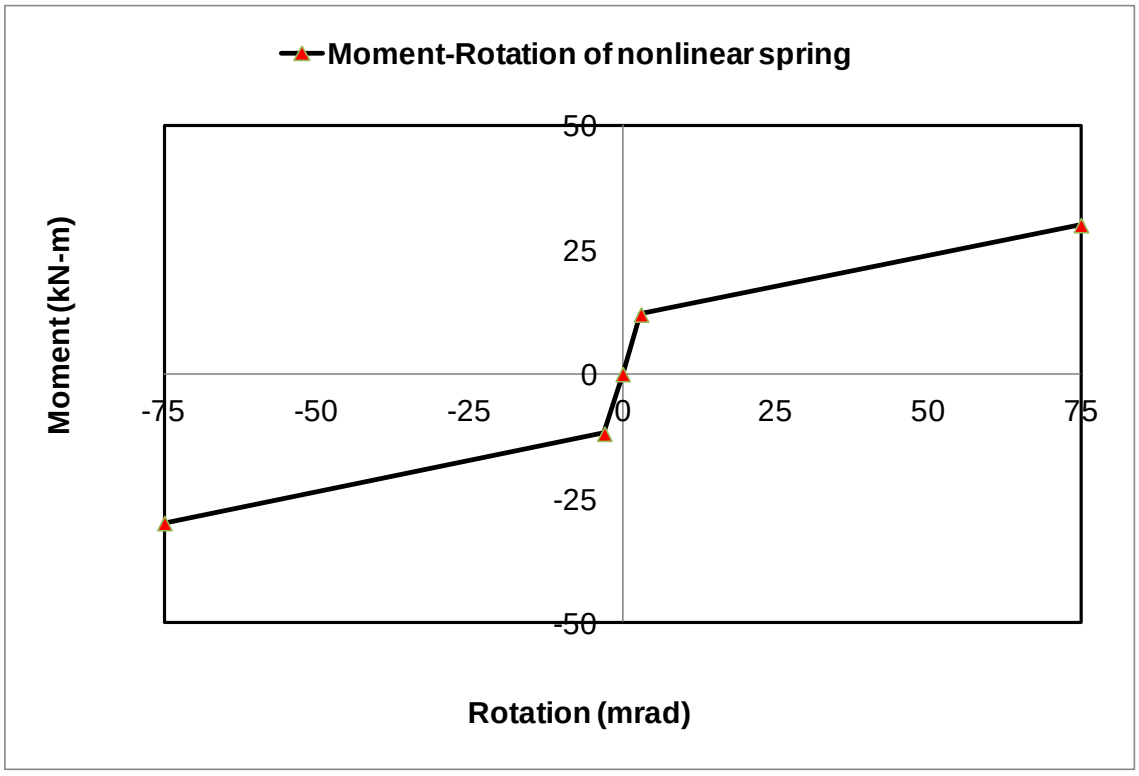

Figure 5.33: Behaviour of shear studs

5.8.3.4. Boundary conditions and load conditions

All of the test boundary conditions were modelled as close to reality as possible. The top and bottom of the column was assumed fixed in the FE model so as to represent the base plates. The final 3-D finite element model is shown in Figure 5.34.

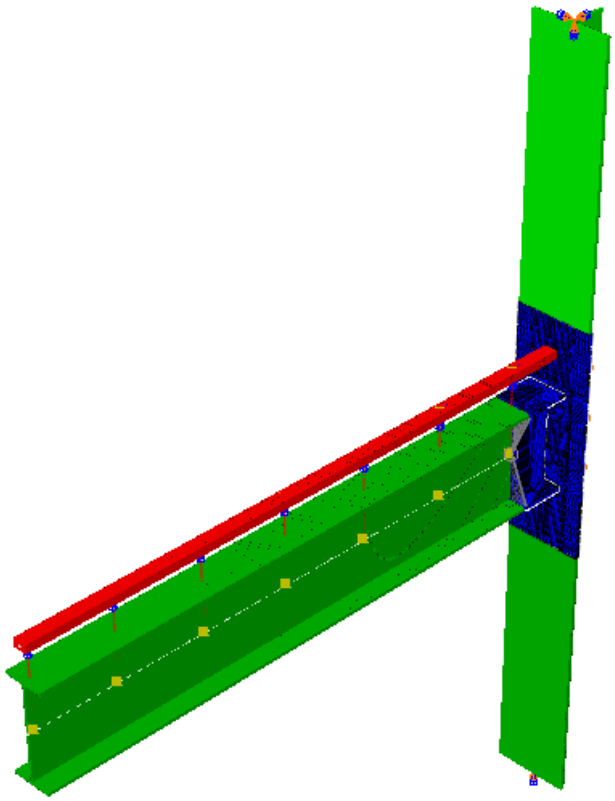

Figure 5.34: The final 3-D finite element model

5.8.3.5. Validity of the finite element model

The 3-D finite element model was validated by comparing the corresponding moment–rotation curves from the test carried out by (Li et al., 1996). The preliminary validation was carried out against the experimental behaviour of a pure steel connection in order to assess the ability of the modelling procedures to capture the actual behaviour of a steelwork connection. The validity of a composite connection model was then evaluated against the experimental behaviour of a composite connection. Figure 5.35 shows the resultant deformed shape of the composite connection. In addition, Figure 5.36 shows good agreement between the moment-rotation curve from the test and finite element analysis. The small discrepancy between them may be related to the fact that the stress-strain behaviour of steel components was assumed to be bilinear. This comparison clearly indicates the applicability of the proposed model to capture the actual behaviour

of a composite connection for a reinforced concrete slab. The extended part in Figure 5.36 of the resultant ABAQUS curve for the behaviour of SJS-1 is related to the extension of the stress-strain curve of steel, as explained in Section 5.8.3.1.3.

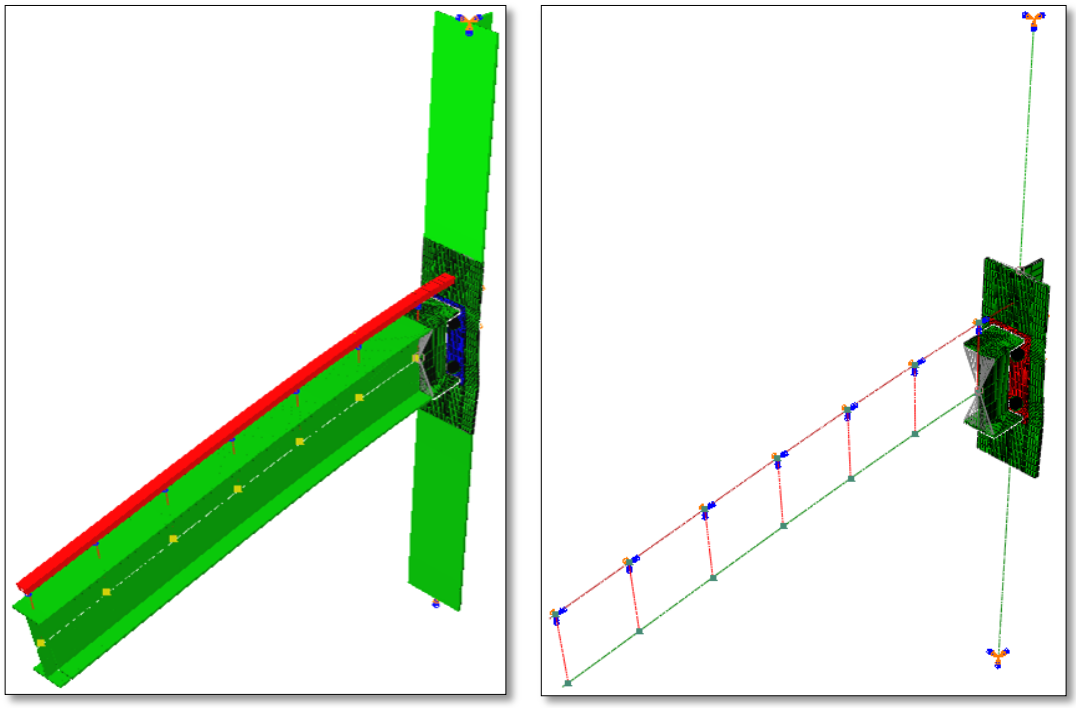

Figure 5.35: Deformed shape of the composite connection

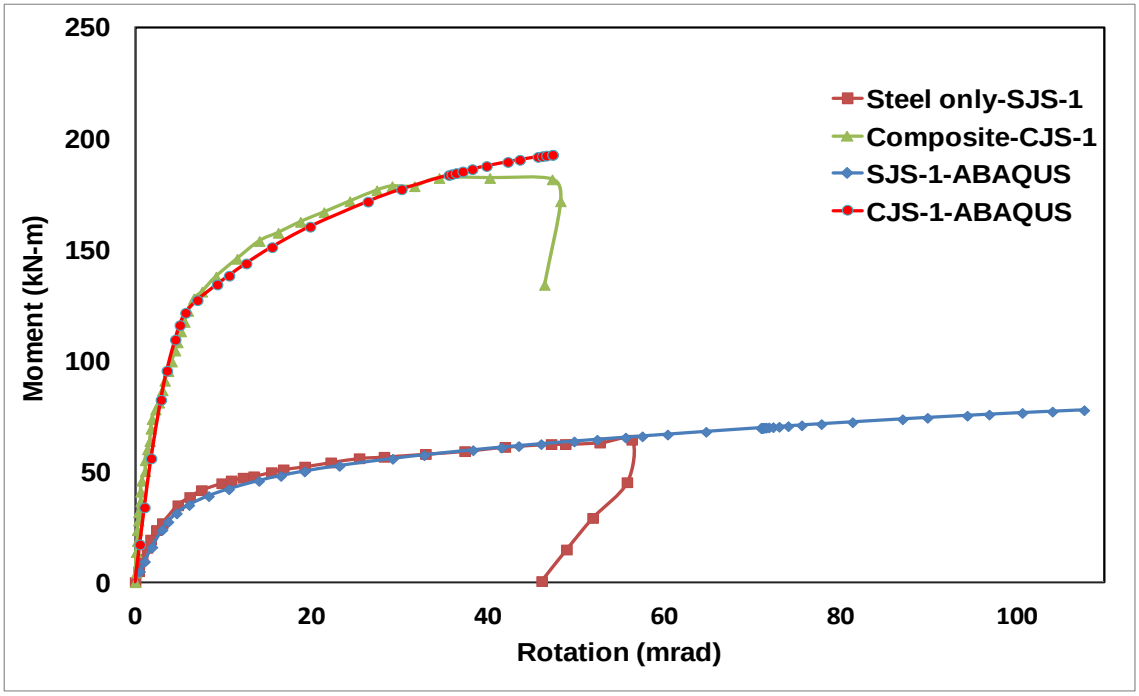

Figure 5.36: Comparison of the moment-rotation curves for experimental and numerical modelling

5.9. Parametric study to investigate the effect of k_{RCC}/k_{sc} on K_{lump}

A parametric study using the proposed expressions was carried out in order to investigate the effect of the relative stiffness of the (RCC) to that of the shear stud component (S) on the resultant stiffness (i.e. "lump'' stiffness). ABAQUS was then used to check all the results.

Before carrying out the parametric study, the range of some important factors should be found first.

5.9.1. Maximum and minimum ratios of k_{RCC}/k_{sc}

Eurocode 4 (2004) states that the minimum and maximum spacing of shear connectors are five times the diameter of the stud and 800 mm respectively. Therefore, the practical range of geometry and properties of the materials for a composite connection are listed in Table 5.1.

Table 5.1: Practical range of properties

E_m (kN/mm^2)		A_r (mm^2)		l_r (mm)		k_{RCC} (kN/mm)		k_{sc} (kN/mm)		k_{RCC}/k_{sc}	
Min.	Max.	Min.	Max.	Min.	Max.	Min.	Max.	Min.	Max.	Min.	Max.
200	300	4ϕ12mm	15ϕ12mm	80	800	113	6360	100	250	0.45	63

In this table, the relative stiffness k_{RCC}/k_{sc} varies between 0.45 and 63. In the parametric study, it was taken to be between 0.01 and 100 in order to investigate other possible values including the range given in the above table. The selected range also refers to the range between the low partial shear connection (k_{RCC}/k_{sc} = 100) and nearly full interaction (k_{RCC}/k_{sc} = 0.01) of a composite connection. Therefore, the main objectives of this parametric study are:

1. Investigate the effect of using stiff or soft shear studs on the distribution of forces in the shear studs and reinforcement along the composite slab.

2. Investigate the effect of shear connection ratio on the distribution of forces in the composite slab.

3. Estimate the maximum number of "active'' shear studs in the shear span in relation to the shear connection ratio.

4. Obtain the relationship between the required number of shear studs for a full shear connection and the maximum number of "active'' shear studs in the shear span.

5.9.2. ABAQUS model

The same modelling procedure detailed in Section 5.7 (i.e. a spring model) was used; this is shown in Figure 5.37.

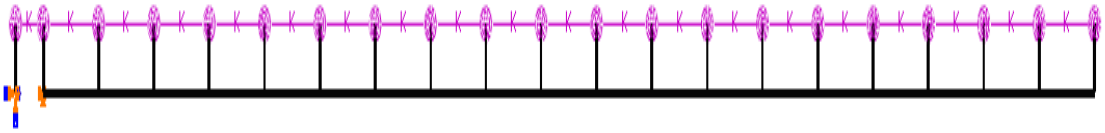

Figure 5.37: Sample of ABAQUS Model for parametric study (20 studs) (same as Figure 5.17, but with different number of studs)

5.9.3. Results and discussion

Effect of shear stud stiffness

The effect of the stiffness of a shear stud on the distribution of forces along the composite connection was investigated by performing four sets of calculation on 13 sets of shear stud in composite connections, with the number of shear studs varying between 2 and 20. Each set of calculation had constant k_{RCC}/k_{sc}, with the stiffness of the shear stud varying between 100 kN/mm and 250 kN/mm. The k_{RCC}/k_{sc} varied between 1.0 and 100. The results of these calculations are shown in Figure 5.38 to Figure 5.41. By comparing the results from every cycle of calculation (i.e. constant k_{RCC}/k_{sc} with varying k_{sc}), it is clear that the stiffness of a shear stud has little effect on the distribution of forces acting on the shear studs along the composite connection for constant values of k_{RCC}/k_{sc}. However, comparison of the results for the same k_{sc} and different k_{RCC}/k_{sc} shows the significant effect of k_{RCC}/k_{sc} on this distribution of forces. As k_{RCC}/k_{sc} increases (i.e. shear connection ratio decreases), greater redistribution of forces between shear studs is achieved and more of shear studs will take a share of the total tensile force in the reinforcement. This consequently means that the effective length of reinforcement increases.

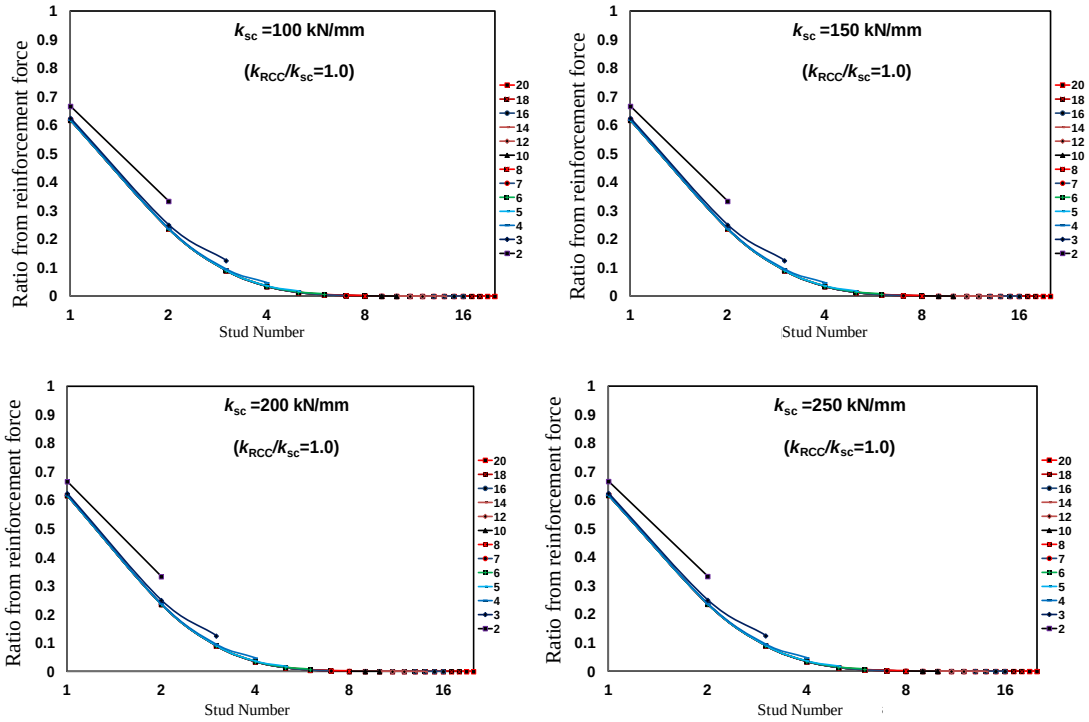

Figure 5.38: Distribution of forces in shear studs for k_{RCC}/k_{sc} =1.0

(The legend shows the number of studs for every connection)

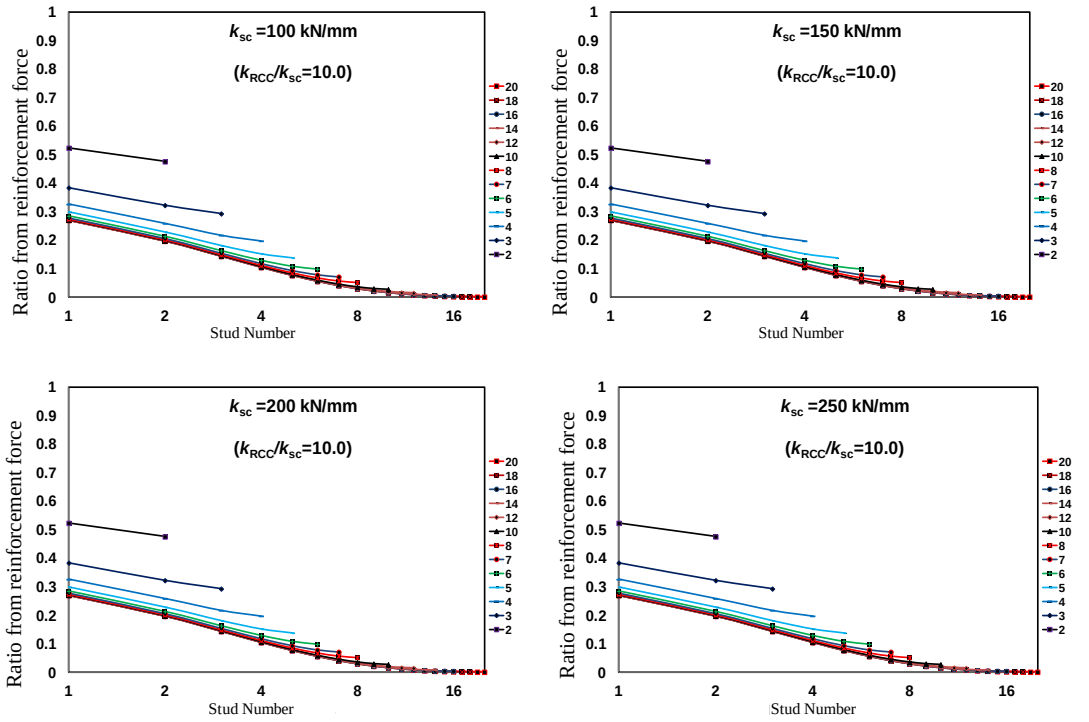

Figure 5.39: Distribution of forces in shear studs for k_{RCC}/k_{sc} =10

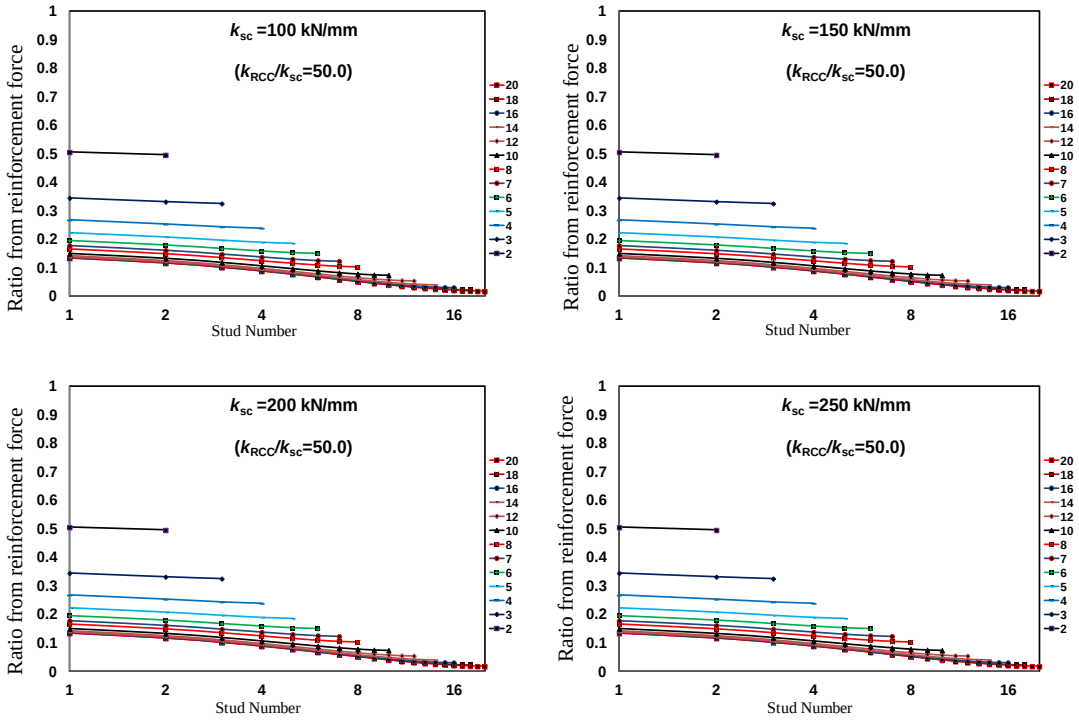

Figure 5.40: Distribution of forces in shear studs for k_{RCC}/k_{sc} =50

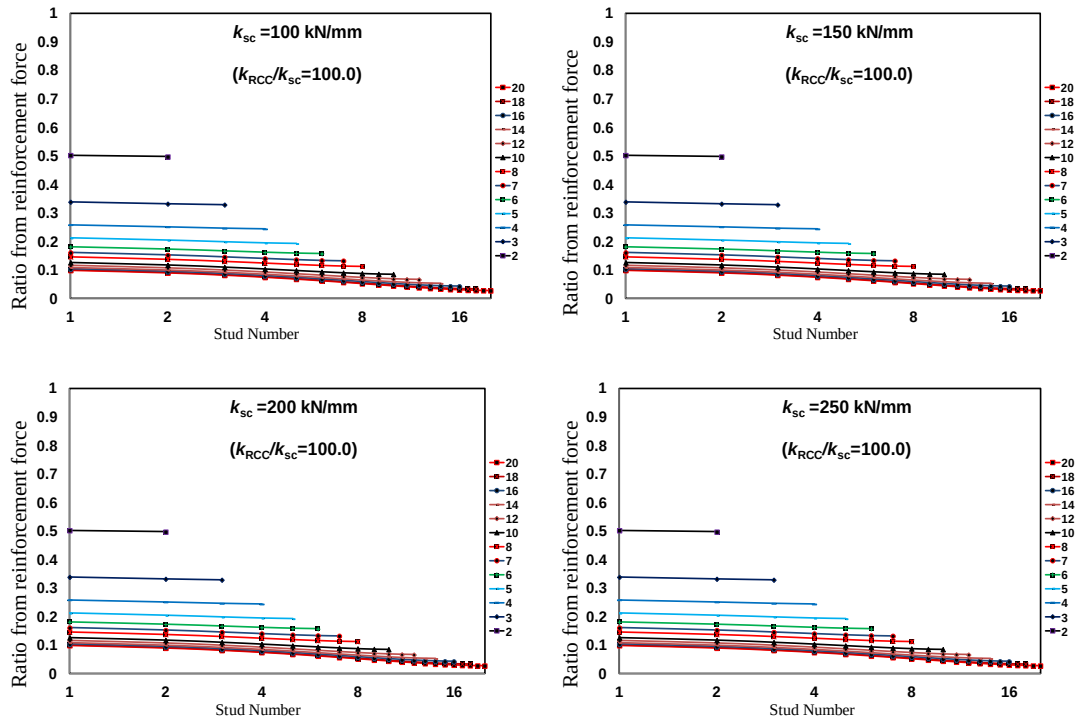

Figure 5.41: Distribution of forces in shear studs for k_{RCC}/k_{sc} =100

Effect of changing k_{RCC}/k_{sc} with constant k_{sc}

Following the observations from the previous part of the parametric study, a constant value of (k_{sc}=150 kN/mm) was used in this part, with values of k_{RCC}/k_{sc} varying from 0.01 to 100 (i.e. full interaction to partial shear connection range). The results from 12 sets of calculation for 13 cases of composite connection with number of shear studs ranging from 2 to 20 are shown in Figure 5.42.

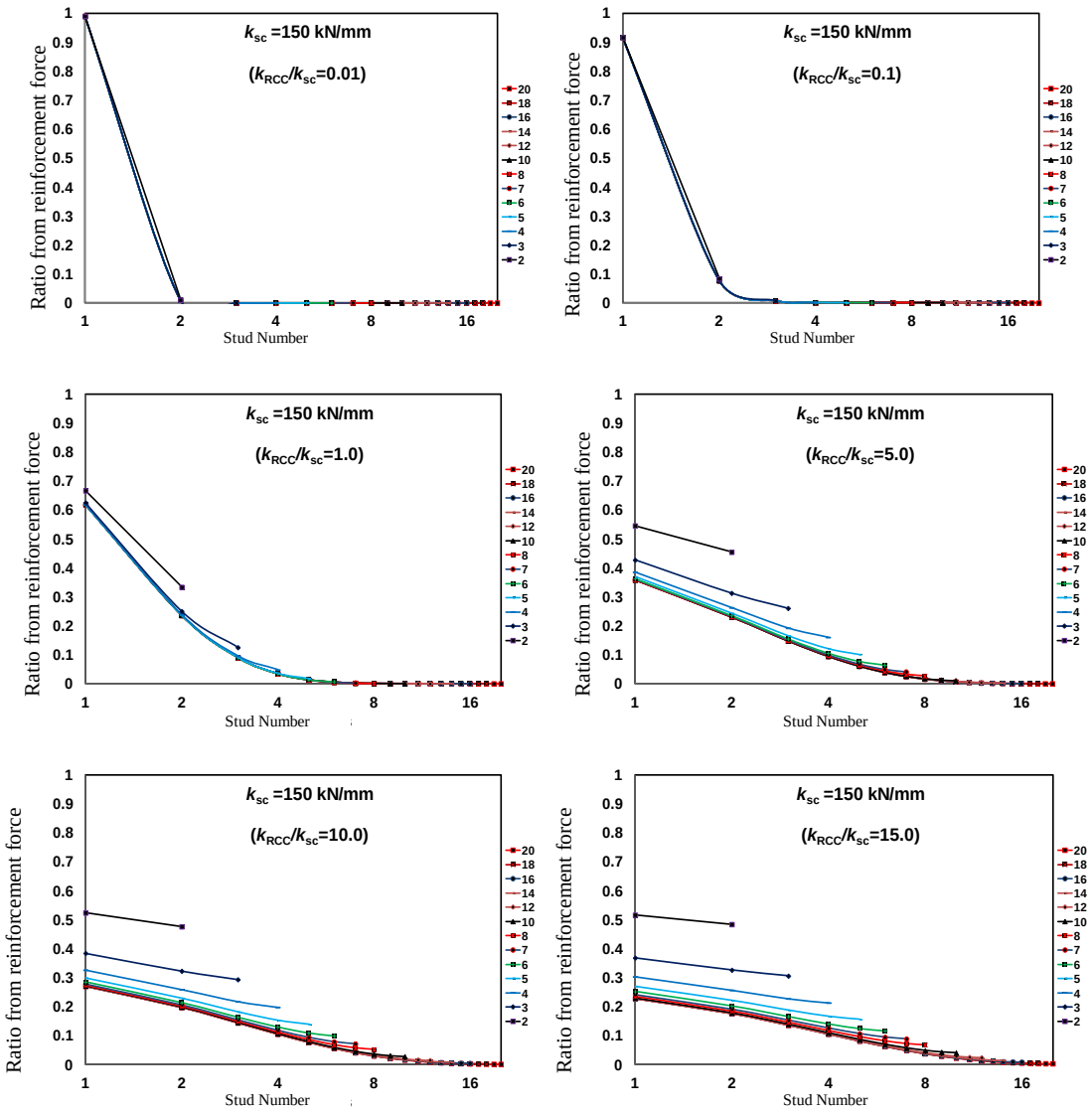

Continue in next page

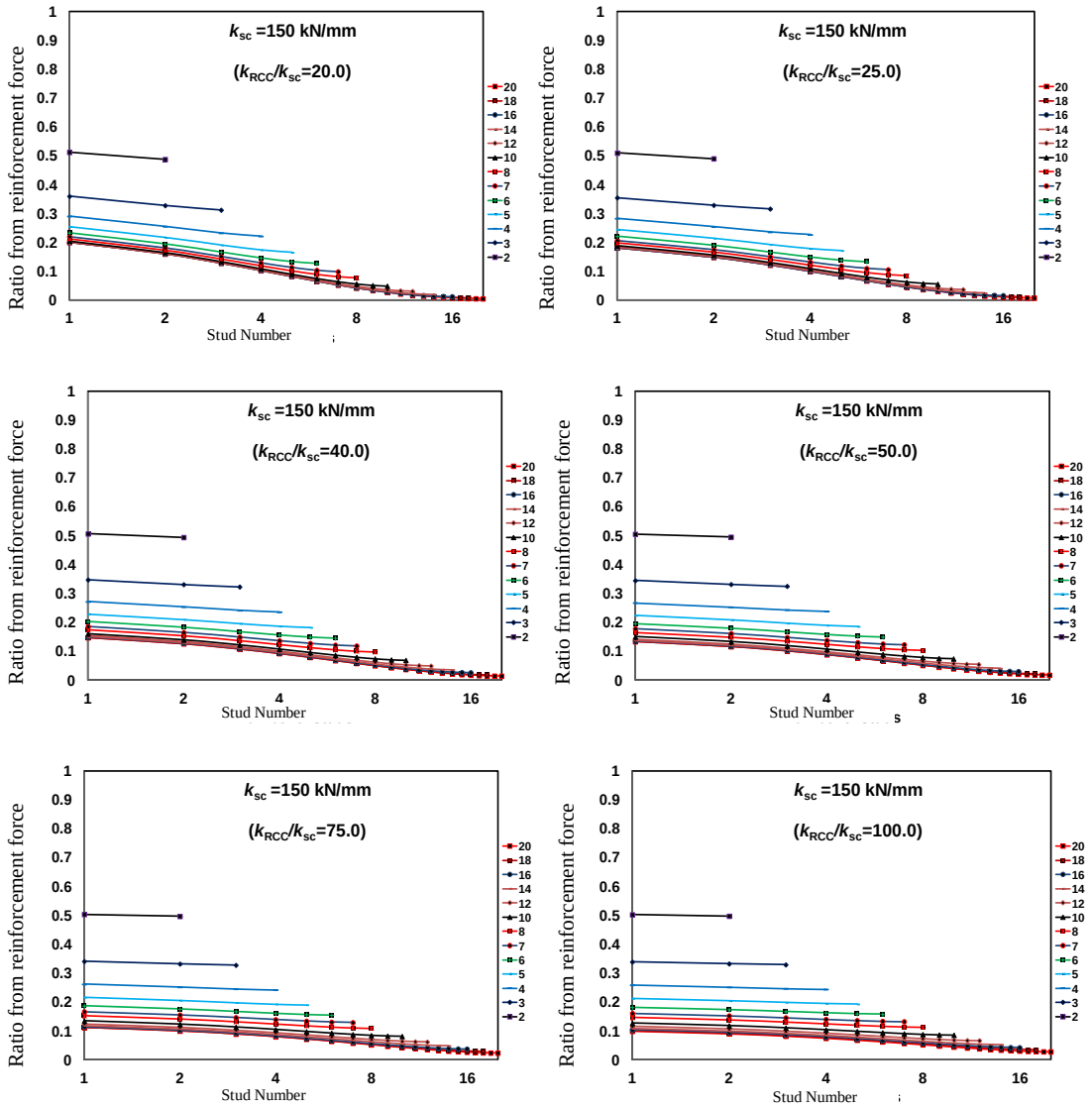

Figure 5.42: Distribution of forces in shear studs for k_{sc}=150kN/mm and k_{RCC}/k_{sc} =0.01 to 100

The results of the analysis show the significant effect of k_{RCC}/k_{sc} on the distribution of forces along the composite connection. When the k_{RCC}/k_{sc} value is small (i.e. a high shear connection), only the shear studs nearer the column will share the total tensile force and the contribution from the other remaining shear studs is insignificant. However, almost all shear studs will share the total tensile force but with a linearly decreasing ratio in cases with a high value of k_{RCC}/k_{sc} (i.e. a low shear connection). Since the stiffness and strength of a shear stud are related, as explained in Chapter Four and Eq. (4.3), the results indicate that the assumption of (Anderson and Najafi, 1994) of using only the first shear studs in their calculation of the initial stiffness of a composite connection is valid only for very stiff shear studs or low reinforcement ratio cases, even though the first stud has the largest percentage of resistance for all cases. This

percentage is reduced abruptly as k_{RCC}/k_{sc} increases or the partial shear connection ratio decreases, since more shear studs will take part in the resistance of the total tensile force at the steel-concrete interface. All shear studs transfer approximately the same amount of shear force for very low shear connection ratios. This behaviour is described in Figure 5.43.

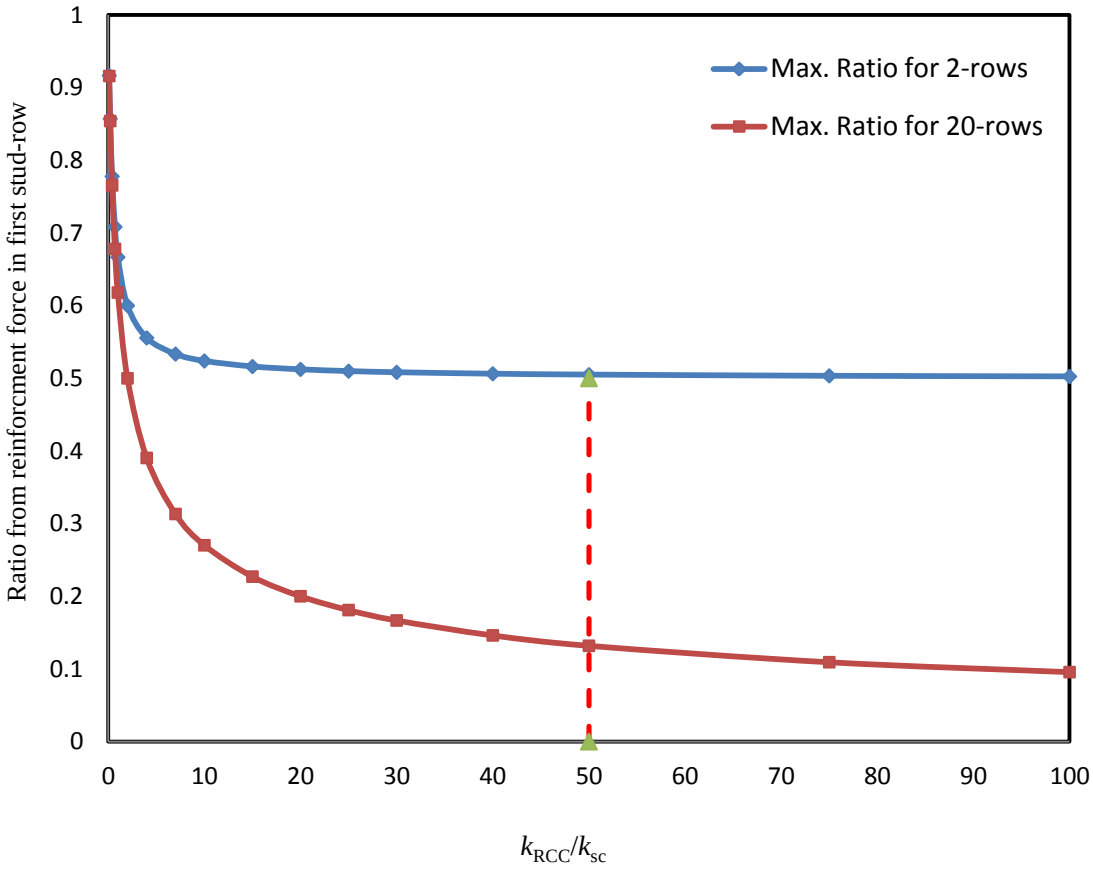

Figure 5.43: First stud force ratio from reinforcement force with varying k_{RCC}/k_{sc}

Furthermore, these results confirm the results of the finite element parametric study conducted by (Ahmed and Nethercot, 1996) on composite connections with different shear connection ratios. They concluded that it is better to use a higher number of soft shear studs with a lower strength than to use fewer stiff shear studs with high strength in order to avoid local concrete failure.

Maximum number of "active'' shear studs

In the present work, the "active'' shear stud is defined as the stud that transfers more than 5% of the total tensile force at the steel-concrete interface. Therefore, the maximum number of "active'' shear studs can be estimated by plotting the relationship

between k_{RCC}/k_{sc} and the maximum number of "active'' shear studs from the results of 156 cases of composite connections (13 composite connections with different numbers of shear studs and 12 values of k_{RCC}/k_{sc}). The relationship is shown in Figure 5.44, and can be best fitted with the following logarithmic expression:

$$N_{active} = \ln(\frac{k_{RCC}}{k_{sc}}) + 3.75 \tag{5.37}$$

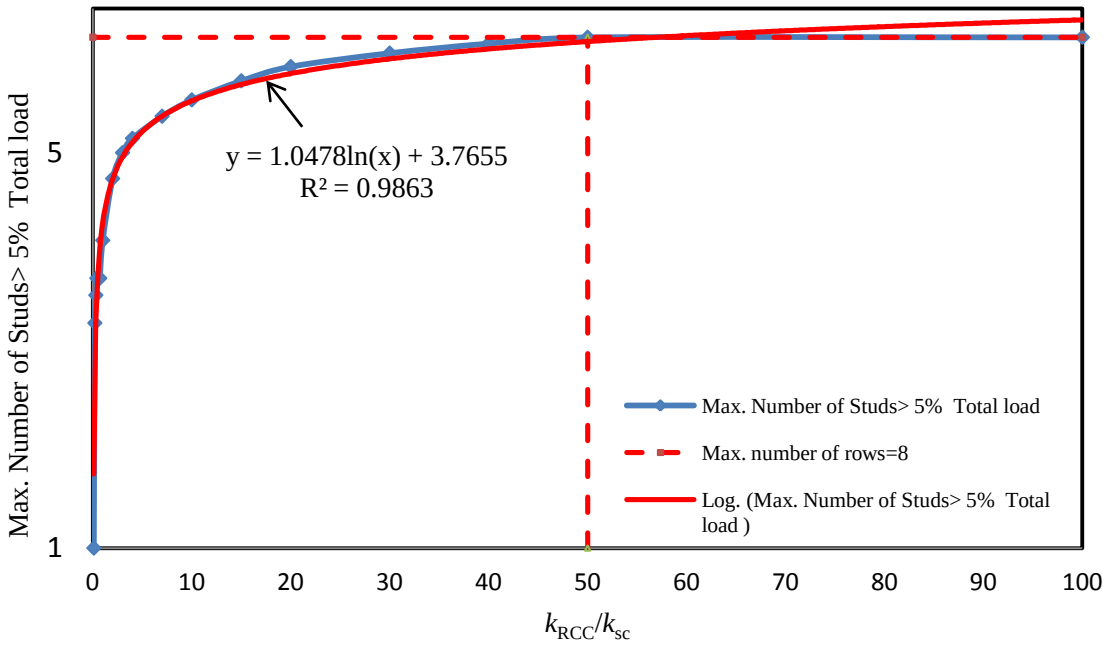

Figure 5.44: Relationship between the maximum number of "active'' shear studs and k_{RCC}/k_{sc}.

Relationship between N_{full} and N_{act}

In order to derive the relationship between the maximum number of shear studs for a full shear connection, N_{full}, and the number of "active'' shear studs, N_{act}, Eq. (5.38) is rewritten as:

$$N_{act} = \ln(\frac{E_m A_r}{p k_{sc}}) + 3.75 \le 8 \tag{5.38}$$

The relationship between the stiffness and strength of a shear stud was defined in Chapter Four (i.e. Eq. (4.3)) as:

$$k_{sc} = \gamma F_{sc,max}$$

where γ was assumed equal to 1.47 as explained in Chapter Four (Section 4.3). Then,

$$N_{act} = \ln(\frac{E_m A_r}{p\gamma F_{sc,\max}}) + 3.75 \le 8$$

since $$N_{full} = \frac{A_r f_{r,y}}{F_{sc,\max}} \Rightarrow \frac{A_r}{F_{sc,\max}} = \frac{N_{full}}{f_{r,y}}$$

then,

$$N_{act} = \ln(N_{full}) + \ln(\frac{E_m}{p\gamma f_{r,y}}) + 3.75 \le 8 \quad (5.39)$$

Therefore, if the number of shear studs for a full shear connection is fewer than eight, it is preferable to increase this number to eight by using shear studs of lower strength. Also, if this number of shear studs is greater than eight, it is preferable to decrease this number to eight by using shear studs of higher strength. The required minimum strength of a shear stud can be calculated as:

$$\min F_{sc,\max} = \frac{A_r f_{r,y}}{8} \quad (5.40)$$

5.11. Modified mechanical model of initial stiffness for a composite connection

In Chapter Three, a mechanical model was proposed to calculate the initial stiffness of a composite connection, as shown in Figure 5.45.

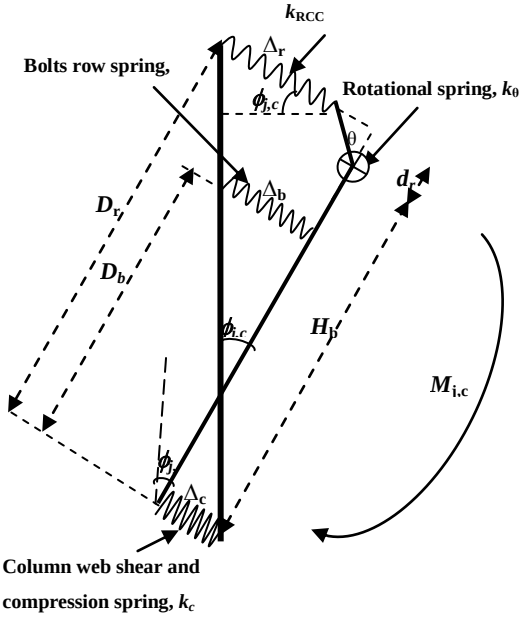

Figure 5.45: The proposed mechanical model

In this model, the reinforcement and shear stud components were modelled separately. The proposed mechanical model can be modified in order to account for the tension-stiffening effect and "active'' shear studs. This modification is only valid to calculate the initial stiffness of a composite connection, but the original model with a rotational spring will be required for the analysis of a composite connection in post-linear range. This modification can be achieved using different methods:

Method 1

In the first method, the same mechanical model shown in Figure 5.45 is used with the following modifications to the stiffness of the reinforcement and shear studs:

i. Stiffness of "active'' shear studs, k_s

There are many procedures to calculate the stiffness of shear studs, as explained in details in Chapter Three. However, none of them consider the concept of an "active'' shear stud or the diminishing share of shear resistance in proportion to the distance from the centreline of the column. This stiffness should be calculated considering the logarithmic decrease in contribution of an "active'' shear stud in total stiffness proportional to its distance from the column. In order to calculate the initial stiffness of a composite connection, the average stiffness of shear connectors can be approximated as follows:

$$k_s = \frac{N_{act}}{2} k_{sc} \quad \text{where} \quad N_{act} \le N_{all} \tag{5.41}$$

ii. Stiffness of embedded reinforcement

Generally, the stiffness of the reinforcement is calculated using the axial stiffness equation for a bar:

$$k_r = \frac{E_r A_r}{l_r} \tag{5.42}$$

where A_r, E_s is the area and modulus of elasticity of the reinforcement. l_r is the effective length of the reinforcement or the distance from the centreline of the column up to the point where the tensile stress decrease to about half the maximum stress. In Chapter Three (Sections 3.9.3), various procedures to estimate the effective length were described, which give considerably different results. In this study, the tension-stiffening effect is taken into account by

replacing E_s with E_m as explained in Section 5.5 (see Figure 5.11), and the effective length is calculated as follows:

$$l_r = \frac{h_c}{2} + \frac{N_{act}\, p}{4} \tag{5.43}$$

where h_c and p are the depth of the column and the spacing of the shear studs respectively. These modifications will ensure that the requirements of effective length definition and stiffness of embedded reinforcement k_{RCC} are met.

Method 2

The second method of modification of the proposed mechanical model can be achieved by replacing both the reinforcement and shear studs springs with a "lump'' spring, as explained in Section 5.5. The stiffness of the "lump'' spring can be calculated using Eq. (5.30). The final modified model is shown in Figure 5.46.

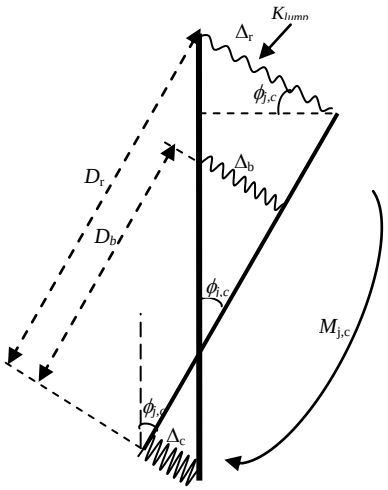

Figure 5.46: Final modified mechanical model

5.12. Summary and conclusions

In this chapter, a new component model for a composite slab has been developed. This model combines the effects of embedded reinforcement and concrete in one component (RCC). The tension-stiffening effect of concrete was considered implicitly in the stiffness of the (RCC) by way of the modified modulus of elasticity concept E_m. In addition, the component model was further simplified by replacing all (RCC) components along the composite connection with equivalent springs. Shear studs were modelled as linear or non-linear springs depending on the expected range of loading. Furthermore, a simplified procedure was proposed to calculate the "lump'' stiffness of

the (RCC) and the shear stud (S) springs. The proposed models and calculation procedures were verified against finite element and experimental results for the selected composite connections. A parametric study was carried out to investigate the effect of the relative values of (RCC) to S stiffnesses on the distribution of forces acting on all components of (RCC) and shear stud springs along the composite connection. A new procedure to find the maximum number of ‘‘active’’ studs was developed. The relationship between the number of ‘‘active’’ shear studs and the maximum number of shear studs required for a full shear connection was derived. Finally, modification of the proposed mechanical model to calculate the initial stiffness of a composite connection was performed using two approaches. The first approach was achieved by developing new expressions to calculate the stiffness of ‘‘active’’ shear studs and the modified embedded reinforcement. The second approach used a single spring in place of the reinforcement and shear stud springs in the original mechanical model. The validity of all the proposed models and equations were verified using ABAQUS software as well as the results from experimental tests in the literature and they are in well agreement.

Chapter Six

Moment resistance and Ductility of a flush end-plate composite connection

6.1. Introduction

In most of the previous works, the moment resistance and rotation capacity of composite connections had been dealt with separately. However, the values of the moment resistance and rotation capacity depend significantly on the mode of failure of connection. In addition, the composite connection cannot attain the plastic moment without sufficient rotation capacity to ensure the redistribution of forces between the components of connection. For that reason, there are many experimental cases where the test had to stop before the composite connection attained its plastic moment due to excessive deformation in just one of their components such as (Li et al., 1996)'s experimental tests. Also, there are some cases where the composite connection failed just at the expected moment resistance due to fracture of one component with very limited rotation capacity such as S8FD specimen which was tested by (Anderson and Najafi, 1994).

Therefore, the choice of a procedure to estimate the moment resistance or rotation capacity of composite connection should be dependent on the mode of failure.

The objectives of this chapter are:

1. Develop a simple flowchart to predict the failure mode of a flush end-plate composite connection,
2. Develop a procedure to estimate the moment resistance of a flush end-plate composite connection by modifying the existence procedures in literature to incorporate the partial shear connection effect and to be compatible with the proposed flowchart of mode failure,
3. Develop a new procedure to estimate the rotation at first yield and rotation capacity of a flush end-plate composite connection.

6.2 Prediction of failure mode of a flush end-plate composite connection

The procedure to predict the failure mode of composite connection was developed by studying a number of experimental tests of composite connections in the literature. The main parameters that govern failure mode are:

1. reinforcement ratio (ρ),
2. shear connection ratio based on the yield strength of reinforcement (η_y), and shear connection ratio based on the ultimate strength of reinforcement (η_u),
3. beam depth (H_b), and
4. whether the column web is stiffened or unstiffened.

The tests from the literature are listed in Table 6.1. The proposed flowchart to predict the failure mode of a flush end-plate composite connection is shown in Figure 6.1.

It should be noted that the proposed flowchart was constructed based on the practical range of shear connection ratio (η_y>0.4). Also, the reinforcement ratio was assumed in the range of (0.5<ρ<1.7%) since most of the experimental tests in the literature were in this range. The normal range of reinforcement ratio in composite connections is in between 0.7% to 1.4% according to (Xiao et al., 1996). There are many other cases reported in the literature where the reinforcement ratio or shear connection ratio are either very high or very low compared to the above ranges. These cases are not considered in the present work.

Table 6.1: Parameters of experimental test of composite connections

Ref.	Specimen	Column Web stiffened	ρ%	Moment resistance	Rotation		Shear Studs		SLIP	Failure Mode
					Ult.	Max.	No.	η_y%		
Anderson and Najafi	S4F	YES	0.55	179	15.7	26.6	7	300	N.A	B
	S8F	YES	1.1	262	28	35.8	7	150	N.A	E,B
	S12F	YES	1.65	302	22.7	55.7	7	100	N.A	E
	S8FD	YES	1.1	416	14	14	7	150	N.A	B
Xiao et. al.(1994)	SCJ3	Non	0.2	85.7	7.2	26.6	6	500	N.A	B
	SCJ4	Non	1.0	202.9	23.4	41.1	6	120	N.A	D,C
	SCJ5	yes	1.0	240.8	26	35	6	120	N.A	E
	SCJ6	Non	1.0	157.6	11.5	23	6	120	N.A	D,C
	SCJ7	plate	1.2	204.5	26.5	46.9	6	100	N.A	E
Li et. al. (1996)	CJS-1	Non	1.2	181.5	47	N.A	7	300	N.A	E,B
	CJS-2	Non	1.2	176	42	N.A	7	300	N.A	E,B
	CJS-3	Non	1.2	148.5	18	N.A	7	300	N.A	D,B
	CJS-4	Non	1.2	177.5	58	N.A	7	300	N.A	E,B
	CJS-5	Non	1.2	197.5	60	N.A	7	300	N.A	E,B
	CJS-6	Non	1.2	174	23	N.A	7	300	N.A	E,B
Liew et. al. (2000)	SCCB1	YES	0.5	271	24.9	N.A	7	155	N.A	B
	SCCB2	YES	1.12	441	51.9	N.A	14	140	N.A	E
	SCCB3	YES	1.56	449	37.3	N.A	10	145	N.A	E
Loh et. al. (2006)	CJ1	C-F-SH	1.29	185.5	30	58	5	110	0.5	E
	CJ2	Fill-C	1.29	187.9	38	53	3	66	4.5	E
	CJ3	Fill-C	1.29	178.9	45	55	2	44	7.4	E
	CJ4	Fill-C	0.65	143.3	21	50	3	133	1.1	SLAB
	CJ5	Fill-C	1.94	192.1	19	30	8	118	0.2	E
Fu and Lam (2006)	CJ1	Non	0.6	370	35.4	N.A	7	275	0.34	B
	CJ2	Non	0.6	363	33.5	N.A	4	157	0.8	B
	CJ3	Non	0.6	250	6.1	N.A	2	78	5.8	G
	CJ4	Non	0.6	368	37.4	N.A	3	98	3.5	G
	CJ5	Non	0.6	363	31.7	N.A	3	98	3.5	G
	CJ6	Non	0.6	425	46.8	N.A	6	120	0.84	B
	CJ7	Non	0.6	274	30	N.A	2	120	0.4	B
	CJ8	Non	0.6	439	42.3	N.A	4	120	1.6	B

B: fracture of the mesh reinforcement;

C: excessive deformation of column flange;

D: buckling of column web;

E: buckling of beam flange;

F: buckling of beam web;

G: shear studs failure.

C-F-SH: concrete-filled square hollow section.

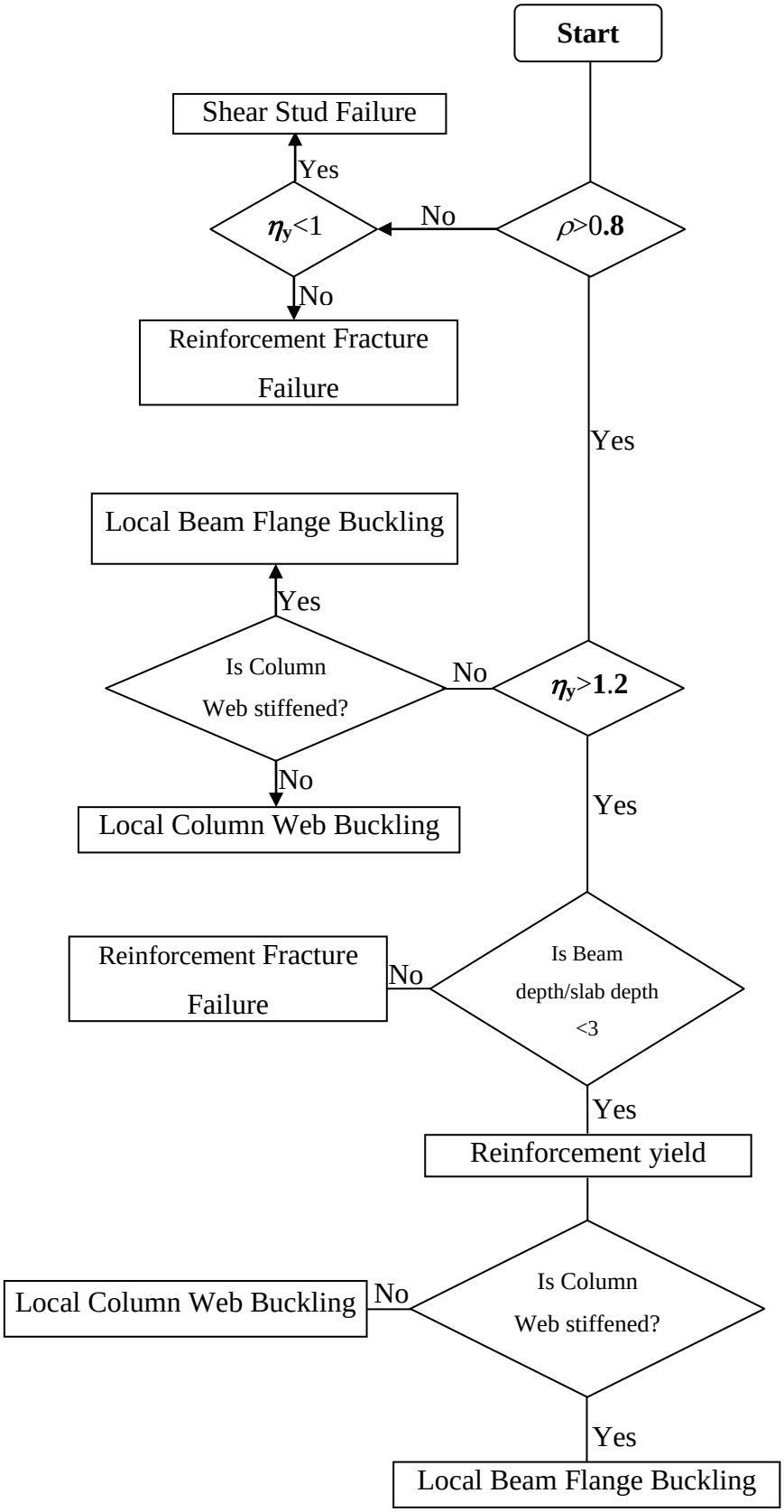

Figure 6.1: Flowchart for failure mode predication

6.3. Moment resistance of a flush end-plate composite connection

6.3.1. Brief literature review

In the literature, there are two main procedures to estimate the moment resistance of composite connection. Both of them predict the moment resistance of composite connection using the concept of a rigid-plastic, stress blocks approach. In this approach, stresses in each components of a connection are represented by rectangular stress blocks. Consequently, these methods sometimes are known as blocks analysis methods.

The moment resistance of a flush end-plate composite connection is mainly provided by three components:

1. slab reinforcement;
2. top row of bolts in tension; and
3. steel beam bottom flange and web in compression.

The main procedures to estimate the moment resistance of a flush-end composite connection are:

Procedure One

The moment resistance of composite connection is calculated using rigid plastic analysis in which the strength of each of the components is multiplied by their lever arms. The moment resistance, $M_{\mathrm{j,Rd}}$ is calculated using the following expression:

$$M_{j,Rd} = F_r D_r + F_b D_b \tag{6.1}$$

where D_{r} and D_{b} are the distances from the reinforcement and top row of bolts to the centre of compression respectively. These forces and distances depend on the location of the neutral axis. Three general cases of locations are associated with three groups of assumptions:

1. Neutral axis is in the bottom beam flange:

(i). Force in the reinforcement $F_r = A_r f_{r,y}$ (6.2)

(ii). Force in the top row of bolts $F_b = R_b$ (6.3)

where R_b is the strength force of top row of bolts which is determined using the procedure that will be explained in the next section. The centre of compression is assumed to be in the mid-thickness of bottom beam flange.

2. Neutral axis is in the beam web below the top row of bolts:

   (i). Force in the reinforcement is determined using Eq. (6.2).

   (ii). Force in the top row of bolts is determined using Eq. (6.3).

   The centre of compression is calculated using equilibrium condition by assuming that the bottom flange and possibly part of the beam web is fully yielded.

3. Neutral axis is in the beam web above the top row of bolts

   (i). Force in the reinforcement is determined using Eq. (6.2).

   (ii). Force in the top row of bolts is zero.

   The centre of compression is calculated using the same procedure in case (2) above.

This procedure was adopted by most researchers such as (Anderson and Najafi, 1994; Li et al., 1996; Ren and Crisinel, 1996; Ahmed and Nethercot, 1997; Crisinel and Carretero, 1997).

Procedure two

This procedure was proposed by (Brown and Anderson, 2001). The preliminary calculations of moment resistance are generally similar to procedure one using Eq. (6.1) to Eq. (6.3). The main differences are:

1. The strength of bottom beam flange is assumed to increase up to 1.4 times of yield stress (i.e. strain hardening) in order to satisfy the equilibrium requirement between tension and compression forces. On the other hand, if this increase is not enough to satisfy equilibrium requirement, the compressive resistance is extended into the beam web but the strength of the bottom beam flange and part of beam web is assumed to be 1.2 times of yield stress.

2. The tension forces in the top row of bolts are assumed to be equal to its maximum capacity, R_b, if the height between the bolt and the plastic neutral axis (d_b) is more than 200 mm to ensure that there is adequate straining of the bolt to reach its

maximum capacity. If this condition is not satisfied, the bolt force is reduced proportionally by a factor of *(d_b/200)*.

6.3.2. Proposed procedure to calculate moment resistance of a flush end-plate composite connection

In the present work, the same principles of the previous procedures are considered in order to develop an appropriate procedure which is compatible with the proposed mechanical model in Chapter Three (see Figure 6.2). In addition, it should be compatible with the proposed flowchart in Figure 6.1 and with the procedure to estimate the rotation at failure which will be developed in the following section. Furthermore, the previous methods dealt with full interaction of composite connection. Therefore, the force of the top row of bolts was ignored in some methods such as (Ren and Crisinel, 1996) or was assumed to have maximum capacity for all cases such as (Anderson and Najafi, 1994; Brown and Anderson, 2001). However, the force of the top row of bolts depends on the properties of the composite connection. The force of the top row of bolts may be negligible in the composite connections with full interaction and high reinforcement ratio. However, it may be at ultimate for connections with full interaction and low reinforcement ratio. For partial interaction, the bolt forces will be in-betweens. Ignoring the bolt forces lead to underestimation of the compression force on the column in the lower part of the connection and this may lead to an unsafe design (Loh et al., 2006). In the present work, the force of the top row bolts is included.

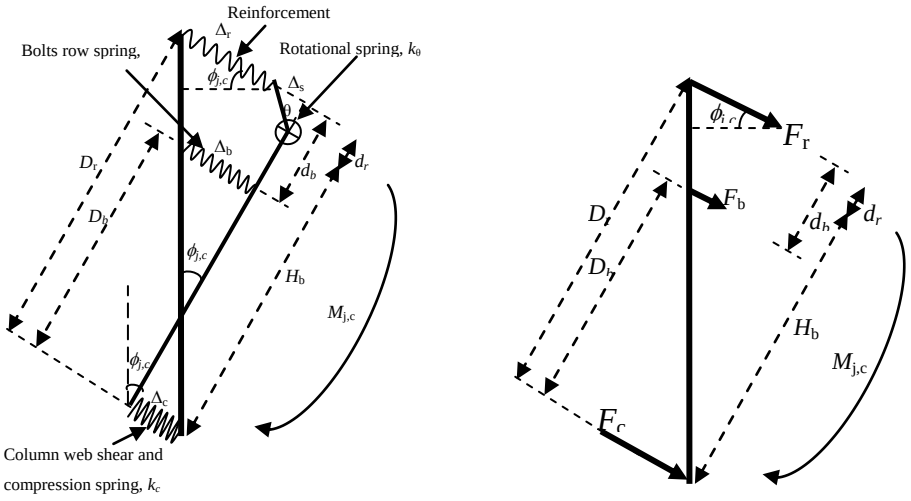

a) Deformations b) Free-body diagram

Figure 6.2: Proposed mechanical model with free-body diagram

6.3.2.1. Shear stud failure mode

This mode of failure occurs when insufficient number of shear stud is used in the shear span. Often this failure mode is associated with the minimum moment resistance and rotation capacity of a composite connection. Consequently, this mode of failure is not preferable for practical use because it does not utilize the available reserve strength and ductility in the components of composite connection. This condition is characterized by:

$$\rho < 0.8 \quad \text{and} \quad 0.4 < \eta_y \le 1 \qquad \text{where} \quad \eta_y = \frac{N_{sc} F_{sc,\max}}{A_r f_{r,y}} \tag{6.4}$$

From the equilibrium considerations of the composite slab, we get:

$$F_r = F_s = N_{sc} F_{sc,\max} \tag{6.5}$$

In addition, since the force in the top row of bolts, F_b, develops as a result of the extension of bolt group component caused mainly by the extension of reinforcement (see Figure 6.2-a), this force needs to be checked whether it is in the elastic range or ultimate stage due to limited extension in the reinforcement. Further, the centre of compression can be assumed in the mid-thickness of bottom flange for the same reason. Consequently, Eq. (3.37) and Eq. (3.39) in Chapter Three to compute the force in the top row of bolts and the force in the reinforcement are still valid but after replacing the elastic stiffness of shear connectors, k_s, by plastic stiffness, $k_{s,p}$, to take into account the slip in shear connectors in the post-linear range:

$$k_{s,p} = \frac{N_{sc} F_{sc,\max}}{s_{sc,c}} \tag{6.6}$$

where $s_{sc,c}$ is the slip capacity of shear connector. Eq. (3.37) and Eq. (3.39) can be rewritten as:

$$F_r = \frac{\left(D_r - D_b \left(\frac{k_b}{k_c + k_b} \right) \right)}{\left(\frac{1}{k_r} + \frac{1}{k_{s,p}} + \frac{1}{(k_c + k_b)} \right)} \phi \tag{6.7}$$

$$F_b = \frac{\frac{k_b}{(k_c + k_b)} \left[D_b k_c \left(\frac{1}{k_r} + \frac{1}{k_{s,p}} + \frac{1}{(k_c + k_b)} \right) - \left(D_r - D_b \left(\frac{k_b}{k_c + k_b} \right) \right) \right]}{\left(\frac{1}{k_r} + \frac{1}{k_{s,p}} + \frac{1}{(k_c + k_b)} \right)} \phi \tag{6.8}$$

Then,

$$w = \frac{F_b}{F_r} = \frac{D_b\left(\frac{1}{k_r} + \frac{1}{k_{s,p}}\right) - \frac{d_b}{k_c}}{\frac{D_r}{k_b} + \frac{d_b}{k_c}} \tag{6.9}$$

For stiffened web column case (i.e. $k_c \approx \infty$)

$$w \approx \frac{D_b k_b\left(\frac{1}{k_r} + \frac{1}{k_{s,p}}\right)}{D_r} \tag{6.10}$$

$$F_b = wF_r \le R_b \tag{6.11}$$

where, R_b, is the strength of the top bolt-row. The R_b can be calculated using Eurocode 3 (2005) §6.2.7.2 requirements:

$$R_b = \text{the smallest value of the resistance for} \begin{cases} \text{(i) column web in tension} \\ \text{(ii) column flange in bending} \\ \text{(iii) end-plate in bending} \\ \text{(iv) beam web in tension} \\ \text{(v) bolt in tension} \end{cases}$$

Also, Li et al. (1996) simplified Eurocode 3 procedure to calculate the resistance of column flange and end-plate in bending. The final equations for the resistance of bolt-row are:

$$R_b = \text{the smallest of} \begin{cases} \text{(i) } b_{eff,t,cw} t_{cw} f_{y,cw} \\ \text{(ii) } (4.32 - 0.039m + 0.0116e + 0.009p) t_{cf}^2 f_{cf} \\ \text{(iii) } (5.5 - 0.021m + 0.017e) t_p^2 f_p \\ \text{(iv) } b_{eff,t,bw} t_{bw} f_{y,bw} \\ \text{(v) } 1.8 A_b f_b \end{cases} \tag{6.12}$$

It should be noted that all partial safety factors are removed from the above equations.

The moment resistance of composite connection can be determined using Eq. (6.1).

6.3.2.2. Reinforcement fracture

This condition is characterized by:

$$\rho < 0.8 \quad \text{and} \quad \eta_y > 1 \tag{6.13}$$

In this mode of failure, the resistance force in the reinforcement, R_r, is calculated as follows:

$$R_r = A_r f_{r,u} \tag{6.14}$$

The moment resistance of composite connection depends on the resistance forces offered by the reinforcement as well as the bolts. The resistance of the top row of bolts, R_b, can be calculated using Eq. (6.12). The same procedure in the previous mode of failure is used to calculate the moment resistance of composite connection but with slight modification. The centre of compression should be checked whether it is in the mid-thickness of bottom flange of beam or in the web. This checking is performed using the following procedure:

$$\text{if} \quad R_r + R_b \le A_{bf} f_{b,y} \quad \rightarrow \qquad M_{j,Rd} = R_r D_r + R_b D_b \tag{6.15}$$

$$\text{if} \quad R_r + R_b > A_{bf} f_{b,y} \quad \rightarrow \qquad M_{j,Rd} = R_r D'_r + R_b D'_b \tag{6.16}$$

where D'_r and D'_b can be calculated as follows:

$$D'_r = D_r - \frac{y_c}{2} \quad \text{and} \quad D'_b = D_b - \frac{y_c}{2} \tag{6.17}$$

$$y_c = \frac{A_{bf} t_{bf} / 2 + t_{bw} y_w (t_{bf} + y_w / 2)}{A_{bf} + t_{bw} y_w} \quad \& \quad y_w = \frac{R_r + R_b - A_{bf} f_{b,y}}{t_{bw} f_{b,y}} \tag{6.18}$$

6.3.2.3. Local buckling of beam flange or column web

This condition is characterized by

$$\rho > 0.8 \quad \text{and} \quad \eta_y \le 1.2 \tag{6.19}$$

The force in the reinforcement and shear connectors are calculated as follows:

$$F_r = F_s = \text{smaller of} \begin{cases} N_{sc} F_{sc,\max} \\ A_r f_{r,y} \end{cases} \tag{6.20}$$

Since the strain in reinforcement may be at the onset of hardening, it should be checked if the force in the top row of bolts is in elastic range or ultimate resistance. The force in the top row of bolts, F_b, is calculated using Eq. (6.11).

***Unstiffened column web* (*Local buckling of column web*)**

The resistance of column web in compression and buckling can be calculated using (Eurocode 3, 2005) §6.2.6.2 as follows:

$$F_{c,cw,Rd} = \text{smaller}\begin{cases}\text{(i) column web in compression}\\ \text{(ii) column web in buckling}\end{cases}$$

$$F_{c,cw,Rd} = \text{smaller}\begin{cases}\text{(i) } b_{eff,cw}t_{cw}f_{y,cw}\\ \text{(ii) } b_{eff}t_{cw}f_{y,cw}\left[\frac{1}{\bar{\lambda}}\left(1-\frac{0.2}{\bar{\lambda}}\right)\right]\end{cases} \quad (6.21)$$

$$\bar{\lambda} = \sqrt{\frac{b_{eff,cw}t_{cw}f_{y,cw}}{F_{cr}}} \Rightarrow \bar{\lambda} = \sqrt{\frac{b_{eff,cw}t_{cw}f_{y,cw}}{\left(\frac{\pi E t_{cw}^3}{3(1-\nu^2)d_{cw}}\right)}} \Rightarrow \bar{\lambda} = 0.93\sqrt{\frac{b_{eff,cw}d_{cw}f_{y,cw}}{Et_{cw}^2}} \quad (6.22)$$

$$b_{eff,cw} = t_{bf} + 2\sqrt{2}a_p + 5(t_{cf} + r_c) + s_p \quad (6.23)$$

s_p is the length obtained by dispersion at 45° through the end-plate ($t_p \le s_p \le 2t_p$).

$$\text{if} \quad F_{c,cw,Rd} \ge F_r + F_b \rightarrow M_{j,Rd} = F_r D_r' + F_b D_b' \quad (6.24)$$

$$\text{if} \quad F_{c,cw,Rd} < F_r + F_b \Rightarrow F_b' = F_{c,cw,Rd} - F_r \ge 0 \Rightarrow M_{j,Rd} = F_r D_r' + F_b' D_b' \quad (6.25)$$

where D_r' and D_b' can be calculated using Eq. (6.17) and Eq. (6.18) respectively.

<u>Stiffened column web (Local buckling of beam flange)</u>

The resistance of beam flange in compression can be calculated using (Eurocode 3, 2005) §6.2.6.7 and the simplified equation by (Li et al., 1996) as follows:

$$F_{c,bf,Rd} = \text{smaller}\begin{cases}\text{(i) column flange in compression}\\ \text{(ii) beam bottom flange in compression}\\ \text{(iii) beam bottom flange in buckling}\end{cases}$$

$$F_{c,bf,Rd} = \text{smaller}\begin{cases}\text{(i) } b_{eff,c,cw}t_{cw}f_{y,cw}\\ \text{(ii) } b_{bf}t_{bf}f_{y,bf}\\ \text{(iii) } 22t_{fb}^2\sqrt{235/f_{y,bf}}\end{cases} \quad (6.26)$$

$$\text{if} \quad F_{c,bf,Rd} \geq F_r + F_b \quad \rightarrow M_{j,Rd} = F_r D'_r + F_b D'_b \tag{6.27}$$

$$\text{if} \quad F_{c,bf,Rd} < F_r + F_b \quad \Rightarrow F'_b = F_{c,bf,Rd} - F_r \geq 0 \quad \Rightarrow M_{j,Rd} = F_r D'_r + F'_b D'_b \tag{6.28}$$

where D'_r and D'_b can be calculated using Eq. (6.17) and Eq. (6.18) respectively.

6.3.2.4. Yielding of reinforcement with buckling of column web or beam flange

This condition is characterized by:

$$\rho > 0.8 \quad \text{and} \quad \eta_y > 1.2 \tag{6.29}$$

In this mode of failure, the force in the top row of bolts, F_b, and reinforcement, F_r, are calculated using Eq. (6.11) and Eq. (6.14) respectively. The expected fracture of reinforcement is associated with buckling of column web or beam flange. For the unstiffened and stiffened column webs, similar procedure described in the previous section is followed.

6.3.3. Validity of the proposed procedure to calculate the moment resistance of a flush end-plate composite connection

The validity of the proposed procedure is compared against 31 available experimental tests in the literature. It consists of tests with partial shear connection, full shear connection and full interaction. Also, reinforcement ratios range between 0.3% to 1.94%. All failure modes are considered. Predictions and test values are compared in Table 6.2 and Figure 6.3.

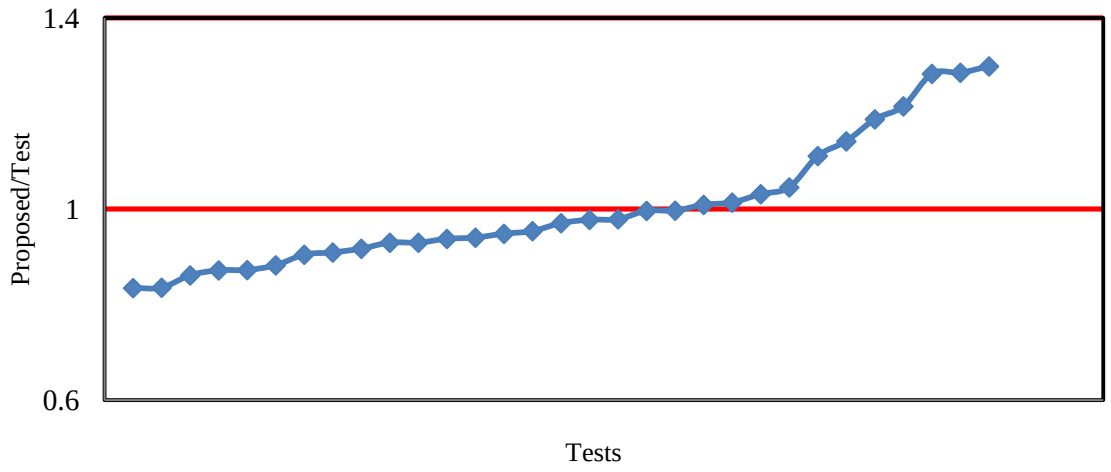

Figure 6.3: Validity of proposed procedure to calculate the moment resistance of composite connection

It can be seen that the prediction of moment resistance of a flush end-plate composite connection from the proposed procedure agrees well with the experimental results for most cases. From Table 6.2, it can be seen that the proposed procedure gives an average of 1.001 with a standard deviation of 0.13. In addition, the maximum and minimum of prediction/test ratios are 1.28 and 0.84 respectively. Ahmed and Nethercot (1997) evaluated their procedure (procedure 1) against 32 experimental tests, some of which are not included in this study due to non-availability of data. They found that this procedure gives an average of 1.04 with a standard deviation of 0.15 and the maximum and minimum of prediction/test ratios are 1.33 and 0.82 respectively. The incorporation of expected failure mode and partial shear connection effect in the calculation of the moment resistance of composite connection are the merits of the proposed procedure over the other previous procedures. As the most of available experimental data are related to full shear connection cases, this merits are not clearly revealed in comparison. Also, Brown and Anderson (2001) investigated the applicability of their procedure (procedure 2) to predict moment resistance of composite connection against eight experimental tests. It was found that this procedure gives an average of 0.819 with a standard deviation of 0.033 and the maximum and minimum of prediction/test ratios are 0.87 and 0.74 respectively. It is clear that the (Brown and Anderson, 2001)'s procedure underestimate the moment resistance of composite connection for most of the cases. From the above discussion, it is clear that the proposed procedure in this study can give the best average, standard deviation, maximum and minimum prediction/test ratios.

Table 6.2:Comparison of test and predicted results of moment resistance

Reference	Specimen	ρ	Ultimate Moment (T)	Shear Studs			W	Components forces						Modified distances (mm)				Proposed (P)	P/T
				No.	η_y	η_u		F_{b1}	R_b	F_r	F_{cc}	F_{cb}	F_b	y_w	y_c	$D_{r,m}$	$D_{b,m}$		
Anderson and Najafi (1994)	S4F	0.55	179	7	3.76	2.61	1.92	429.11	238.22	322	3506.61	504.9	182.9	0	5.1	395	254	173.65	0.97
	S8F	1.1	262	7	1.91	1.32	0.97	429.11	238.22	634.2	3506.61	504.9	0	71.83	13.46	388.27	247.27	246.24	0.94
	S12F	1.65	302	7	1.19	0.88	0.65	429.12	238.22	952	3506.61	504.9	0	248.39	65.82	362.09	221.09	344.71	1.14
	S8FD	1.1	416	7	1.91	1.32	1.09	481.42	318.15	634.2	3517.18	498.35	0	59.58	13	578.5	443.5	366.88	0.88
Xiao et. al.(1994)	SCJ3	0.3	85.7	6	6.41	4.45	3.62	406.24	238.22	161.7	343.8	538.56	182.1	0	5.1	395	254	110.13	1.28
	SCJ4	1	202.9	6	2	1.39	1.21	434.01	238.22	518	343.8	538.56	0	0	5.1	395	254	204.61	1.01
	SCJ5	1	240.8	6	2	1.39	1.09	393.67	238.22	518	3438.05	538.56	20.56	0	5.1	395	254	209.83	0.87
	SCJ6	1	157.6	6	2	1.39	1.21	434.01	238.22	518	343.8	538.56	0	0	5.1	395	254	204.61	1.28
	SCJ7	1.2	204.5	6	1.67	1.16	1.01	434.01	238.22	621.6	3438.05	538.56	0	43.25	8.67	390.66	249.66	242.84	1.19
Li et. al. (1996)	CJS-1	1.2	181.5	14	4.61	3.37	1.14	417	190.02	498.55	3056.07	350.94	0	60	14.33	330.84	194.84	164.94	0.91
	CJS-2	1.2	176	14	4.61	3.37	1.14	417.01	190.02	498.55	3056.07	350.94	0	60	14.33	330.84	194.84	164.94	0.94
	CJS-3	1.2	148.5	14	4.61	3.37	1.14	417.01	190.02	498.55	3056.07	350.94	0	60	14.33	330.84	194.84	164.94	1.11
	CJS-4	1.2	177.5	14	4.61	3.37	1.14	417.01	190.02	498.55	3056.07	350.94	0	60	14.33	330.84	194.84	164.94	0.93
	CJS-5	1.2	197.5	14	4.61	3.37	1.14	417.02	190.02	498.55	3056.07	350.94	0	60	14.33	330.84	194.84	164.94	0.84
	CJS-6	1.2	174	14	4.61	3.37	1.14	417.02	190.02	498.55	3056.07	350.94	0	60	14.33	330.84	194.84	164.94	0.95
Liew et. al. (2000)	SCCB1	0.5	271	7	1.69	1.55	1.16	575.72	233.15	543	3491.46	731.69	188.69	0	6.85	400	254	265.13	0.98
	SCCB2	1.12	441	14	1.52	1.39	0.52	575.72	233.15	1206.6	3491.46	731.69	0	187.86	46.52	376.74	230.74	454.58	1.03
	SCCB3	1.56	449	20	1.55	1.42	0.37	575.72	233.15	1689	3491.46	731.69	0	378.68	118.05	340.98	194.98	575.91	1.28
Loh et. al. (2006)	CJ1	1.29	185.5	5	1.09	1.04	1.14	523.23	208.04	480	3428.85	446.25	0	16.07	6.02	336.99	180.99	161.75	0.87
	CJ2	1.29	187.9	3	0.65	0.63	1.04	312.06	208.04	480	3428.85	446.25	0	16.07	6.02	336.99	180.99	161.75	0.86
	CJ3	1.29	178.9	2	0.43	0.42	0.89	177.6	208.04	480	3428.85	446.25	0	16.07	6.02	336.99	180.99	161.75	0.9
	CJ4	0.65	143.3	3	1.3	1.25	2.27	523.24	208.04	240	3428.85	446.25	206.25	0	5.1	340	184	119.55	0.83
	CJ5	1.94	192.1	8	1.16	1.11	0.76	523.25	208.04	720	3428.85	446.25	0	130.36	31.82	324.09	168.09	233.34	1.21
Fu and Lam (2006)	CJ1	0.6	370	7	2.5	2.11	1.91	641.04	273.4	398.15	14115.55	1708.5	273.4	0	8.85	634	399	361.51	0.98
	CJ2	0.6	363	4	1.43	1.21	1.91	641.04	273.4	398.15	14115.55	1708.5	273.4	0	8.85	634	399	361.51	1
	CJ3	0.6	250	2	0.71	0.6	2.43	584.23	273.4	335.98	14115.55	1708.5	273.4	0	8.85	634	399	322.1	1.28
	CJ4	0.6	368	3	1.07	0.9	2.69	903.45	273.4	360	14115.55	1708.5	273.4	0	8.85	634	399	337.33	0.92
	CJ5	0.6	363	3	1.07	0.9	2.97	998.92	273.4	360	14115.55	1708.5	273.4	0	8.85	634	399	337.33	0.93
	CJ6	0.6	425	6	1.68	1.42	1.84	788.12	273.4	507.2	14115.55	1708.5	273.4	0	8.85	634	399	430.65	1.01
	CJ7	0.6	274	2	1.12	0.95	5.26	1126.68	273.4	240	14115.55	1708.5	273.4	0	8.85	634	399	261.25	0.95
	CJ8	0.6	439	4	1.12	0.95	1.97	842.77	273.4	480	14115.55	1708.5	273.4	0	8.85	684	399	437.41	1
																	AVERAGE		1.001
																	STDEV.		0.13
																	MAX.		1.28
																	MIN.		0.84

6.4. Ductility of a flush end-plate composite connection

Ductility means the ability of a structure to sustain deformations after its initial yield, without any significant reduction in the ultimate strength. The ductility of composite connection can be defined as:

$$\mu_j = \frac{\phi_{j,c}}{\phi_{j,y}} \tag{6.30}$$

where

$\phi_{j,c}$ is the rotation of composite connection at failure (i.e. rotation capacity).

$\phi_{j,y}$ is the rotation of composite connection when the first component yields.

Since the proposed mechanical model (Figure 6.2) to calculate the initial stiffness is based on the equilibrium and compatibility requirements that must be satisfied at all load stages. Hence it can be used to calculate the rotation of a flush end-plate composite connection at yield and failure after making some necessary modification on stiffness of its components.

6.5. Brief literature review

6.5.1. Rotation at yield

Eurocode 3 (2005) §6.1.2.1(2) emphasises the determination of moment resistance, rotational stiffness and rotational capacity of connections. The rotational capacity refers to the rotation at failure. However to calculate connection ductility, the rotation at yield is essential as described in the previous paragraph. The information on the latter is virtually non-existent in the literature.

Anderson and Najafi (1994) proposed the following equation to compute the rotation of a flush end-plate composite connection at yield of reinforcement:

$$\phi_{j,y} = \frac{\left(1+\frac{k_s}{k_r}\right)}{k_s H_b} F_y \tag{6.31}$$

$$k_s = 200 \text{ kN/mm} ; \qquad k_r = \frac{E_r A_r}{\left(\frac{D_c}{2} + p_0\right)} ; \qquad F_y = f_{r,y} A_r \tag{6.32}$$

where A_r is the reinforcement area and all the others parameters are as defined previously. These expressions assumed that the first component in the connection to yield is the reinforcement. This assumption may be valid for a flush end-plate composite connection with full shear interaction. However, for the connection with partial shear connection the reinforcement may yield only after the yielding of shear connectors or may not yield at all. In addition, the effect of deformation in the compression zone was not included since these expressions were derived for composite connection with stiffened column web.

Aribert (1996) proposed an approach to predict the whole moment-rotation of a flush end-plate composite connection. This approach was developed based on the analysis of composite beams with partial shear connection under uniformly distributed loading. As part of this approach, the rotation at yield was calculated using an iterative procedure. This procedure can be simplified as follows:

$$\phi_{j,y} = \frac{\left(\frac{1}{k_r} + 2k_s\right)}{D_r} F_y \tag{6.33}$$

$$k_s = \frac{N_{sc} k_{sc}}{\left(\beta - ((\beta - 1)/(1+\alpha)) \frac{(H_b + d_r)}{(H_b/2 + d_r)}\right)} ; \qquad k_r = \frac{E_r A_r}{\left(\frac{D_c}{2}\right)} \tag{6.34}$$

$$\alpha = \frac{(EI)_b}{(H_b/2 + d_r)^2 (EA)_r}; \qquad \beta = \sqrt{\left(\frac{1}{\alpha} + 1\right) \frac{N k_{sc} L_b}{(EA)_r}} \tag{6.35}$$

where L_b is the length of the beam under hogging bending moment adjacent to the connection. E_b and E_r are the moduli of elasticity of steel beam and reinforcement, I_b is the second moment of area of the steel beam section, and A_r is the area of the reinforcement. The yield force, F_y, is calculated as follows:

$$F_y = \begin{cases} f_{r,y} A_r & \text{when} \quad \eta_y > 1 \\ N_{sc} F_{sc,\max} & \text{when} \quad \eta_y < 1 \end{cases} \tag{6.36}$$

Eq. (6.36) assumed that the yielding may start in reinforcement or shear connectors depending on the shear connection ratio. These expressions overcome some shortcoming in the (Anderson and Najafi, 1994) procedure. However, the effect of deformation in compression zone was not included since it was derived for composite connection with stiffened column web.

6.5.2. Rotation capacity

In literature, there are many procedures to compute the rotation capacity of composite connection. All these procedures are based on compatibility requirement of connection at failure. Further, all of these procedures used the conventional mechanical models for composite connection but the number of basic components being different from one model to another as seen in Figure 6.4.

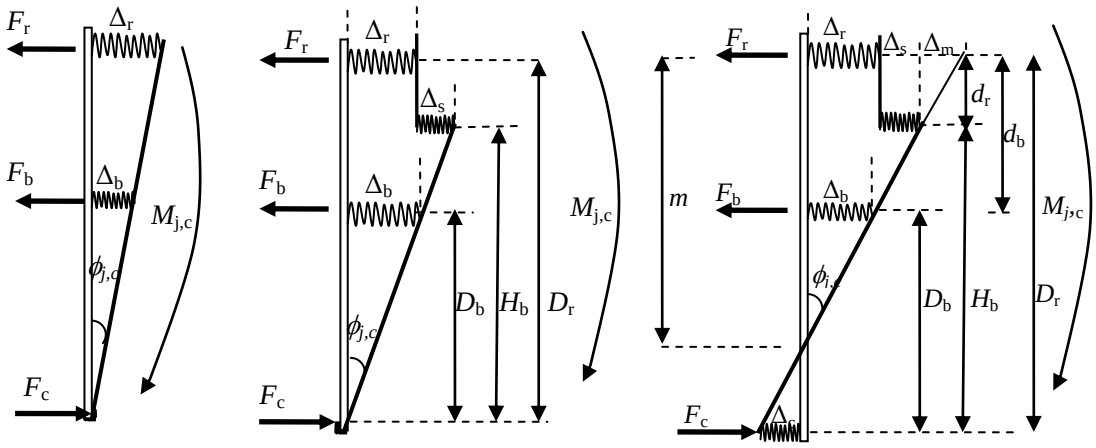

Figure 6.4: Conventional mechanical models: a) Benussi and Noe's model; (b) Anderson and Najafi's model; c) Ahmed and Nethercot model

Based on deformation of only one component; elongation of reinforcement, Δ_r,SCI Report (1992) suggested the following simplified relationship to calculate the rotation capacity of composite connection (see Figure 6.4-a):

$$\phi_{j,c} = \frac{\Delta_r}{D_r} \tag{6.37}$$

This simple relation did not take into account the effect of slip in shear connection which has significant effect on rotation especially for partial shear connection cases (Aribert, 1996). Also, the deformation of compression zone was ignored even though this effect may be considerable for composite connection with high reinforcement ratio or when the column web is unstiffened. Therefore, this relation may underestimate the rotation capacity for many cases. Xiao et al. (1992) proposed an expression to calculate the rotation capacity of composite connection. It is same as Eq. (6.37) but with different procedure to calculate, Δ_r, as will be explained in the next section.

Xiao (1994) carried out twenty experimental tests with four different types of steel connection: seating cleat with double web cleats, flush end-plates, partial depth end-plates and finplate. The objectives were to investigate the effect of the interaction properties of composite connection on the connections' moment resistance, rotational stiffness and rotation capacity. Based on the results of these tests, Xiao et al. (1996) developed the following equation to calculate the rotation capacity of a flush end-plate composite connection with any number of bolt-rows:

$$\phi_{ult} = \frac{\Delta_r}{m} + \frac{\Delta_s}{m - d_r} \tag{6.38}$$

where m is the distance from the reinforcement to the centre of rotation (see Figure 6.4-c) and it was calculated using the following equation:

$$m = d_r + p_1 + p(i + 2/3) \tag{6.39}$$

where p_1 is the distance of the first bolt-row from the top of beam flange and p is the bolt-row pitch. The variable i is the integer part of the number of bolt-rows in tension (k). This number (k) was calculated as follows:

$$k = \frac{f_{b,y} b_{bf} t_{bf} \; - F_r \; + f_{b,y} t_{bw} (H_b - p_1 - t_{bf} + \frac{p}{3})}{F_b \; + f_{b,y} t_{bw} p} \tag{6.40}$$

where $f_{b,y}$ is the yield strength of steel beam, and all other parameters are as defined previously. The deformation distance, Δ_m was ignored in derivation of Eq. (6.38) (see Figure 6.4). This will lead to underestimation of the first part of this equation. Ahmed and Nethercot (1997) investigated the validity of Eq. (6.38) and Eq. (6.39) against some

experimental tests of composite connection with two bolt-rows and found that these expressions gave an unacceptable result for the depth considered for the calculation of rotation capacity, *m*. In some cases, this depth becomes greater than the combined beam and slab depth.

Ren and Crisinel (1996) extended their equation for rotational stiffness which was discussed in Chapter Three (Eq. (3.14)) to calculate the rotation capacity of a flush end-plate composite connection but with different values of component stiffness. This equation takes the form:

$$\phi_{j,c} = \frac{D_r^2}{\frac{1}{k_r} + \frac{1}{k_s} + \frac{1}{k_c}} \tag{6.41}$$

where D_r, k_r, k_s, k_c have the same definition as before. It was assumed that the reinforced-concrete slab is at the plastic cracked state. Also, it was assumed that steelwork connection factor, k_c, is not the critical factor for causing failure, therefore it was calculated using the same equation for initial stiffness. This assumption may be valid for composite connection with relatively low amount of reinforcement ratio and with stiffened column web but it could be unsafe for other cases. In addition, it was assumed that stiffness of shear connector, k_s, can be calculated using the same expressions for initial stiffness but with maximum slip of shear connector even though it was assumed that the maximum force in shear connector is about 60% of ultimate strength of shear connector. This assumption may be valid only for composite connection with high or full shear connection as explained in (section 6.3).

Based on the compatibility of deformations in the connection zone, Aribert (1996) proposed the following approximate equation to calculate the rotation capacity:

$$\phi_{j,c} = \frac{\Delta_r + \Delta_s}{D_r} \tag{6.42}$$

This equation was validated against three experimental tests of full and partial shear connection of flush end-plate composite connections with 1.34, 0.95 and 0.63 of shear connection ratio and showed good agreement with experimental results. Nevertheless, this equation ignored the deformation of column web or flange in the compression zone since all of the above experimental tests were stiffened with the column web stiffener. This effect may be significant for high value of reinforcement ratio in composite connection without column web stiffener.

Ahmed and Nethercot (1997) proposed an equation to calculate the rotation capacity of composite connection based on the deformation of three components: elongation of reinforcement (Δ_r), slip of shear studs (Δ_s), and extension of tension bolts (Δ_r). The rotation capacity is calculated using the following equation:

$$\phi_{j,c} = \frac{\Delta_r}{D_r - d_{c,bw}} + \frac{\Delta_s}{D_r - d_{c,bw} - d_r} + \frac{\Delta_b}{D_r - d_{c,bw} - d_b} \tag{6.43}$$

where $d_{c,bw}$ is the extended distance of compression zone in the beam web and can be calculated from equilibrium considerations. This equation overestimates the rotation capacity of connection since the rotation part due to the deformation of bolt-row, Δ_b, is already included in other two part of rotation in Eq. (6.43) (see Figure 6.4-c). Therefore, this equation doubles up the effect of bolts deformation.

Anderson et al. (2000) proposed the following equation to calculate the rotation capacity of composite connection:

$$\phi_{j,c} = \frac{\Delta_r}{D_r} + \frac{\Delta_s + \Delta_c}{H_b} \tag{6.44}$$

It was assumed that the centre of compression is in the mid-thickness of bottom beam flange. This assumption is valid for connection with low ratio of reinforcement so that the compression force in bottom flange can be in balance with tension forces in reinforcement and top row of bolts. As the reinforcement ratio is increased, the compression zone is extended to the beam web and the denominator of the two parts of Eq. (6.44) needs to modify, otherwise the rotation capacity will be underestimated.

Kemp and Nethercot (2001) proposed an approach to calculate the available rotation in continuous composite beams with semi-rigid connection. The same approach with required modifications was used to calculate the rotation capacity of composite connection. The final equation is:

$$\phi_{j,c} = \frac{\Delta_r}{D_r} + \frac{\Delta_c}{d_c} \tag{6.45}$$

where d_c is the distance from the mid-thickness of bottom beam flange to the centre of rotation. This equation ignored the effect of slip in shear connectors since it was originally derived for the cases of composite beams with full interaction. This equation underestimates the rotation capacity of connection with partial shear connection.

It should be noted that even though the same symbols were used to represent the deformation of reinforcement (Δ_r), slip of shear connector (Δ_s), bolt-row deformation (Δ_b), and deformation of compression zone (Δ_c), but each method used different procedure to calculate each of them as will be demonstrated in the following sections.

6.6. Proposed procedure to predict the rotation at yield and rotation capacity of a flush end-plate composite connection

It was demonstrated in Chapter Three that one of the advantages of the proposed mechanical model to calculate the rotational stiffness of composite connection is its applicability in the post-linear range of moment-rotation curve using appropriate component values. Therefore, this model is used to calculate the rotations of composite connection at first yield and at failure. This model with the required deformations and distances terms is shown in Figure 6.5.

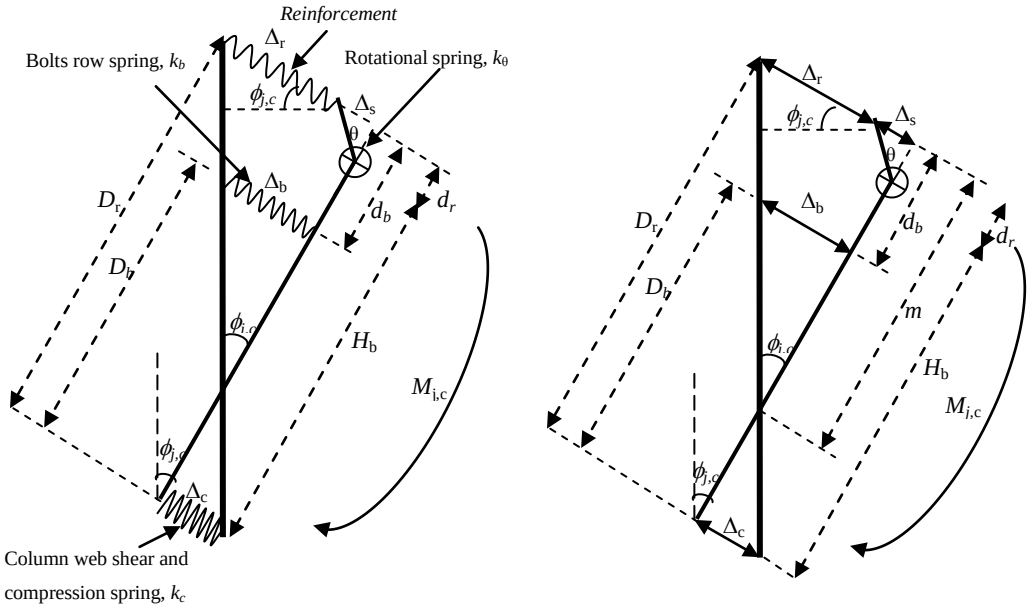

Figure 6.5: Mechanical model for calculating the rotations at yield and ultimate

6.6.1. Rotation at yield

It was found in Chapter Three that the elastic forces in reinforcement and top row of bolts can be calculated using Eq. (3.37) and Eq. (3.39) which was rewritten in (section 6.3) as Eq. (6.7) and Eq. (6.8). Also, in section 6.4, the rotation at yield, $\phi_{j,y}$, was

defined as the rotation of composite connection when the first component yields. In addition, all of the previous experimental and numerical studies demonstrated clearly that for normal range of reinforcement ratios in composite connections (0.7% to 1.4%), the reinforcement or shear connectors are the first expected component to yield depending on the shear connection ratios. Therefore, it can be assumed that Eq. (6.7) is valid up to the first component yield (i.e. reinforcement or shear connectors). Then, the rotation at yield can be calculated as follows:

$$\phi_{j,y} = \frac{\left(\frac{1}{k_r} + \frac{1}{k_s} + \frac{1}{(k_c + k_b)}\right)}{\left(D_r - D_b\left(\frac{k_b}{k_c + k_b}\right)\right)} F_y \tag{6.46}$$

Therefore, the rotation at yield and the associated moment, $M_{j,y}$, can be calculated depending on the shear connection ratio as follows:

1. **Full interaction case ($\eta_y \geq 1.1$)**: for this perfect interaction between steel beam and composite slab, it is expected that the reinforcement will yield first and the strain in reinforcement will control the rotation of composite connection since the slip in shear connectors is negligible. Therefore, the yield force, F_y, is calculated as follows:

$$F_y = f_{r,y} A_r \tag{6.47}$$

   The force of top row of bolts, F_b, is calculated using Eq. (6.9), Eq. (6.11) and Eq. (6.12). The yield moment can be calculated as follows:

$$M_{j,y} = F_y D_r + F_b D_b \tag{6.48}$$

2. **High to full shear connection case ($0.8 \leq \eta_y < 1.1$)**: for this high ratio of shear connection, the yield of reinforcement and shear connectors are expected to take place simultaneously. Therefore, the rotation at yield is computed using Eq. (6.46) with the yield force computed as:

$$F_y = \text{smaller}\begin{cases} f_{r,y} A_r \\ N_{sc} F_{sc,y} \end{cases} \tag{6.49}$$

   The linear range of the stiffness of shear connector can be assumed to be valid up to 50% of its strength as explained in Chapter Three (section 3.6.4) and Chapter Four

(section 4.3). This range can be extended up to 60% of its strength as suggested by (Ren and Crisinel, 1996) or up to 70% as stated by (Eurocode 4, 2004) §A.3. In the present work, the ratio of 60% was selected since it's the average value. Therefore, the yield force of shear connector is calculated as follows:

$$F_{sc,y} = 0.6F_{sc,\max} \tag{6.50}$$

The yield moment is calculated using the same procedure as in the previous case.

3. **Partial shear connection case ($0.4 \leq \eta_y < 0.8$)**: for this low ratio of shear connection, it is expected that the shear connector yields first. Therefore, the rotation at yield is computed using Eq. (6.46) with the yield force being computed as:

$$F_{s,y} = 0.6N_{sc}F_{sc,\max} \tag{6.51}$$

The yield moment is calculated using the same procedure as in case 1.

6.6.2. Rotation capacity

The proposed mechanical model is used to compute the rotation capacity of a flush end-plate composite connection as follows:

$$\phi_{j,c} = \frac{\Delta_r + \Delta_s}{m} \tag{6.52}$$

Also, the compatibility of deformations in composite connection leads to the following equations:

$$\frac{\Delta_r + \Delta_s}{m} = \frac{\Delta_b}{m - d_b}$$

$$m = d_b\left(\frac{\Delta_r + \Delta_s}{\Delta_r + \Delta_s - \Delta_b}\right) \tag{6.53}$$

Then,

$$\phi_{j,c} = \frac{\Delta_r + \Delta_s - \Delta_b}{d_b} \tag{6.54}$$

It should be noted that the effect of compression zone, Δ_c, is taken implicitly in Eq. (6.54) since its value is proportional to the deformation of other components.

The advantages of the proposed equation (Eq. (6.54)) upon all other previous models are:

1. It considered the deformation of all the effective components of composite connection (i.e. reinforcement, shear connectors, bolts and compression zone).

2. It can be used to calculate the rotation of a flush end-plate composite connection for the whole range of moment-rotation behaviour with appropriate value of its parameters since the equilibrium and compatibility are always satisfied under increasing loading. The other models were derived for special stage of rotation.

3. It can be used for a flush end-plate composite connection with all degrees of shear connection (i.e. full and partial shear connection) and for stiffened or unstiffened column web cases.

4. It is simple to use and contain the least number of variables (i.e. three variable) since other models used the estimated deformation of components (Δ_r, Δ_s, Δ_c, and Δ_b) in addition to the variable distances such as (D_r, d_c, $d_{c,bw}$ and H_b) which may change with the magnitude of loading due to the position of the centre of compression being at a higher level than the bottom compression flange. Therefore, the accumulated error from all the variables will be the minimum in the proposed expression in relative to other expressions.

As with moment resistance procedure, the calculation of rotation capacity of a flush end-plate composite connection depends on the expected mode of failure. As explained in (section 6.3), there are four modes of failure for composite connection:

6.6.2.1. Shear stud failure mode (ρ<0.8 and 0.4<η_y≤1)

The deformation in reinforcement, shear connector and bolt-row are:

$$\Delta_r = \varepsilon_r l_r; \quad \Delta_s = s_{sc,c}; \quad \Delta_b = \frac{F_b}{k_b} \tag{6.55}$$

$$\therefore \phi_{j,c} = \frac{\varepsilon_r l_r + s_{sc,c} - \frac{F_b}{k_b}}{d_b}$$

where ε_r, l_r and $S_{sc,c}$ are as defined in (section 6.3.1). The force of top row of bolts, F_b, is calculated using Eq. (6.9), Eq. (6.11) and Eq. (6.12).

6.6.2.2. Reinforcement fracture failure (ρ<0.8 and η_y>1)

For this high shear connection ratio, the shear connector is assumed to be in elastic range and the slip is calculated as:

$$\Delta_s = \frac{A_r f_{r,u}}{k_s} \le s_{sc,c} \tag{6.56}$$

Also, the deformation in the top row of bolts is calculated as:

$$\Delta_b = \frac{F_b}{k_b} \tag{6.57}$$

Anderson et al. (2000) proposed the following procedure to determine the deformation of embedded reinforcement at ultimate strain as:

$$\Delta_{u,r} = 2L_t \varepsilon_{smu} \tag{6.58}$$

where ε_{smu} and L_{t} are the ultimate strain of embedded reinforcement and the transmission length of crack respectively which can be calculated using Eq. (5.18) and Eq. (5.23) in Chapter Five.

6.6.2.3. Local buckling of beam flange or column web (ρ>0.8 and η_{y}≤1.2)

Since the strain in reinforcement may be at the onset of hardening, the force in top row of bolts, F_{b}, is calculated using Eq. (6.10), Eq. (6.11) and Eq. (6.12). Whether the reinforcement may yield or not depend on the reinforcement ratio (ρ). Also, by considering the tension-stiffening effect and the conclusions from the available experimental results in literature, the strain in the embedded reinforcement for the composite connection with partial shear connection cannot achieve the onset of the strain hardening (Fu et al., 2010). These conditions can be represented by the following expressions:

$$\varepsilon_r = \begin{cases} \dfrac{N_{sc} F_{sc,\max}}{E_r A_r} & \text{if } \eta_y = \dfrac{N_{sc} F_{sc,\max}}{A_r f_{r,y}} \le 1 \\ \dfrac{\varepsilon_{r,y} + \varepsilon_{r,h}}{2} & \text{if } \eta_y > 1 \end{cases}$$

where $\varepsilon_{\text{r,y}}$ and $\varepsilon_{\text{r,h}}$ are the strains at yield and at the onset of strain hardening of reinforcement. In the absence of enough experimental data, (Amadio and Fragiacomo, 2003) assumed, after their experimental results, that the onset of strain hardening and the modulus in hardening phase are:

$$\varepsilon_{r,h} = 3\varepsilon_{r,y} \quad \text{and} \quad E_{r,h} = 0.02E_{r,y} \tag{6.59}$$

The shear connector is assumed to be in elastic range and its slip is calculated using Eq. (6.56). The deformation in top row of bolts is calculated using Eq. (6.57) and, F_{b} may need to be modified as follows:

Unstiffened column web (*Local buckling of column web*)

$$\text{If} \quad F_{c,cw,Rd} < F_r + F_b \;\Rightarrow F_b' = F_{c,wc,Rd} - F_r \geq 0$$

Stiffened column web (Local buckling of beam flange)

$$\text{If} \quad F_{c,bf,Rd} < F_r + F_b \;\Rightarrow F_b' = F_{c,bf,Rd} - F_r \geq 0$$

6.6.2.4. Yielding of reinforcement with buckling of column web or beam flange (ρ>0.8 and $\eta_y \leq 1.2$)

The same procedures in the previous mode are used to calculate the slip in shear connectors, Δ_s, and the deformation in the top row of bolts, Δ_b. The deformation of embedded reinforcement is calculated using (Anderson et al., 2000)'s procedure as:

$$\Delta_{u,r} = \begin{cases} \left(\frac{D_c}{2} + L_t\right)\varepsilon_{smu} & \text{when } p_0 < L_t \\ \left(\frac{D_c}{2} + L_t\right)\varepsilon_{smu} + \left(p_0 - L_t\right)\varepsilon_{smy} & \text{when } p_0 > L_t \end{cases} \tag{6.60}$$

where D_c and p_0 are the column depth and the distance from the face of column to the first stud. The strains ε_{smy}, ε_{smu} are respectively yield and ultimate strain of embedded reinforcement which can be calculated using Eq. (5.17) and Eq. (5.18) in Chapter Five. The ultimate rotation is calculated using Eq. (6.54).

6.7. Validity of the proposed procedures

6.7.1. Rotation at yield

Three sets of experimental tests were considered to check the validity of the proposed procedure to calculate the rotation at yield. These tests were selected to represent three cases of shear connection (i.e. full interaction, full shear connection and partial shear connection). Only a limited numbers of tests in the literature have the measurement of strain for reinforcement or slip of shear studs in order to check the first component to yield. The selected three sets of tests were conducted by (Aribert, 1996; Li et al., 1996; Fu and Lam, 2006). The results of calculation are presented in Table 6.3. It is clear from the results that the proposed procedure can provide a good estimation of rotation at

yield of composite connections for most cases. The accuracy of the procedure is affected by the accuracy involved in the choice of the behaviour of the components.

Table 6.3: Comparison between the proposed and test results for rotation at yield

Ref	Test	A_r (mm^2)	N_{sc}	$f_{r,y}$ (N/mm^2)	$F_{sc,max}$ (kN)	η_y %	$\phi_{j,y}$	$\phi_{j,y}$ *(test)*	$\phi_{j,y}$ / $\phi_{j,y}$ *(test)*
Li et al. (1996)	CSJ-1	780	14	480	120	>300	5.89	6.5	0.91
	CSJ-5	780	14	480	120	>300	6.1	6.4	0.95
Aribert and Lachal (1992)	C1	405	17	540	30	135	3.91	4.3	0.909
	C2	405	12	540	30	95	4.1	3.8	1.08
	C3	405	8	540	30	63	5.1	4.5	1.13
Fu and Lam (2006)	CJ1	628	7	535	120	234	3.9	4.5	0.866
	CJ3	628	2	535	120	105	4.57	5	0.914
	CJ5	628	3	535	120	66	4.8	5.8	0.83
								Average	0.95
								Stdev	0.103

6.7.2. Rotation capacity

Six sets of experimental tests with 21 cases of composite connection were considered to check the validity of the proposed procedure to calculate the rotation capacity of flush end-plate composite connection. These tests represent the usual cases of failure modes. It consists of full interaction, full shear connection and partial shear connection of composite connections. The results of calculation are presented in Table 6.4.

It is clear from these results that the proposed procedure can estimate the rotation capacity of flush end-plate composite connections for most cases even though it underestimates or over-estimates the rotation for some cases. The accuracy of the procedure is affected by the accuracy of the assumed strain at failure for the steelwork components and reinforcement. Also, it depends on the assumed slip capacity of shear studs for the composite connection with low partial shear connection where the shear studs failure mode is expected. From Table 6.4, it can be seen that the proposed procedure gives an average of 1.08 with a standard deviation of 0.2. In addition, the maximum and minimum of prediction/test ratios are 1.42 and 0.7 respectively. The equation developed by Ahmed and Nethercot (1997) (i.e. Eq. (6.43)) gives an average of 1.04 with a standard deviation of 0.27 and the maximum and minimum of prediction/test ratios are 1.73 and 0.72 respectively.

Table 6.4: Comparison between proposed and test results for rotation capacity

Ref.	Specimen	ρ%	Rotation (mrad)		Shear Studs		L_t	N_{act}	Ahmed and Nethercot (1997) (1)		Proposed (P)	
			At ultimate moment	At failure (T)	No.	η_y	(mm)		Rotation capacity (mrad)	(1)/T	Rotation capacity (mrad)	P/T
Anderson and Najafi (1994)	S4F	0.55	15.70	26.60	7	1.91	121	5.51	30.29	1.14	35.01	1.32
	S12F	1.65	22.70	55.70	7	1.27	81	5.94	61.04	1.10	60.51	1.09
Xiao et. al.(1994)	SCJ3	0.30	7.20	26.60	6	2.00	133	5.28	23.23	0.87	34.86	1.31
	SCJ4	1.00	23.40	41.10	6	2.00	133	5.28	34.94	0.85	58.38	1.42
	SCJ7	1.20	26.50	46.90	6	1.67	111	5.47	40.28	0.86	59.61	1.27
Li et. al. (1996)	CJS-1	1.20	47.00	47.00	14	4.61	111	4.58	43.64	0.93	44.19	0.94
	CJS-2	1.20	42.00	42.00	14	4.61	111	4.58	43.64	1.04	44.19	1.05
	CJS-4	1.20	58.00	58.00	14	4.61	111	4.58	43.64	0.75	44.19	0.76
	CJS-5	1.20	60.00	60.00	14	4.61	111	4.58	43.64	0.73	44.19	0.74
Liew et. al. (2000)	SCB2	1.12	51.90	51.90	14	1.52	119	5.59	90.01	1.73	64.55	1.24
Loh et. al. (2006)	CJ1	1.29	30.00	58.00	5	1.09	103	5.00	51.82	0.89	68.85	1.19
	CJ2	1.29	38.00	53.00	3	0.65	103	3.00	58.20	1.10	67.98	1.28
	CJ3	1.29	45.00	55.00	2	0.43	103	2.00	67.69	1.23	65.14	1.18
	CJ4	0.65	21.00	50.00	3	1.16	69	5.75	46.25	0.92	54.04	1.08
Fu and Lam (2006)	CJ1	0.60	35.40	35.40	7	2.50	222	5.06	29.93	0.85	33.99	0.96
	CJ4	0.60	37.40	37.40	3	1.43	222	4.00	35.84	0.96	35.69	0.95
	CJ5	0.60	31.70	31.70	3	0.71	222	2.00	39.55	1.25	35.69	1.13
	CJ6	0.60	46.80	46.80	6	1.07	222	3.00	37.72	0.81	52.69	1.13
	CJ7	0.60	30.00	30.00	2	1.07	222	3.00	49.30	1.64	35.69	1.19
	CJ8	0.60	42.30	42.30	4	1.68	222	5.29	42.22	1.00	29.43	0.70
									Average	1.04		1.08
									Stdev	0.27		0.2
									Maximum	1.73		1.42
									Minimum	0.72		0.7

6.8 Relation between the ductility of connection and ductility of frame

A steel frame with three bays and four storeys was used to demonstrate the relation between the ductility of connection and ductility of frame (see Figure 6.6).

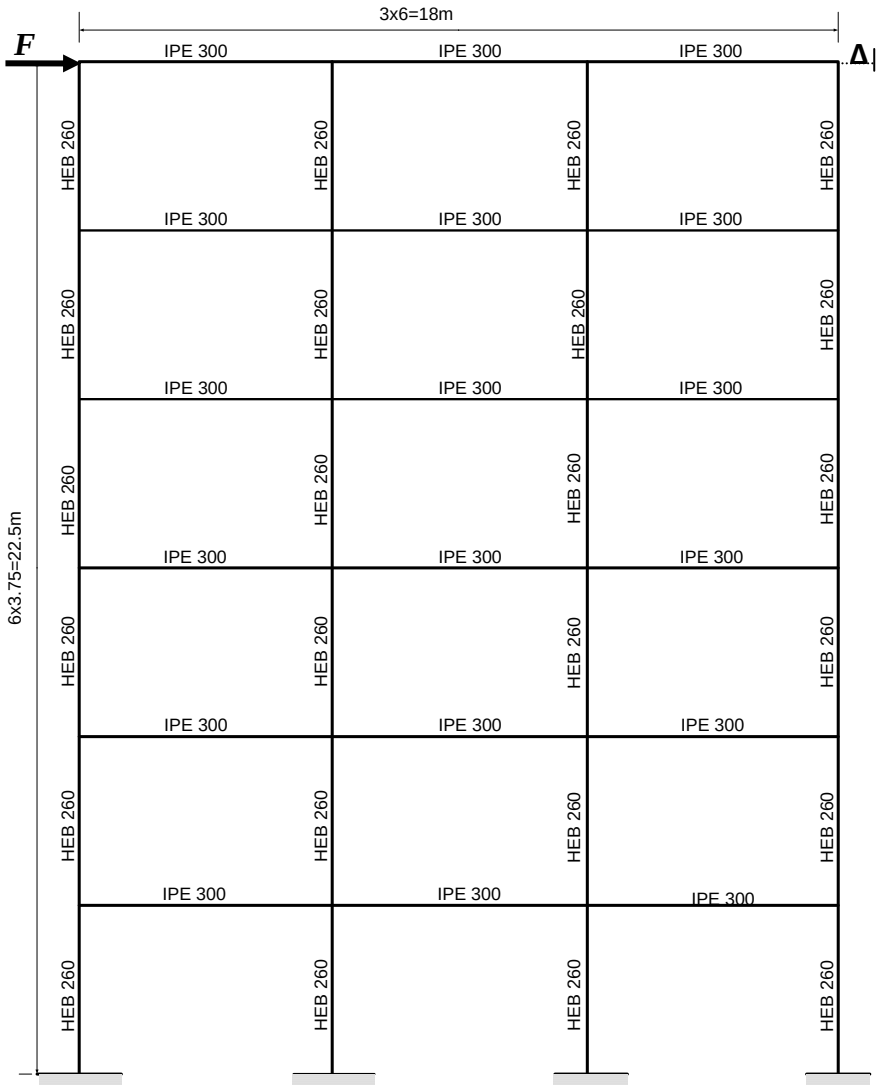

Figure 6.6: Steel frame

Two different flush end-plate connections are used to evaluate the effect of ductility of connection on the ductility of steel frame. These connections were tested by (Davison et al., 1987) and the moment-rotation curves of these connections are shown in Figure 6.7. They are considered as semi-rigid connections, as shown in Figure 6.8.

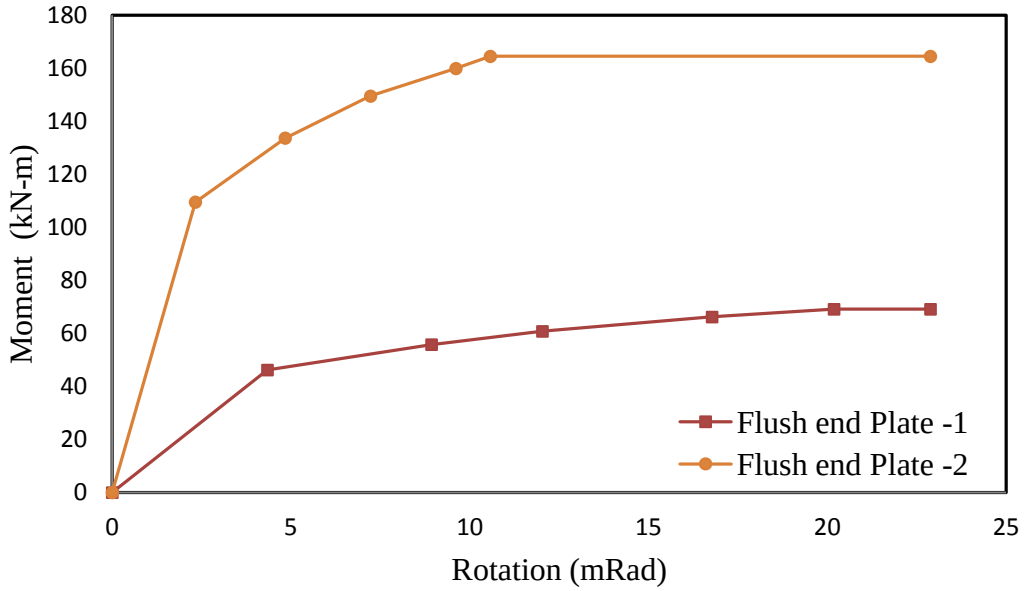

Figure 6.7: Moment-rotation curve of isolated connections

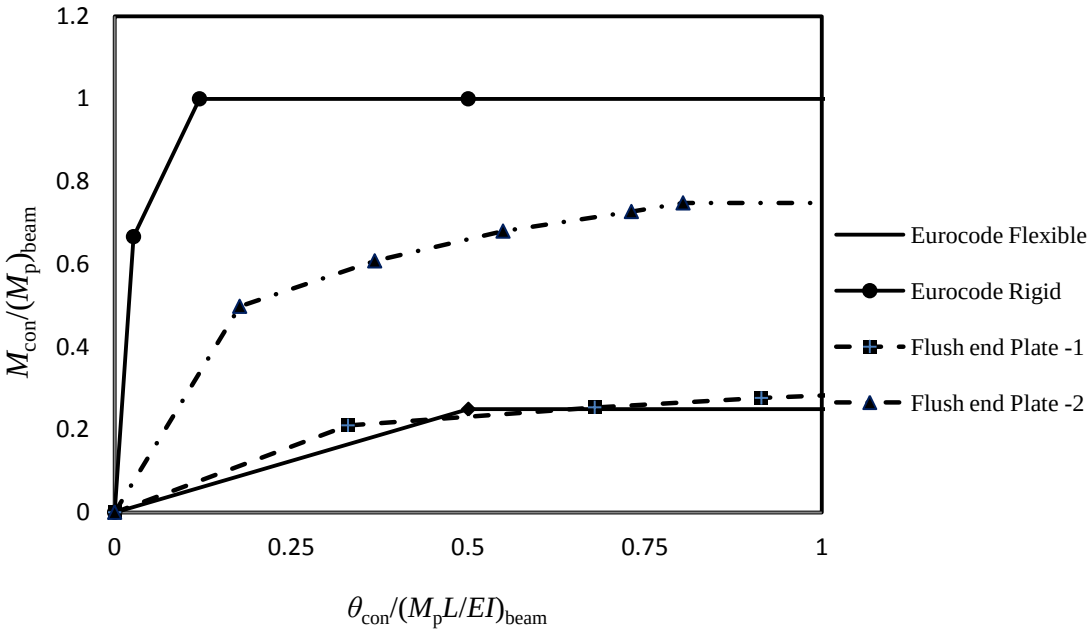

Figure 6.8: Connection classification

The ductility of frame is calculated using the following relation

$$\mu_f = \frac{\Delta_u}{\Delta_y}$$

where μ_f is the ductility of frame. Δ_y, Δ_u are respectively the top horizontal displacement at first yield and ultimate load due to horizontal point load at the top of frame. The ductility of connection is calculated using Eq. (6.30), as:

$$\mu_j = \frac{\phi_{j,c}}{\phi_{j,y}}$$

The available ductility of isolated connections (see Figure 6.7) are:

Flash end-plate-1 (*Conn*-1)

$$\mu_{j,av} = \frac{22.88}{4.34} = 5.25$$

Flash end-plate-2 (*Conn*-2)

$$\mu_{j,av} = \frac{22.88}{2.32} = 9.86$$

6.8.1. Finite element modelling

The analysis of the frame in Figure 6.6 with one type of connection each time was performed using ABAQUS package. All columns and beams were modelled using B31 beam element. The concentred load and boundary conditions were simulated, as shown in Figure 6.6. Steel elastic material was assigned to all columns and beams. This option ensures that the whole behaviour of the frame will control by only its connections behaviour. All connections were modelled using connector elements with non-linear behaviour. The constant extrapolation option in connector section was selected for connection curve. This option ensures that the curve of connection will continue with zero slope up to unlimited value in order to ensure that the connection can reach unlimited ductility. Also, it ensures that the frame can reach ultimate resistance and then its resistance is reduced due to accumulative deformations of all columns, beams and connections without any local failure of connection. Furthermore, this option permits to plot the relation between the instantaneous ductility of frame with the associated ductility of control connection.

Results and discussions

Figure 6.9 shows the deflected frame under lateral concentrated load at top left point.

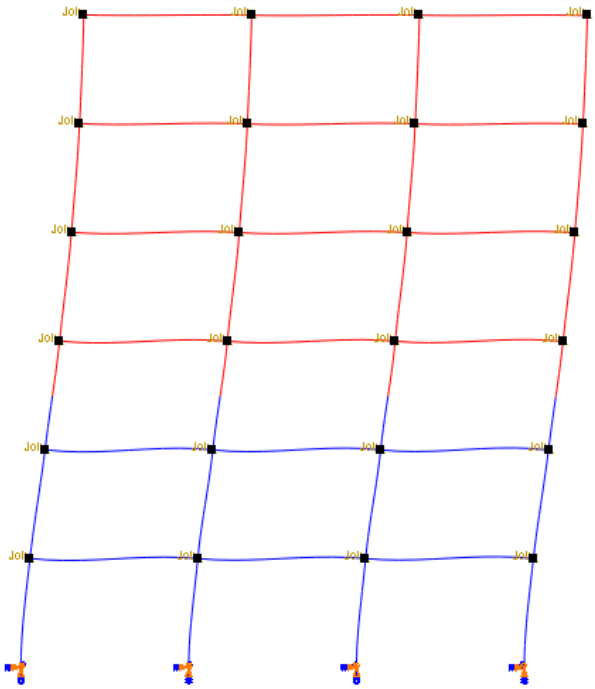

Figure 6.9: Deflected shape of frame

Figure 6.10 and Figure 6.11 show the load-rotation curves for all connections in the frame up to the ultimate load. Some of these connections have positive rotations and other have negative rotations depend on its location in the frame. Also, it is clear that many of the connections reached the experimental rotation capacity before the frame reached its ultimate resistance whereas other connections varied between the linear and post linear ranges.

Figure 6.12 shows the load-displacement curve for the frame with each type of connection. The horizontal point load at first yield of connection is 100 kN for the frame with Conn-1 and 225 kN for the frame with Conn-2. The associated horizontal displacement at top of the frame is 160 mm for the frame with Conn-1 and 225 mm for the frame with Conn-2. Also, the ultimate horizontal point load is 410 kN and the associated displacement is 1843 mm for the frame with Conn-1. The ultimate horizontal point load is 533 kN and the associated displacement is 735 mm for the frame with Conn-2.

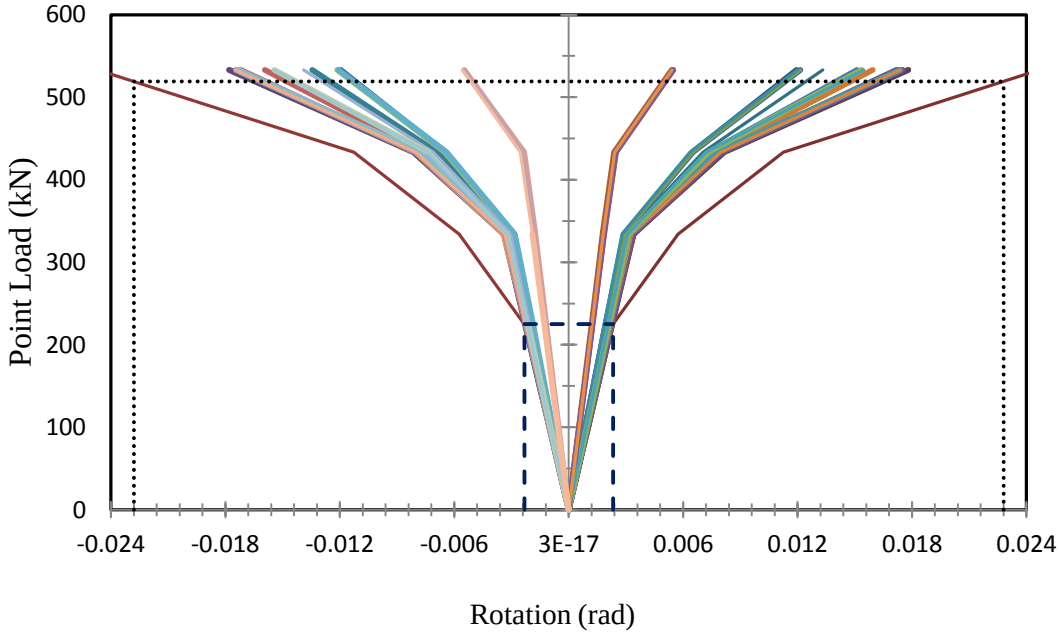

Figure 6.10: load-rotation curves of connection in the frame with Conn-1 (the black dash line represents the yield limit of connection and black dots line represent the rotation capacity of connection)

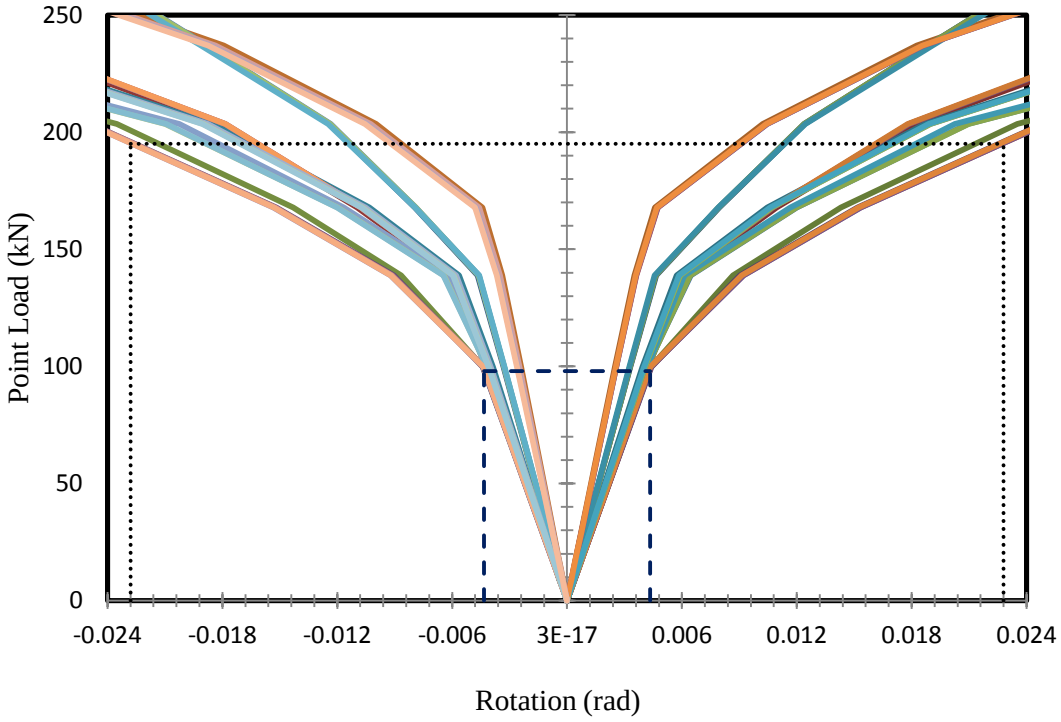

Figure 6.11: load-rotation curves of connection in the frame with Conn-2 ((the black dash line represents the yield limit of connection and black dots line represent the rotation capacity of connection)

Calculation of the ductility of frame and connection can be summarized as follows:

Available ductility of the frame

(i) Frame with Conn-1

$$\left(\mu_f\right)_{av} = \frac{\Delta_{u,c}}{\Delta_{y,c}} = \frac{485}{160} = 3.0$$

where $\Delta_{y,c}$ is the top horizontal displacement of the frame when rotation of any connection in the frame reaches the yield rotation. $\Delta_{u,c}$ is the top horizontal displacement of the frame when the rotation of any connection in the frame reaches the rotation capacity.

(ii) Frame with Conn-2

$$\left(\mu_f\right)_{av} = \frac{650}{225} = 2.9$$

Required ductility of the frame to reach its ultimate resistance

i. Frame with Conn-1

$$\left(\mu_f\right)_{req} = \frac{1843}{160} = 11.5$$

ii. Frame with Conn-2

$$\left(\mu_f\right)_{req} = \frac{735}{225} = 3.27$$

Required ductility of the connection to provide the required ductility of frame

The required ductility of the connection in order to provide the required ductility for the frame in order to reach its ultimate resistance is:

i. Frame with Conn-1

$$\left(\mu_c\right)_{req} = \frac{95.9}{4.43} = 21.6$$

ii. Frame with Conn-2

$$(\mu_c)_{req} = \frac{24.7}{2.32} = 10.6$$

The percentage of available connection ductility to the required ductility

i. Frame with Conn-1

$$\frac{(\mu_c)_{av}}{(\mu_c)_{req}} = \frac{5.25}{21.6} \times 100 = 24.3\%$$

ii. Frame with Conn-2

$$\frac{(\mu_c)_{av}}{(\mu_c)_{req}} = \frac{9.86}{10.6} \times 100 = 93\%$$

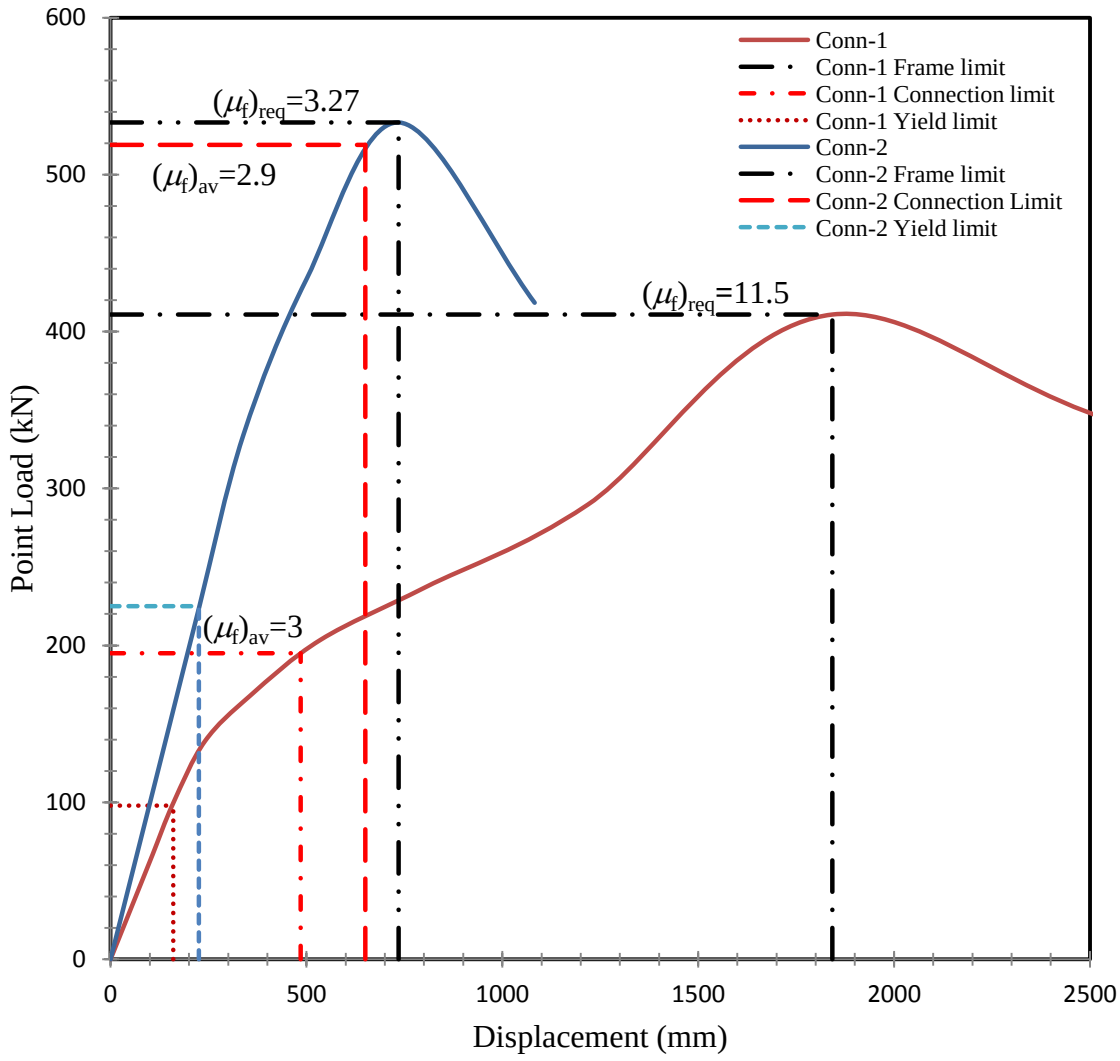

Figure 6.12: load-displacement curve of frame

Figure 6.13 shows the moment rotation of the connection in the frame up to failure of frame. It demonstrates the advantage of extending the moment-rotation curve horizontally in the modelling of connection to overcome the possibility of terminating the processing of ABAQUS programme due to failure in connection before the frame reaches its maximum load resistance. Figure 6.14 shows the relation between the top horizontal displacements of frame with the associated rotation of control connection in the frame.

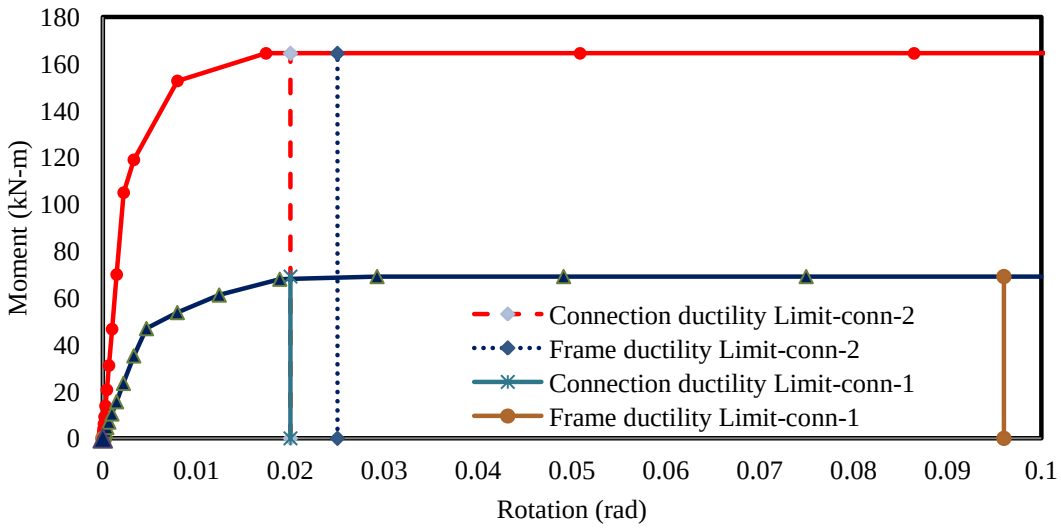

Figure 6.13: Moment-Rotation of connection in the frame

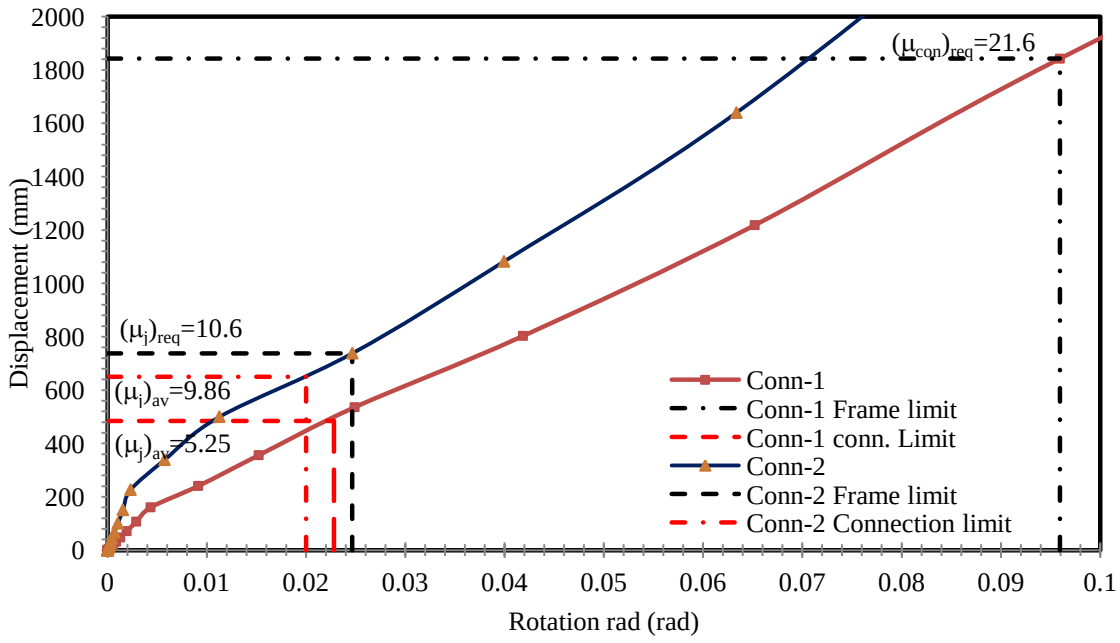

Figure 6.14: Frame displacement-connection rotation curve

The above results show that both types of connection provide the nearly same available ductility to the frame. However, this value of available ductility is equal to about 93 % of the required ductility for the frame with Conn-2 to reach its ultimate resistance but it is only equal to about 24% of the required ductility for the frame with Conn-1.

Furthermore, the frame with (Conn-1) has much ductility with less load resistance than the same frame with (Conn-2), as the moment resistance of the (Conn-1) is less than the moment resistance of (Conn-2).

The results from Figure 6.12, Figure 6.13 and Figure 6.14 were used to construct the relation between the *instantaneous ductility* of connection and the *instantaneous ductility* of frame, as shown in Figure 6.15. It is clear from these figures that the ductility of any frame is strongly dependent on moment resistance and ductility of its connection.

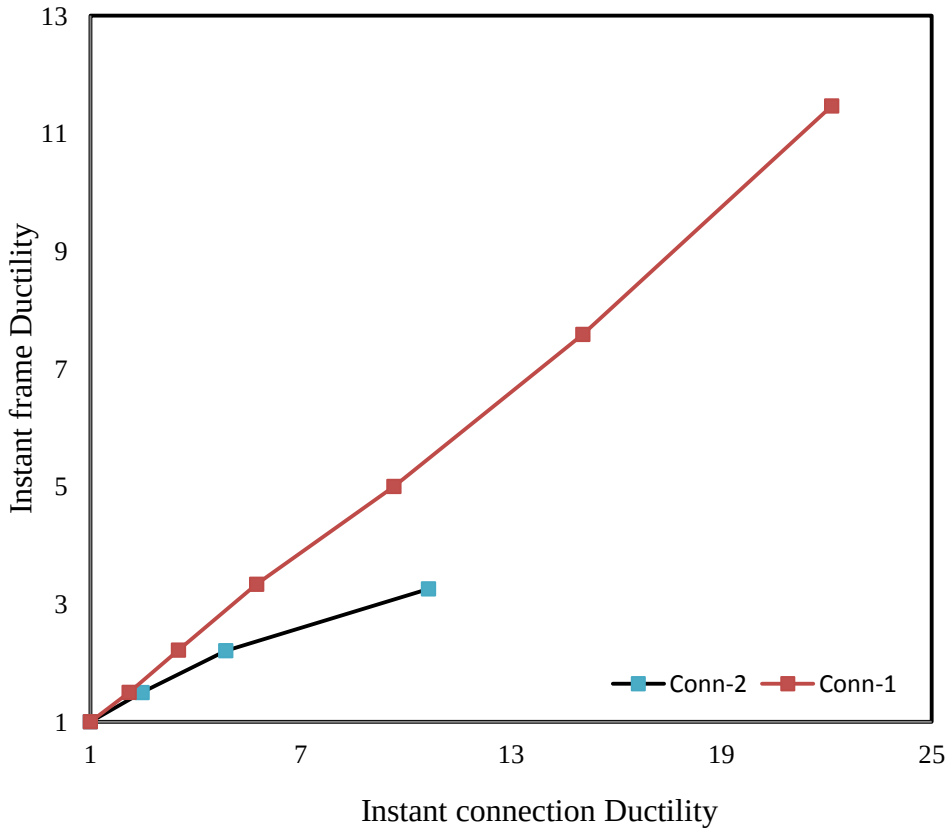

Figure 6.15: Instant frame ductility-Instant connection ductility relationship

6.9. Summary and conclusions

1. A flowchart to predict the failure mode of composite connection has been developed based on the practical range of shear connection ratio (η_y>0.4) and reinforcement ratio (0.5<ρ<1.7%).

2. A procedure to calculate the moment resistance of composite connection has been developed using the concept of a rigid-plastic, stress blocks. This procedure is compatible with the proposed flowchart in Figure 6.1 and with the procedure to estimate the rotation at failure. Also, it considered the cases of full interaction, full shear connection and partial shear connection.

3. The prediction of moment resistance of composite connection from the proposed procedure is in agreement with the experimental results for most cases. The ratio of the results from the proposed procedure and the experiments gives an average of 1.001 with a standard deviation of 0.13. In addition, the maximum and minimum of prediction/test ratios are 1.28 and 0.84 respectively.

4. The proposed mechanical model to calculate the rotational stiffness of composite connection is extended to calculate the rotations at yield and at failure using the appropriate post-linear values of its components.

5. The validity of the proposed procedure to calculate the rotation at yield was evaluated against three sets of experiments. These tests were selected to represent three cases of shear connection (i.e. full interaction, full shear connection and partial shear connection). The results from the proposed procedure can estimate well the rotation at yield of composite connections for most cases.

6. Six sets of experimental tests with 21 cases of composite connection were considered to check the validity of the proposed procedure to calculate the rotation at failure. These tests represent all of the usual failure modes. The proposed procedure can estimate the rotation at failure of composite connections for most cases.

7. The relationship between connection ductility and frame ductility was investigated. It was found that the moment resistance and ductility of connection affect significantly the whole behaviour of frame.

Chapter Seven

Analysis of a uniform beam with semi-rigid connections under gravity loading

7.1. Introduction

The semi-rigid behaviour of a connection significantly affects the overall behaviour of the structural member to which its ends are attached. Deflection of a structural member is greatly influenced by the flexibility of the connections involved. Many approximate practical procedures have been used to compute the deflection of a beam with semi-rigid connections at its ends. Recently, (Ahmed, 2001; Ahmed et al., 2008) proposed a new practical procedure to determine the maximum deflection of a beam under gravity loading with semi-rigid connections using basic structural principles. Based on this maximum deflection, they constructed practical charts to evaluate the practical allowable span/depth ratio for rectangular and UB sections. Even though this method can give good predictions of the maximum deflection of a beam with semi-rigid connection, it has many shortcomings which are listed below:

1. This method entails the use of explicit expressions for the maximum deflection of a beam which are subject to only three standard cases of loading: central, third point and uniformly loading. As a result, it can provide only an approximate result for other types of loading.

2. It only gives the deflection at the estimated point of maximum deflection. It cannot be used to calculate the deflection at other points.

3. It cannot be extended to calculate the shear force or bending moment under serviceability loading.

4. It deals with statically indeterminate members.

In the following section, a new procedure which can be used to calculate the deflection for a beam with semi-rigid connections under any arbitrary loading will be proposed. This procedure will overcome the shortcomings of the procedure used by (Ahmed et al., 2008). The proposed procedure has the following virtues:

1. It is based on the flexibility parameters of a simply-supported beam which means that all calculations deal with a statically determinate member.
2. It can be used to calculate the deflection at any point of the beam.
3. It can be used to calculate the deflection for an arbitrary loading without any approximation.
4. It can be also used to compute shear force and bending moment as well.
5. It can be extended to compute the deflection of a composite steel-concrete member after making some modifications to account for beam stiffness.

7.2. Proposed procedure

The beam with a semi-rigid connection in Figure 7.1 is used for the derivation of the required parameters. The beam can be subjected to any arbitrary type of loading. The procedure is based on the principle of superposition to find the rotation at the two ends of the simply-supported beam using the moment-area method or any other simple methods.

Derivation of the required parameters

The slope deflection equations for a beam with semi-rigid connections are:

$$M_A = \frac{2EI}{L}\left(2\phi_A + \phi_B\right) \qquad \& \qquad M_B = \frac{2EI}{L}\left(2\phi_B + \phi_A\right) \tag{7.1}$$

where E, I and L are the modulus of elasticity, second moment of inertia and length of beam. In order to show the effect of the semi-rigid end-springs, Eq. (7.1) can be rewritten as:

$$M_A = \frac{2EI}{L}(2S_A\theta_A + S_{BA}\theta_B) \quad \& \quad M_B = \frac{2EI}{L}(2S_B\theta_B + S_{AB}\theta_A) \tag{7.2}$$

where $$\phi_A = \theta_A - \frac{M_A}{k_A} \qquad \text{and} \qquad \phi_B = \theta_B - \frac{M_B}{k_B} \tag{7.3}$$

From (Wong et al., 2007):

$$S_A = \frac{1}{R}(1+3R_B), \quad S_B = \frac{1}{R}(1+3R_A) \quad \& \quad S_{AB} = S_{BA} = \frac{1}{R} \tag{7.4}$$

$$R_A = \frac{EI}{Lk_A} \quad \& \quad R_B = \frac{EI}{Lk_B} \quad \& \quad R = 1 + 4(R_A + R_B) + 12R_AR_B \tag{7.5}$$

$$\therefore M_A = \frac{2EI}{LR}((6R_B + 2)\theta_A + \theta_B) \quad \& \quad M_B = \frac{2EI}{LR}((6R_A + 2)\theta_B + \theta_A) \tag{7.6}$$

$$\therefore M_A = \frac{2EI}{L}\left(\frac{(6R_B + 2)}{R}\theta_A + \frac{1}{R}\theta_B\right) \quad \& \quad M_B = \frac{2EI}{L}\left(\frac{(6R_A + 2)}{R}\theta_B + \frac{1}{R}\theta_A\right)$$

$$\therefore M_A = \frac{2EI}{L}\left(\frac{f_A}{R}\theta_A + \frac{1}{R}\theta_B\right) \quad \& \quad M_B = \frac{2EI}{L}\left(\frac{f_B}{R}\theta_B + \frac{1}{R}\theta_A\right) \tag{7.7}$$

$$f_A = 6R_B + 2 \quad \& \quad f_B = 6R_A + 2 \tag{7.8}$$

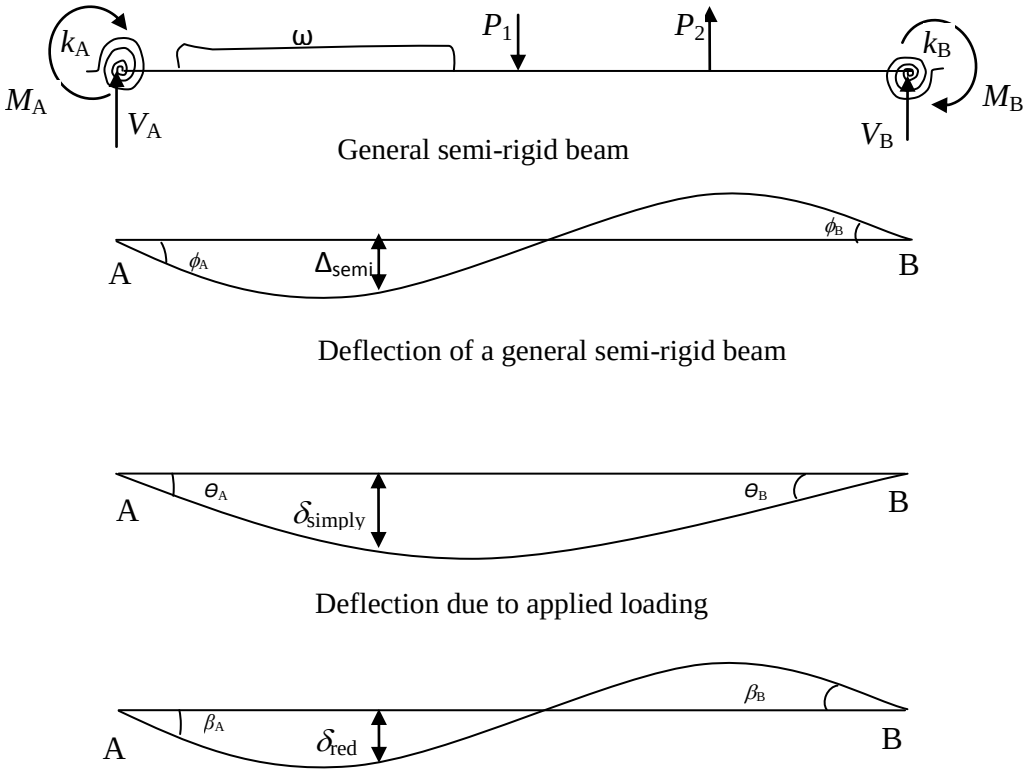

Figure 7.1: Semi-rigid beam with a general load system

7.3. Eurocode 3 (2005) classification for joints

Eurocode 3 (2005) classifies joints for braced and unbraced steel structures as:

1. Rigid a) braced $\frac{EI}{Lk_s} \geq \frac{1}{8}$ b) unbraced $\frac{EI}{Lk_s} \geq \frac{1}{25}$
2. Semi-rigid a) braced $\frac{1}{8} < \frac{EI}{Lk_s} < 2$ b) unbraced $\frac{1}{25} < \frac{EI}{Lk_s} < 2$ (7.9)
3. Pinned $\frac{EI}{Lk_s} \leq 2$

where k_s is the stiffness of the connection. EI and L are the flexural stiffness and length of the beam respectively. Therefore, the semi-rigid range for unbraced steel structure joints:

$$0.04 < \left(R_A \& R_B\right) < 2$$

7.4. Comparison with (Ahmed et al., 2008)'s equations

The equations proposed in Section 7.2 are for semi-rigid beams with symmetrical or asymmetrical loading. However, (Ahmed et al., 2008)'s equations are for semi-rigid beams with symmetrical loading only (i.e. θ_A/θ_B =-1).

In order to compare the result from the proposed equations with (Ahmed et al., 2008)'s equation for symmetrical loading, the same definition used by (Ahmed et al., 2008) for semi-rigid factors are used:

Assume $$R_A = \frac{EI}{Lk_A} = m \quad \text{and} \quad n = \frac{k_B}{k_A} \quad \Rightarrow R_B = \frac{m}{n} \tag{7.10}$$

$$\therefore\ R = 1 + 4m\left(1 + \frac{1}{n}\right) + 12\frac{m^2}{n}$$

Eqs. (7.7) and (7.8) are rewritten in terms of m and n:

$$f_A = \frac{6m}{n} + 2 \qquad \& \quad f_B = 6m + 2 \tag{7.11}$$

$$M_A = \frac{2EI}{L}\frac{\left(f_A\theta_A + \theta_B\right)}{1 + 4m\left(1 + \frac{1}{n}\right) + 12\frac{m^2}{n}} \qquad \& \qquad M_B = \frac{2EI}{L}\frac{\left(f_B\theta_B + \theta_A\right)}{1 + 4m\left(1 + \frac{1}{n}\right) + 12\frac{m^2}{n}} \tag{7.12}$$

For all cases of symmetrical loading:

$$\theta_A = -\theta_B \tag{7.13}$$

$$\therefore M_A = \frac{2EI}{L}\frac{(f_A - 1)}{\left(1 + 4m(1 + \frac{1}{n}) + 12\frac{m^2}{n}\right)}\theta \quad \text{and} \quad M_B = \frac{2EI}{L}\frac{(f_B - 1)}{\left(1 + 4m(1 + \frac{1}{n}) + 12\frac{m^2}{n}\right)}\theta \tag{7.14}$$

In order to find the end moments for a fixed end case with symmetrical loading (M_{FA} and M_{FB}), then:

$$k_A = k_B = \infty$$

from Eq. (7.10): $\therefore R_A = 0 \Rightarrow m = 0 \quad \& \quad n = 1 \quad \Rightarrow R_B = 0$

from Eq. (7.11): $(f_A)_{Fix} = (f_B)_{Fix} = 2 \Rightarrow M_{FA} = \frac{2EI}{L}\theta \quad \& \quad M_{FB} = \frac{2EI}{L}\theta$

Then, by substituting (M_{FA} and M_{FB}) in Eq. (7.14) the proposed equations for symmetrical loading:

$$\therefore M_A = M_{FA}\frac{(f_A - 1)}{\left(1 + 4m(1 + \frac{1}{n}) + 12\frac{m^2}{n}\right)} \quad \& \quad M_B = M_{FB}\frac{(f_B - 1)}{\left(1 + 4m(1 + \frac{1}{n}) + 12\frac{m^2}{n}\right)} \tag{7.15}$$

Eq. (7.15) can be rewritten as:

$$\therefore M_A = M_{FA} f_1 \quad \& \quad M_B = M_{FB} f_2 \tag{7.16}$$

Comparing Eq. (7.16) and Eq. (7.15) gives:

$$f_1 = \frac{(f_A - 1)}{\left(1 + 4m(1 + \frac{1}{n}) + 12\frac{m^2}{n}\right)} \quad \& \quad f_2 = \frac{(f_B - 1)}{\left(1 + 4m(1 + \frac{1}{n}) + 12\frac{m^2}{n}\right)} \tag{7.17}$$

$$\therefore f_1 = \frac{\frac{6EI}{L} + k_B}{\frac{4EI}{L}(\frac{3EI}{Lk_A} + \frac{k_B}{k_A}) + \left(\frac{4EI}{L} + k_B\right)} \quad \text{and} \quad f_2 = \frac{k_B\left(\frac{6EI}{Lk_A} + 1\right)}{\frac{4EI}{L}(\frac{3EI}{Lk_A} + \frac{k_B}{k_A}) + \left(\frac{4EI}{L} + k_B\right)}$$

From (Ahmed et al., 2008)'s equations for symmetrical loading:

$$(f_1)_{\text{Ahmed}} = \frac{\frac{6EI}{L} + k_B}{\frac{4EI}{L}\left(\frac{3EI}{Lk_A} + \frac{k_B}{k_A}\right) + \left(\frac{4EI}{L} + k_B\right)} \tag{7.18}$$

$$(f_2)_{\text{Ahmed}} = \frac{k_B\left(\frac{6EI}{Lk_A} + 1\right)}{\frac{4EI}{L}\left(\frac{3EI}{Lk_A} + \frac{k_B}{k_A}\right) + \left(\frac{4EI}{L} + k_B\right)} \tag{7.19}$$

It is clear that f_1 and f_2 in Eq. (7.17) are identical to Eq. (7.18) and Eq. (7.19). In addition, the above discussion show that the proposed equations and (Ahmed et al., 2008)'s equation are equivalent for symmetrical loading cases. The proposed equations are for semi-rigid beams with symmetrical or asymmetrical loading. However, (Ahmed et al., 2008)'s equations are for semi-rigid beams with symmetrical loading only (i.e. θ_A/θ_B =-1). Therefore, it is clear that (Ahmed et al., 2008)'s equations are only special case from the proposed equations.

7.5. Deflection of a semi-rigid beam

Based on the pre-determined values of fixed end moments at two ends of a beam, (Ahmed et al., 2008) proposed design charts to calculate only the maximum deflection at the point of maximum moment for only three standard cases of symmetrical loading. However, the proposed equations (i.e. Eqs. (7.7) & (7.8) can be used to calculate deflection at any point along the beam and for any arbitrary type of loading.

The proposed procedure is based on the principle of superposition by considering the beam as simply-supported to find the deflection at a point, δ_{simply}, using any conventional methods such as the moment area method or the virtual work method. Reduction factors are then used to account for the semi-rigid effect. The net deflection at any point is:

$$\Delta_{semi} = \delta_{simply} + (\delta_{red})_{M_A} + (\delta_{red})_{M_B} \tag{7.20}$$

$$(\delta_{red})_{M_A} = \left(\frac{M_A}{6EI}\right)\left(3x^2 - x^3/L - 2Lx\right) \qquad 0 < x < L \quad \text{from point A} \tag{7.21}$$

$$\left(\delta_{red}\right)_{M_B} = \left(\frac{M_B}{6EI}\right)\left(3x^2 - x^3 / L - 2Lx\right) \qquad 0<x<L \text{ from point B} \tag{7.22}$$

7.6. Steps for analysis of a beam with a semi-rigid connection under gravity loading

7.6.1 End moment and reaction V_A and V_B

(i) Compute θ_A & θ_B for simply-supported boundary condition by any conventional method such as the moment area method or the virtual work method. Also, if the fixed end moment is already known (M_{FA} &M_{FB}) for this kind of loading then:

$$\theta_A = \frac{L}{6EI}\left(2\,M_{FA} - M_{FB}\right) \quad \& \quad \theta_B = \frac{L}{6EI}\left(2M_{FB} - M_{FA}\right) \tag{7.23}$$

(ii) Use Eqs. (7.7) & (7.8) to compute M_A and M_B.

(iii) Use the principle of superposition method to plot the bending moment diagram for the whole beam.

(iv) Use the equilibrium equations to calculate the end reactions and a shear force diagram.

7.6.2. Deflection at any point

(i) Calculate the deflection at any point for simply-supported boundary conditions (δ_{simply}) by any conventional method.

(ii) Using M_A and M_B, compute the reduction in deflection (δ_{red}) due to the semi-rigid effect using Eqs. (7.21)& (7.22).

(iii) Calculate the net deflection at any point using Eq. (7.20).

Example 1: For the semi-rigid beam shown in Figure 7.2: (b=0.2 m, h=0.4 m, L=20 m, E=200GN/m^2, I= 107x10^{-5} m4, k_A=1000 N-m/rad, k_B=10000 N-m/rad)

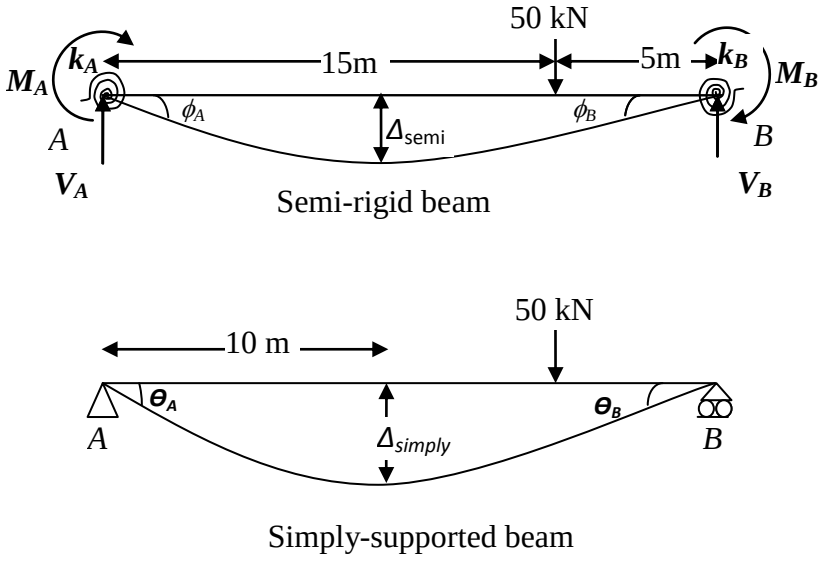

Figure 7.2: Example 1

End moments

1. Compute θ_A & θ_B for simply-supported boundary condition by any conventional method.

$$\theta_A = \frac{50000 \times 5 \times 15 \times (20+5)}{6EIL} = 0.00366 \text{ rad} \quad \& \quad \theta_B = 0.00513 \text{ rad}$$

2. Use Eq. (7.5) to compute:

$$R_A = \frac{EI}{Lk_A} = 10.7 \quad \& \; R_B = \frac{EI}{Lk_B} = 1.07 \quad \& \; R = 1 + 4(R_A + R_B) + 12R_AR_B = 184$$

3. Use Eq. (7.7) to find:

$$M_A = \frac{2 \times 107 \times 10^5}{185}(2(1+3 \times 1.07) \times 0.00366 - 0.00513) = 2.96 \text{ kNm}$$

$$M_B = \frac{2 \times 107 \times 10^5}{185}(2(1+3 \times 10.7) \times 0.00513 - 0.00366) = 38.7 \text{ kNm}$$

Reactions V_A and V_B

Using the equilibrium equations, end reactions can be calculated as:

$$V_A = \frac{2.96 + 50 \times 5 - 38.7}{20} = 10.7 \text{ kN} \qquad \Rightarrow V_A = 50 - 10.7 = 39.3 \text{ kN}$$

Deflection at a distance of* 10 m *from point A

1. Calculate the deflection at 10m from point *A* for simply-supported boundary condition (δ_{simply}):

$$(\delta_{simply})=0.0269 \text{ m}$$

2. Using M_A and M_B, compute the reduction in deflection (δ_{red}) due to semi-rigid effect:

$$\left(\delta_{red}\right)_{M_A}=\left(\frac{2.96\times10^3}{6\times200\times10^9\times106.7\times10^{-5}}\right)\left(3\times10^2-\frac{10^3}{20}-2\times20\times10\right)=\text{-0.000347m}$$

$$\left(\delta_{red}\right)_{M_B}=\left(\frac{38.7\times10^3}{6\times200\times10^9\times106.7\times10^{-5}}\right)\left(3\times10^2-\frac{10^3}{20}-2\times20\times10\right)=\text{-0.00453m}$$

3. Calculate the *net deflection* at the point:

$$\Delta_{semi}=\delta_{simply}+\left(\delta_{red}\right)_{MA}+\left(\delta_{red}\right)_{MB}=0.0268-0.000347-0.00453=0.0219\text{m}=21.9\text{mm}$$

Comparison with ABAQUS results

The same beam was analysed using the ABAQUS software. The steel beam was modelled with beam element and the semi-rigid connections were simulated as rotational springs at the ends. The JOINT option was used in conjunction with the *SPRING* option to simulate the connections as stated in (ABAQUS/ Keywords Reference Manual §18.29). Euler-Bernoulli cubic beam elements (B23) available in ABAQUS/Standard were used to simulate the beam, as this element is highly accurate for simulations of dynamic vibration analyses (Getting Started with ABAQUS §6.3). An analysis step with a FREQUENCY procedure option was used to obtain natural frequencies of the beam. A Static, general step was used to calculate the reaction forces at two ends of the beam. Table 7.1 shows the comparison of the results from the proposed procedure and the ABAQUS results.

Table 7.1: Comparison of the results of the proposed procedure with those given by ABAQUS

Parameters	End moment		Reaction		Deflection (mm)
	M_A (kNm)	M_B (kNm)	V_A (kN)	V_B (kN)	
Proposed	2.964	38.71	10.71	39.29	21.98
ABAQUS	2.965	38.70	10.71	39.29	21.99
Proposed/ABAQUS	100%	100%	100%	100%	100%

It is clear from Table 7.1 that the proposed procedure can give results that are nearly identical to those given by ABAQUS modelling for this simple example.

7.7. Natural frequency of a uniform beam with semi-rigid connections using the effective length concept

For most practical cases, the stiffness of two end connections are equal (i.e. $k_A=k_B$). Therefore, the concept of *effective length* can be used to compute the natural frequency of a beam with semi-rigid connections. The procedure is based on the natural frequency of a simply-supported beam in conjunction with the effect of a semi-rigid connection using the effective length concept as follows:

For simply-supported beam ($k_A=k_B=0$)

$$f_{\text{pin}} = \frac{9.869}{2\pi}\sqrt{\frac{EI}{WL^3}} = \frac{1}{2\pi}\sqrt{\frac{EI}{W}\frac{\pi^4}{L^3}} \tag{7.24}$$

For a fixed-end beam ($k_A=k_B=\infty$)

$$f_{fix} = \frac{22.37}{2\pi}\sqrt{\frac{EI}{WL^3}} = \frac{1}{2\pi}\sqrt{\frac{EI}{W}\frac{\pi^4}{(0.579L)^3}} \tag{7.25}$$

where W is the total mass of beam. f_{pin} and f_{fix} are the natural frequency of a beam with pinned-pinned and fixed-fixed boundary conditions respectively. The natural frequency for general cases of boundary conditions is:

$$f = \frac{1}{2\pi}\sqrt{\frac{EI}{W}\frac{\pi^4}{(\kappa L)^3}} \tag{7.26}$$

where κL is the effective length of the beam and κ is the effective length factor. The value of κ depends on the boundary conditions of the beam, as shown in Figure 7.3. This value can be determined from the chart in Figure 7.4. This chart was developed by normalising the natural frequency of a beam to the natural frequency of the simply-supported condition and assuming that ($k_{pin} \approx 0.5EI/L$), as in the Eurocode 3 (2005) classification.

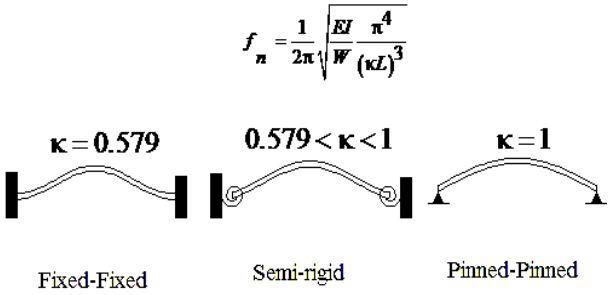

Figure 7.3: Natural frequency for beams of uniform mass with different boundary conditions

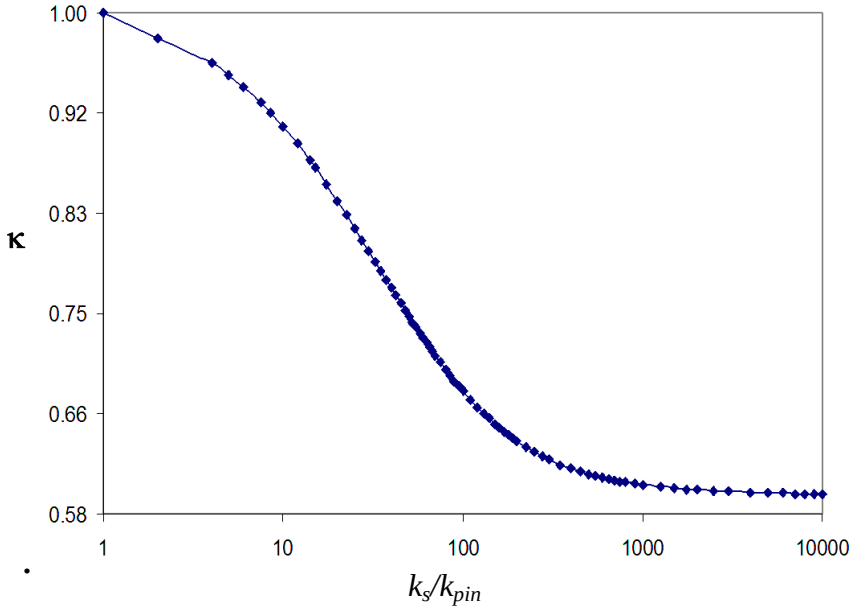

Figure 7.4: Effective length factor [ABAQUS results]

Example 2: The same beam as in Figure 7.2 was used to verify the proposed procedure with ABAQUS software for different stiffnesses and loading. (b=0.1m, h=0.2m, L=20m, E=200GPa)

7.8. Results and conclusion

It can be seen from Table 7.2 that the results of deflection and frequency given by the proposed procedure are well in agreement with the results of finite element modelling for different rotational stiffnesses. The proposed method however does not take into account any shear deformation or rotational inertia.

Table 7.2: Comparison with ABAQUS software for different stiffnesses and loading

P (N)	K_A=K_B	M_A	M_B	δ_{simply}	$(\delta_{red})_{MA}$	$(\delta_{red})_{MB}$	Δ_{semi}	f	Δ_{semi} ABAQUS	f ABAQUS
10000	1000	11.7	16.4	0.0859	-2.19E-05	-3.07E-05	0.0859	1.15	0.0858	1.14
20000	1E4	232	326	0.172	-0.000435	-0.000611	0.1708	1.15	0.171	1.15
30000	1E5	3238	4611	0.258	-0.00607	-0.00864	0.2431	1.18	0.243	1.18
40000	1E6	24644	39645	0.344	-0.0462	-0.0743	0.2232	1.41	0.223	1.42
50000	1E7	49238	116204	0.429	-0.0923	-0.2179	0.1195	2.14	0.119	2.13

Chapter Eight

A simplified procedure to calculate by hand the natural periods of semi-rigid steel frames

8.1. Introduction

In the literature, far too little attention has been paid to incorporate the effect of beam-column joint stiffness in approximate formulae in order to calculate by hand the natural periods of semi-rigid steel frames, which is the aim of this chapter. The proposed formulae have been developed by modifying the existing formulae in literature for rigid-jointed plane steel frames. The accuracy of these approximate formulae has been verified by finite element analysis using ABAQUS software. Finally, a parametric study has been conducted to quantify the effects of semi-rigid connections on the natural periods of vibration of plane steel frames. The parametric study highlights the justification for incorporating the effect of connection stiffness in estimating natural vibration period.

8.2. Brief literature review

Traditionally, the beam-to-column connection is assumed to be either absolutely pinned or ideally rigid. However, a number of previous experimental investigations clearly demonstrated that almost all types of connections of a steel frame are semi-rigid with different degree of flexibility (Davison et al., 1987; Chen and Kishi, 1989; Kishi et al., 1997). Conventionally, frames with semi-rigid connections were considered to be unsuitable for use in seismic area due to their flexibility. Subsequently, experimental studies found that semi-rigid frames have considerable potential in resisting seismic loads due to their higher energy dissipation capacities (Astaneh et al., 1989; Elnashai and Elghazouli, 1994; Nader and Astaneh, 1996). Also, analytical studies by (Rosales, 1991; Sekulovic et al., 2002) showed that the increase in flexibility of semi-rigid frames may significantly reduce the vibration frequencies, especially the fundamental frequency, and thus semi-rigid frames attract lesser inertia forces (Nader and Astaneh, 1991). This may result in a more satisfactory earthquake-resistant structure, even in the areas of moderate to high peak ground motion.

Previous research works including design codes provide empirical formulae to estimate the fundamental period for buildings. These formulae are usually dependent on the building material (steel, reinforced concrete, etc.), building type (frame, shear wall, etc.) and overall dimensions (Goel and Chopra, 1997; BS EN 1998-1, 2004). None of these empirical formulae takes into account the joint behaviour. The period of a semi-rigid frame, which is the category that most real frames will fall into, can be twice that of a rigid frame (Smith and Crowe, 1986). It must be mentioned that the actual vibration period of a real building is most likely to be affected by many factors, including non-structural members and fixtures.

In this study, a simple hand-calculation procedure is proposed to calculate the first three natural periods of steel frames with semi-rigid connections, which is not available in the literature. The proposed procedure is based on a shear-flexure cantilever model of rigid frames (Smith and Crowe, 1986), which in turn was based on the models of other authors such as (Skattum, 1971; Heidebrecht and Smith, 1973; Rutenberg, 1975). The accuracy of the proposed simplified procedure has been verified by finite element analysis of a plane steel frame with semi-rigid connections using ABAQUS software. The procedure is limited to plane frames with uniform geometric and material properties along their height. Finally, a parametric study has been conducted to quantify the effects of the flexibility of connections on the natural frequencies of vibration of plane steel frames with semi-rigid connections.

8.3. Derivation of an approximate formula to calculate the natural periods of a cantilever beam

Heidebrecht and Smith (1973) assumed a plane framed structure to be a combination of shear-flexural cantilever beams. The free vibration of this beam is governed by the following differential equation:

$$\frac{\partial^4 y}{\partial x^4} - \alpha^2 \frac{\partial^2 y}{\partial x^2} + \frac{m}{EI} \frac{\partial^2 y}{\partial t^2} = 0 \tag{8.1}$$

where y is the horizontal deflection, x is the axial coordinate of the beam. m is the mass per unit length of the assumed beam. The parameter α account for the effect of flexural and shear rigidity (EI and GA) of the assumed cantilever beam as follows:

$$\alpha^2 = \frac{GA}{EI} \tag{8.2}$$

where *E, G* are the Young's modulus of elasticity and modulus of rigidity respectively. *A, I* are the second moment and the cross-sectional area of the beam respectively.

Rutenberg (1975) introduced a characteristic parameter, *k,* in Eq. (8.1) in order to consider the effect of axial rigidity:

$$k^2 = 1 + \frac{\mathrm{I}}{Ac^2} \tag{8.3}$$

where *c* is a distance parameter that will later be explained in the context of a frame. The modified version of Eq. (8.1) will be in the following form:

$$\frac{\partial^4 y}{\partial x^4} - (\alpha k)^2 \frac{\partial^2 y}{\partial x^2} + \frac{m}{EI}\frac{\partial^2 y}{\partial t^2} = 0 \tag{8.4}$$

The assumed product solution for Eq. (8.1) or (8.4) is:

$$y(x,t) = \psi(x)T(t) \tag{8.5}$$

where $T(t)$ is a harmonic function with a circular frequency of ω. Using the boundary conditions for a cantilever beam of length *H,* fixed at $x = 0$ and free at $x = H$:

$$y(0,t) = 0\,, \qquad \left(\frac{\partial y}{\partial x}\right)_{(0,t)} = 0, \qquad V(H,t) = 0, \quad M(H,t) = 0 \tag{8.6}$$

where *V,* and *M* are shear force and bending moment respectively. Heidebrecht and Smith (1973) derived the following characteristic equation for the shear-flexural motion (Eq. (8.4)) of a prismatic cantilever with height *H* as:

$$2 + \left[\left(\frac{\lambda_1}{\lambda_2}\right)^2 + \left(\frac{\lambda_2}{\lambda_1}\right)^2\right]\cos\lambda_1 H \cosh\lambda_1 H + \left[\frac{\lambda_2}{\lambda_1} - \frac{\lambda_1}{\lambda_2}\right]\sin\lambda_2 H \sinh\lambda_2 H = 0 \tag{8.7}$$

The eigenvalues λ_1 and λ_2 are written as follows:

$$\lambda_1^2 = \sqrt{\frac{(\alpha k)^4}{4} + \omega^2 \frac{m}{EI}} - \frac{(\alpha k)^2}{2} \tag{8.8}$$

$$\lambda_2^2 = \sqrt{\frac{(\alpha k)^4}{4} + \omega^2 \frac{m}{EI}} + \frac{(\alpha k)^2}{2} \tag{8.9}$$

and

$$\lambda^2 = \omega\sqrt{\frac{m}{EI}} \tag{8.10}$$

Then, by substituting Eq. (8.10) in Eq. (8.8) and Eq. (8.9) the following is obtained:

$$\lambda_1^2 = \sqrt{\frac{(\alpha k)^4}{4} + \lambda^4} - \frac{(\alpha k)^2}{2} \Rightarrow \lambda^4 = \lambda_1^4 \left(1 + \left(\frac{\alpha k}{\lambda_1}\right)^2\right) \tag{8.11}$$

$$\lambda_2^2 = \sqrt{\frac{(\alpha k)^4}{4} + \lambda^4} + \frac{(\alpha k)^2}{2} \quad \Rightarrow \quad \lambda_2^2 = \lambda_1^2 + (\alpha k)^2 \tag{8.12}$$

By multiplying Eq. (8.11) with H^2 and rearranging it, it gives:

$$(\lambda H)^2 = (\lambda_1 H)^2 \sqrt{\left(1 + \left(\frac{\alpha k H}{\lambda_1 H}\right)^2\right)} \tag{8.13}$$

And substituting Eq. (8.11) and Eq. (8.12) into Eq. (8.7) gives:

$$2 + \left[2 + \left(\frac{\alpha k H}{\lambda H}\right)^4\right] \cos(\lambda_1 H) \cosh(\lambda_1 H) + \left[\frac{\alpha k H}{\lambda H}\right]^2 \sin\left(\frac{\lambda^2}{\lambda_1} H\right) \sinh\left(\frac{\lambda^2}{\lambda_1} H\right) = 0 \tag{8.14}$$

8.3.1. Purely flexural motion (i.e. $\lambda = \lambda_f$)

In the case of the purely flexural motion, the parameter α is

$$\alpha^2 = \frac{GA}{EI} = 0 \tag{8.15}$$

Substituting Eq. (8.15) in Eq. (8.11) and Eq. (8.12) gives:

$$\lambda = \lambda_1 = \lambda_2 \quad \text{and } \lambda = \lambda_f \tag{8.16}$$

Further substituting Eq. (8.15) and Eq. (8.16) in Eq. (8.14) gives:

$$1 + \cos(\lambda_f H) \cosh(\lambda_f H) = 0 \tag{8.17}$$

The eigenvalues of purely flexural vibration, λ_f of Eq. (8.17) are:

$$(\lambda_f H)_1 = 1.875; \qquad (\lambda_f H)_n = (n - 0.5)\pi \quad \text{for } n = 2, 3, 4, ..$$

or $$(\lambda_f H)_n = a_n \Rightarrow a_n = \begin{cases} 1.875 & \text{for } n = 1 \\ (n - 0.5)\pi & \text{for } n = 2, 3, 4, .. \end{cases} \tag{8.18}$$

8.3.2. Coupled shear-flexural motion (i.e. $\lambda=\lambda_{sf}$)

In the case of shear-flexural motion, Eq. (8.13) and Eq. (8.14) gives:

$$\left(\lambda_{sf}H\right)^2=\left(\lambda_1 H\right)^2\sqrt{\left(1+\left(\frac{\alpha kH}{\lambda_1 H}\right)^2\right)} \tag{8.19}$$

$$2+\left[2+\left(\frac{\alpha kH}{\lambda_{sf}H}\right)^4\right]\cos\left(\lambda_1 H\right)\cosh\left(\lambda_1 H\right)+\left[\frac{\alpha kH}{\lambda_{sf}H}\right]^2\sin\left(\frac{\lambda^2}{\lambda_1}H\right)\sinh\left(\frac{\lambda^2}{\lambda_1}H\right)=0 \tag{8.20}$$

For values of $k\alpha H\geq 6$, Skattum (1971) proposed the following equation:

$$\lambda_{sf}^2=\frac{\left(n-0.5\right)\pi\left(1+k\alpha H\right)}{H^2}\qquad \text{for}\quad k\alpha H\geq 6 \tag{8.21}$$

For a practical range of ($0<k\alpha H<6$), Heidebrecht and Smith (1973) obtained:

$$\lambda_1 H\cong\lambda_f H \tag{8.22}$$

Substituting in Eq. (8.13) gives:

$$\left(\lambda_{sf}H\right)^2=\left(\lambda_f H\right)^2\sqrt{\left(1+\left(\frac{\alpha kH}{\lambda_f H}\right)^2\right)}\qquad \text{for}\quad k\alpha H<6 \tag{8.23}$$

8.3.3. Combined effect of pure flexural and shear-flexural free vibration

According to the assumption of isolated components of motion by (Rutenberg, 1975) the lateral deflection can be written as:

$$y=\frac{1}{k^2}y_{sf}+\left(1-\frac{1}{k^2}\right)y_f \tag{8.24}$$

The Southwell-Dunkerley approximation could then be used to compute the frequencies of vibration as:

$$\frac{1}{\omega^2}\approx\frac{1}{\omega_1^{\,2}}+\frac{1}{\omega_2^{\,2}}=\left(\frac{1}{k^2}\right)\frac{1}{\omega_{sf}^2}+\left(1-\frac{1}{k^2}\right)\frac{1}{\omega_f^2} \tag{8.25}$$

Thus,

$$\frac{1}{\lambda^2}\approx\sqrt{\left(\frac{1}{k^2}\right)\frac{1}{\lambda_{sf}^4}+\left(1-\frac{1}{k^2}\right)\frac{1}{\lambda_f^4}} \tag{8.26}$$

and $$T = \frac{2\pi}{\lambda^2}\sqrt{\frac{m}{EI}} \tag{8.27}$$

8.4. Approximate formulae for natural periods

Based on Eqs. (8.26 and 8.27), the natural period can be expressed as:

$$T \cong 2\pi\sqrt{\frac{m}{EI}}\sqrt{\left(\frac{1}{k^2}\right)\frac{1}{\lambda_{sf}^4}+\left(1-\frac{1}{k^2}\right)\frac{1}{\lambda_f^4}} \tag{8.28}$$

Using Eqs. (8.18, 8.21, 8.23 and 8.28), and after rearranging the parameters, the natural period of vibration can be written as:

$$T_n = \left(T_f\right)_n\sqrt{1+\frac{1}{k^2}\left(\frac{1}{R_n}-1\right)} \tag{8.29}$$

where $\left(T_f\right)_n = \dfrac{2\pi H^2}{k{a_n}^2}\sqrt{\dfrac{m}{EI}}$ and $R_n = \begin{cases} 1+\left(\dfrac{k\alpha H}{a_n}\right)^2 & \text{for } k\alpha H < 6 \\ \left(\left(n-0.5\right)\pi\left(\dfrac{1+k\alpha H}{{a_n}^2}\right)\right)^2 & \text{for } k\alpha H \geq 6 \end{cases}$

8.5. Evaluation of characteristic parameters

The concept of modelling a plane framed structure as a shear-flexural cantilever beam is applicable for any type of uniform frame structure, provided that the centres of mass and resistance are coincident (Smith and Crowe, 1986). The characteristic parameters of a frame can be expressed in terms of geometrical and material parameters as:

$$\alpha^2 = \frac{GA}{\sum_{j=1}^{r} EI_{cj}} \tag{8.30}$$

$$k^2 = \frac{\sum_{j=1}^{r} I_{cj} + \sum_{j=1}^{r} A_{cj}c_j^2}{\sum_{j=1}^{r} A_{cj}c_j^2} \tag{8.31}$$

Also, the equivalent *GA* for rigid frame is:

$$GA = \frac{12E/h}{\frac{1}{\sum_{j=1}^{r} \frac{I_{cj}}{h}} + \frac{1}{\sum_{i=1}^{z} \frac{I_{bi}}{l_{bi}}}} \tag{8.32}$$

where A_{cj} and I_{cj} are the cross-sectional area and second moment of area of the j-th column; h is the storey height; I_{bi} and l_{bi} represent the second moment of area and span of the beam in the i-th bay. The term c_j denotes the distance of the j-th column from the centroid of the column assembly.

8.6. Simplified procedure to calculate natural periods of a steel frame

1. Calculate the equivalent shear rigidity of the steel frame using Eq. (8.32).
2. Calculate the characteristic parameters of the steel frame, k^2 and α^2 using Eqs. (8.30 and 8.31).
3. Calculate $k\alpha H$
4. Calculate the natural periods, T_n, using Eq. (8.29).

8.7. Effect of connection flexibility on natural frequency of steel frames

To investigate the effect of the flexibility of connection on the natural frequency of a steel frame, a simple portal steel frame was used. The beam had UB 254×146×37 section, and the columns were of UC 203×203×60 sections. (ABAQUS, 2005) was used to compute the natural frequencies. Rotational spring elements were attached to the beam ends to simulate the effect of connection flexibility of beam-to-column connections. The stiffness of the springs ranged from those close to *perfectly-pinned* to an almost *perfectly-rigid* connection. The same modelling procedure that detailed in Chapter Seven (Section 7.6.2) was used to simulate the steel frame. A parametric study was carried out for various ratios of the second moment of area of the beam (0.25, 0.5, 2, 4 and 8) from the original (I=5537 mm^4) in order to show the effect of flexural stiffness of a beam on the natural frequency of a steel frame.

The results of the frequency analysis are non-dimensionalised using the pinned case as zero and the natural frequency of a rigid case as one, as shown in Figure 8.1. The spring stiffness ratio, $k_s/(EI/L)_b$, was used as abscissa instead of the spring stiffness as

the effect of flexibility of connection is highly affected by the flexural stiffness of the beam to which it is attached.

It is evident from Figure 8.1 that the flexibility of the connection must be taken into account in any frequency analysis of steel frames. This means that the original equations used to calculate the characteristic parameters, α^2 and k^2, of a steel frame should be modified to account for the flexibility of the connections.

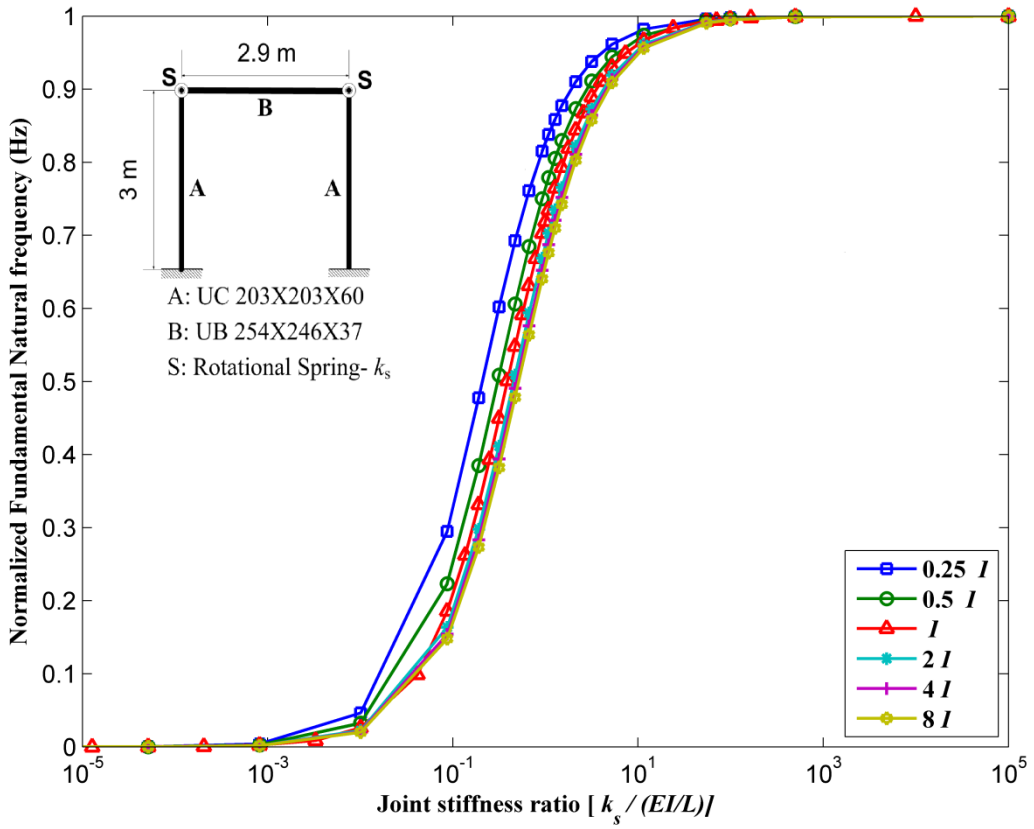

Figure 8.1: Plots of normalized fundamental Natural Frequency versus the joint stiffness ratio. The variable *I* in the legend indicates the second moment of area of the beam cross-section

8.8. Modification of the approximate formulae for semi-rigid frames

The approximate formulae for determining the natural periods for rigid frames cannot be used directly for frames with semi-rigid connections. The difference is appreciable in the range of stiffness ratio between 0.01 to 100 (see Figure 8.1). The flexural stiffness of beams needs to be modified to take into account the effect of the flexibility of connections.

Many procedures for the modification the stiffness of a beam to consider the effect of the flexibility of end connections are detailed in the literature, such as the procedures developed by (Chen and Lui, 1985; Chui and Chan, 1997; Wong et al., 2007). For this work, the procedure suggested by (Chen and Lui, 1985) was adopted to assess the stiffness of beams because it is applicable for both braced and unbraced frames. The modified second moment of area of a beam, $\bar{I}_b$, can be calculated using the equation:

$$\bar{I}_b = \frac{I_b}{\left(1+\frac{\beta E I_b}{l_b k_s}\right)} \tag{8.33}$$

where β=6 and 2 for unbraced and braced frames respectively, and k_s is the rotational stiffness of semi-rigid connections. This modified second moment of inertia of a beam, $\bar{I}_b$, should be used in Eq. (8.32).

Example: In order to investigate the accuracy of the proposed procedure and the effect of joint stiffness, a three-bay, six-storey plane steel frame (Figure 8.2) was analysed for a wide range of flexibilities of beam-to-column connections. The span of each bay was 6 m and the storey height was 3.75 m. The section properties of columns and beams were HEB 260 and IPE 300 respectively. The properties of the steel frame are shown in Table 8.1. The same procedure as that detailed in Section 7.6.2 was used to simulate the beams, columns, boundary conditions and connections.

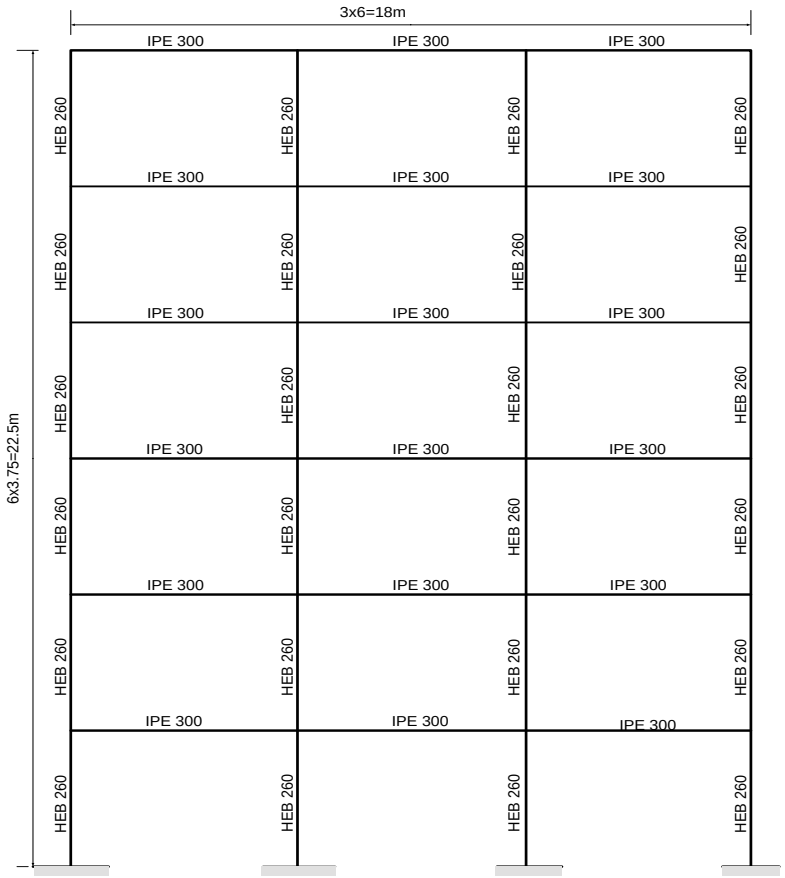

Figure 8.2: Three-bay, six-storey steel frame

Table 8.1: Properties of the steel frame shown in Figure 8.2

Section	l (m)	A (m^2)	I (m^4)	E (GPa)	Density (kg/m^3)
IPE 300	6	0.00538	$8.36x10^{-4}$	200	7800
HEB 260	3.75	0.0118	0.000149	200	7800

Sample calculations

All calculations were carried out using Microsoft Excel spreadsheets. In the following section, sample of calculations for an almost rigid connection and one case for a semi-rigid connection are shown using the proposed steps.

A. Rigid connection case

(i) Calculate the equivalent shear rigidity of a steel frame using Eq. (8.32).

$$GA = \frac{12E}{3.75\left[\dfrac{1}{4\times\left(\dfrac{0.000149}{3.75}\right)}+\dfrac{1}{3\times\left(\dfrac{0.0000835}{6}\right)}\right]} = 2.12\times10^4 \text{ kN}$$

(ii) Calculate the characteristic parameters of a steel frame, k^2 and α^2 using Eqs. (8.30 and 8.31).

$$\alpha^2 = \frac{GA}{\sum_{j=1}^{n}\left(EI_c\right)_j} = \frac{2.12\times10^7}{4\times200\times10^9\times\left(0.000149\right)} = 0.177\ \frac{1}{\text{m}^2}$$

$$k^2 = 1+\frac{\sum_{j=1}^{n}EI_{cj}}{\sum_{j=1}^{n}EA_{cj}c_j^2} = 1+\frac{4E\left(0.000149\right)}{E\times0.0118\times\left(2\times9^2+2\times3^2\right)} = 1.00028$$

(iii) Calculate $k\alpha H$

$$k\alpha H = \sqrt{\left(1.00028\times0.178\right)}\ \times 22.5 = 9.48 > 6$$

(iv) Calculate T_n using Eq. (8.29)

$$\left(T_f\right)_n = \frac{2\pi\times(22.5)^2}{1.00028\times a_n{}^2}\sqrt{\frac{573}{11.9\times10^7}} = \frac{6.97}{a_n{}^2}$$

$$R_n = \begin{cases} 1+\left(\dfrac{9.479}{a_n}\right)^2 & \text{for } k\alpha H < 6 \\ \left(\left(n-0.5\right)\pi\left(\dfrac{10.479}{a_n{}^2}\right)\right)^2 & \text{for } k\alpha H \geq 6 \end{cases}$$

The natural frequencies were calculated for f_1 to f_5 (f=1/T_n) using both parts of Eq. (8.29) and ABAQUS modelling. The results of the calculations and finite element analysis are presented in Table 8.2 and Figure 8.3.

Table 8.2: Result of natural frequencies from the proposed equation and ABAQUS modelling for the rigid connection case

n	a_n	$(T_f)_n$	$k\alpha H < 6$		$k\alpha H \geq 6$		ABAQUS
			R_n	$f_n = 1/T_n$	R_n	$f_n = 1/T_n$	
1	1.875	1.982	26.557	2.59	21.921	2.35	2.29
2	4.712	0.314	5.047	7.15	4.946	7.08	7.37
3	7.854	0.113	2.456	13.87	1.78	11.80	13.73
4	11.0	0.057	1.742	22.90	0.907	16.53	21.64
5	14.137	0.035	1.449	34.53	0.549	21.26	30.78

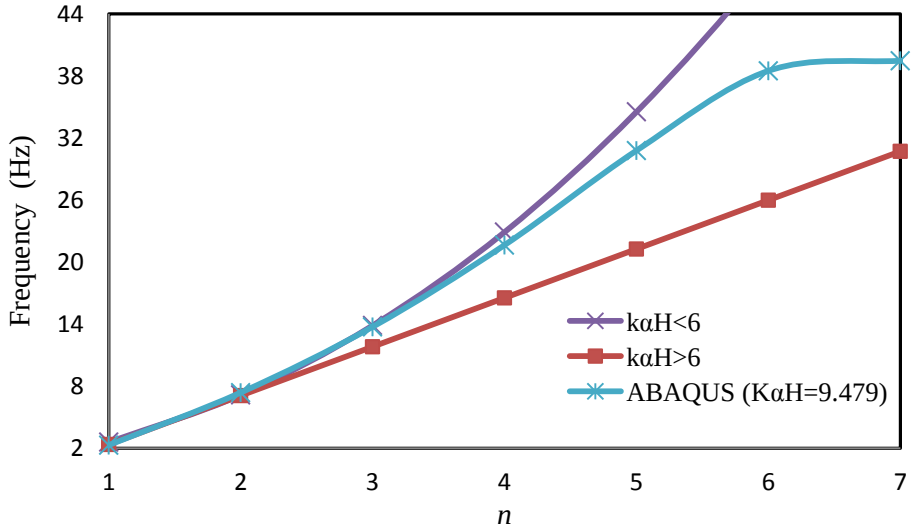

Figure 8.3: Natural frequencies from the proposed equation and ABAQUS for the rigid connection case.

The results of the calculations from the proposed equations and finite element modelling show clearly that both parts of Eq. (8.29) work well for the fundamental and second natural frequencies. From f_3 to f_6, the first part of Eq. (8.29) (i.e. $k\alpha H$ <6) dominate the frequency behaviour of the frame, even though the ($k\alpha H$) values in these cases are more than 6. After f_6, the second part of Eq. (8.29) becomes more effective in controlling the frequency of the frame.

Therefore, as the second part of Eq. (8.29) underestimated the frequency in the range between f_3 to f_6 and the first part of Eq. (8.29) overestimated the frequency after f_6, it was recommended to calculate the natural frequency for the first and second frequencies using the relevant equations, then using both parts of Eq. (8.29) for the third frequency and above. The selection of lowest frequency (i.e. lowest stiffness for safe design) or highest frequency depends on the main purpose of the analysis under consideration.

B. Semi-rigid connection case [$k_s/(EI/L)_b$ =7.18]

(i) Calculate the modified second moment of inertia of a beam using Eq. (8.33).

$$\bar{I}_b = \frac{I_b}{\left(1+\frac{\beta E I_b}{l_b k_s}\right)} = \frac{I_b}{1+\frac{6}{7.18}} = 0.5447 I_b$$

(ii) Calculate the equivalent shear rigidity of a steel frame using Eq. (8.32).

$$GA = \frac{12E}{3.75\left[\frac{1}{4\times\left(\frac{0.000149}{3.75}\right)}+\frac{1}{3\times 0.545\times\left(\frac{0.0000836}{6}\right)}\right]} = 12740\,\text{kN}$$

(iii) Calculate the characteristic parameters of a steel frame, k^2 and α^2, using Eqs. (8.30, 8.31).

$$\alpha^2 = \frac{GA}{\sum_{j=1}^{n}(EI_c)_j} = \frac{12740000}{4\times 200\times 10^9\times(0.000149)} = 0.107\frac{1}{m^2}$$

$$k^2 = 1+\frac{\sum_{j=1}^{n}(EI_c)_j}{\sum_{j=1}^{n}(EA_c c^2)_j} = 1+\frac{4E(0.0001492)}{E\times 0.0118\times(2\times 9^2+2\times 3^2)} = 1.000281$$

(iv) Calculate $k\alpha H = \sqrt{(1.00028\times 0.107)}\times 22.5 = 7.35 > 6$

(v) Calculate T_n using Eq. (8.29)

$$(T_f)_n = \frac{6.97}{a_n^{\,2}}$$

$$R_n = \begin{cases} 1+\left(\frac{7.35}{a_n}\right)^2 & \text{for } k\alpha H < 6 \\ \left((n-0.5)\pi\left(\frac{8.35}{a_n^{\,2}}\right)\right)^2 & \text{for } k\alpha H \geq 6 \end{cases}$$

As with the rigid connection case, the natural frequencies are calculated for f_1 to f_5 using both the proposed equations and ABAQUS modelling. The results of calculation and finite element analysis are presented in Table 8.3 and Figure 8.4.

Table 8.3: Result of natural frequencies from the proposed equation and ABAQUS modelling for the semi-rigid connection case.

n	a_n	$(T_f)_n$	$k\alpha H < 6$		$k\alpha H \geq 6$		ABAQUS
			R_n	$f_n = 1/T_n$	R_n	$f_n = 1/T_n$	
1	1.875	1.982	16.373	2.035	13.935	1.878	1.874
2	4.712	0.314	3.431	5.903	3.138	5.645	6.235
3	7.854	0.113	1.875	12.124	1.129	9.411	12.159
4	11.0	0.057	1.446	20.872	0.576	13.177	20.0
5	14.137	0.035	1.270	32.331	0.348	16.942	29.50

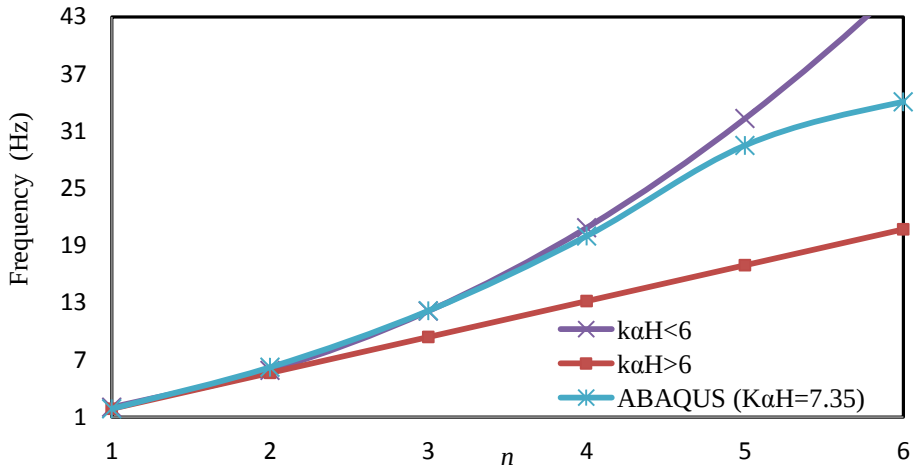

Figure 8.4: Natural frequencies from the proposed equation and ABAQUS for the semi-rigid connection case

As with the rigid connection case, the results of the calculations show clearly that both parts of Eq. (8.29) work well for the fundamental and second natural frequencies. Then, the first part of Eq. (8.29) (i.e. $k\alpha H$ <6) is seen to dominate the frequency behaviour of the frame. After f_6, the second part of Eq. (8.29) resumes the control of the frequency of the frame.

Therefore, the same recommended procedure for the rigid connection case was used with the semi-rigid connection case to calculate frequency.

Also, the fundamental natural time periods (T_1) obtained from the hand-calculations (Eqs. 8.29-8.33) were compared in Table 8.4.

Table 8.4: Comparisons of fundamental time period

Type of Frame	T_1 -Proposed Eqs. (8.31) (1)	ABAQUS (2)	(1)/(2)
Rigid –Frame	0.425 s	0.4366 s	0.971
Semi-rigid Frame	0.5324 s	0.5336 s	0.999

In order to investigate the whole range of the semi-rigid connection, a parametric study using the proposed procedure and ABAQUS for the same frame with different stiffness of connections was carried out. The value of stiffness varied from approaching perfectly pinned to approaching perfectly rigid. The results of the parametric study are presented in Figure 8.5, Figure 8.6 and Figure 8.7.

It can be observed that the fundamental natural frequency calculated by the proposed procedure is very similar to the ABAQUS results for the whole range of semi-rigid connection.

The proposed procedure is sensitive to any changes in connection stiffness. In addition, it was found that the frames with connections of low and very low stiffness always gave values of ($k\alpha H$) that were less than 6. On the other hand, the relatively rigid frames give values of ($k\alpha H$) greater than 6.

The results for the second and third natural frequencies were also close between the ABAQUS and the proposed procedures, with a maximum difference of about 6%. This is the case if the recommended procedure in the previous section is followed by calculating the natural frequency using both parts of Eq. (8.29), as explained previously.

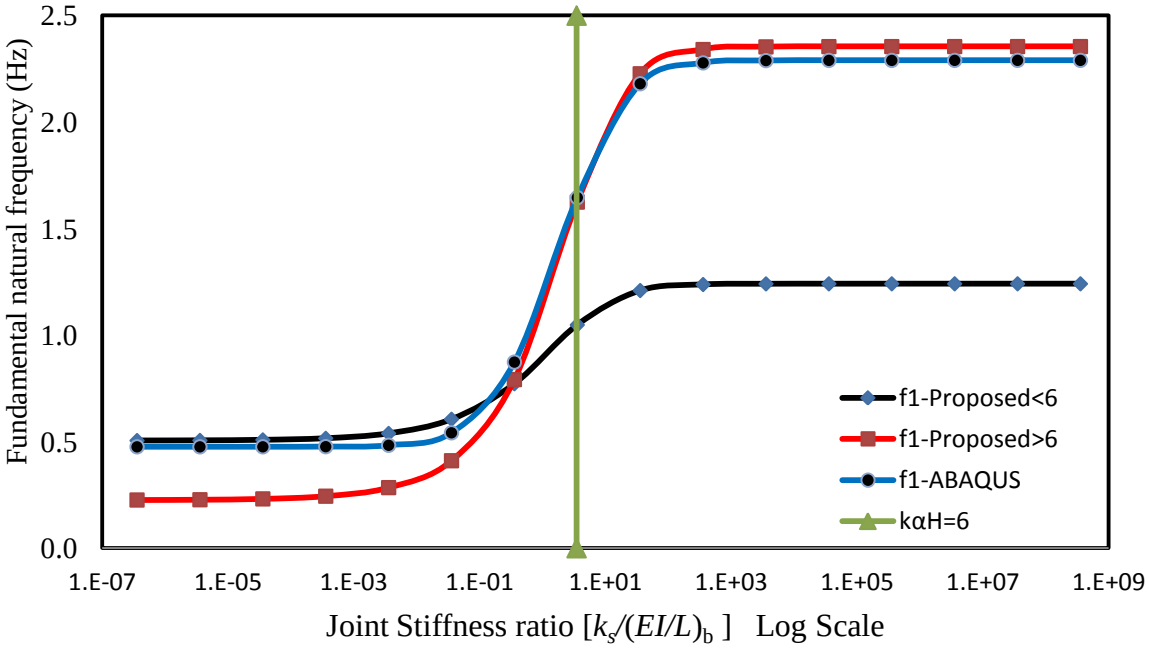

Figure 8.5: Joint stiffness ratio versus the fundamental natural frequency of the steel frame shown in Figure 8.2

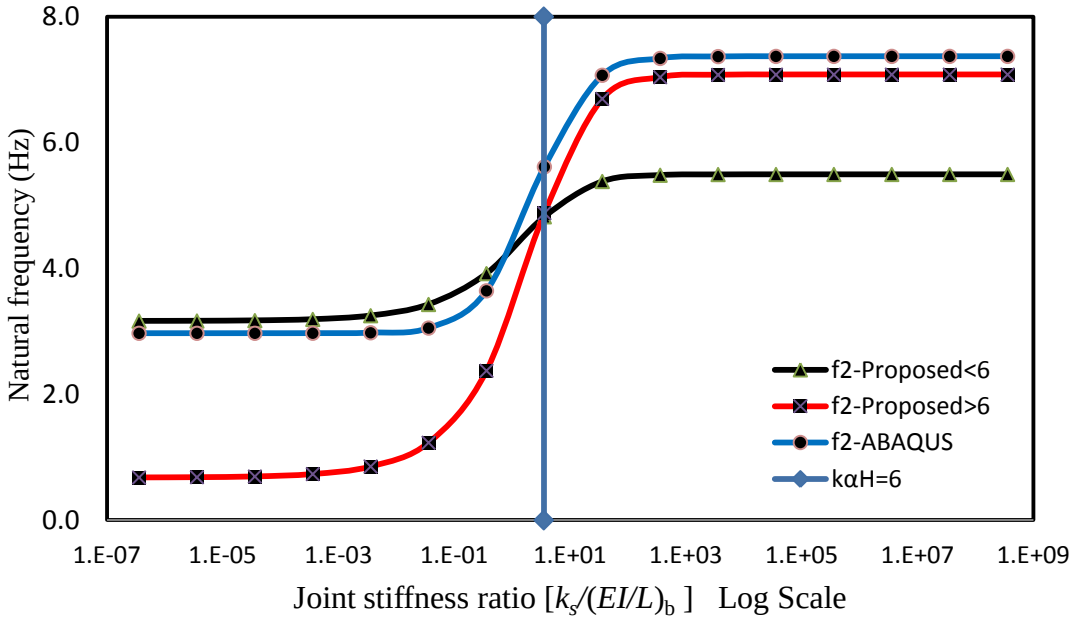

Figure 8.6: Joint stiffness ration versus the second natural frequencies of the steel frame shown in Figure 8.2

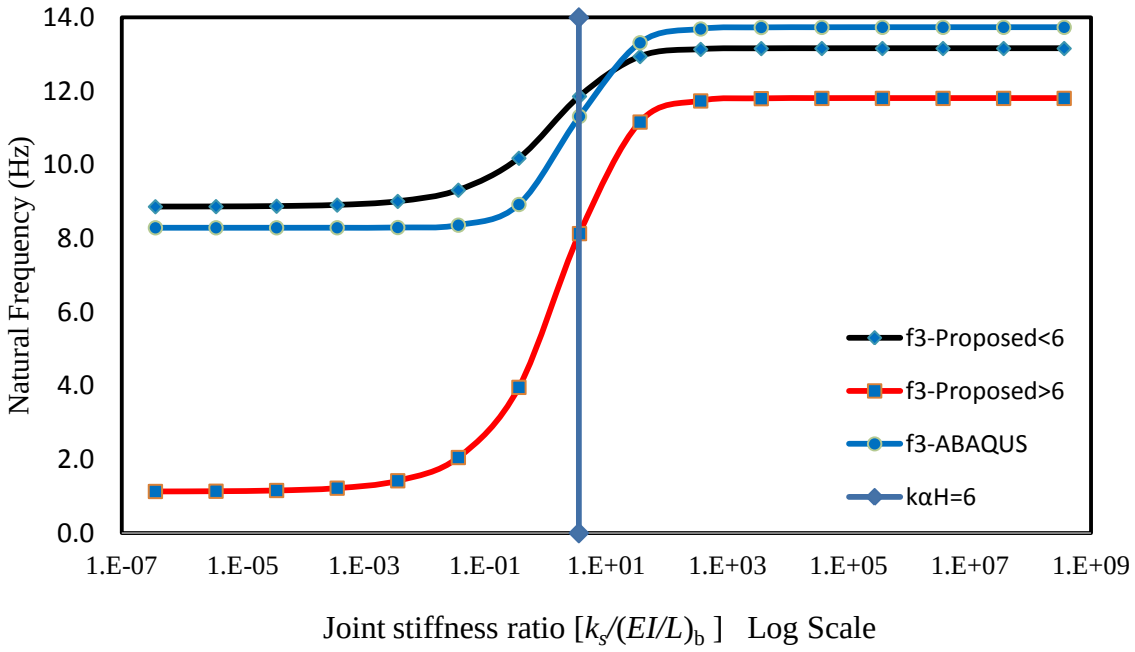

Figure 8.7: Joint stiffness ration versus the third natural frequencies of the steel frame shown in Figure 8.2

8.9. Parametric study on the effect of different $k\alpha H$ values

The parametric study involved evaluating the effect of the following factors:

1. Height of the frame, H
2. Flexibility of the connections, and
3. Axial, flexural and shear rigidity of the frame.

It is clear from Eq. (8.31) that the parameter k considers the effect of relative ratio of flexural stiffness to axial stiffness, and its value will approach unity for axially rigid columns. The parameter α incorporates the effect of relative ratio of shear stiffness to the summation of flexural stiffness of the columns and beams. Using Eqs. (8.21, 8.23 and 8.29), the ratio of shear-flexural period to total period can be expressed as:

$$\frac{T_{sf}}{T_n} \approx \frac{1}{\sqrt{\frac{1}{k^2}(1-R_n)+R_n}} \tag{8.34}$$

For the fundamental period (i.e. n=1 and a_n=1.875) and for $k\alpha H=6$

$$\frac{T_{sf}}{T_1} = \frac{1}{\sqrt{9.782 - 8.782\frac{1}{k^2}}}$$

For k^2=1 (i.e. flexural stiffness/axial stiffness→0)

$$\frac{T_{sf}}{T_1} = 1$$

and for k^2=∞ (i.e. flexural stiffness/axial stiffness→∞)

$$\frac{T_{sf}}{T_1} = 0.319$$

For any given values of α and k, as the height of a frame (H) increases, the percentage of pure-flexural period will increase proportionally, and the ratio of shear-flexural to total period (T_{sf} /T_1) will decrease, as shown in Figure 8.8. In summary, the percentage of shear-flexural period to the total period is inversely proportional to the height of the frame, connection flexibility, and the flexural to shear rigidity ratio.

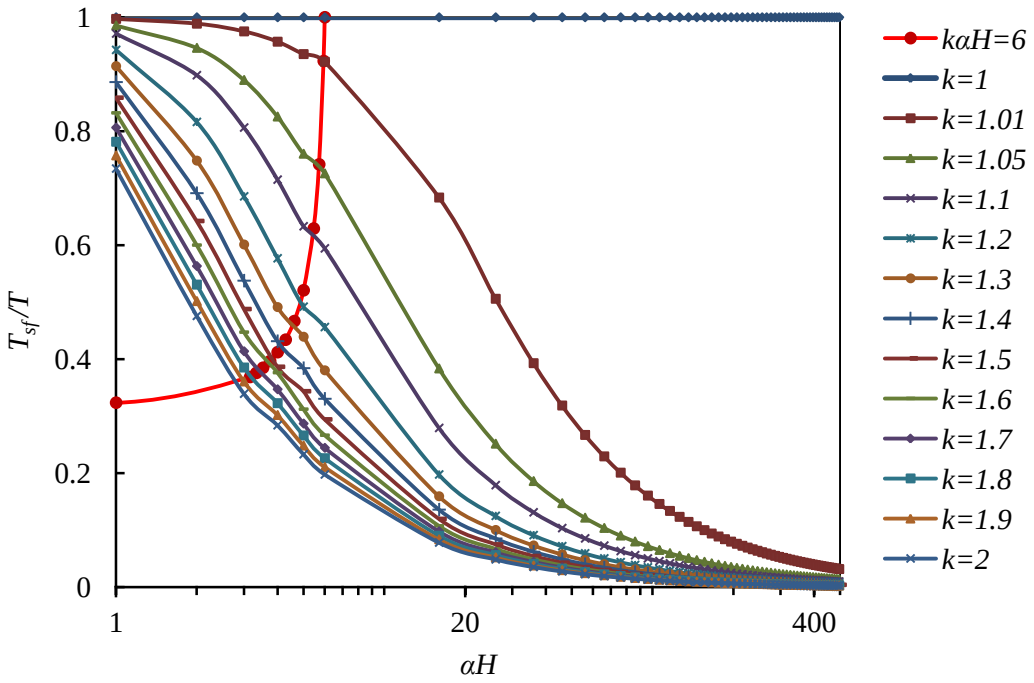

Figure 8.8: Effect of frame parameters on shear-flexural to total periods.

8.10. Summary and conclusions

It is evident from Figure 8.1, Figure 8.5, Figure 8.6 and Figure 8.7 that the flexibility of a connection has a considerable effect on the natural frequencies (or natural periods) of a steel frame. Further to this, the "Ideal-Rigid" assumption for beam-to-column connections may lead to overestimation of the natural frequency or underestimation of the natural periods of a frame. Inaccurate values for the fundamental period may result in unsafe design, as the design value of the seismic base shear force depends on the fundamental period (BS EN 1998-1, 2004), Clause 4.3.3.2.2.(1). In addition, Figure 8.5 and Figure 8.6 show clearly that the proposed procedure can predict the natural periods of a frame for a wide range of flexibilities of beam-to-column connections. The validity of the proposed procedure is confirmed by comparing the results with the results obtained from ABAQUS, and good agreement between them was demonstrated.

Chapter Nine

An approximate analytical method for calculating the natural periods of unbraced steel frames with semi-rigid connections

9.1. Introduction

Recently, increasing attention has been paid to the study of the effect of seismic ground motion on the behaviour of steel buildings. The calculation of the design base shear force plays a centre role in these considerations. This force greatly depends on the fundamental period of vibration of the structure, as well as other factors such as soil conditions and level of ductility. In turn, the mass, strength and stiffness of the structure are factors which affect the magnitude of the fundamental period of vibration.

The stiffness of a structure greatly depends on the stiffness of its beam-to-column connections. As mentioned in the previous chapters, for reasons of simplicity and lack of understanding of the response characteristics of semi-rigid connections under seismic loading, beam-column connections are conventionally assumed to be either perfectly pinned or perfectly rigid. Additionally, it was mentioned in Chapter Eight that the semi-rigid frames were regarded as inappropriate for use in seismic areas due to their flexibility, even though they offer significant gains in resisting seismically-induced loads due to their ability to attract lesser inertia forces and higher energy dissipation capacities.

9.2. Brief literature review

Natural periods of any structure can be found by using finite element packages such as ABAQUS, ANSYS and ADINA. However, due to the amount computational cost and time that these calculations require, they are not appropriate for routine design work, except when it is not feasible to use simplified methods.

Current seismic design codes provide empirical equations which relate the fundamental period to the height of the frame. Eurocode 8 (2004) §4.2.3.3 gives the

following empirical expression to determine the fundamental natural period for the steel frames for heights (H) up to 40 m:

$$T_1 = 0.085H^{3/4} \tag{9.1}$$

In addition, there are many other empirical formulae in the literature which have the same general form as Eq. (9.1) but with different constants depending on the structural forms.

Considering the limitations of the empirical equations, the design codes allow for estimation of the fundamental natural period using alternative methods, such as Rayleigh's method or computer-based eigenvalue analysis. These methods require more complex procedures and computer programmes which make them impractical for many situations. Therefore, many researchers have investigated the applicability of using approximate hand-calculation methods, which have the merits of simplicity with enough accuracy (Rutenberg, 1975; Smith and Crowe, 1986; Qiusheng et al., 1994; Goel and Chopra, 1998; Zalka, 2001; Chrysanthakopoulos et al., 2006). All of the above approximate methods assumed the beam-column connections as rigid even though the period of a semi-rigid frame can be twice to that of a rigid frame (Smith and Crowe, 1986).

In this Chapter, a simple hand-calculation method is presented to calculate the fundamental natural period of steel frames with rigid or semi-rigid connections. The original equations of the well-known Muto's method are firstly improved by introducing new factors to take into account the following:

(i) the actual position of the inflection point in the beams,

(ii) the effect of the boundary condition of the first storey on the upper stories, and

(iii) the effect of applied load at any storey on the deflection of the adjacent unloaded upper storey**.**

The improved equations were then combined with the conventional matrix method for vibration analysis to construct a simple "hand'' procedure in order to determine the first three natural periods of a structure. The lumped-mass idealization and the concept of "master'' degree of freedom were used to formulate the "dynamic matrix" of the structure. The power method was used to find the eigenvalues and eigenvectors for the dynamic matrix. A step-by-step worked example with instructions was presented as a

guide for using the proposed procedure. The accuracy and sensitivity of the approximate procedure were validated by finite element analysis of semi-rigid jointed steel frames using ABAQUS.

9.3. Muto's original method (D value method)

Muto (1974) proposed an approximate analytical method for the analysis of multi-storey frames with rigid connections. It is considered the most accurate manual method for the elastic analysis of sway frames with rigid connections (Wong et al., 2007). The assumptions of this method are:

1. At each floor, the above and below columns equally utilize the stiffness of the beam.
2. The rotations of adjacent beam-column connections are equal.
3. The sum of beam stiffness at the top and bottom of any storey are similar and approximately equal to the average stiffness.

Using these assumptions, the storey drift of a multi-storey frame was approximated by

$$\Delta_i = \frac{V_i}{\sum_{j=1}^{j=r} D_{i,j}} \quad \text{where } V_i = \sum_{j=1}^{j=r} F_{i,j} \tag{9.2}$$

where V_i and $\sum D_{i,j}$ are the shear and the lateral stiffness of the i-th storey respectively. Figure 9.1 shows an example of a frame with multi-degrees of freedom and Figure 9.2 shows the sub-frame which is used in the derivation of the D-values.

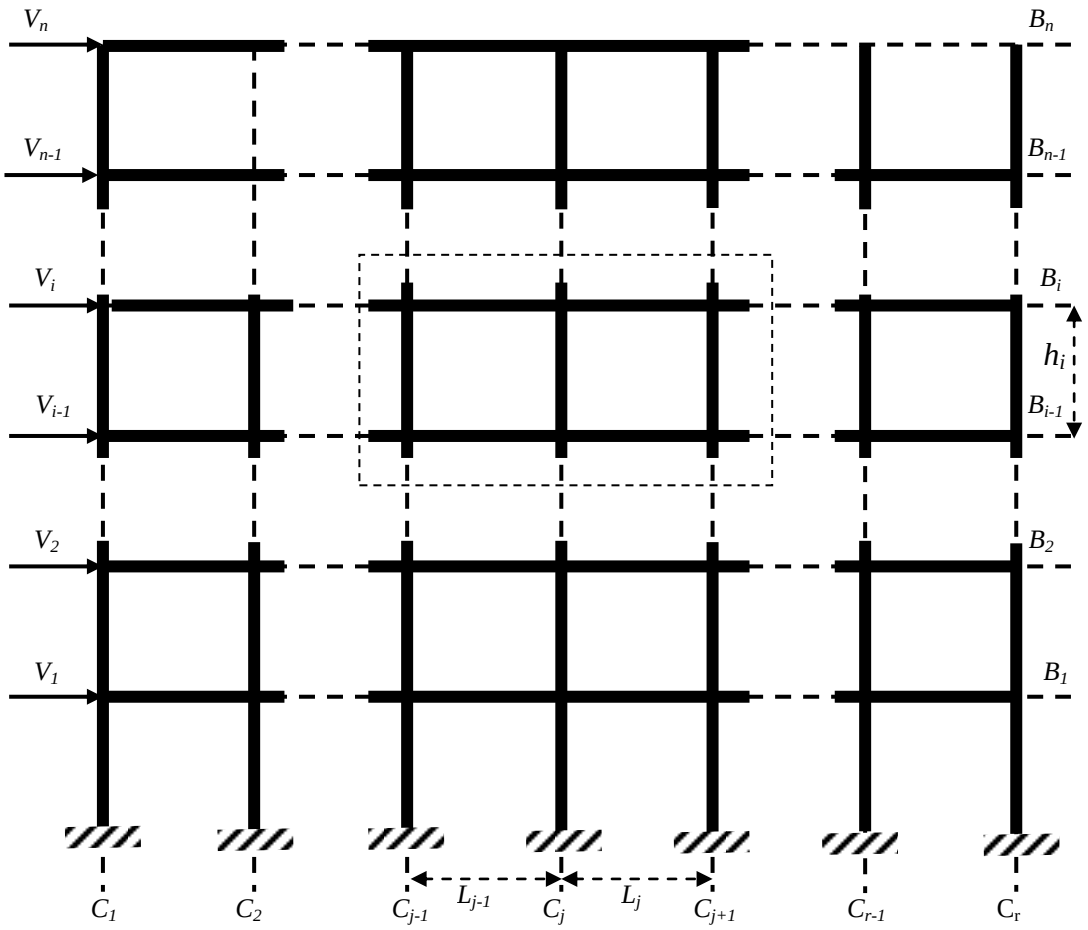

Figure 9.1: Steel frame with multi-degree of freedom

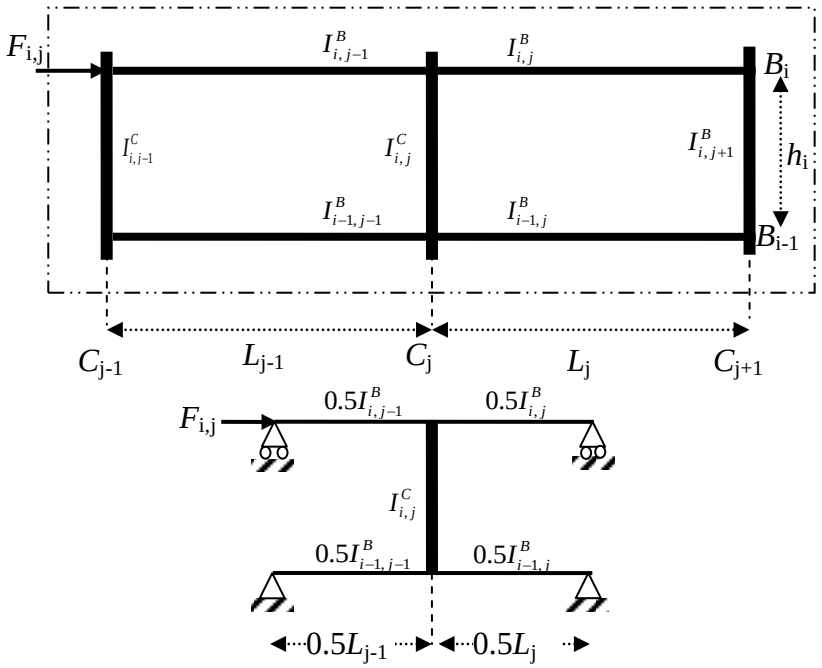

Figure 9.2: Simplified sub-frame used for lateral force analysis

9.3.1. Equations of Muto's original method

First storey

1. Fixed base

$$D_{1,j} = \frac{F_{1,j}}{\Delta_1} = \left[\frac{12E}{h_1^2}\right] k_{c,1,j} \left(\frac{0.5 + 3\alpha \bar{K}_{1,j}}{2 + 3\alpha \bar{K}_{1,j}}\right) \tag{9.3}$$

where $k_{c,i,j} = \frac{I_{c,i,j}}{h_i}$; $k_{B,i,j} = \frac{I_{B,i,j}}{L_{B,i,j}}$; $\bar{K}_{i,j} = \frac{k_{B,i,j-1} + k_{B,i,j}}{k_{c,i,j}}$

and α is the factor which depends on $\bar{K}_{i,j}$. It was taken as 1/3 for the first storey.

2. Pinned base

$$D_{1,j} = \frac{F_{1,j}}{\Delta_1} = \left[\frac{12E}{h_1^2}\right] k_{c,1,j} \left(\frac{0.5\alpha \bar{K}_{1,j}}{1 + 2\bar{K}_{1,j}}\right) \tag{9.4}$$

and α is the factor which depends on $\bar{K}_{i,j}$. It was taken as 1 for the first storey.

Middle and top stories (i >1)

$$D_{i,j} = \frac{F_{i,j}}{\Delta_i} = \left[\frac{12E}{h_i^2}\right] k_{c,i,j} \left(\frac{\bar{K}_{i,j}}{1 + \bar{K}_{i,j}}\right) \tag{9.5}$$

where $\bar{K}_{i,j} = \frac{k_{B,i,j-1} + k_{B,i,j} + k_{B,i-1,j-1} + k_{B,i-1,j}}{2k_{c,i,j}}$

Position of inflection point of column in the first storey

$$y_{c,1,j} = \frac{3\bar{K}_{1,j} + 1}{6\bar{K}_{1,j} + 1} \tag{9.6}$$

The distance to the inflection point, $y_{c,1,j}$ is measured from the base.

9.4. Improvements of Muto's method

The proposed procedure to calculate the vibration period of a structure depends on the accuracy of the calculated flexibility matrix. This matrix is calculated by sequentially applying unit lateral load at each storey and the resultant deflections are found. One of the main objectives of the present work is to improve the original Muto's method in order to take into account the factors which affect this deflection. This improvement requires the introduction of new factors to account for the effect which are listed in Section 9.2.

9.4.1. The position of inflection point of beams

It can be clearly seen from the simplified model in Figure 9.2 that the derivation of *D values* for Muto's method was based on the assumption that the position of inflection point in all beams is located at the mid-length of the beam. In fact, there are many situations where this assumption is not valid, and consequently inadequate results may be given due to the shift of the inflection point from the middle of the beam. The magnitude of this shifting depends on the relative stiffness of two adjacent columns at the same level, and could be significant if the stiffness ratio is three or more. Therefore, a modified factor (*m*) is introduced in Muto's original equations to account for this effect.

The derivations of the modified equations are illustrated in appendix A. The resultant modified equations are:

First storey

1. Fixed base

$$D_{1,j-1} = \left[\frac{12E}{h_1^{\,2}}\right] k_{c,1,j-1} \left(\frac{3\bar{K}_{1,j-1} + m_{1,j-1}}{3\bar{K}_{1,j-1} + 4m_{1,j-1}}\right) \tag{9.7}$$

$$D_{1,j} = \left[\frac{12E}{h_1^{\,2}}\right] k_{c,1,j} \left(\frac{3\bar{K}_{1,j} - m_{1,j-1} + 1)}{3\bar{K}_{1,j} - 4m_{1,j-1} + 4}\right) \tag{9.8}$$

$$m_{1,j-1} = \frac{3\bar{K}_{1,j} + 4}{3\left(\bar{K}_{1,j-1} + \bar{K}_{1,j}\right) + 8} \tag{9.9}$$

2. Pinned base

$$D_{1.j-1} = \left[\frac{12E}{h_1^{\,2}}\right] k_{c,1,j-1} \left(\frac{\bar{K}_{1,j-1}}{4\bar{K}_{1,j-1} + 4m_{1,j-1}}\right) \tag{9.10}$$

$$D_{1,j} = \left[\frac{12E}{h_1^{\,2}}\right] k_{c,1,j} \left(\frac{\left(1-m_{1,j-1}\right)\bar{K}_{1,j}}{4\left(1-m_{1,j-1}\right)\bar{K}_{1,j-1} + 4\left(1-m_{1,j-1}\right)^2}\right) \tag{9.11}$$

$$m_{1,j-1} = \frac{\bar{K}_{1,j} + 1}{\left(\bar{K}_{1,j-1} + \bar{K}_{1,j} + 2\right)} \tag{9.12}$$

Middle and top stories

$$D_{i,j-1} = \left[\frac{12E}{h_i^{\,2}}\right] k_{c,i,j-1} \left(\frac{\bar{K}_{i,j-1}}{\bar{K}_{i,j-1} + 2m_{i,j-1}}\right) \tag{9.13}$$

$$D_{i,j} = \left[\frac{12E}{h_i^{\,2}}\right] k_{c,i,j} \left(\frac{\bar{K}_{i,j}}{\bar{K}_{i,j} + 2(1-m_{i,j-1})}\right) \tag{9.14}$$

$$m_{i,j-1} = \frac{\bar{K}_{i,j} + 2}{\left(\bar{K}_{i,j-1} + \bar{K}_{i,j} + 4\right)} \tag{9.15}$$

Position of inflection point of column in first storey

$$y_{1,j-1} = \frac{3\bar{K}_{1.j-1} + 2m_{1,j-1}}{6\bar{K}_{1,j-1} + 2m_{1,j-1}} \tag{9.16}$$

$$y_{1,j} = \frac{3\bar{K}_{1,j} + 2(1-m_{1,j-1})}{6\bar{K}_{1,j} + 2(1-m_{1,j-1})} \tag{9.17}$$

In Muto's original method, the position of the inflection point of the beam is at the centre of the span (*i.e.* m=0.5). This case requires that $\bar{K}_{\mathrm{i,j-1}} \approx \bar{K}_{\mathrm{i,j}}$. If this equality is substituted in Eqs. (9.9), (9.12) and (9.15), we get m=0.5 for the three cases discussed above. Also, if m=0.5 is substituted in Eqs. (9.7), (9.8), (9.10), (9.11), (9.13), (9.14) and (9.16), the original Muto's equations will be obtained.

9.4.2. Effect of boundary conditions of columns at the first storey on the deflection of upper storey

It can be seen in the original Muto's equation for the first storey that there is a factor (α) which represents the distribution factor of the moments between beams and upper and lower columns. This factor depends on $\bar{K}_{i,j-1}$ and $\bar{K}_{i,j}$ and on the relative stiffness of the column at the first and second storey. It was assumed as 1/3 for the fixed base case and 1 for the pinned base case. In the present work, the actual effect is accounted for introducing new relative stiffness factors, $\beta_{i,j}, \bar{K}^{u}_{i,j}$, $\bar{K}^{d}_{i,j}$ for the upper and lower storeys.

9.4.3. Storey deflection due to load applied at immediately beneath the storey in question

The effect due to load applied at any storey on the deflection of the adjacent unloaded upper storey is taken into account by introducing a new factor, $\Delta_{i,j}^{u}$, in the improved equations.

The definitions of the above new factors and derivations of the modified equations are illustrated in Appendix B. Only the final equations and selected sub-frames are presented in the next section.

9.5. Improved equations and corresponding sub-frames

First storey (for the case *m*=0.5)

1. Fixed base

$$D_{1,j} = \frac{12E}{h_1^{\,2}} k_{1,j}^{C} \left(1 - \left[\frac{3\beta_{1,j}\left(1+6\bar{K}^{u}_{2,j}\right)}{\left(1+4\beta_{1,j}+6\bar{K}^{d}_{1,j}\right)\left(1+6\bar{K}^{u}_{2,j}\right)-1} \right] \right) \tag{9.18}$$

$$\Delta^{u}_{1,j} = \left[\frac{6\beta_{1,j}\left(1+3\bar{K}^{u}_{2,j}\right)}{\left(1+4\beta_{1,j}+6\bar{K}^{d}_{1,j}\right)\left(1+6\bar{K}^{u}_{2,j}\right)-1} \right] \Delta_{1,j} \tag{9.19}$$

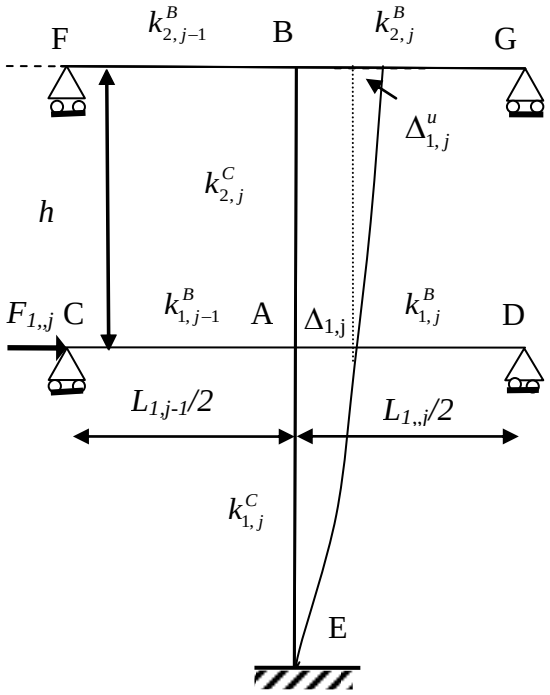

Figure 9.3: First storey-fixed base

2. Pinned base

$$D_{1,j} = \left[\frac{12E}{h_1^{\,2}}\right] k^C_{1,j} \left(\frac{\left(\bar{K}^d_{1,j} + \bar{K}^u_{2,j} + 6\bar{K}^d_{1,j}\bar{K}^u_{2,j}\right)}{4\left[\frac{\beta_{1,j}}{2} + 3\beta_{1,j}\bar{K}^u_{2,j} + \bar{K}^d_{1,jd} + \bar{K}^u_{2,j} + 6\bar{K}^d_{1,j}\bar{K}^u_{2,j}\right]} \right) \tag{9.20}$$

$$\Delta^{u}_{1,j} = \left[\frac{3\beta_{1,j}\left(1+3\bar{K}^u_{2,j}\right)}{\left(1+3\beta_{1,j}+6\bar{K}^d_{1,j}\right)\left(1+6\bar{K}^u_{2,j}\right)-1} \right] \Delta_{1,j} \tag{9.21}$$

where

$$\beta_{1,j} = \frac{k^C_{1,j}}{k^C_{2,j}}; \quad \bar{K}^d_{1,j} = \frac{k^B_{1,j\text{-}1} + k^B_{1,j}}{k^C_{2,j}}; \quad \bar{K}^u_{2,j} = \frac{k^B_{2,j\text{-}1} + k^B_{2,j}}{k^C_{2,j}}$$

$$k^B_{2,j\text{-}1} = \frac{I^B_{2,j\text{-}1}}{2L_{2,j\text{-}1}} \;\; ; \;\; k^B_{2,j} = \frac{I^B_{2,j}}{2L_{2,j}} \;\; ; \;\; k^B_{1,j\text{-}1} = \frac{I^B_{1,j\text{-}1}}{L_{1,j\text{-}1}}; \;\; k^B_{1,j} = \frac{I^B_{1,j}}{L_{1,j}}$$

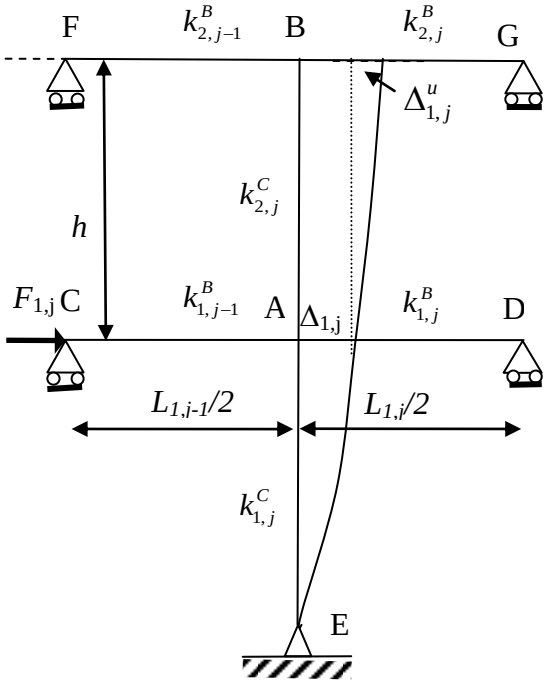

Figure 9.4: First storey-pinned base

Middle stories (for case *m*=0.5)

$$D_{i,j}=\left[\frac{12E}{h_i^{\,2}}\right]k^C_{i,j}\left(\frac{1}{2}\left(\frac{1+6\bar{K}^D_{i,j}}{2+3\bar{K}^D_{i,j}}\right)-\left[\frac{3\beta\left(\dfrac{1+3\bar{K}^D_{i,j}}{2+3\bar{K}^D_{i,j}}\right)^2}{\left(1+4\beta_{i,j}+6\bar{K}^d_{i+1,j}-\dfrac{2\beta}{\left(2+3\bar{K}^D_{i,j}\right)}-\dfrac{1}{1+6\bar{K}^u_{i+1,j}}\right)}\right]\right) \tag{9.22}$$

$$\Delta^u_{i+1,j}=\left[\frac{6\beta_{i,j}\left(1+3\bar{K}^D_{i,j}\right)\left(1+3\bar{K}^u_{i+1,j}\right)}{\left(1+4\beta_{i,j}+6\bar{K}^d_{i+1,j}\right)\left(1+6\bar{K}^u_{i+1,j}\right)\left(2+3\bar{K}^D_{i,j}\right)-\beta_{i,j}\left(2+12\bar{K}^u_{i+1,j}\right)-\left(2+3\bar{K}^D_{i,j}\right)}\right]\Delta_{i,j} \tag{9.23}$$

where

$$\bar{K}^u_{i+1,j}=\frac{k^B_{i+1,j-1}+k^B_{i+1,j})}{k^C_{i+1,j}}\;;\quad k^B_{i+1,j-1}=\frac{I^B_{i+1,j-1}}{2L_{i+1,j-1}}\;;\; k^B_{i+1,j}=\frac{I^B_{i+1,j}}{2L_{i+1,j}}$$

$$\bar{K}^d_{i,j}=\frac{k^B_{i,j-1}+k^B_{i,j}}{k^C_{i+1,j}}\;;\; k^B_{i,j-1}=\frac{I^B_{i,j-1}}{L_{i,j-1}}\;;\; k^B_{i,j}=\frac{I^B_{i,j}}{L_{i,j}}$$

$$\overline{K}^{D}_{i\text{-}1,j} = \frac{k^{B}_{i\text{-}1,j\text{-}1} + k^{B}_{i\text{-}1,j}}{k^{C}_{i,j}} \quad ; \quad k^{B}_{i\text{-}1,j\text{-}1} = \frac{I^{B}_{i\text{-}1,j\text{-}1}}{2L_{i\text{-}1,j\text{-}1}} \quad ; \quad k^{B}_{i\text{-}1,j} = \frac{I^{B}_{i\text{-}1,j}}{2L_{i\text{-}1,j}}$$

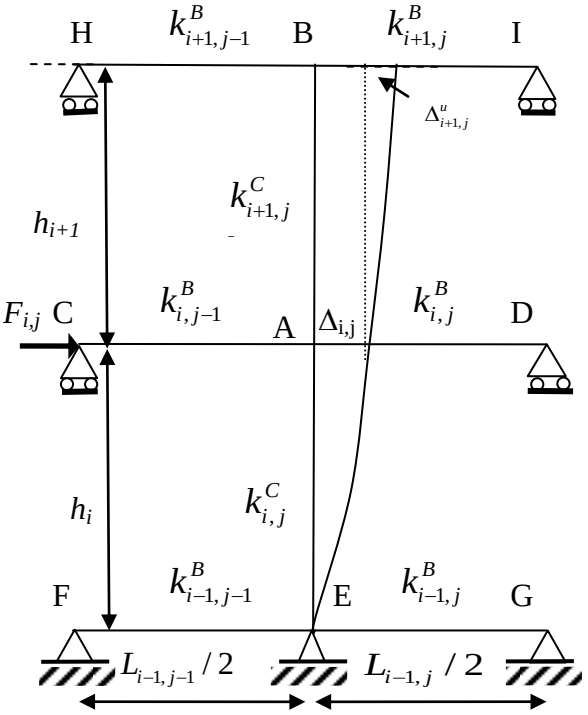

Figure 9.5: Middle storey model

Top storey (for the case *m*=0.5)

$$D_{n,j} = \left[\frac{12E}{h_n^{\,2}}\right] k^{C}_{n,j} \left(\frac{\left(\bar{K}^{d}_{n-1,j} + \bar{K}^{u}_{n,j} + 6\bar{K}^{d}_{n-1,j}\bar{K}^{u}_{n,j}\right)}{2\left(1 + 2\bar{K}^{u}_{n,j} + 2\bar{K}^{d}_{n-1,j} + 3\bar{K}^{d}_{n-1,j}\bar{K}^{u}_{n,j}\right)} \right) \tag{9.24}$$

where

$$\bar{K}^{u}_{n,j} = \frac{k^{B}_{n,j\text{-}1} + k^{B}_{n,j}}{k^{C}_{n,j}} \;; k^{B}_{n,j\text{-}1} = \frac{I^{B}_{n,j,j\text{-}1}}{L_{n,j\text{-}1}} \;;\; k^{B}_{n,j} = \frac{I^{B}_{n,j}}{L_{n,j}}$$

$$\bar{K}^{d}_{n\text{-}1,j} = \frac{k^{B}_{n\text{-}1,j\text{-}1} + k^{B}_{n\text{-}1,j}}{k^{C}_{n,j}} \;; k^{B}_{n\text{-}1,j\text{-}1} = \frac{I^{B}_{n\text{-}1,j\text{-}1}}{2L_{n\text{-}1,j\text{-}1}} \;;\; k^{B}_{n\text{-}1,j} = \frac{I^{B}_{n\text{-}1,j}}{2L_{n\text{-}1,j}}$$

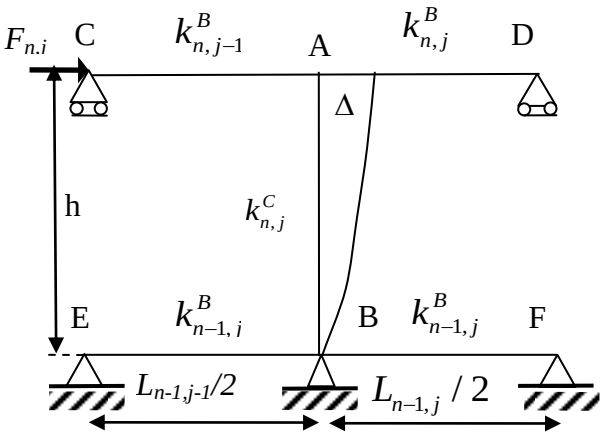

Figure 9.6: Top storey model

9.6. Proposed procedure to compute flexibility matrix for plane frame structures

Since the flexibility matrix of a frame is symmetrical, only half of the flexibility matrix needs to be computed. Moreover, the most important coefficients of flexibility matrix are the coefficients in and around the diagonal region. The effect of coefficients far from the diagonal is minimal. The conventional matrix method is used to determine the "*condensed*'' flexibility matrix. This matrix is computed by applying unit load at one of the "*Master*'' degrees of freedom of the frame at a time. The resultant lateral deflections are calculated by using the improved equations based on Muto's method. The axial deformation of the beams and columns are neglected by omitting the corresponding degrees of freedom. The steps of the calculation are as follows:

1. Calculate $k^c_{i,j}, k^B_{i,j}$ for each bay of the frame**.**
2. Calculate $\bar{K}_{i,j}$ for each bay.
3. Apply unit load at one of the "master'' degrees of freedom at a time. The horizontal displacement of any floor is the master degree of freedom which is associated with inertia forces (lumped-mass idealization).
4. Calculate $m_{i,j}$ **(**i.e. position of the point of inflection) for each bay.
5. Calculate *D*-values for each column.

6. Calculate the summation of the *D*-values for all columns in the same storey (*i.e.* $\sum D$).

7. Calculate the deflection of master degrees of freedom due to shear force (unit load) in the storey using the following equation:

$$\Delta_i = \frac{V_i}{\sum_{j=1}^{j=r} D_{i,j}} \tag{9.25}$$

8. From the results of the deflections in step 7, the symmetrical condensed flexibility matrix, $\bar{\boldsymbol{F}}$, is constructed.

It should be noted that all of the above calculations can be carried out easily by hand for two or three storey frames and an Excel spreadsheet will be sufficient for multi-storied frames. The procedure can also be programmed using any programming language for day-to-day use.

9.7. Lumped-mass matrix for a multi-storey plane frame

Lumped-mass idealisation is very popular in practice due to its simplicity. The lumped-mass matrix, $\overline{M}$, is a diagonal matrix. Each coefficient on the diagonal represents the mass associated with the corresponding master degree of freedom in each storey. This mass represents the mass of all the beams in the relevant storey added to the percentage of column mass. This percentage ranges between 35% and 50%, as stated by (Chan and Lui, 2005) depending on the stiffness of the connection. These coefficients are usually calculated by "hand'' and a lumped-mass matrix can easily be constructed. It takes this form:

$$\bar{M} = \begin{bmatrix} M_1 & 0 & 0 \\ 0 & M_2 & 0 \\ 0 & 0 & M_3 \end{bmatrix} \tag{9.26}$$

9.8. Fundamental period of a multi-storey plane frame

The conventional matrix method of vibration is used to find the fundamental period of a multi-storey plane frame. This procedure consists of the following simple steps:

1. Calculate the "*dynamic matrix*'' $\overline{DM}$ by simply multiplying the flexibility matrix, $\bar{F}$, with the lumped-mass matrix, $\overline{M}$.

$$\overline{DM} = \bar{F}\bar{M} \tag{9.27}$$

2. The resulting dynamic matrix is not symmetrical. The dominant eigenvalue of this matrix is the reciprocal of the square of the circular natural frequency $\frac{1}{\omega_1^2}$ of the system, which corresponds to the natural period $T_1 = \frac{2\pi}{\omega_1}$ (or the natural frequency $f_1 = \frac{1}{T_1}$.

3. The well-known "power method'' is used to find the eigenvalues. This simple method is suitable for "hand-calculation'' and can be easily programmed depending on the number of degrees of freedom, as it merely involves multiplying the "dynamic matrix'' with an arbitrary unit vector, $\bar{\varphi}_0$, to yield another vector, $\bar{\varphi}_1$, as follows:

$$\overline{DM}\,\bar{\varphi}_0 = \bar{\varphi}_1 = \frac{1}{\boldsymbol{\omega}_1^2}\bar{\varphi}_0 \qquad \text{where} \qquad \left[\bar{\varphi}_0\right]^T = \begin{bmatrix}1 & 1 & 1\end{bmatrix} \tag{9.28}$$

4. If $\bar{\varphi}_0$ is already the correct eigenvector, the corresponding eigenvalue $\frac{1}{\omega_1^2}$ is the correct eigenvalue. In contrast, if $\bar{\varphi}_0$ is only distantly related to the true eigenvector, then $\bar{\varphi}_1$ is a better approximation of the "first mode shape''. Multiplying $\overline{DM}$ by $\bar{\varphi}_1$ for the second time will give a more accurate eigenvalue (by up to 95%) in most cases. Repeated multiplication will improve the results to desired accuracy. The procedure can also be used to determine the largest eigenvalue which corresponds to the largest natural period and the lowest frequency and corresponding mode shape by first inverting the dynamic matrix $\overline{DM}$ and applying the previous procedure with $\overline{DM}^{-1}$**.** In addition, all of the

remaining eigenvalues and eigenvectors can be found by the same method, as explained in details in textbooks such as that by (Meskouris, 2000).

9.9. Modified Muto's method for a semi- rigid framed structure

Muto's method was originally derived to analyse plane frames with rigid connections. Recently, a simplified modification was proposed by (Wong et al., 2007) in order to make Muto's method suitable for plane frames with semi-rigid connections. This modification is based on the concept of "equivalent" beam stiffness for beams with elastic springs attached at two ends. Figure 9.7 shows a hybrid beam element with rotational springs of stiffness k_{si} and k_{sj} at its two ends.

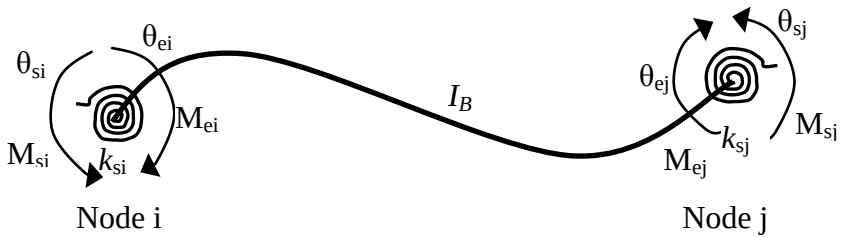

Figure 9.7: Hybrid beam element with connection springs attached

The equivalent bending stiffness $i^i_{B,eq.}$ and $i^j_{B,eq.}$ of the hybrid beam element at end nodes *i* and *j* respectively are defined as:

$$i^i_{B,eq.} = \Psi^i i_B \quad \& \quad i^j_{B,eq.} = \Psi^j i_B \tag{9.29}$$

where $i_B = \frac{EI_B}{L_B}$; $\Psi^i = \frac{1+2R_i}{R}$; $\Psi^j = \frac{1+2R_j}{R}$

$$R_i = \frac{i_B}{k_{si}};\ R_j = \frac{i_B}{k_{sj}};\ R = 1+4\left(R_i + R_j\right)+12R_iR_j$$

The procedure given in Section 9.8 can be used for rigid and semi-rigid frames using the nominal or equivalent bending stiffness of the beams.

Example: The following example is given to investigate the accuracy of the proposed procedure by comparing the results of the frequencies with the corresponding results from the ABAQUS software package. The example also illustrates the effect of semi-rigid connections on natural periods (i.e. frequencies). The steel frame, (E_s =200Gpa and density is 7800 kg/m^3), under consideration has four bays and six storeys, as shown in Figure 9.8. The frame is analysed for rigid and semi-rigid connection cases. For simplicity, the same rotational stiffness is used for all of the spring connections. Two values are used for the stiffness of the rotational springs, which are 1x10^{22} N-mm/rad for the rigid case, and 1.076x10^{10} N-mm/rad for the semi-rigid case.

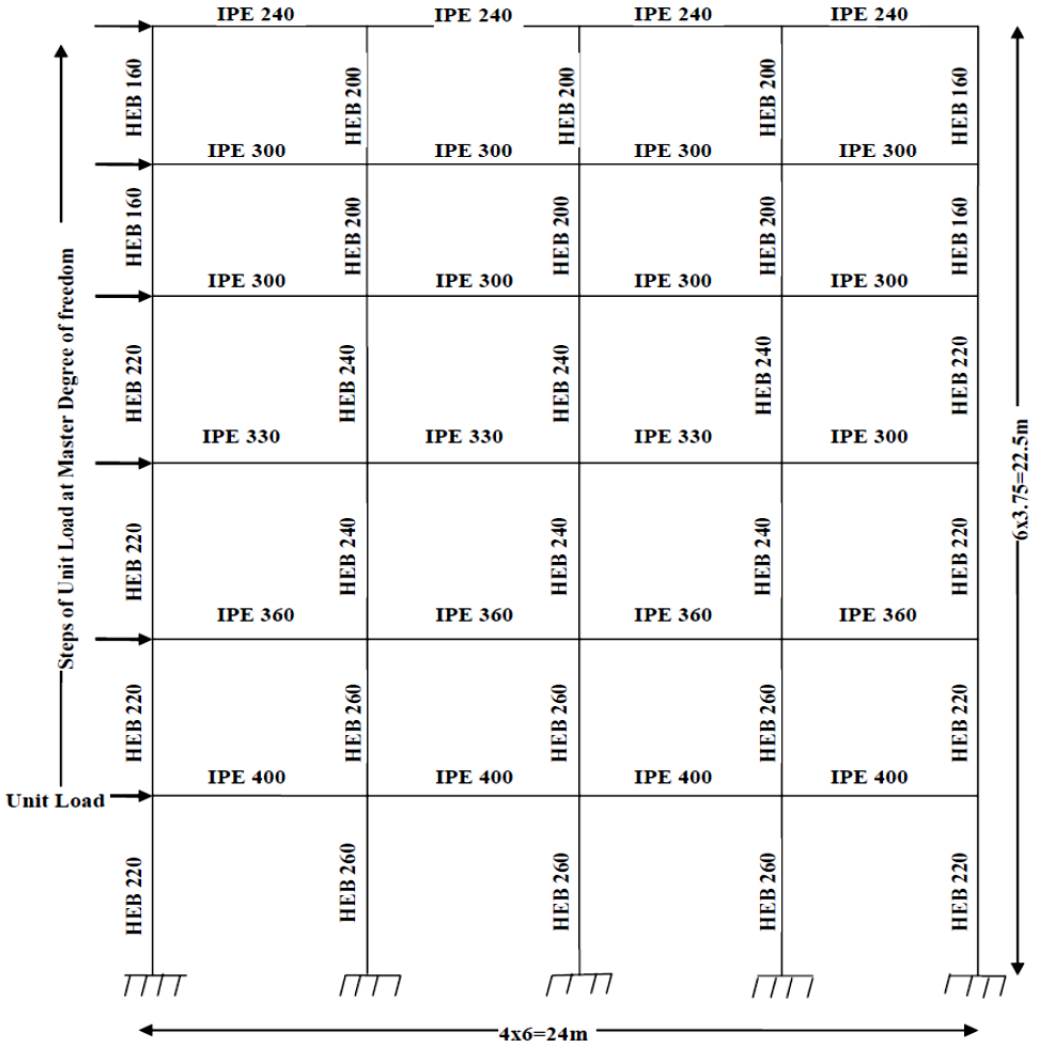

Figure 9.8: Layout of the steel frame

Table 9.1: Properties of the steel frame shown in Figure 9.8

Section	l (m)	A (m^2)	I(m^4)
IPE 240	6	0.00391	$3.89x10^{-4}$
IPE 300	6	0.00538	$8.36x10^{-4}$
IPE 330	6	0.00626	$11.77x10^{-4}$
IPE 360	6	0.00727	$16.27x10^{-4}$
IPE 400	6	0.00845	$23.13x10^{-4}$
HEB 160	3.75	0.0054	0.000025
HEB 200	3.75	0.0078	0.000057
HEB 220	3.75	0.0091	0.000081
HEB 240	3.75	0.0106	0.000113
HEB 260	3.75	0.0118	0.000149

- **Results and discussions:**

For the sake of brevity, only the final coefficients of the dynamic matrices, $\overline{DM}$ **,** using the proposed procedure are shown below:

$$\overline{DM}_{Rigid} = 10^{-7} \times \begin{bmatrix} 1255 & 1393 & 1267 & 1178 & 979 & 830 \\ 1535 & 3141 & 3109 & 2891 & 2403 & 2038 \\ 1535 & 3585 & 5168 & 5253 & 4366 & 3708 \\ 1535 & 3585 & 5707 & 7556 & 6783 & 5752 \\ 1535 & 3585 & 5707 & 8259 & 9942 & 8894 \\ 1535 & 3585 & 5707 & 8259 & 10494 & 12096 \end{bmatrix}$$

$$\overline{DM}_{Semi-Rigid} = 10^{-7} \times \begin{bmatrix} 1897 & 2749 & 2661 & 2473 & 2056 & 1743 \\ 2981 & 7017 & 7449 & 6925 & 5756 & 4880 \\ 3222 & 8318 & 12061 & 13125 & 10909 & 9250 \\ 3222 & 8318 & 14118 & 17909 & 16519 & 14007 \\ 3222 & 8318 & 14118 & 19875 & 21709 & 19848 \\ 3222 & 8318 & 14118 & 19875 & 23407 & 25028 \end{bmatrix}$$

The results of the natural periods from the proposed procedure and ABAQUS package are shown in Table 9.2.

Table 9.2: Results of natural periods

Period (s)	Proposed procedure			ABAQUS		
	T_1	T_2	T_3	T_1	T_2	T_3
Rigid	0.348	0.14	0.082	0.358	0.141	0.080
Semi-rigid	0.532	0.194	0.109	0.526	0.184	0.10

It can be clearly seen that the results from the proposed procedure are in good agreement with the FE results. The proposed procedure, which takes into account the realistic connection stiffness, reflects the behaviour of the frame with high accuracy. In addition, if the procedure is implemented in a spread sheet program like Excel, the effect of changing the geometric properties of any element can be easily obtained. Furthermore, the merit of the proposed procedure is in its ability to tune the flexibility of the beam-to-column connection in order to get the value of the fundamental natural period within a desired range.

9.10. Sensitivity of the proposed procedure

In order to evaluate the sensitivity of the proposed procedure for changes in the stiffness of semi-rigid connections, the same semi-rigid frame shown in Figure 9.8 was analysed using the proposed procedure for a wide range of semi-rigid connections (i.e. $0.5 \le \frac{Lk_s}{EI} \le 70$).

Eurocode 3 (2005) §5.2 consider connections with relative stiffness (Lk_s/EI) between 0.5 and 25 as semi-rigid connection.

The results from the proposed procedure and ABAQUS for the fundamental period are presented in Figure 9.9. It is clear from this figure that the proposed procedure can accurately predict the fundamental period for a whole range of stiffness. The important results are for the range between 0.5 and 25, which is considered as semi-rigid range by Eurocode 3. In this range, the original equation of Muto's method substantially underestimates the fundamental period, which is unsafe as the original equations are valid for rigid connection only. In addition, this figure shows that the proposed procedure is very sensitive to changes in stiffness, even for low range.

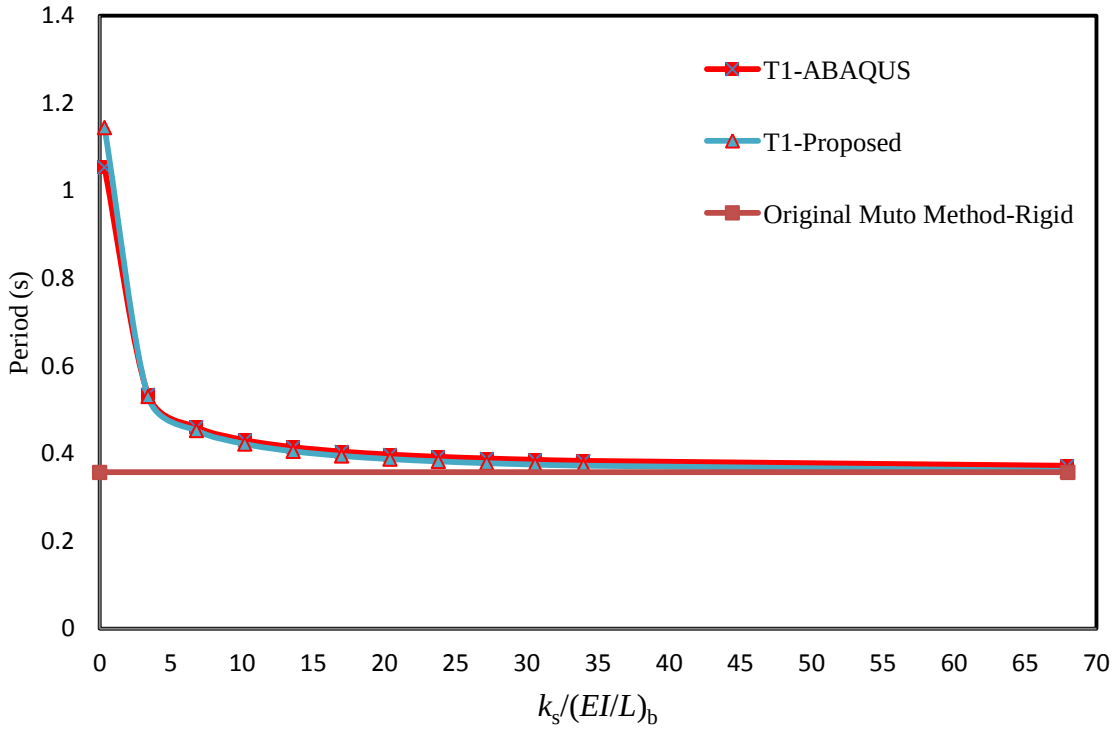

Figure 9.9: Relationship between relative stiffness and fundamental natural period

Figure 9.10 and Figure 9.11show that the proposed procedure can reliably predict the second and third natural periods for a wide range of semi-rigid connections. The discrepancy between the approximate procedure and ABAQUS modelling, particularly when the connection approaches a pinned connection, is expected and acceptable for any approximate procedures.

Furthermore, it can be seen that the decrease in stiffness of semi-rigid frame may significantly increase its natural periods, especially the fundamental period. The semi-rigid frames have longer period and thus attract lesser inertia. This behaviour confirms the results of analytical studies by (Rosales, 1991; Sekulovic et al., 2002) as stated above.

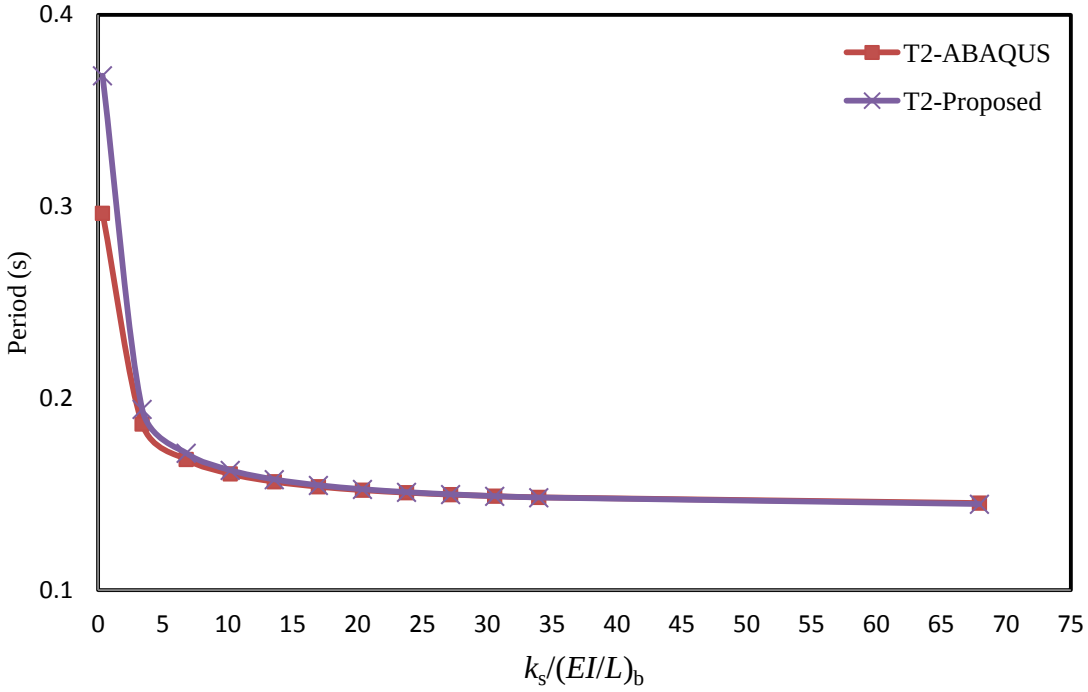

Figure 9.10: Relationship between relative stiffness and second natural period

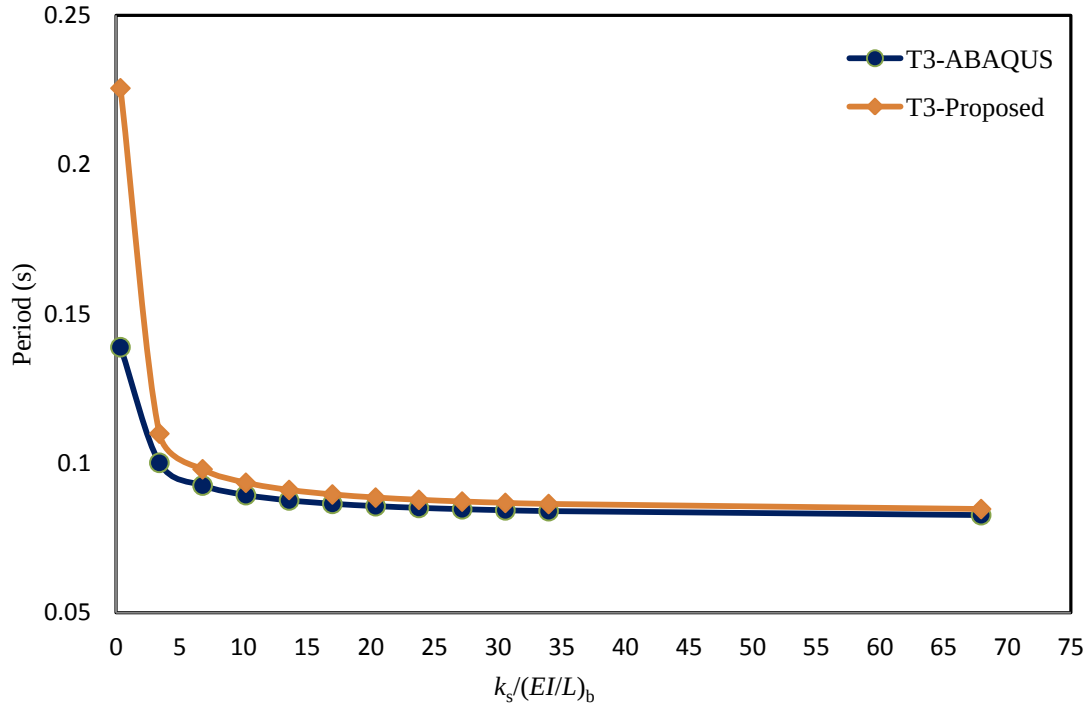

Figure 9.11: Relationship between relative stiffness and third natural period

9.11. Summary and conclusions

A simple "hand'' procedure has been proposed to calculate the fundamental natural period of rigid and semi-rigid plane steel frames. This procedure, based on Muto's method, is capable of calculating the fundamental natural periods of multi-storey steel frames with rigid and semi-rigid connections. The results of the calculations indicate that the concept of semi-rigid design is not optional for designers and must be taken into account for safe design. It has been shown that this simple approximate procedure yields agreeable results compared with other accurate and approximate methods. The small discrepancy between them is due to the overturning of the entire frame, resulting in shortening and elongation of the columns at opposite sides of the frame. The contribution of the overturning moment may be about 10-20% of the total sway for unbraced rigid frames up to 20 to 30 stories. Furthermore, as with any other approximate methods, the results need to be multiplied by an adequate safety factor as some results may underestimate the natural period, which is considered as unsafe. Nevertheless, the accuracy of the proposed procedure is high when compared with the finite element results obtained using ABAQUS. The proposed procedure can easily be extended to unbraced composite frame depending on the modified Muto's method developed by (Wong et al., 2007) for the analysis of unbraced composite frame systems by introducing the concept of improved equivalent beam stiffness.

Chapter Ten

Summary and Conclusions

10.1. Introduction

The importance of inclusion of semi-rigid concept in analysis or design of any structural system has been presented with the help of many experimental and numerical studies in literature. These studies showed clearly that the consideration of the semi-rigid concept is necessary in order to achieve economical and safe design.

The detailed literature review showed that even though the finite element modelling can predict well the behaviour of a semi-rigid connection, the reliable test results are essential to calibrate the model before it can be used for a different connection. In addition, the intensive computational effort and time that is required in finite element modelling make it impractical to analyse large structures. All of these considerations make the component-based mechanical models as potential alternative to the finite element approach.

10.2. Mechanical model for predicting the rotational stiffness of a flush end-plate composite connection incorporating the effect of partial interaction

A new component-based mechanical model was developed to calculate the rotational stiffness of a semi-rigid connection. The effect of each component of connection was well studied and modelled. The traditional axial spring which had been used to model the effect of shear connectors was replaced by a simple rotational spring to consider the actual rotation of concrete slab under loading and to make this model general enough so as to use with steelwork and composite connections. Further, a simple and effective procedure to evaluate the equivalent stiffness of shear connection was developed. The validity of the model was evaluated by comparing with the results from other existing models and experimental results.

Besides the generality of the proposed model for bare steel and composite connections, the model could be implemented in any finite element software and was

able to extend further than the linear region with appropriate input data for component stiffness.

10.3. Prediction of the load-slip behaviour of a stud shear-connector

A simple approach to estimate the secant stiffness and strength of standard diameters of shear connector for different compressive strength of concrete was developed. The proposed chart can be used to estimate the secant stiffness and strength for other diameters of shear connectors by drawing parallel lines at the required levels. Also, a simplified multi-linear curve was derived based on the proposed chart for initial stiffness as well as the derivation of post-yield stiffness from the empirical equations in the literature.

The proposed model is in agreement with the test results. It can be used when no push-out test curve is available since the empirical equations that researchers have used in the past can lead to unrealistic shear stiffness of the shear connector in some cases.

10.4. Stiffness of a reinforced concrete slab in a composite connection

A new component model for composite slab was developed. This model incorporates the components of embedded reinforcement and concrete in one single component (RCC). The tension-stiffening effect of concrete was considered implicitly in the stiffness of (RCC) by modified modulus of elasticity concept E_{m}. In addition, the component model is further simplified by replacing all (RCC) components along the composite connection by equivalent springs. Shear studs was modelled as linear or nonlinear springs depending on the range of loading. Furthermore, a simplified procedure was proposed to calculate the "lump'' stiffness of (RCC) and shear studs (S) springs. The proposed models and calculation procedures were verified against finite element and experimental results for some selected composite connections.

A parametric study was carried out to investigate the effect of relative stiffness of (RCC) to (S) on the distribution of forces on all components of (RCC) and shear stud springs along a composite connection. The results of the parametric study show clearly that the first and second shear studs and first and second reinforcement zones provide the most resistance to the longitudinal shear force in the composite connection. Also, the results of the parametric study show that the stiffness of a shear stud has little effect on the distribution of forces acting on the shear studs along the composite connection

for constant values of k_{RCC}/k_{sc}. However, comparison of the results for the same k_{sc} and different k_{RCC}/k_{sc} shows the significant effect of k_{RCC}/k_{sc} on this distribution of forces.

The proposed a mechanical component model for an (RCCS) can be used as a simplified model in the finite element modelling of a composite connection to overcome the convergence problems in explicit modelling of concrete when the concrete slab begins to crack. This will also reduce the computational time significantly with adequate accuracy.

The analytical expression for the initial stiffness of (RCCS) can be used in the manual calculation of the initial stiffness of an overall composite connection. This expression can be used to overcome the shortcoming in the estimation of the effective length of reinforcement, l_r in calculating the stiffness of the reinforcement component (k_r).

A new procedure to find the maximum number of "active'' studs was developed. The relation between the number of "active'' shear studs and maximum number of shear studs for full shear connection requirement was derived. Modification to the proposed mechanical model to calculate the initial stiffness of composite connection was performed by two approaches. The first approach was achieved by developing new expressions to calculate the stiffness of "active'' shear studs and modified embedded reinforcement. The second approach was undertaken by replacing both the springs for reinforcement and shear studs by a "lump'' spring in the original mechanical model.

Furthermore, it was concluded that it is preferable to use a higher number of soft shear studs with a lower strength than to use fewer stiff shear studs with high strength in order to avoid local concrete failure.

10.5. Moment resistance and ductility of flush end-plate composite connections

A flowchart to predict the failure mode of composite connection had been developed based on the practical range of shear connection ratio (η_y>0.4) and reinforcement ratio (0.5<ρ<1.7%). Then, a procedure to calculate the moment capacity of composite connection was developed using the concept of a rigid-plastic, stress blocks. This procedure is compatible with the proposed flowchart and with the procedure to estimate

the rotation at failure. Also, it considered the cases of full interaction, full shear connection and partial shear connection.

The prediction of moment capacity of composite connection from the proposed procedure is in agreement with the experimental results for most cases.

The proposed mechanical model to calculate the rotational stiffness of composite connection was extended to calculate the rotations at yield and at failure using the appropriate post-linear values of the components. The validity of the proposed procedure to calculate the rotation at yield was evaluated against three sets of experimental test data. These tests were selected to represent three cases of shear connection (i.e. full interaction, full shear connection and partial shear connection) and covered the usual cases of failure modes.

The proposed procedure was observed to be applicable for estimation the rotation at yield and rotation capacity of a flush end-plate composite connection.

10.6. Analysis of a beam with semi-rigid connections under gravity loading

A new analysis procedure for beam with semi-rigid connections under gravity load was developed. The proposed procedure was based on the principle of superposition. The accuracy of this procedure has been verified by a finite element analysis using the ABAQUS software. It overcomes the shortcomings of Ahmed et al. (2008)'s procedure, where only certain symmetrical loadings were allowed. In contrast, the proposed procedure is applicable to any arbitrary loading. Also, it can be used to calculate the deflection at any point of the beam and to compute shear force and bending moment as well. It can be extended to compute the deflection of a composite steel-concrete member after making some modifications to account for beam stiffness.

10.7. A simplified procedure to calculate by hand the natural periods of semi-rigid steel frames

Simplified formulae to calculate by hand the natural periods of semi-rigid steel frames are presented. The proposed formulae have been developed after modifications of existing formulae in literature for rigid-jointed plane steel frames. A parametric study has been conducted to quantify the effects of semi-rigid connections on the natural

periods of vibration of plane steel frames. The results of the parametric study show clearly that the flexibility of a connection has a considerable effect on the natural frequencies of a steel frame. Inaccurate values for the fundamental period may result in unsafe design.

The proposed procedure can predict the natural periods of a frame for a wide range of flexibilities of beam-to-column connections. The validity of the proposed procedure is confirmed by comparing the results with the results obtained from ABAQUS, and good agreement between them was demonstrated.

10.8. An approximate analytical method for calculating the natural periods of unbraced steel frames with semi-rigid connections

A simple "hand'' procedure has been proposed to calculate the fundamental natural period of rigid and semi-rigid plane steel frames. This procedure, based on Muto's method, is capable of calculating the fundamental natural periods of multi-storey steel frames with rigid and semi-rigid connections. The results of the calculations indicate that the concept of semi-rigid design is not optional for designers and must be taken into account for safe design. It has been shown that this simple approximate procedure yields agreeable results compared with other accurate and approximate methods. Also, the accuracy of the proposed procedure is high when compared with the finite element results obtained using ABAQUS. The proposed procedure can easily be extended to unbraced composite frame depending on the modified Muto's method developed by (Wong et al., 2007) for the analysis of unbraced composite frame systems by introducing the concept of improved equivalent beam stiffness.

10.9. Recommendation for future work

1. The proposed mechanical model for calculating the rotational spring need further improvement by adding another springs in appropriate position such as the spring to consider the effect of concrete around column flange. This spring can be active only in asymmetrical cases of connection or in external connection. The stiffness of this spring needs more experimental and numerical work to be evaluated. Another suggestion is to use a spring to take into account the effect of concrete in compression zone around the shear connectors but the stiffness and strength of this spring needs more experimental and numerical work to be evaluated.

2. The proposed chart of strength and stiffness of shear connector may need more improvement since it is based on a limited number of numerical and experimental tests. Nevertheless, it can be used for estimating the strength and stiffness of shear connector if push out test data is not available. In addition, the experimental and numerical data for other diameters of shear connector are needed to extend this chart for other diameters.

3. Due to very few experimental tests in the literature on isolated composite slab, the proposed model for lump component (RCCS) was validated using the results from finite element modelling and available test data in the literature. This can substantially reduce the amount of calculation required to evaluate stiffness of composite connections. Therefore, the procedure needs further validation using experimental test data for full and partial shear interaction.

4. The proposed procedures for evaluating the frequency of semi-rigid frames need to extend to composite structure. Combining an equivalent stiffness of composite beam with the springs simulating the semi-rigid connection can be used for this purpose. However, the validity of such modelling needs the computational power of a super computer to run the required finite element model of composite frame. Experimental tests are essential to validate the approximate analytical model as well as the validity of finite element model in order to carry out a parametric study on the combined effect of flexibility of connection and shear connection ratio on the frequency of composite structure.

References

ABAQUS. 2005. Theory manual, version 6.10.Hibbit, Karlsson&Sorenson.

Ahmed, B. (2001). "Deflection of semi-rigidly connected beams." *Journal of Civil Engineering*, CE 29(2), 133-150.

Ahmed, B., Li , T. Q., and Nethercot, D. A. "Deflection of semi-rigidly connected beams " *Proc., International Conference on Structures and Granular Solids - From Scientific Principles to Engineering Applications*, CRC Press-Taylor & Francis Group,2008, 293 - 303

Ahmed, B., and Nethercot, D. A. (1996). "Effect of high shear on the moment capacity of composite cruciform endplate connections." *Journal of Constructional Steel Research*, 40(2), 129-163.

Ahmed, B., and Nethercot, D. A. (1997). "Design of flush endplate connections in composite beams." *The Structural Engineer*, 75(14), 233-244.

Ahmed, B., and Nethercot, D. A. (1997). "Prediction of initial stiffness and available rotation capacity of major axis composite flush endplate connections." *Journal of Constructional Steel Research*, 41(1), 31-60.

Ahmed, B., Nethercot, D. A., and Li, T. Q. "Modelling composite connection response." *Connections in Steel Structures III: Behaviour, Strength and Design, ed. R. Bjorhovde, A. Colson and R. Zandonini. Proceedings of the Third International Workshop, Trento University, 29-31 May 1995.*,1996: 259-268.

Al-Jabri, K. S. (2004). "Component-based model of the behaviour of flexible end-plate connections at elevated temperatures." *Composite Structures*, 66(1-4), 215-221.

Amadio, C., and Fragiacomo, M. (2003). "Analysis of rigid and semi-rigid steel–concrete composite joints under monotonic loading. Part I: Finite element modelling and validation." *Steel and Composite Structures*, 3(5), 349-369.

An, L., and Cederwall, K. (1996). "Push-out tests on studs in high strength and normal strength concrete." *Journal of Constructional Steel Research*, 36(1), 15-29.

Anderson, D., Aribert, J. M., Bode, H., and Kronenburger, H. J. (2000). "Design rotation capacity of composite joints." *Structural engineer London*, 78(6), 25-29.

Anderson, D., and Najafi, A. A. (1994). "Performance of composite connections: Major axis end plate joints." *Journal of Constructional Steel Research*, 31(1), 31-57.

Aribert, J.-M., and Al Bitar, A. (1989). "Optimisation du dimensionnement en connexion partielle des poutres de planchers mixtes r´ealises avec un bac en tˆole mince nervur´ee." *Construction m´etallique*, 43-55 (in French).

Aribert, J. M. "Influence of slip of the shear connection on composite joint behaviour." *Proceedings of the 3rd International Workshop on Connections in Steel Structures*, Trento, Italy,1996: 11–22.

Aribert, J. M., and Dinga, O. N. "Modeling and experimental investigation of bolted flush end-plate composite beam-to-column joints." *Composite Construction in Steel and Concrete IV,*, Banff, Alta.,2000: 711-724.

Aribert, J. M., and Labib, A. G. (1982). "Model of elasto-plastic design for composite beams with partial interaction." *Modele de calcul elato-plastique de poutrres mixtes a connexion partielle*, 19(4), 3-51.

Aribert, J. M., and Lachal, A. "Experimental investigation of composite connections in global interpretation ", *Proceedings of COST C 1 conference on semi-rigid Joints*, Strasbourg, France,1992: 158-169.

Astaneh, A., Nader, M. N., and Malik, L. (1989). "Cyclic behavior of double angle connections." *Journal of structural engineering New York, N.Y.*, 115(5), 1101-1118.

Azizinamini, A., and James, B. R. (1989). "Static and cyclic performance of semi-rigid steel beam-to-column connections." *Journal of Structural Engineering*, 115(12), 2979-2999.

Brown, N. D., and Anderson, D. (2001). "Structural properties of composite major axis end plate connections." *Journal of Constructional Steel Research*, 57(3), 327-349.

BS EN 1998-1 (2004). "Design of structures for earthquake resistance." *part 1: General rules, seismic actions and rules for buildings*, European Committee for Standardization (CEN), Brussels.

BSI. BS 5400-5:Steel, concrete and composite bridges, Part 5: Code of practice for the design of composite bridges. London, British Standards Institution; 2005.

Bursi, O. S., and Jaspart, J. P. (1997). "Benchmarks for finite element modelling of bolted steel connections." *Journal of Constructional Steel Research*, 43(1-3), 17-42.

Bursi, O. S., and Jaspart, J. P. (1998). "Basic issues in the finite element simulation of extended end plate connections." *Computers and Structures*, 69, 361-382.

Cabrero, J. M., and Bayo, E. (2007). "The semi-rigid behaviour of three-dimensional steel beam-to-column joints subjected to proportional loading. Part I. Experimental evaluation." *Journal of Constructional Steel Research* 63, 1241-1253.

CEB-FIP model code 1990. Comite Euro-International du Beton, General models. London, Thomas Telfored Services Ltd.

Chan, S.-L., and Chui, P.-T. (2000). *Non-linear static and cyclic analysis of steel frames with semi-rigid connections*, ELSEVIER SCIENCE Ltd, The Boulevard, Langford Lane, Kidlington, Oxford OX5 1GB, UK.

Chan, S. L., and Lui, E. M. (2005). *Hand book of structural engineering*

Chen, W. F., and Kishi, N. (1989). "Semirigid steel beam-to-column connections: Data base and modeling." *Journal of structural engineering New York, N.Y.*, 115(1), 105-119.

Chen, W. F., and Lui, E. M. (1985). "Stability design criteria for steel members and frames in the United States." *Journal of Constructional Steel Research*, 5(1), 31-74.

Chrysanthakopoulos, C., Bazeos, N., and Beskos, D. E. (2006). "Approximate formulae for natural periods of plane steel frames." *Journal of Constructional Steel Research*, 62(6), 592-604.

Chui, P. P. T., and Chan, S. L. (1997). "Vibration and deflection characteristics of semi-rigid jointed frames." *Engineering Structures*, 19(12), 1001-1010.

Crisinel, M., and Carretero, A. "Simple prediction method for moment-rotation properties of composite beam-to-column joints."1997: 823-835.

da S. Vellasco, P. C. G., de Andrade, S. A. L., da Silva, J. G. S., de Lima, L. R. O., and Brito Jr, O. (2006). "A parametric analysis of steel and composite portal frames with semi-rigid connections." *Engineering Structures*, 28(4), 543-556.

Dabaon, M. A., El-Boghdadi, M. H., and Kharoob, O. F. (2009). "Experimental and numerical model for space steel and composite semi-rigid joints." *Journal of Constructional Steel Research*, 65(8-9), 1864-1875.

Dai, Y. M., and Liao, S. (2005). "Experimental study on stud shear connectors in composite steel-fdpcp beams." *Build. Tech. Dev.*, , 32(5), 27–28.

Davison, J. B., Kirby, P. A., and Nethercot, D. A. (1987). "Rotational stiffness characteristics of steel beam-to-column connections." *Journal of Constructional Steel Research*, 8(C), 17-54.

Davison, J. B., Kirby, P. A., and Nethercot, D. A. (1987). "Rotational stiffness characteristics of steel beam-to-column connections." *Journal of Constructional Steel Research*, 8, 17-54.

Dhillon, B. S., and Malley, J. W. O. (1999). "Interactive design of semi-rigid steel frames." *Journal of Structural Engineering* 125(5), 556-564.

Ellobody, E., and Young, B. (2006). "Performance of shear connection in composite beams with profiled steel sheeting." *Journal of Constructional Steel Research*, 62(7).

Elnashai, A. S., and Elghazouli, A. Y. (1994). "Seismic behaviour of semi-rigid steel frames." *Journal of Constructional Steel Research*, 29(1-3), 149-174.

Eurocode 3. BS EN 1993-1-8:2005: Design of steel structures Part 1-8: Design of joints. European Committee of Standardization.

Eurocode 4. EN1994-1-1:2004 : Design of composite steel and concrete structures part 1-1: general rules and rules for buildings. European Committee of Standardization.

Eurocode 8. Design of structures for earthquake resistance Part 1:general rules. Brussels, CEN (European Committee for Standardization).

Fu, F., and Lam, D. (2006). "Experimental study on semi-rigid composite joints with steel beams and precast hollowcore slabs." *Journal of Constructional Steel Research* 62 771-782.

Fu, F., Lam, D., and Ye, J. (2007). "Parametric study of semi-rigid composite connections with 3-D finite element approach." *Journal of Engineering Structures*, 29 888-898.

Fu, F., Lam, D., and Ye, J. (2008). "Modelling semi-rigid composite joints with precast hollowcore slabs in hogging moment region." *Journal of Constructional Steel Research*, 64(12), 1408-1419.

Fu, F., Lam, D., and Ye, J. (2010). "Moment resistance and rotation capacity of semi-rigid composite connections with precast hollowcore slabs." *Journal of Constructional Steel Research*, 66(3), 452-461.

Gattesco, N., and Giuriani, E. (1996). "Experimental study on stud shear connectors subjected to cyclic loading." *Journal of Constructional Steel Research*, 38(1), 1-21.

Gattesco, N., Giuriani, E., and Gubana, A. (1997). "Low-cycle fatigue test on stud shear connectors." *Journal of Structural Engineering*, 123(2), 145-150.

Gerstle, K. H. (1988). "Effect of connections on frames." *J. Construct. Steel Research* 10 (1988), 241-267.

Gil, B., and Bayo, E. (2008). "An alternative design for internal and external semi-rigid composite joints. Part II: Finite element modelling and analytical study." *Engineering Structures*, 30(1), 232-246.

Gizejowski, M. A., Barcewicz, W., and Salah, W. (2010). "Finite element modelling of the behaviour of a certain class of composite steel-concrete beam-to-column joints." *Archives of Civil Engineering*, 56(1), 19-56.

Goel, R. K., and Chopra, A. K. (1997). "Period formulas for moment-resisting frame buildings." *Journal of Structural Engineering*, 123(11), 1454-1461.

Goel, R. K., and Chopra, A. K. (1998). "PERIOD FORMULAS FOR CONCRETE SHEAR WALL BUILDINGS." *Journal of structural Engineering*, 124(4), 426-433.

Gupta, A., and Maestrini, S. (1990). "Tension-stiffness model for reinforced concrete bars." *Journal of Structural Engineering, ASCE*, 116(3), 769-790.

Heidebrecht, A. C., and Smith, B. S. (1973). "Approximate analysis of tall wall-frame structures " *ASCE J Struct Div*, 99(ST2), 199-221.

Heidebrecht, A. C., and Smith, B. S. (1973). "Approximate analysis of tall wall-frame structures." *Journal of the Structural Division*, 99(ST2), 199-221.

Hwang, L. S., and Rizkalla, S. H. (1983). "Behavior of reinforced concrete in tension at post-cracking range." *Engineering Report*, Department of Civil Engineering, University of Manitoba, Winnipeg, Canada.

Ihaddoudène, A. N. T., Saidani, M., and Chemrouk, M. (2009). "Mechanical model for the analysis of steel frames with semi rigid joints." *Journal of Constructional Steel Research* 65(2009), 631-640.

Jaeyeol, C., Namso, C., Namsik, K., and Youngsun, C. "Stress-strain relationship of reinforced concrete subjected to biaxial tension." *Proc., Transactions of the 17th International Conference on Structural Mechanics in Reactor Technology (SMiRT 17), August 17 -22*,2003.

Johnson, R. P., and May, I. M. (1975). "Partial-interaction design of composite beams." *Structural Engineer*, 53(8), 305-311.

Johnson, R. P., and Molenstra, N. (1991). "Partial shear connection in composite beams for buildings." *Proceedings - Institution of Civil Engineers. Part 2. Research and theory*, 91, 679-704.

Jones, S. w., Kirby, P. A., and Nethercot, D. A. (1983). "The analysis of frames with semi-rigid connections-A Stata-of the Art Report." *Journal of Constructional Steel Research*, 3(2), 2-13.

Kattner, M., and Crisinel, M. (1997). "Finite element modelling of semi-rigid composite joints." *FE-modellierung halbsteifer verbundknoten*, 66(12), 819-829.

Kattner, M., and Crisinel, M. (2000). "Finite element modelling of semi-rigid composite joints." *Journal of Computers and Structures* 78 341-353.

Kemp, A. R., and Nethercot, D. A. (2001). "Required and available rotations in continuous composite beams with semi-rigid connections." *Journal of Constructional Steel Research*, 57(4), 375-400.

Kim, B., Wright, H., and Cairns, R. (2001). "The behaviour of through-deck welded shear connectors: an experimental and numerical study." *Journal of Constructional Steel Research*, 57, 1359-1380.

Kishi, N., and Chen, W. F. (1986). "Data base of steel beam-to-column connections." *Struct. EnonO Rap. No. CE-STR-86-26*, I and ll, School of Civil Engineering, Purdue University, West Lafayette.

Kishi, N., Hasan, R., Chen, W. F., and Goto, Y. (1997). "Study of Eurocode 3 steel connection classification." *Engineering Structures*, 19(9), 772-779.

Kwak, H.-G., and Kim, D.-Y. (2006). "Cracking behavior of RC panels subject to biaxial tensile stresses." *Computers and Structures*, 84 305-317.

Lam, D. (2007). "Capacities of headed stud shear connectors in composite steel beams with precast hollowcore slabs." *Journal of Constructional Steel Research* 63 1160-1174.

Lam, D., and El-Lobody, E. (2005). "Behavior of headed stud shear connectors in composite beam." *Journal of Structural Engineering*, 131(1), 96-107.

Lawson, R. (1989). "Design of composite slabs and beams with steel decking." *SCI Publication 055*, The Steel Construction Institute, Ascot.

Li, T. Q., Nethercot, D. A., and Choo, B. S. (1996). "Behaviour of flush end-plate composite connections with unbalanced moment and variable shear/moment ratios - I. Experimental behaviour." *Journal of Constructional Steel Research*, 38(2), 125-164.

Li, T. Q., Nethercot, D. A., and Choo, B. S. (1996). "Behaviour of flush end-plate composite connections with unbalanced moment and variable shear/moment ratios - II. Prediction of moment capacity." *Journal of Constructional Steel Research*, 38(2), 165-198.

Liew, J. Y. R., Teo, T. H., Shanmugam, N. E., and Yu, C. H. (2000). "Testing of steel-concrete composite connections and appraisal of results." *Journal of Constructional Steel Research*, 56(2), 117-150.

Loh, H. Y., Uy, B., and Bradford, M. A. (2004). "The effects of partial shear connection in the hogging moment regions of composite beams Part II - Analytical study." *Journal of Constructional Steel Research*, 60(6), 921-962.

Loh, H. Y., Uy, B., and Bradford, M. A. (2006). "The effects of partial shear connection in composite flush end plate joints Part i - Experimental study." *Journal of Constructional Steel Research*, 62(4), 378-390.

Loh, H. Y., Uy, B., and Bradford, M. A. (2006). "The effects of partial shear connection in composite flush end plate joints Part II - Analytical study and design appraisal." *Journal of Constructional Steel Research*, 62(4), 391-412.

McGuire, J. (1995). "Notes on Semi-Rigid Connections." Jim Loughlin - NASA Goddard Space Flight Center.

Meskouris, K. (2000). *Structural dynamics : models, methods, examples*, Ernst & Sohn, Berlin.

Mottram, J. T., and Johnson, R. P. (1990). "Push tests on studs welded through profiled steel sheeting." *Structural engineer London*, 68(10), 187-193.

Muto, K. (1974). *Aseismic design analysis of buildings* Maruzen Company,Ltd., Tokyo.

Nader, M. N., and Astaneh, A. (1991). "Dynamic behavior of flexible, semirigid and rigid steel frames." *Journal of Constructional Steel Research*, 18 179--192.

Nader, M. N., and Astaneh, A. (1991). "Dynamic behavior of flexible, semirigid and rigid steel frames." *Journal of Constructional Steel Research*, 18(3), 179-192.

Nader, M. N., and Astaneh, A. (1996). "Shaking table tests of rigid, semirigid, and flexible steel frames." *Journal of Structural Engineering*, 122(6), 589-596.

Nethercot, D. A. (1995). "Semirigid joint action and the design of nonsway composite frames." *Engineering Structures*, 17(8), 554-567.

Nethercot, D. A., Davison, J. B., and Kirby, P. A. (1988). "Connection flexibility and beam design in non-sway frames." *Engineering Journal / AISC*, THIRD QUARTER/1988, 99-108.

Nie, J., Fan, J., and Cai, C. S. (2004). "Stiffness and deflection of steel-concrete composite beams under negative bending." *Journal of Structural Engineering*, 130(11), 1842-1851.

Oehlers, D. J., and Coughlan, C. G. (1986). "The shear stiffness of stud shear connections in composite beams." *Journal of Constructional Steel Research*, 6, 273-284.

Ohi, K., and Hyoukchoi, J. (2006). "Hybrid simulation on semi-rigid partial-strength connection." *International Journal of Modern Physics B* 20(25), 4445-4450.

Ollgaard, J. G., Slutter, R. G., and Fisher, J. W. (1971). "Shear strength of stud connectors in lightweight and normalweight concrete." *Eng J Amer Inst Steel Constr*, 8(2), 55-64.

Qiusheng, L., Hong, C., and Guiqing, L. (1994). "Analysis of free vibrations of tall buildings." *Journal of Engineering Mechanics - ASCE*, 120(9), 1861-1876.

Queiroz, F. D., Queiroz, G., and Nethercot, D. A. (2009). "Two-dimensional FE model for evaluation of composite beams, I: Formulation and validation." *Journal of Constructional Steel Research*, 65(5), 1055-1062.

Queiroz, F. D., Queiroz, G., and Nethercot, D. A. (2009). "Two-dimensional FE model for evaluation of composite beams, II: Parametric study." *Journal of Constructional Steel Research*, 65(5), 1063-1074.

Queiroz, G., Mata, L., and Franco, J. (2005). " Analysis of composite connections in unbraced frames subjected to wind and gravity loading." *Journal of Constructional Steel Research*, 61, 1075-1093.

Queiroza, F. D., Vellascob, P. C. G. S., and Nethercota, D. A. (2007). "Finite element modelling of composite beams with full and partial shear connection." *Journal of Constructional Steel Research*, 63, 505-521.

Rassati, G. A., Leon, R. T., and Noe, S. (2004). "Component modeling of partially restrained composite joints under cyclic and dynamic loading." *Journal of Structural Engineering* 130(2), 343-351.

Razaqpur, A. G., and Nofal, M. (1989). "A finite element for modelling the nonlinear behavior of shear connectors in composite structures." *Computers and Structures*, 32(1), 169-174.

Ren, P., and Crisinel, M. "Prediction method for moment-rotation behaviour of composite beam-to-column connection." *Connections in Steel Structures III:Behaviour, Strength and Design, ed. R. Bjorhovde, A. Colson and R. Zandonini. Proceedings of the Third International Workshop, Trento University, 29-31 May 1995.* , Pergamon, Oxford,1996: 33-46.

Rex, C. O., and Easterling, S. (2000). "Behavior and modelling of reinforced composite slab in tension." *Journal of Structural Engineering*, 126(7), 762-771.

Rocha, J. D. B., Arrizabalaga, E. M., Quevedo, R. L., and Morfa, C. A. R. (2012). "Behavior and strength of welded stud shear connectors in composite beam." *Rev. Fac. Ing. Univ. Antioquia* (63), 93-104.

Rosales, J. G. P. (1991). "Seismic resistance of steel frames with semi-rigid connections." MSc dissertation, University of London, London, UK.

Rosales, J. G. P. (1991). "Seismic resistance of steel frames with semi-rigid connections. ." MSc dissertation, Imperial College, University of London, London, UK.

Rutenberg, A. (1975). "Approximate natural frequencies for coupled shear walls." *Earthquake Engineering and Structural Dynamics*, 4, 95-100.

Rutenberg, A. (1975). "Approximate natural frequencies for coupled shear walls " *Earthquake Engineering and Structural Dynamics*, 4(1), 95-100.

Rutenberg, A. (1975). "Approximate natural frequencies for coupled shear walls." *Earthquake Engineering and Structural Dynamics*, 4(1), 95-100.

Salvatore, W., Bursi, O. S., and Lucchesi, D. (2005). "Design, testing and analysis of high ductile partial-strength steel–concrete composite beam-to-column joints." *Journal of Computers and Structures* 83 2334-2352.

SCI Report. Partial strength moment resisting connections in composite frames. The Steel Construction Institute April, 1992.

Sekulovic, M., Salatic, R., and Nefovska, M. (2002). "Dynamic analysis of steel frames with flexible connections." *Computers and Structures*, 80(11), 935-955.

Shim, C. S., Lee, P. G., and Yoon, T. Y. (2004). "Static behavior of large stud shear connectors." *Engineering Structures*, 26(12), 1853-1860.

Silva, S. d., Santiago, A., and Real, P. V. (2002). "Post-limit stiffness and ductility of end-plate beam-to-column steel joints." *Computers and Structures* 80 (2002), 515-531.

Skattum, K. S. (1971). "Dynamic analysis of coupled shear walls and sandwich beams."PhD Thesis, California Institute of Technology, Pasadena, California.

Skattum, K. S. (1971). "Dynamic analysis of coupled shear walls and sandwich beams." PhD Thesis, California Institute of Technology, Pasadena, California.

Smith, B. S., and Crowe, E. (1986). "Estimating periods of vibration of tall buildings." *Journal of structural engineering New York, N.Y.*, 112(5), 1005-1019.

Smith, S. B., and Crowe, E. (1986). "Estimating periods of vibration of tall buildings " *Journal of structural engineering New York, N.Y.*, 112(5), 1005-1019.

Tamai, S., Shima, H., Izumo, J., and Okamura, H. "Average stress-strain relationship in post yield range of steel bar in concrete." *Concrete Library of JSCE*,1988: 117-129.

Tamai, S., Shima, H., Izumo, J., and Okamura, H. (1988.). "Average stress-strain relationship in post yield range of steel bar in concrete." *Concrete Library of JSCE* 11, 117-129.

Titoum, M., Tehami, M., and Achour, B. (2009). "Effects of partial shear connection on the behavior of semi-continuous composite beams." *International Journal of Steel Structures*, 9(4), 301-313.

Titoum, M., Tehami, M., Achour, B., and Jaspart, J. P. (2008). "Analysis of semi-continuous composite beams with partial shear connection using 2-D finite element approach." *Asian Journal of Applied Sciences*, 1(3), 185-205.

Vasdravellis, G., Valente, M., and Castiglioni, C. A. (2009). "Behavior of exterior partial-strength composite beam-to-column connections: Experimental study and numerical simulations." *Journal of Constructional Steel Research* 65 23-35.

Vellascoa, P. C. G., Andradec, S. A. L., and Silvab, J. G. S. (2006). "A parametric analysis of steel and composite portal frames with semi-rigid connections." *Journal of Engineering Structures*, 28 543-556.

Wang, Q., Liu, Y., Luo, J., and Lebet, J. P. "Experimental study on stud shear connectors with large diameter and high strength." Lushan,2011: 340-343.

Wang, Y. C. (1998). "Deflection of steel-concrete composite beams with partial shear interaction." *Journal of Structural Engineering*, 124(10), 1159-1165.

Weynand, K., Jaspart, J. P., and Steenhuis, M. "The Stiffness Model of revised Annex J of Eurocode 3." *Connections in steel structures III [Proceedings of the 3rd international workshop on connections in steel structures]*,1996: 441-452.

Wong, Y. L., Yu, T., and Chan, S. L. (2007). "A simplified analytical method for unbraced composite frames with semi-rigid connections." *Journal of Constructional Steel Research*, 63(7), 961-969.

Wong, Y. L., Yu, T., and Chan, S. L. (2007). "A simplified analytical method for unbraced composite frames with semi-rigid connections." *Journal of Constructional Steel Research* 63 961-969.

Xiao, Y. (1994). "Behaviour of composite connections in steel and concrete."PhD Thesis, Department of Civil Engineering, University of Nottingham, UK.

Xiao, Y., Choo, B. S., and Nethercot, D. A. (1994). "Composite connections in steel and concrete. I. Experimental behaviour of composite beam-Column connections." *Journal of Constructional Steel Research*, 31(1), 3-30.

Xiao, Y., Choo, B. S., and Nethercot, D. A. (1996). "Composite connections in steel and concrete. Part 2 Moment Capacity of End Plate Beam to Column Connections." *Journal of Constructional Steel Research*, 37(1), 63-90.

Xiao, Y., Nethercot, D. A., and Choo, B. S. (1992). *Design of semi-rigid composite beam-column connections* ,F. K. Garas et al. E & FN Spon, London.

Xue, D., Liu, Y., Yu, Z., and He, J. (2012). "Static behavior of multi-stud shear connectors for steel-concrete composite bridge." *Journal of Constructional Steel Research*, 74, 1-7.

Xue, W., Ding, M., Wang, H., and Luo, Z. (2008). "Static behavior and theoretical model of stud shear connectors." *Journal of Bridge Engineering*, 13(6), 623-634.

Xue, W., Ding, M., Wang, H., and Luo, Z. (2009). "Experimental studies on behavior of stud shear connectors under monotonic loads." *Jianzhu Jiegou Xuebao/Journal of Building Structures*, 30(1), 95-100.

Zalka, K. A. (2001). "A simplified method for calculation of the natural frequencies of wall-frame buildings." *Engineering Structures*, 23(12), 1544-1555.

Appendix-A1

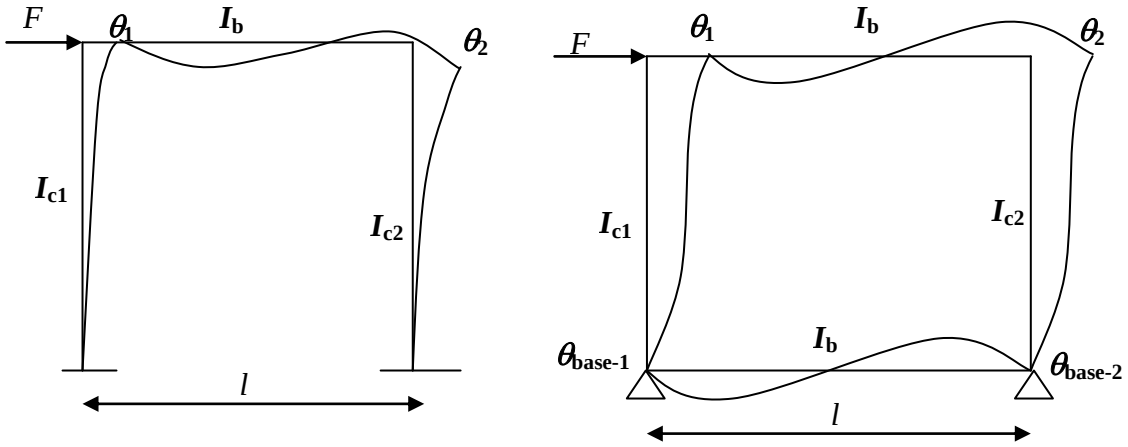

a) b)

Figure A. 1: a) First b) Middle and Top storey frames

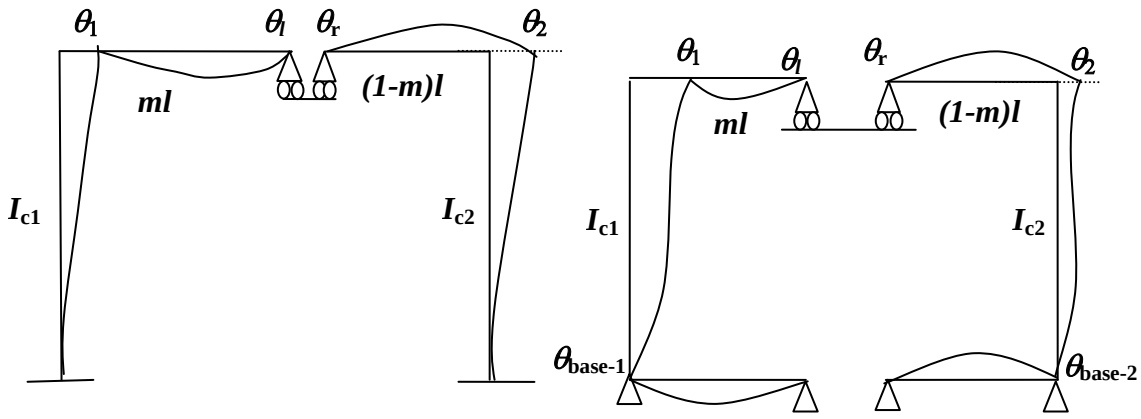

a) b)

Figure A. 2: a) First storey model b) Middle and top storeys model

1. Derivation of the main equations:

Let $S_1 = 2 + \frac{\theta_{base}}{\theta_1}$ and $S_2 = 2 + \frac{\theta_{base}}{\theta_2}$

Left side of model (a and b)

$$M_{c1} = \frac{2EI_{c1}}{h}\left(S_1\theta_1 - \frac{3\Delta}{h} \right) \qquad \text{(A.1)}$$

$$M_{b\text{-}l} = \frac{2EI_b}{ml}\left(2\theta_1 + \theta_l\right) \tag{A.2}$$

Right side of model:

$$M_{c2} = \frac{2EI_{c2}}{h}\left(S_2\theta_2 - \frac{3\Delta}{h}\right) \tag{A.3}$$

$$M_{b\text{-}r} = \frac{2EI_b}{(1-m)L}\left(2\theta_2 + \theta_r\right) \tag{A.4}$$

At virtual hinge:

$$M_{o\text{-}l} = \frac{2EI_b}{ml}\left(2\theta_{l+}\theta_1\right) = 0 \qquad \rightarrow \qquad \theta_l = -\frac{\theta_1}{2} \tag{A.5}$$

$$M_{o\text{-}r} = \frac{2EI_b}{(1-m)l}\left(2\theta_r + \theta_2\right) = 0 \qquad \rightarrow \qquad \theta_r = -\frac{\theta_2}{2} \tag{A.6}$$

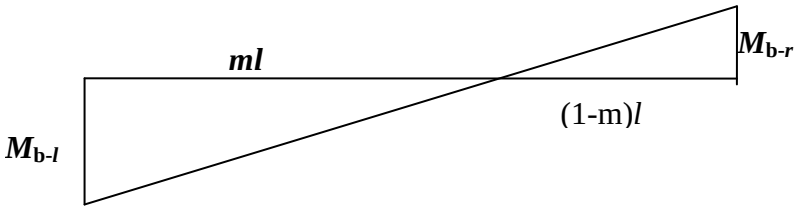

Figure A. 3: Bending moment diagram of beam

From Figure A.3, it is seen that**:**

$$\frac{M_{b\text{-}l}}{M_{b\text{-}r}} = \frac{ml}{(1-m)l} = \frac{m}{(1-m)} \tag{A.7}$$

$$\because \frac{M_{b\text{-}l}}{M_{b\text{-}r}} = \frac{\frac{2EI_b}{ml}\left(2\theta_1 + \theta_l\right)}{\frac{2EI_b}{(1-m)l}\left(2\theta_2 + \theta_r\right)} = \frac{(1-m)\left(2\theta_1 + \theta_l\right)}{(m)\left(2\theta_2 + \theta_r\right)}$$

$$\therefore \frac{M_{b\text{-}l}}{M_{b\text{-}r}} = \frac{(1-m)\left(2\theta_1 - \frac{\theta_1}{2}\right)}{(m)\left(2\theta_2 - \frac{\theta_2}{2}\right)} = \frac{(1-m)\left(\theta_1\right)}{(m)\left(\theta_2\right)} \tag{A.8}$$

From Eq. (A.7) & Eq. (A.8), results:

$$\frac{\theta_1}{\theta_2} = \frac{(m)^2}{(1-m)^2} \tag{A.9}$$

$$\because M_{c1} + M_{b\text{-}l} = 0 \qquad \& \quad M_{c2} + M_{b\text{-}r} = 0$$

$$\frac{2EI_{c1}}{h}\left(S_1\theta_1 - \frac{3\Delta}{h}\right) + \frac{2EI_b}{ml}\left(2\theta_1 + \theta_l\right) = \frac{2EI_{c1}}{h}\left(S_1\theta_1 - \frac{3\Delta}{h}\right) + \frac{2EI_b}{ml}\left(2\theta_1 - \theta_1/2\right) = 0$$

and $$\frac{2EI_{c2}}{h}\left(S_2\theta_2 - \frac{3\Delta}{h}\right) + \frac{2EI_b}{(1-m)l}\left(2\theta_2 - \theta_2/2\right) = 0$$

Let $$k_{c1} = \frac{I_{c1}}{h} \quad \& \quad k_{c2} = \frac{I_{c2}}{h} \quad \& \quad k_b = \frac{I_b}{l}$$

$$\overline{K}_1 = \frac{k_{b1}}{k_{c1}} \quad \& \; \overline{K}_2 = \frac{k_b}{k_{c2}}$$

$$\therefore \frac{\Delta}{h} = \frac{\theta_1}{3}\left(S_1 + \frac{3\overline{K}_1}{2m}\right) = \frac{\theta_2}{3}\left(S_2 + \frac{3\overline{K}_2}{2(1-m)}\right) \tag{A.10}$$

From Eq. (A.9) and Eq. (A.10), results:

$$\frac{(m)^2}{(1-m)^2} = \frac{\left(S_2 + \frac{3\overline{K}_2}{2(1-m)}\right)}{\left(S_1 + \frac{3\overline{K}_1}{2m}\right)} = \frac{m}{(1-m)} \frac{\left(2S_2(1-m) + 3\overline{K}_2\right)}{\left(2S_1 m + 3\overline{K}_1\right)}$$

$$\therefore \frac{m}{(1-m)} = \frac{\left(2S_2(1-m) + 3\overline{K}_2\right)}{\left(2S_1 m + 3\overline{K}_1\right)}$$

$$2m^2\left(S_1 - S_2\right) + m\left(3\overline{K}_1 + 3\overline{K}_2 + 4S_2\right) - \left(2S_2 + 3\overline{K}_2\right) = 0 \tag{A.11}$$

2. Determine *S* & *m*

First storey

1. Fixed base

$$\because M_{c1} = 2Ek_{c1}\left(2\theta_1 - \frac{3\Delta}{h}\right) \quad \& \; M_{c2} = 2Ek_{c2}\left(2\theta_2 - \frac{3\Delta}{h}\right)$$

By comparing with Eq. (A.1) & Eq. (A.3):

$$\therefore S_1 = S_2 = 2 \tag{A.12}$$

By substituting Eq. (A.12) in Eq. (A.11), results:

$$m = \frac{3\overline{K}_2 + 4}{3\left(\overline{K}_1 + \overline{K}_2\right) + 8} \tag{A.13}$$

2. Pinned base

$$\because M_{c1} = 2Ek_{c1}\left(2\theta_1 + \theta_{base\text{-}1} - \frac{3\Delta}{h}\right) \quad \& \; M_{base\text{-}1} = 2Ek_{c1}\left(2\theta_{base\text{-}1} + \theta_1 - \frac{3\Delta}{h}\right) = 0$$

$$\therefore \theta_{base-1} = -\frac{\left(\theta_1 - \frac{3\Delta}{h}\right)}{2} \quad \& \; M_{c1} = 3Ek_{c1}\left(\theta_1 - \frac{\Delta}{h}\right) \tag{A.14}$$

By substituting Eq. (A.14) in Eq. (A.1), results:

$$3Ek_{c1}\left(\theta_1 - \frac{\Delta}{h}\right) = 2Ek_{c1}\left(S_1\theta_1 - \frac{3\Delta}{h}\right)$$

$$\therefore \frac{\Delta}{h} = \frac{\theta_1}{3}\left(2S_1 - 3\right) \tag{A.15}$$

By substituting Eq. (A.15) in Eq. (A.10), results:

$$S_1 = \left(3 + \frac{3\overline{K}_1}{2m}\right) \tag{A.16}$$

In the same manner, it can be found that:

$$S_2 = \left(3 + \frac{3\overline{K}_2}{2(1-m)} \right) \tag{A.17}$$

By substituting S_1 & S_2 in Eq. (A.11), results that:

$$m^2\left(\overline{K}_1 + \overline{K}_2 + 2\right) - m\left(\overline{K}_1 + 2\overline{K}_2 + 3\right) + \left(\overline{K}_2 + 1\right) = 0$$

$$\therefore m = \frac{\overline{K}_2 + 1}{\left(\overline{K}_1 + \overline{K}_2 + 2\right)} \tag{A.18}$$

Middle and top stories

$$\because M_{c1} = 2Ek_{c1}\left(3\theta_1 - \frac{3\Delta}{h}\right) \quad \& \quad M_{c2} = 2Ek_{c2}\left(3\theta_2 - \frac{3\Delta}{h}\right)$$

By comparing with Eq. (A.1) and (A.3), results:

$$\therefore S_1 = S_2 = 3 \tag{A.19}$$

By substituting S1 & S2 in Eq. (A.11), results that:

$$m = \frac{\overline{K}_2 + 2}{\left(\overline{K}_1 + \overline{K}_2 + 4\right)} \tag{A.20}$$

3. Determine D_{value} in term of m

First storey

1. Fixed base

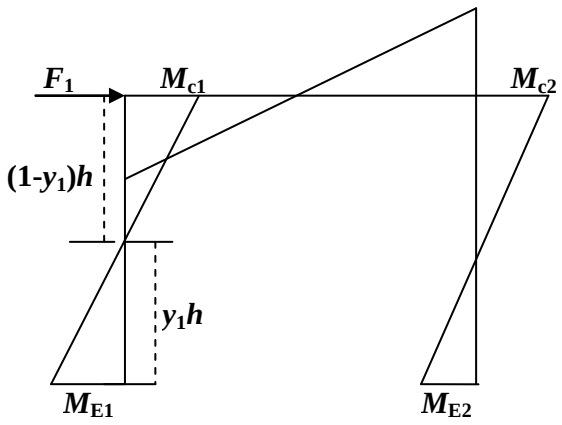

Figure A. 4: First storey-fixed ends

$$\because -F_1 h = M_{c1} + M_{E1} \qquad \& \qquad -F_2 h = M_{c2} + M_{E2}$$

$$\therefore -F_1 h = 2Ek_{c1}\left(2\theta_1 - \frac{3\Delta}{h}\right) + 2Ek_{c1}\left(\theta_1 - \frac{3\Delta}{h}\right) = 12Ek_{c1}\left(\frac{\theta_1}{2} - \frac{\Delta}{h}\right)$$

$$\therefore F_1 = \left[\frac{12E}{h^2}\right]k_{c1}\left(\Delta - \frac{h\theta_1}{2}\right) \qquad \text{(A.21)}$$

By substituting Eq. (A.10) and Eq. (A.12) in Eq. (A.21), results that:

$$D_1 = \frac{F_1}{\Delta} = \left[\frac{12E}{h^2}\right]k_{c1}\left(\frac{3\overline{K}_1 + m}{3\overline{K}_1 + 4m}\right) \quad \& \quad D_2 = \frac{F_2}{\Delta} = \left[\frac{12E}{h^2}\right]k_{c2}\left(\frac{3\overline{K}_2 - m + 1)}{3\overline{K}_2 - 4m + 4}\right)$$

2. Pinned base

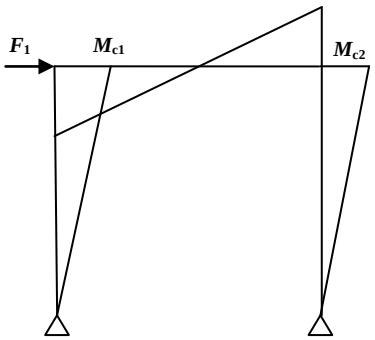

Figure A. 5: First storey-pinned ends

$$\because -F_1 h = M_{c1} \quad \& \quad -F_2 h = M_{c2}$$

$$\therefore -F_1 h = 2Ek_{c1}\left(S_1\theta_1 - \frac{3\Delta}{h}\right) \qquad \text{(A.22)}$$

By substituting Eq. (A.10) and Eq. (A.16) in Eq. (A.22), results that:

$$-F_1 h = 2Ek_{c1}\left(\left(3 + \frac{3\overline{K}_1}{2m}\right)\left(\frac{3\Delta}{h\left(3 + \frac{3\overline{K}_1}{m}\right)}\right) - \frac{3\Delta}{h}\right)$$

$$D_1 = \frac{F_1}{\Delta} = \left[\frac{12E}{h^2}\right]k_{c1}\left(\frac{\overline{K}_1}{4\overline{K}_1 + 4m}\right) \quad \& \quad D_2 = \frac{F_2}{\Delta} = \left[\frac{12E}{h^2}\right]k_{c2}\left(\frac{\overline{K}_2}{4\overline{K}_2 + 4(1-m))}\right)$$

Middle and top stories

$$\because -F_1 h = 2M_{c1} \quad \& \quad -F_2 h = 2M_{c2} \tag{A.23}$$

By substituting Eq. (A.1), Eq. (A.10) and Eq. (A.19) in Eq. (A.23), results that:

$$-F_1 h = 4Ek_{c1}\left(3\left(\frac{3\Delta}{h\left(3+\frac{3\overline{K}_1}{2m}\right)}\right)-\frac{3\Delta}{h}\right)$$

$$D_1 = \frac{F_1}{\Delta} = \left[\frac{12E}{h^2}\right]k_{c1}\left(\frac{\overline{K}_1}{\overline{K}_1+2m}\right) \quad \& \quad D_2 = \frac{F_2}{\Delta} = \left[\frac{12E}{h^2}\right]k_{c2}\left(\frac{\overline{K}_2}{\overline{K}_2+2(1-m)}\right)$$

Position of inflection point of column in first storey

$$M_{c1} = 2Ek_{c1}\left(2\theta_1 - \frac{3\Delta}{h}\right) \quad \& \quad M_{E1} = 2Ek_{c1}\left(\theta_1 - \frac{3\Delta}{h}\right) \tag{A.24}$$

$$M_{c2} = 2Ek_{c2}\left(2\theta_2 - \frac{3\Delta}{h}\right) \quad \& \quad M_{E2} = 2Ek_{c2}\left(\theta_2 - \frac{3\Delta}{h}\right) \tag{A.25}$$

$$\frac{M_{E1}}{M_{c1}} = \frac{y_1}{(1-y_1)} \tag{A.26}$$

$$\therefore \frac{\left(\theta_1 - \frac{3\Delta}{h}\right)}{\left(2\theta_1 - \frac{3\Delta}{h}\right)} = \frac{y_1}{(1-y_1)} \quad \rightarrow \quad \frac{\Delta}{h} = \frac{\theta_1}{3}\left[\frac{(1-3y_1)}{(1-2y_1)}\right] \tag{A.27}$$

By substituting Eq. (A.10) and Eq. (A.12) in Eq. (A.27), results that:

$$\left[\frac{(1-3y_1)}{(1-2y_1)}\right] = \left(2+\frac{3\overline{K}_1}{2m}\right)$$

$$y_1 = \frac{3\overline{K}_1+2m}{6\overline{K}_1+2m} \quad \& \quad y_2 = \frac{3\overline{K}_2+2(1-m)}{6\overline{K}_2+2(1-m)} \tag{A.29}$$

Appendix-B

First storey (for case m=0.5)

1. Fixed base (Figure 9.3)

$$M_{AB} = 2Ek_{2,j}^{C}\left(2\theta_A + \theta_B - 3\frac{\Delta_{1,j}^{u}}{h}\right) \;;\quad M_{BA} = 2Ek_{2,j}^{C}\left(2\theta_B + \theta_A - 3\frac{\Delta_{1,j}^{u}}{h}\right) \tag{B.1}$$

$$M_{AB} + M_{BA} = 0 \rightarrow 2Ek_{2,j}^{C}\left(2\theta_A + \theta_B - 3\frac{\Delta_{1,j}^{u}}{h}\right) + 2Ek_{2,j}^{C}\left(\theta_A + 2\theta_B - 3\frac{\Delta_{1,j}^{u}}{h}\right) = 0 \tag{B.2}$$

let $\quad k_c = \frac{I_c}{h} \;;\quad k_b = \frac{I_b}{L} \;;\quad \beta_{1,j} = \frac{k_{1,j}^{C}}{k_{2,j}^{C}}$

$$\therefore \left(\theta_A + \theta_B\right) = 2\frac{\Delta_{1,j}^{u}}{h} \tag{B.3}$$

$$M_{BA} + M_{BG} + M_{BF} = 0 \tag{B.4}$$

$$2Ek_{2,j}^{C}\left(2\theta_B + \theta_A - 3\frac{\Delta_{1,j}^{u}}{h}\right) + 4Ek_{2,j-1}^{B}\left(\frac{3}{2}\theta_B\right) + 4Ek_{2,j}^{B}\left(\frac{3}{2}\theta_B\right) = 0$$

$$\left(2\theta_B + \theta_A - 3\frac{\left(\theta_A + \theta_B\right)}{2}\right) + 3\theta_B\left(\frac{k_{2,j-1}^{B} + k_{2,j}^{B}}{k_{2,j}^{C}}\right) = 0$$

$$\theta_B = \frac{\theta_A}{1 + 6\left(\frac{k_{2,j-1}^{B} + k_{2,j}^{B}}{k_{2,j}^{C}}\right)} \quad \rightarrow \quad \theta_B = \frac{\theta_A}{1 + 6\overline{K}_{2,j}^{u}} \tag{B.5}$$

From Eq. (B.3) and Eq. (B.5), results:

$$\therefore \frac{\Delta_{1,j}^{u}}{h} = \frac{1}{2}\theta_A\left(\frac{2 + 6\overline{K}_{2,j}^{u}}{1 + 6\overline{K}_{2,j}^{u}}\right) \tag{B.6}$$

$$M_{AB} + M_{AE} + M_{AC} + M_{AD} = 0 \tag{B.7}$$

$$2Ek_{2,j}^{C}\left(2\theta_A + \theta_B - 3\frac{\Delta_{1,j}^{u}}{h}\right) + 2Ek_{1,j}^{C}\left(2\theta_A - 3\frac{\Delta_{1,j}}{h}\right) + 4Ek_{1,j-1}^{B}\left(\frac{3}{2}\theta_A\right) + 4Ek_{1,j}^{B}\left(\frac{3}{2}\theta_A\right) = 0$$

$$k_{2,j}^{C}\left(2\theta_A+\theta_B-3\frac{(\theta_A+\theta_B)}{2}\right)+k_{1,j}^{C}\left(2\theta_A-3\frac{\Delta_{1,j}}{h}\right)+3\theta_A\left(k_{1,j-1}^{B}+k_{1,j}^{B}\right)=0$$

$$\theta_A\left(\frac{1}{2}+2\beta_{1,j}+3\left(\frac{k_{1,j-1}^{B}+k_{1,j}^{B}}{k_{2,j}^{C}}\right)\right)-\frac{\theta_B}{2}=3\beta_{1,j}\frac{\Delta_{1,j}}{h}$$

$$\theta_A=\frac{\left(3\beta_{1,j}\frac{\Delta_{1,j}}{h}+\frac{\theta_B}{2}\right)}{\left(\frac{1}{2}+2\beta_{1,j}+3\frac{k_{1,j-1}^{B}+k_{1,j}^{B}}{k_{2,j}^{C}}\right)}\quad\rightarrow\quad\theta_A=\frac{\left(3\beta_{1,j}\frac{\Delta_{1,j}}{h}+\frac{\theta_B}{2}\right)}{\left(\frac{1}{2}+2\beta_{1,j}+3\overline{K}_{1,j}^{d}\right)}\tag{B.8}$$

$$\theta_A=\left[\frac{6\beta_{1,j}\left(1+6\overline{K}_{2,j}^{u}\right)}{\left(1+4\beta_{1,j}+6\overline{K}_{1,j}^{d}\right)\left(1+6\overline{K}_{2,j}^{u}\right)-1}\right]\frac{\Delta_{1,j}}{h}\tag{B.9}$$

From Eq. (B.6) and Eq. (B.9), results:

$$\Delta_{1,j}^{u}=\left[\frac{6\beta_{1,j}\left(1+3\overline{K}_{2,j}^{u}\right)}{\left(1+4\beta_{1,j}+6\overline{K}_{1,j}^{d}\right)\left(1+6\overline{K}_{2,j}^{u}\right)-1}\right]\Delta_{1,j}\tag{B.10}$$

$$-F_{1,j}h=M_{AE}+M_{EA}\tag{B.11}$$

$$-F_{1,j}h=2Ek_{1,j}^{C}\left(2\theta_A-3\frac{\Delta_{1,j}}{h}\right)+2Ek_{1,j}^{C}\left(\theta_A-3\frac{\Delta_{1,j}}{h}\right)$$

$$-F_{1,j}h=6Ek_{1,j}^{C}\left(\theta_A-2\frac{\Delta_{1,j}}{h}\right)\tag{B.12}$$

By substituting Eq. (B.9) in Eq. (B.12), results:

$$F_{1,j}h=6Ek_{1,j}^{C}\frac{\Delta_{1,j}}{h}\left(2-\left[\frac{6\beta_{1,j}\left(1+6\overline{K}_{2,j}^{u}\right)}{\left(1+4\beta_{1,j}+6\overline{K}_{1,j}^{d}\right)\left(1+6\overline{K}_{2,j}^{u}\right)-1}\right]\right)$$

$$D_{1,j}=\frac{F_{1,j}}{\Delta_{1,j}}=\left[\frac{12E}{h^2}\right]k_{1,j}^{C}\left(1-\left[\frac{3\beta_{1,j}\left(1+6\overline{K}_{2,j}^{u}\right)}{\left(1+4\beta_{1,j}+6\overline{K}_{1,j}^{d}\right)\left(1+6\overline{K}_{2,j}^{u}\right)-1}\right]\right)\tag{B.13}$$

where

$$\overline{K}^{u}_{2,j} = \frac{k^{B}_{2,j\text{-}1} + k^{B}_{2,j}}{k^{C}_{2,j}} \quad ; \quad k^{B}_{2,j\text{-}1} = \frac{I^{B}_{2,j\text{-}1}}{2L_{2,j\text{-}1}} \quad ; \; k^{B}_{2,j} = \frac{I^{B}_{2,j}}{2L_{2,j}}$$

$$\overline{K}^{d}_{1,j} = \frac{k^{B}_{1,j\text{-}1} + k^{B}_{1,j}}{k^{C}_{2,j}} \quad ; k^{B}_{1,j\text{-}1} = \frac{I^{B}_{1,j\text{-}1}}{L_{1,j\text{-}1}} ; k^{B}_{1,j} = \frac{I^{B}_{1,j}}{L_{1,j}}$$

2. Pinned base (see Figure 9.4)

$$M_{AB} = 2Ek^{C}_{2,j}\left(2\theta_A + \theta_B - 3\frac{\Delta^{u}_{1,j}}{h}\right) \; ; \qquad M_{BA} = 2Ek^{C}_{2,j}\left(2\theta_B + \theta_A - 3\frac{\Delta^{u}_{1,j}}{h}\right) \tag{B.14}$$

$$M_{AB} + M_{BA} = 0 \rightarrow 2Ek^{C}_{2,j}\left(2\theta_A + \theta_B - 3\frac{\Delta^{u}_{1,j}}{h}\right) + 2Ek^{C}_{2,j}\left(\theta_A + 2\theta_B - 3\frac{\Delta^{u}_{1,j}}{h}\right) = 0 \tag{B.15}$$

$$\left(\theta_A + \theta_B\right) = 2\frac{\Delta^{u}_{1,j}}{h} \tag{B.16}$$

$$M_{EA} = 0 \rightarrow 2Ek^{C}_{1,j}\left(2\theta_E + \theta_A - 3\frac{\Delta_{1,j}}{h}\right) = 0 \rightarrow \theta_E = \frac{1}{2}\left(3\frac{\Delta_{1,j}}{h} - \theta_A\right) \tag{B.17}$$

$$M_{BA} + M_{BF} + M_{BG} = 0 \tag{B.18}$$

$$2Ek^{C}_{2,j}\left(2\theta_B + \theta_A - 3\frac{\Delta^{u}_{1,j}}{h}\right) + 4Ek^{B}_{2,j\text{-}1}\left(\frac{3}{2}\theta_B\right) + 4Ek^{B}_{2,j}\left(\frac{3}{2}\theta_B\right) = 0$$

$$\left(2\theta_B + \theta_A - 3\frac{\left(\theta_A + \theta_B\right)}{2}\right) + 3\theta_B\left(\frac{k^{B}_{2,j\text{-}1} + k^{B}_{2,j}}{k^{C}_{2,j}}\right) = 0$$

$$\theta_B = \frac{\theta_A}{1 + 6\left(\frac{k^{B}_{2,j\text{-}1} + k^{B}_{2,j}}{k^{C}_{2,j}}\right)} \rightarrow \theta_B = \frac{\theta_A}{1 + 6\overline{K}^{u}_{2,j}} \tag{B.19}$$

From Eq. (B.16) and Eq. (B.19), results:

$$\frac{\Delta^{u}_{1,j}}{h} = \frac{1}{2}\theta_A\left(\frac{2 + 6\overline{K}^{u}_{2,j}}{1 + 6\overline{K}^{u}_{2,j}}\right) \tag{B.20}$$

$$M_{AB} + M_{AE} + M_{AC} + M_{AD} = 0 \tag{B.21}$$

$$2Ek^{C}_{2,j}\left(2\theta_A + \theta_B - 3\frac{\Delta^{u}_{1,j}}{h}\right) + 2Ek^{C}_{1,j}\left(2\theta_A + \theta_E - 3\frac{\Delta_{1,j}}{h}\right) + 6E\theta_A\left(k^{B}_{1,j\text{-}1} + k^{B}_{1,j}\right) = 0$$

$$\left(2\theta_A+\theta_B-3\frac{(\theta_A+\theta_B)}{2}\right)+\beta_{1,j}\left(2\theta_A+\theta_E-3\frac{\Delta_{1,j}}{h}\right)+3\theta_A\left(\frac{k^B_{1,j\text{-}1}+k^B_{1,j}}{k^C_{2,j}}\right)=0$$

$$\theta_A\left(\frac{1}{2}\left(1+3\beta_{1,j}\right)+3\left(\frac{k^B_{1,j\text{-}1}+k^B_{1,j}}{k^C_{2,j}}\right)\right)=\frac{1}{2}\left(3\beta_{1,j}\frac{\Delta_{1,j}}{h}+\theta_B\right)$$

$$\theta_A\left(\frac{1}{2}\left(1+3\beta_{1,j}\right)+3\overline{K}^d_{1,j}\right)=\frac{1}{2}\left(3\beta_{1,j}\frac{\Delta_{1,j}}{h}+\frac{\theta_A}{1+6\overline{K}^u_{2,j}}\right)$$

$$\theta_A=\left[\frac{3\beta_{1,j}\left(1+6\overline{K}^u_{2,j}\right)}{\left(1+3\beta_{1,j}+6\overline{K}^d_{1,j}\right)\left(1+6\overline{K}^u_{2,j}\right)\text{-}1}\right]\frac{\Delta_{1,j}}{h} \qquad \text{(B.22)}$$

From Eq. (B.20) and Eq. (B.22), results:

$$\Delta^u_{1,j}=\left[\frac{3\beta_{1,j}\left(1+3\overline{K}^u_{2,j}\right)}{\left(1+3\beta_{1,j}+6\overline{K}^d_{1,j}\right)\left(1+6\overline{K}^u_{2,j}\right)-1}\right]\Delta_{1,j}$$

$$\text{-}F_{1,j}h=M_{AE} \qquad \text{(B.23)}$$

$$\text{-}F_{1,j}h=2Ek^C_{1,j}\left(2\theta_A+\theta_E-3\frac{\Delta_{1,j}}{h}\right)=3Ek^C_{1,j}\left(\theta_A-\frac{\Delta_{1,j}}{h}\right)$$

$$F_{1,j}h=3Ek^C_{1,j}\frac{\Delta_{1,j}}{h}\left(\frac{6\left(\overline{K}^d_{1,j}+\overline{K}^u_{2,j}+6\overline{K}^d_{1,j}\overline{K}^u_{2,j}\right)}{\left(1+3\beta_{1,j}+6\overline{K}^d_{1,j}\right)\left(1+6\overline{K}^u_{2,j}\right)\text{-}1}\right)$$

$$D_{1,j}=\frac{F_{1,j}}{\Delta_{1,j}}=\left[\frac{12E}{h^2}\right]k^C_{1,j}\left(\frac{\left(\overline{K}^d_{1,j}+\overline{K}^u_{2,j}+6\overline{K}^u_{2,j}\overline{K}^d_{1,j}\right)}{4\left[\frac{\beta_{1,j}}{2}+3\beta_{1,j}\overline{K}^u_{2,j}+\overline{K}^d_{1,j}+\overline{K}^u_{2,j}+6\overline{K}^u_{2,j}\overline{K}^d_{1,j}\right]}\right) \qquad \text{(B.24)}$$

where:

$$\overline{K}^u_{2,j}=\frac{k^B_{2,j\text{-}1}+k^B_{2,j}}{k^C_{2,j}}\ ;\ k^B_{2,j\text{-}1}=\frac{I^B_{2,j\text{-}1}}{2L_{2,j\text{-}1}}\ ;\ k^B_{2,j}=\frac{I^B_{2,j}}{2L_{2,j}}$$

$$\overline{K}^d_{1,j}=\frac{k^B_{1,j\text{-}1}+k^B_{1,j}}{k^C_{2,j}}\ ;\ k^B_{1,j\text{-}1}=\frac{I^B_{1,j\text{-}1}}{L_{1,j\text{-}1}}\ ;k^B_{1,j}=\frac{I^B_{1,j}}{L_{1,j}}$$

Middle stories (for case m=0.5) (see Figure 9.5)

$$M_{AB} = 2Ek^{C}_{i+1,j}\left(2\theta_A + \theta_B - 3\frac{\Delta^{u}_{i+1,j}}{h}\right) \quad ; \quad M_{BA} = 2Ek^{C}_{i+1,j}\left(2\theta_B + \theta_A - 3\frac{\Delta^{u}_{i+1,j}}{h}\right) \tag{B.25}$$

$$M_{AB} + M_{BA} = 0 \rightarrow 2Ek^{C}_{i+1,j}\left(2\theta_A + \theta_B - 3\frac{\Delta^{u}_{i+1,j}}{h}\right) + 2Ek^{C}_{i+1,j}\left(\theta_A + 2\theta_B - 3\frac{\Delta^{u}_{i+1,j}}{h}\right) = 0 \tag{B.26}$$

Let $\quad k_c = \frac{I_c}{h} \;\; ; \;\; k_b = \frac{I_b}{L} \;\; ; \; \beta_{i,j} = \frac{k^{C}_{i,j}}{k^{C}_{i+1,j}}$

$$\left(\theta_A + \theta_B\right) = 2\frac{\Delta^{u}_{i+1,j}}{h} \tag{B.27}$$

$$M_{EA} + M_{EF} + M_{EG} = 0 \tag{B.28}$$

$$2Ek^{C}_{i,j}\left(2\theta_E + \theta_A - 3\frac{\Delta_{i,j}}{h}\right) + 4Ek^{B}_{i\text{-}1,j\text{-}1}\left(\frac{3}{2}\theta_E\right) + 4Ek^{B}_{i\text{-}1,j}\left(\frac{3}{2}\theta_E\right) = 0$$

$$\theta_E = \frac{\left(3\frac{\Delta_{i,j}}{h} - \theta_A\right)}{\left(2 + 3\left(\frac{k^{B}_{i\text{-}1,j\text{-}1} + k^{B}_{i\text{-}1,j}}{k^{C}_{i,j}}\right)\right)} \rightarrow \theta_E = \frac{\left(3\frac{\Delta_{i,j}}{h} - \theta_A\right)}{\left(2 + 3\overline{K}_D\right)} \tag{B.29}$$

$$M_{BA} + M_{BH} + M_{BI} = 0 \tag{B.30}$$

$$2Ek^{C}_{i+1,j}\left(2\theta_B + \theta_A - 3\frac{\Delta^{u}_{i+1,j}}{h}\right) + 4Ek^{B}_{i+1,j\text{-}1}\left(\frac{3}{2}\theta_B\right) + 4Ek^{B}_{i+1,j}\left(\frac{3}{2}\theta_B\right) = 0$$

$$\left(2\theta_B + \theta_A - 3\frac{\left(\theta_A + \theta_B\right)}{2}\right) + 3\theta_B\left(\frac{k^{B}_{i+1,j-1} + k^{B}_{i+1,j}}{k^{C}_{i+1,j}}\right) = 0$$

$$\theta_B = \frac{\theta_A}{1 + 6\left(\frac{k^{B}_{i+1,j-1} + k^{B}_{i+1,j}}{k^{C}_{i+1,j}}\right)} \rightarrow \theta_B = \frac{\theta_A}{1 + 6\overline{K}^{u}_{i+1,j}} \tag{B.31}$$

From Eq. (B.27) and Eq. (B.31), results:

$$\frac{\Delta^{u}_{i+1,j}}{h} = \frac{1}{2}\theta_A\left(\frac{2 + 6\overline{K}^{u}_{i+1,j}}{1 + 6\overline{K}^{u}_{i+1,j}}\right) \tag{B.32}$$

$$0\, M_{AB} + M_{AE} + M_{AC} + M_{AD} = 0 \tag{B.33}$$

$$2Ek_{i+1,j}^{C}\left(2\theta_A+\theta_B-3\frac{\Delta_{i+1,j}^{u}}{h}\right)+2Ek_{i,j}^{C}\left(2\theta_A+\theta_E-3\frac{\Delta_{i,j}}{h}\right)+6E\theta_A\left(k_{i,j\text{-}1}^{B}+k_{i,j}^{B}\right)=0$$

$$\left(\frac{1}{2}\theta_A+2\beta_{i,j}-\frac{1}{2}\theta_B\right)+\beta_{i,j}\left(\frac{\left(3\frac{\Delta_{i,j}}{h}-\theta_A\right)}{\left(2+3\overline{K}_{i\text{-}1,j}^{D}\right)}-3\frac{\Delta_{i,j}}{h}\right)+3\theta_A\left(\frac{k_{i,j\text{-}1}^{B}+k_{i,j}^{B}}{k_{i+1,j}^{C}}\right)=0$$

$$\theta_A\left(\frac{1}{2}+2\beta_{i,j}-\frac{\beta_{i,j}}{\left(2+3\overline{K}_{i\text{-}1,j}^{D}\right)}+3\overline{K}_{i,j}^{d}\right)=3\beta_{i,j}\frac{\Delta_{i,j}}{h}\left(\frac{1+3\overline{K}_{i\text{-}1,j}^{D}}{\left(2+3\overline{K}_{i\text{-}1,j}^{D}\right)}\right)+\frac{1}{2}\theta_B$$

$$\theta_A\left(\frac{1}{2}+2\beta_{i,j}-\frac{\beta_{i,j}}{\left(2+3\overline{K}_{i\text{-}1,j}^{D}\right)}+3\overline{K}_{i,j}^{d}-\frac{1}{2+12\overline{K}_{i+1,j}^{u}}\right)=3\beta_{i,j}\frac{\Delta_{i,j}}{h}\left(\frac{1+3\overline{K}_{i\text{-}1,j}^{D}}{\left(2+3\overline{K}_{i\text{-}1,j}^{D}\right)}\right)$$

$$\theta_A=\left[\frac{3\beta_{i,j}\left(\frac{1+3\overline{K}_{i-1,j}^{D}}{2+3\overline{K}_{i-1,j}^{D}}\right)}{\left(\frac{1}{2}+2\beta_{i,j}+3\overline{K}_{i,j}^{d}-\frac{\beta_{i,j}}{\left(2+3\overline{K}_{i-1,j}^{D}\right)}-\frac{1}{2+12\overline{K}_{i+1,j}^{u}}\right)}\right]\frac{\Delta_{i,j}}{h} \tag{B.34}$$

$$\Delta_{i+1,j}^{u}=\left[\frac{6\beta_{i,j}\left(1+3\overline{K}_{i-1,j}^{D}\right)\left(1+3\overline{K}_{i+1,j}^{u}\right)}{\left(1+4\beta_{i,j}+6\overline{K}_{i,j}^{d}\right)\left(1+6\overline{K}_{i+1,j}^{u}\right)\left(2+3\overline{K}_{i-1,j}^{D}\right)-\beta_{i,j}\left(2+12\overline{K}_{i+1,j}^{u}\right)-\left(2+3\overline{K}_{i-1,j}^{D}\right)}\right]\Delta_{i,j} \tag{B.35}$$

$$-F_{i,j}h=M_{AE+}M_{EA} \tag{B.36}$$

$$-F_{i,j}h=2Ek_{i,j}^{C}\left(2\theta_A+\theta_E-3\frac{\Delta_{i,j}}{h}\right)+2Ek_{i,j}^{C}\left(2\theta_E+\theta_A-3\frac{\Delta_{i,j}}{h}\right)$$

$$-F_{i,j}h=2Ek_{i,j}^{C}\left(3\theta_A+3\theta_E-6\frac{\Delta_{i,j}}{h}\right)=6Ek_{i,j}^{C}\left(\theta_A+\theta_E-2\frac{\Delta_{i,j}}{h}\right)$$

$$-F_{i,j}h = 6Ek_{i,j}^{C}\left(\theta_A\left(\frac{1+3\overline{K}_{i\text{-}1,j}^{D}}{2+3\overline{K}_{i\text{-}1,j}^{D}}\right)-\left(\frac{1+6\overline{K}_{i\text{-}1,j}^{D}}{2+3\overline{K}_{i\text{-}1,j}^{D}}\right)\frac{\Delta_{i,j}}{h}\right)$$

$$-F_{i,j}h = 6Ek_{i,j}^{C}\left(\left[\frac{3\beta_{i,j}\left(\frac{1+3\overline{K}_{i\text{-}1,j}^{D}}{2+3\overline{K}_{i\text{-}1,j}^{D}}\right)^{2}}{\left(\frac{1}{2}+2\beta_{i,j}+3\overline{K}_{i,j}^{d}-\frac{\beta_{i,j}}{\left(2+3\overline{K}_{i\text{-}1,j}^{D}\right)}-\frac{1}{2+12\overline{K}_{i+1,j}^{u}}\right)}\right]-\left(\frac{1+6\overline{K}_{i\text{-}1,j}^{D}}{2+3\overline{K}_{i\text{-}1,j}^{D}}\right)\right)\frac{\Delta_{i,j}}{h}$$

$$D_{i,j}=\frac{F_{i,j}}{\Delta_{i,j}}=\left[\frac{12E}{h^2}\right]k_{i,j}^{C}\left(\frac{1}{2}\left(\frac{1+6\overline{K}_{i\text{-}1,j}^{D}}{2+3\overline{K}_{i\text{-}1,j}^{D}}\right)-\left[\frac{3\beta_{i,j}\left(\frac{1+3\overline{K}_{i\text{-}1,j}^{D}}{2+3\overline{K}_{i\text{-}1,j}^{D}}\right)^{2}}{\left(1+4\beta_{i,j}+6\overline{K}_{i,j}^{d}-\frac{2\beta_{i,j}}{\left(2+3\overline{K}_{i\text{-}1,j}^{D}\right)}-\frac{1}{1+6\overline{K}_{i+1,j}^{u}}\right)}\right]\right)$$

where

$$\overline{K}_{i+1,j}^{u}=\frac{k_{i+1,j\text{-}1}^{B}+k_{i+1,j}^{B})}{k_{i+1,j}^{C}}\quad;\quad k_{i+1,j\text{-}1}^{B}=\frac{I_{i+1,j\text{-}1}^{B}}{2L_{i+1,j\text{-}1}}\quad;\quad k_{i+1,j}^{B}=\frac{I_{i+1,j}^{B}}{2L_{i+1,j}}$$

$$\overline{K}_{i,j}^{d}=\frac{k_{i,j\text{-}1}^{B}+k_{i,j}^{B}}{k_{i+1,j}^{C}}\quad;\quad k_{i,j\text{-}1}^{B}=\frac{I_{i,j\text{-}1}^{B}}{L_{i,j\text{-}1}}\quad;\quad k_{i,j}^{B}=\frac{I_{i,j}^{B}}{L_{i,j}}$$

$$\overline{K}_{i\text{-}1,j}^{D}=\frac{k_{i\text{-}1,j\text{-}1}^{B}+k_{i\text{-}1,j}^{B}}{k_{i,j}^{C}}\quad;\quad k_{i\text{-}1,j\text{-}1}^{B}=\frac{I_{i\text{-}1,j\text{-}1}^{B}}{2L_{i\text{-}1,j\text{-}1}}\quad;\quad k_{i\text{-}1,j}^{B}=\frac{I_{i\text{-}1,j}^{B}}{2L_{i\text{-}1,j}}$$

Top storey (for the case *m*=0.5) (see Figure 9.6**)**

$$M_{AB} + M_{AC} + M_{AD} = 0 \tag{B.37}$$

$$2Ek_{n,j}^{C}\left(2\theta_A + \theta_B - 3\frac{\Delta_{n,j}}{h}\right) + 4Ek_{n,j-1}^{B}\left(\frac{3}{2}\theta_A\right) + 4Ek_{n,j}^{B}\left(\frac{3}{2}\theta_A\right) = 0$$

$$\theta_B = 3\frac{\Delta_{n,j}}{h} - \theta_A\left(2 + 3\left(\frac{k_{n,j-1}^{B} + k_{n,j}^{B}}{k_{n,j}^{C}}\right)\right) = 3\frac{\Delta_{n,j}}{h} - \theta_A\left(2 + 3\overline{K}_{n,j}^{u}\right) \tag{B.38}$$

$$M_{BA} + M_{BE} + M_{BF} = 0 \tag{B.39}$$

$$2Ek_c\left(2\theta_B + \theta_A - 3\frac{\Delta_{n,j}}{h}\right) + 4Ek_{n-1,j-1}^{B}\left(\frac{3}{2}\theta_B\right) + 4Ek_{n-1,j}^{B}\left(\frac{3}{2}\theta_B\right) = 0$$

$$\theta_A = 3\frac{\Delta_{n,j}}{h} - \theta_B\left(2 + 3\left(\frac{k_{n-1,j-1}^{B} + k_{n-1,j}^{B}}{k_{n,j}^{C}}\right)\right) = 3\frac{\Delta_{n,j}}{h} - \theta_B\left(2 + 3\overline{K}_{n-1,j}^{d}\right)$$

$$\theta_A = 3\frac{\Delta_{n,j}}{h} - \left(3\frac{\Delta_{n,j}}{h}\left(2 + 3\overline{K}_{n-1,j}^{d}\right) - \theta_A\left(2 + 3\overline{K}_{n,j}^{u}\right)\left(2 + 3\overline{K}_{n-1,j}^{d}\right)\right)$$

$$\theta_A\left(\left(2 + 3\overline{K}_{n,j}^{u}\right)\left(2 + 3\overline{K}_{n-1,j}^{d}\right) - 1\right) = 3\frac{\Delta_{i,j}}{h}\left(1 + 3\overline{K}_{n-1,j}^{d}\right)$$

$$\theta_A = \left[\frac{3\left(1 + 3\overline{K}_{n-1,j}^{d}\right)}{\left(\left(2 + 3\overline{K}_{n,j}^{u}\right)\left(2 + 3\overline{K}_{n-1,j}^{d}\right) - 1\right)}\right]\frac{\Delta_{n,j}}{h} \tag{B.40}$$

$$-F_{n,j}h = M_{AB+}M_{BA} \tag{B.41}$$

$$-F_{n,j}h = 2Ek_{n,j}^{C}\left(2\theta_A + \theta_B - 3\frac{\Delta_{n,j}}{h}\right) + 2Ek_{n,j}^{C}\left(2\theta_B + \theta_A - 3\frac{\Delta_{n,j}}{h}\right)$$

$$-F_{n,j}h = 6Ek_{n,j}^{C}\left(\theta_A + \theta_B - 2\frac{\Delta_{i,j}}{h}\right)$$

$$F_{n,j}h = 6Ek_{n,j}^{C}\left(\theta_A\left(1 + 3\overline{K}_{n,j}^{u}\right) - \frac{\Delta_{n,j}}{h}\right)$$

$$F_{n,j}h = 6Ek_{n,j}^{C}\frac{\Delta_{n,j}}{h}\left(\frac{3\left(1 + 3\overline{K}_{n-1,j}^{d}\right)\left(1 + 3\overline{K}_{n,j}^{u}\right) - \left(\left(2 + 3\overline{K}_{n,j}^{u}\right)\left(2 + 3\overline{K}_{n-1,j}^{d}\right) - 1\right)}{\left(\left(2 + 3\overline{K}_{n,j}^{u}\right)\left(2 + 3\overline{K}_{n-1,j}^{d}\right) - 1\right)}\right)$$

$$F_{n,j}h = 6Ek^{C}_{n,j}\frac{\Delta_{n,j}}{h}\left(\frac{\left(\overline{K}^{d}_{n\text{-}1,j}+\overline{K}^{u}_{n,j}+6\overline{K}^{d}_{n\text{-}1,j}\overline{K}^{u}_{n,j}\right)}{\left(1+2\overline{K}^{u}_{n,j}+2\overline{K}^{d}_{n\text{-}1,j}+3\overline{K}^{d}_{n\text{-}1,j}\overline{K}^{u}_{n,j}\right)}\right)$$

$$D_{n,j} = \left[\frac{12E}{h^2}\right]k^{C}_{n,j}\left(\frac{\left(\overline{K}^{d}_{n\text{-}1,j}+\overline{K}^{u}_{n,j}+6\overline{K}^{d}_{n\text{-}1,j}\overline{K}^{u}_{n,j}\right)}{2\left(1+2\overline{K}^{u}_{n,j}+2\overline{K}^{d}_{n\text{-}1,j}+3\overline{K}^{d}_{n\text{-}1,j}\overline{K}^{u}_{n,j}\right)}\right) \qquad \text{(B.42)}$$

where:

$$\overline{K}^{u}_{n,j} = \frac{k^{B}_{n,j\text{-}1}+k^{B}_{n,j}}{k^{C}_{n,j}} \;\; ; \quad k^{B}_{n,j\text{-}1} = \frac{I^{B}_{n,j,j\text{-}1}}{L_{n,j\text{-}1}} \; ; \quad k^{B}_{n,j} = \frac{I^{B}_{n,j}}{L_{n,j}}$$

$$\overline{K}^{d}_{n\text{-}1,j} = \frac{k^{B}_{n\text{-}1,j\text{-}1}+k^{B}_{n\text{-}1,j}}{k^{C}_{n,j}} \;\; ; \quad k^{B}_{n\text{-}1,j\text{-}1} = \frac{I^{B}_{n\text{-}1,j\text{-}1}}{2L_{n\text{-}1,j\text{-}1}} \; ; \quad k^{B}_{n\text{-}1,j} = \frac{I^{B}_{n\text{-}1,j}}{2L_{n\text{-}1,j}}$$